FLUORESCENT GFP CHROMOPHORES AS POTENTIAL LIGANDS FOR VARIOUS NUCLEAR RECEPTORS

A Dissertation
Presented to
The Academic Faculty

by

Anna Duraj-Thatte

In Partial Fulfillment
of the Requirements for the Degree
Doctorate of Philosophy in the
School of Chemistry and Biochemistry

Georgia Institute of Technology
August 2012

FLUORESCENT GFP CHROMOPHORES AS POTENTIAL LIGANDS FOR VARIOUS NUCLEAR RECEPTORS

Approved by:

Dr. Laren Tolbert, Advisor
School of Chemistry and Biochemistry
Georgia Institute of Technology

Dr. Bahareh Azizi, Advisor
School of Chemistry and Biochemistry
Georgia Institute of Technology

Dr. Andreas Bommarius
School of Chemical and Biomolecular Engineering
Georgia Institute of Technology

Dr. Eric Gauchier
School of Biology
Georgia Institute of Technology

Dr. Loren Williams
School of Chemistry and Biochemistry
Georgia Institute of Technology

Dr. Nicholas Hud
School of Chemistry and Biochemistry
Georgia Institute of Technology

Date Approved: April 10, 2012

I am among those who think that science has great beauty. A scientist in his laboratory is not only a technician: he is also a child placed before natural phenomena which impress him like a fairy tale.

Maria Sklodowska- Curie

This work could not have been completed without endless support and love of my husband, Azam Thatte, who always believed in me, more than I did. Therefore I dedicate this work to him and to my daughter Saay Duraj-Thatte, who brought light into my life. I also dedicate this work to my parents Elzbieta Duraj and Tadeusz Duraj who have sacrificed everything for my education and without their love and support I could not be here today.

ACKNOWLEDGEMENTS

Through the journey of graduate studies, I had opportunity to meet friends, philosophers and guides whose presence has had significant impact on my development not only as a scientist but also as an individual.

First of all, I thank my advisers Dr. Laren Tolbert and Dr Bahareh Azizi for their guidance and support through my graduate studies. Their trust in me and the opportunity they provided to develop my ideas, allowed me to learn and grow as a scientist. Specially, I would like to thank Dr Bahareh Azizi for her hard work and dedication to mentor me through all these years. The current work could not have been possible without her support, guidance and friendship.

I would also like to thank my committee members: Dr. Loren Williams, Dr. Andreas Bommarius, Dr. Nicholas Hud and Dr. Eric Gaucher for their guidance through out my graduate studies.

In addition, my lab members have immensely helped me in this journey through their support and friendship. In particular, I would like to thank Dr. Terry Watt and Dr. Kenyetta Johnson for their guidance in the first year of my graduate studies and Michael Rood for all the scientific and philosophical discussions that I have always enjoyed with him. I would also like to thank James Kratzer for his continual friendship. I am grateful to Dr. Hally Schaffer, Dr. Amanda Ousley, Dr. Hilda Castillo and Dr. Jennifer Taylor for their great friendship and for training me in the cell culture. The presence of these lab mates made all those uncountable hours of experiments to be cheerful and fun. Finally, I would like to thank Dr. Anthony Baldridge, whose work has had a significant impact on my dissertation. He synthesized all the compounds that I have used in my Ph.D research.

I also wish to thank Dr. Adrian Katona and Pritha Bagchi for their friendship and support through all these years.

I am very thankful to the undergraduate students that I have had pleasure to work with. I very much enjoyed mentoring Milad Adloo, Bader Kashlan and Brice Hwang who were all outstanding students. Their work has played a substantial role in my research. I would like to thank Dr. Payne for allowing me to use her lab's confocal microscope. I am grateful to Andrew Shaw, Dr. William Humphries and Dr. Reagan McRae for training me on confocal microscopy.

I wish to specially thank my friends Vrinda Vasudeva, Sahil Girotra, Sonali Tare, Karan Singhal, Bhargavi Chavali and Nilesh Ostwal who were not only great friends but also part of a family.

I love my husband, Dr. Azam Thatte, whose endless love and support made my Ph.D journey possible. He always believed in me and gave me strength to push myself forward through peaks and valleys of this journey. Finally, "Thank You" are too little words to express my feelings towards my parents, Elzbieta Duraj and Tadeusz Duraj whose endless love and hard work has supported my life journey.

TABLE OF CONTENTS

LIST OF TABLES

LIST OF FIGURES

LIST OF SYMBOLS AND ABBREVIATIONS

3-AT	3-amino-1, 2, 4-triazole
Ac	Acetyl group
ACTR	Activator for Thyroid and Retinoid receptors
AD	Activation domain
ADE	Adenine
AF-1	Ligand-independent activation function domain
AF-2	Ligand-dependent activation function domain
-ALW	Minus adenine, leucine and tryptophan
AMI	Arylmethyleneimidazolodinone
APL	Acute promyelocytic leukemia
AR	Androgen receptor
BF-3	Binding function 3
BFP	Blue fluorescent protein
C.A.	Constitutively active
CAR	Constitutive androstane receptor
CC	Chemical complementation
CFP	Cyan fluorescent protein
CMV	Cytomegalovirus
CoAc	Coactivator
CoR	Corepressor
CTE	Carboxy terminal extension

CYP3A4	Cytochrome P450 monooxygenase 3A4
DBD	DNA binding domain
DNA	Deoxyribonucleic acid
DMSO	Dimethylsulfoxide
dNTPs	Deoxyribonucleotide triphosphate
E2	17-β-estradiol
E.coli	*Escherichia coli*
EC_{50}	Half maximal effective concentration
EpPCR	Error-prone PCR
ER	Estrogen receptor
ERR	Estrogen related receptor
FXR	Farnesoid x receptor
GAD	Gal4 activation domain
GBD	Gal4 DNA binding domain
GR	Glucocorticoid receptor
HATs	Histone acetyltransferases
HDAC	Histone deacetylase
HEK 293T	Human embryonic kidney 293T
HIS	Histidine
-HLW	Minus histidine, leucine and tryptophan
HR38	Hormone receptor-like in 38
HSP	Heat shock protein

ID	Intrinsically disordered
LBD	Ligand binding domain
LBP	Ligand bind pocket
LRH-1	Liver receptor homolog-1
-LW	Minus leucine and tryptophan
LXR	Liver X receptor
µg	Microgram
MgCl2	Magnesium chloride
µM	Micromolar
Mm	millimolar
MnCl2	Manganese chloride
MPP	Methyl-piperidino-pyrazole
MR	Mineralocorticoid receptor
NCoR1	Nuclear receptor Corepressor-1
Ng	Nanogram
nM	Nanomolar
NR	Nuclear receptor
Nurr1	Nuclear receptor related 1 protein
OD	Optical density
oligos	oligonucleotides
OFP	Orange fluorescent protein
PCR	Polymerase chain reaction

PDB	Protein Data Bank
p-HBDI	4-(p-hydroxybenzylidene)-5-imidazolinone
PPARs	Peroxisome proliferator-activated receptors
PR	Progesterone receptor
PXR	Pregnane X receptor
PTT	Propylpyrazole triol
r	rat
RAR	Retinoic acid receptor
RE	Response element
RFP	Red fluorescent protein
RLU	Relative light units
rpm	Revolutions per minute
RXR	Retinoid X receptor
SC	Synthetic complete media
SERDs	Selective nuclear receptor downregulators
SF-1	Steroidogenic receptor
SRC-1	Steroid Receptor Coactivator-1
TR	Thyroid hormone receptor
TR3	Orphan receptor TR3
VDR	Vitamin D Receptor
Wt	Wild type
YFP	Yellow fluorescent protein

SUMMARY

Nuclear receptors are ligand-activated transcription factors, where upon binding with small molecule ligands, these proteins are involved in the regulation of gene expression. To date there are approximately 48 human nuclear receptors known, involved in multiple biological and cellular processes, ranging from differentiation to maintenance of homeostasis. Due to their critical role in transcriptional regulation, these receptors are implicated in several diseases. Currently, 13% of prescribed drugs in the market are NR ligands for diseases such as cancer, diabetes and osteoporosis. Issues such as drug resistance, as seen with the highly successful breast cancer therapeutic drug, tamoxifen, present a critical need for the continuous identification of novel small molecules that can serve as potential ligands for these receptors, developing new drugs. In addition to drug discovery, the mechanism of function, mobility and trafficking of these receptors is poorly understood. Gaining insight into the relationship between the function and /or dysfunction of these receptors and their mobility will aid in a better understanding of the role of these receptors.

The green fluorescent protein (GFP) has revolutionized molecular biology by providing the ability to monitor protein function and structure via fluorescence. The fluorescence from this biological marker arises from the chromophore, formed from the polypeptide backbone of three amino acid residues, buried inside 11-stranded β-barrel protein. Synthesis of GFP derivatives is based on the structure of the arylmethyleneimidazolidinone (AMI), creating a molecule that is only weakly fluorescent. Certain AMI derivatives have previously been designed to bind the human

serum albumin (HSA) protein, showing fluorescence upon protein binding. Characterizing these AMI derivatives for other proteins can provide a powerful visualization tool for analysis of protein function and structure. This development could provide a very powerful method for protein analysis *in vitro* and *in vivo*.

Development of such fluorescent ligands will prove beneficial for the nuclear receptors. Current methods for visualizing these receptors involve creating fusion proteins with the green fluorescent protein (GFP). Nuclear receptors are involved in multiple cascades of protein/protein interactions, and the presence of a bulky fluorescence protein might prevent the natural function of the receptor by eliminating the surface area needed for critical protein/protein contacts. Therefore, the development of fluorogens links the fluorescence to a small molecule ligand, more natural to the function of the receptor, serving as the tool needed for visualization and the trafficking of these receptors *in vivo*.

In this work, libraries of AMIs derivatives were synthesized by manipulating various R groups around the core structure, and tested for their ability to serve as nuclear receptor ligands with the ability to fluoresce upon binding. The fluorogens are developed for steroidal and non-steroidal receptors, two general classes of nuclear receptors. Specific AMIs were designed and developed for steroid receptor estrogen receptor α (ERα). These ligands are showed to activate the receptor with an EC_{50} value of 3 μM and the 10-fold activation with AMI 1 and AMI 2 in comparison to the 21-fold activation observed with natural ERα ligand, 17β-estradiol. These novel ligands were not able to display the fluorescence upon binding the receptor. However, fluorescence localized in nucleus was observed in the case of another AMI derivative, AMI 10, which does not

activate the receptor. Such ligands open new avenues for developing fluorescent probes for ERα that do not involve fluorescent conjugates attached to a known ERα ligand core.

AMIs were also characterized for non-steroidal receptors, specifically the pregnane x receptor (PXR) and retinoic acid receptor α (RARα). To date, fluorogens which turn fluorescence upon binding and activate the receptor have not been developed for these receptors. With respect to PXR, several AMI derivatives were discovered to bind and activate this receptor with a fold-activation better than the known agonist, rifampicin. The best characterized AMI derivative, AMI 4, activates the receptor with an EC_{50} of value 6.3 μM and the 154-fold activation in comparison to the 90-fold activation and an EC_{50} value of 1.3 μM seen with rifamipicin. This ligand is not only able to activate PXR but also displays fluorescence upon binding to the receptor. The fluorescence pattern was observed around the nucleus. Besides AMI 4, 16 other AMI derivatives are identified that activate PXR with different activation profiles. Thus, a novel class of PXR ligands with fluorescence ability has been developed.
The AMI derivatives able to bind and activate RAR, also displayed activation profiles that were comparable to the wild-type ligand, all *trans* retinoic acid. These ligands activated the receptor with an EC_{50} value of 220 nM for AMI 109 in comparison to an EC_{50} value of 0.8 nM with the natural ligand for RARα. When these ligands were tested for fluorescence in yeast, the yeast were able to fluoresce only in the presence of the receptor and the AMI derivative, indicating that these agonists also have the ability to fluoresce.

To provide the opportunity to gain further insight into interaction between the ligand and the receptor, these nuclear receptors were also subjected to rounds of

mutagenesis, engineering receptors with the ability to bind AMI derivatives. The most promising of these rounds of mutagenesis was the discovery of an estrogen receptor α variant, E380D that showed an increase in the fold activation from two fold to five fold with AMI 2 in comparison to the wild-type receptor. This variant also showed an enhanced fluorescence with AMI 1 and 2 in comparison to the wild-type receptor. Interestingly, the variants have mutations outside of the ligand binding pocket, showing the importance of residues that are not in direct contact with the ligand and how the secondary shell residues and even those on the surface of the protein could have an allosteric effect on ligand binding.

The discovery of this novel class of ligands, AMIs, for various nuclear receptors indicates that they can serve as strong candidates for these receptors, in terms of drug development and resources for visualizing nuclear receptor mobility and trafficking. These fluorogens hold great promise as perhaps the next generation of novel ligands for various nuclear receptors and will perhaps allow a better understanding of the functionality of these proteins and their mechanism to certain diseases.

CHAPTER 1

NUCLEAR RECEPTORS

1.1 Nuclear Receptor Superfamily

The control of gene expression is essential for development, metabolism and cell function. Nuclear receptors are a large family of ligand dependent transcription factors that regulate gene transcription. They play crucial roles in a number of important biological and physiological processes [1-3]. Hormones, endogenous small molecules, act as ligands to the nuclear receptors to control expression of specific genes [4].

Due to their essential functions, nuclear receptors are present even in the simplest of the organisms, and first appeared around 635 million years ago [5]. However, it is hypothesized that the original nuclear receptors were primarily environmental sensors due to the lack of endocrine organs present at that time in the simple life form [1, 6, 7]. The development of the complex endocrine system in evolution of bilateral animals caused the nuclear receptors to evolve in binding various hormones, thus serving as transcription factors. To date, 900 nuclear receptor genes have been identified in every species[5]. Mammals, including humans, have 48 nuclear receptors [8, 9]. While about half of these receptors have ligands that have been identified, several others do not have a known “natural” ligand associated with them and are called “orphan nuclear receptors”. However, in such cases several metabolic intermediates have been identified as potential ligands [10, 11]. A few nuclear receptors, such as Nurr1 and HR38, do not possess the typical binding pocket, as their pocket is filled with the side chain amino acids, serving as constitutively active receptors[12, 13].

The majority of nuclear receptors bind a variety of small, hydrophobic molecules that are derivatives of fatty acids, retinoids, vitamins and hormones. Based on the types of small molecules these receptors bind, the superfamily of nuclear receptors is divided into subfamilies [8, 14]. Thus, estrogen receptor (ERα-β), estrogen related receptor (ERRα-γ), glucocorticoid receptor (GR), mineralocorticoid receptor (MR), progesterone receptor (PR) and androgen receptor (AR) belong to the steroid family of nuclear receptors as they bind to the derivatives of the steroids[15]. Other nuclear receptors are activated by retinoids or fatty acids, such as retinoid x receptor and peroxisome proliferator activated receptor (PPARγ), therefore creating the non-steroidal subfamily[16] [17, 18]. The pregnane x receptor (PXR) is the example of an orphan nuclear receptor, due to the lack of an identified natural ligand for it but is found to be activated by various xenobiotic ligands [19, 20]. The wide diversity of ligands that bind and activate the nuclear receptors in nanomolar affinity and with high specificity, allow these receptors to perform their specific functions, such as controlling embryonic development and homeostatis [21]. Due to their critical role in transcriptional regulation, these receptors are implicated in several diseases. Hence, there is a vast interest in discovering ligands for these receptors as potential therapeutic drugs [22]. Currently, 13% of prescribed drugs in the market (e.g. Advair, Avandia and Faslodex) are NR ligands for diseases such as cancer, diabetes and osteoporosis[5, 23], while the nuclear receptor ligands such as dibenzodiazepine derivatives have recently been developed for schizophrenia, autism and Parkinson's disease [24, 25]. However, the issues such as drug resistance and toxicity indicate that there is a critical need for the identification of a novel class of small molecules as potential ligands for such nuclear receptors.

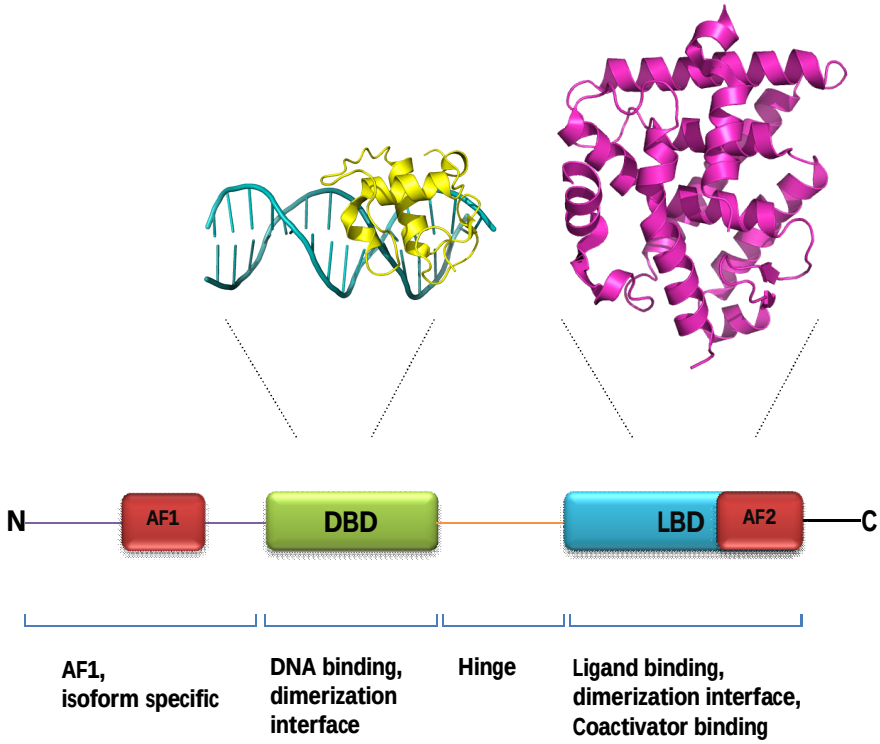

Figure 1.1 Scheme of nuclear receptors structure. The visual structure of DBD (yellow) and LBD (pink).

1.2 Structure of Nuclear Receptors

Nuclear receptors share a common structural organization, which includes five main domains: the N- terminal A/B domain containing transcriptional activation function 1 domain (AF-1), the C domain known as the central DNA binding domain (DBD), a flexible hinge D region and the E domain containing the carboxy terminal ligand binding domain (LBD) with the activation function 2 domain (AF-2) (Figure 1.1) [14, 26, 27].

Nuclear receptors contain two transcriptional activation domains which interact with co-regulatory proteins. The AF-1 domain is the least conserved domain among the nuclear receptor domains, significantly varying in length and sequence composition. This trans-activational domain is also thought to be intrinsically disordered (ID), making the analysis of the structure - function relationship difficult [28,29]. More recently, it has been discovered that this domain is able to interact with many co-regulatory proteins [30]. Even though this domain acts as ligand independent transcriptional activator, it synergizes its action with AF-2 domain, which is responsible for interactions with the co-activators.

The DNA binding domain (DBD) is the most conserved structural domain within the nuclear receptor superfamily. In case of the DBD, structural data has been reported for many nuclear receptors, and has been shown to consist of helices interacting with the major groove and specific bases, while the second helix stabilizes the domain (Figure 1.2). The crucial role in binding DBD is played by two zinc finger motifs that are created from two zinc ions which are coordinated by four cysteine residues [1, 15, 26, 31]. All nuclear receptors interact with a specific DNA sequence called response

Figure 1.2 Structure of DNA binding domain. DNA binding domain as heterodimer (green and blue), response elements (orange) and Zn (II) ions (red). PDB:1DSZ

elements (RE). Response elements are located relatively close to the gene of interest that is activated by nuclear receptor. They are created from direct or indirect (palindromic) repeats of specific sequence 5'-AGAACA-3' or 5'-AGGTCA-3', that are separated by few nucleotides[1].

Nuclear receptors can be subdivided into three groups based on the way they bind to the response elements: steroids receptors such as ER and GR that bind to DNA as homodimers, receptors that can interact with response elements as heterodimers (e.g. VDR, LXR and RAR) and nuclear receptors that bind as monomers (e.g. steroidogenic receptor (SF-1) and ERR) .

The DBD is connected to the ligand binding domain (LBD) via a hinge region. However, recent studies have indicated that the hinge region is not only the flexible linker that allows for correct DNA binding and dimerization but also a part of it, which includes about 12 residues called a carboxy terminal extension (CTE), that directly participates in binding to the DNA [32, 33]. This region is not conserved among all the nuclear receptors and creates significantly different structural motifs. Thus, the CTE of thyroid hormone receptor (TR) creates a helix that interacts with the DNA along with the other two helices that are part of the DBD [34].

The LBD is the most characterized domain of nuclear receptors. Extensive structural studies have revealed a great amount of information about the structure - function relationship of this domain. The LBD of the most nuclear receptors consists of a canonical fold containing about 10-13 α helices, two to five β strands, and the variable loops, which are arranged into an anti-parallel, three-layered sandwich (Figure 1.3)[35].

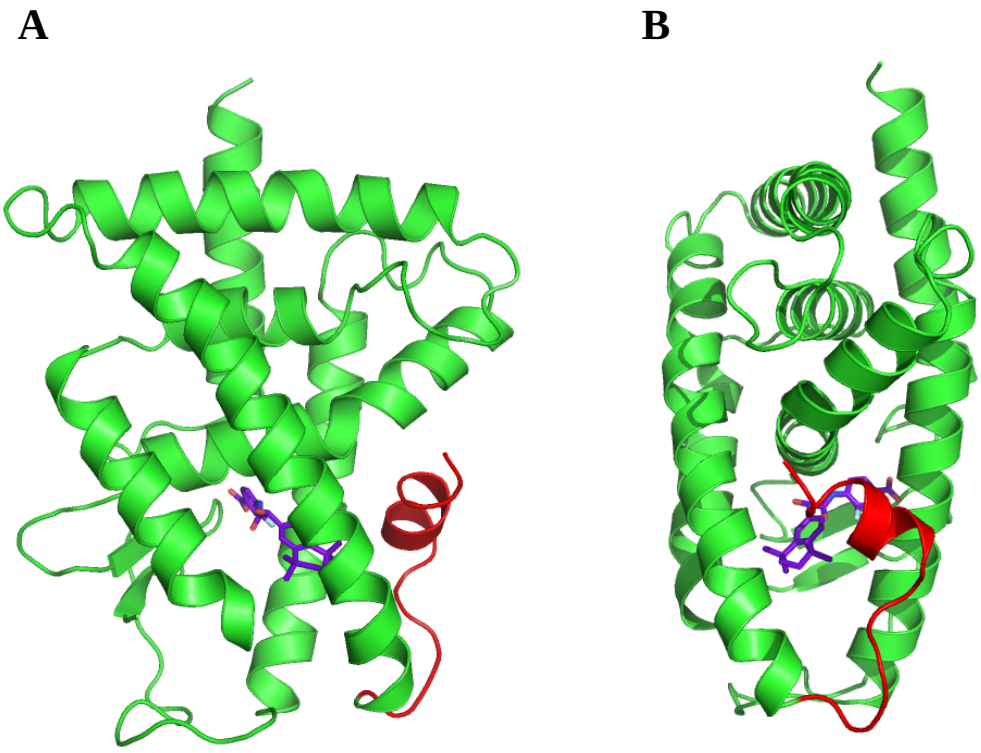

Figure 1.3 Structure of the ligand binding domain. A and B LBD shown from different side. Helix 12 is shown in red, ligand (purple). PDB: 4LBD

The LBD's primary role is the binding of a small molecule ligand, in its ligand binding pocket (LBP). The LBP is formed from helices 3, 7, 10 and β-turn, creating a predominantly hydrophobic pocket. However, several polar residues are responsible for the crucial interactions with the ligand[9]. Due to a wide range of ligands that bind and activate nuclear receptors, the size and shape of LBP varies depending on the type of nuclear receptor, ranging from 400 $Å^3$ observed with ERα to 1600 $Å^3$, observed with PXR[8, 36].

The role of helix 12 of the LBD is crucial in these receptors. Upon ligand binding, helix 12 changes its conformation, from a freely mobile structure in solvent to a more stabilized conformation, moving to the surface of the protein (Figure 1.4) [37]. A part of this helix is the ligand regulated transcriptional activation function domain (AF-2), which is responsible for allosteric interaction with co-regulators. In the absence of the ligand (apo) or in the presence of an antagonist, the LBD interacts with the nuclear receptor corepressor such as NCoR1 and SMRT [38, 39]. However, agonist binding leads to a conformational change of helix 12, positioning the AF2 domain in the orientation for co-activator binding. Conformational flexibility of helix 12 is crucial for creating transcriptional response based on the antagonist or the agonist binding [18].

Crystal structures solved for many DBDs and LBDs revealed several structural details about the function of the nuclear receptor domains. However, domain-domain interactions were not well defined due to the lack of various full length ligand-bearing nuclear receptors. To date, there is only one full length crystal structure of a nuclear

receptor that includes LBD and DBD of PPARγ as a heterodimer with RXRα, bound to DNA and the co-activator peptides (Figure 1.5)[40].

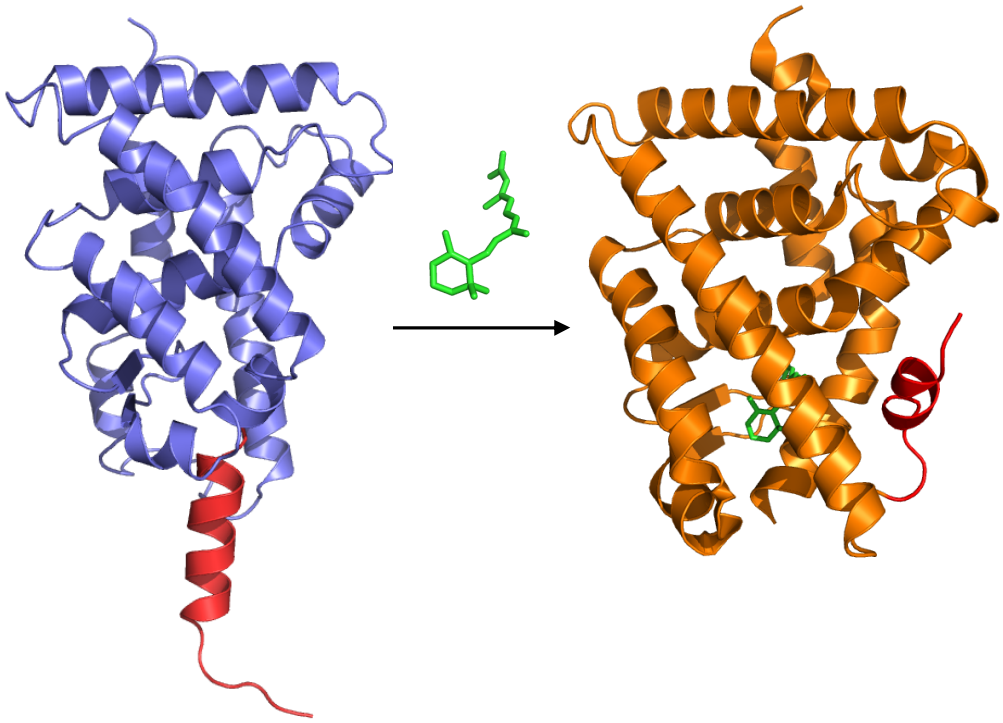

Figure 1.4 Ligand binding induces conformational change of the LBD of nuclear receptor. Helix 12 is shown in red, ligand (9cRA) in green. PDB:1LBD, 1FBY

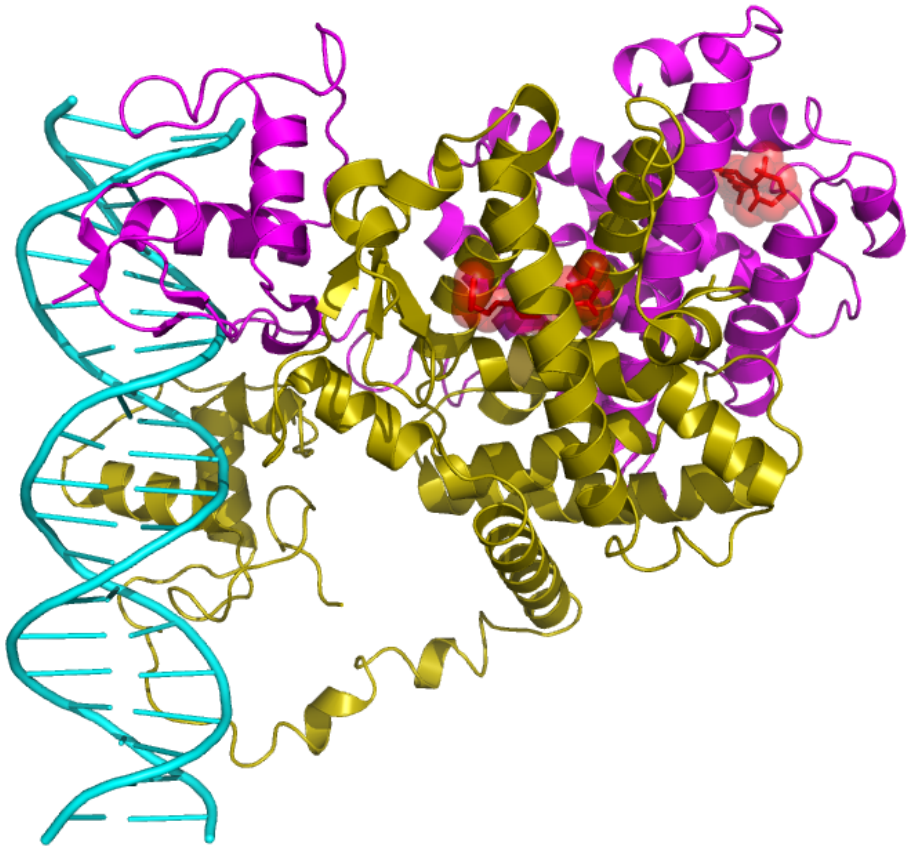

Figure 1.5 Full length crystal structure of PPARγ with RXRα bound to DNA.

1.3 Function of Nuclear Receptors

Each of the 48 members of the human nuclear receptor family is able to turn on the transcription of various genes by binding to specific response elements. Without ligand, the nuclear receptor interacts with corepressor, such as nuclear receptor corepressor 1 (NCoR1) or silencing mediator for retinoid and thyroid hormone receptor (NCoR2, SMRT). These proteins bind to hydrophobic grooves created between helices 3 and 4, forming a corepressor nuclear receptor box [41]. Corepressor proteins in turn recruit histone deacetylases (HDAC), which are responsible for condensation of chromatin above the gene promoter and the repressor of gene transcription [42]. When the agonist binds to the nuclear receptor, helix 12 undergoes a conformational change that leads to corepressor dissociation and creation of coactivator binding site. Coactivators, such as the steroid receptor coactivator 1 (SRC-1) and the activator for thyroid and retinoid receptors (ACTR) interact with LBD through LXXLL NR box, where L is leucine and X is any amino acid [43, 44]. Coactivators create complexes with histone acetyltransferase (HAT), which acetylate the lysine residues on the histones, thus weakening the interactions between the DNA and the histones. This in turn allows for the recruitment of the RNA polymerase and initiates the transcription (Figure 1.6) [45].

Next to coactivator and corepressor site, the nuclear receptor function is also modulated by the other protein–protein interaction by binding function–3 (BF-3). This recently found site brings a new site for the allosteric control of nuclear receptors [46, 47]. This site is highly conserved among the nuclear receptors and the mutations in this region were implicated in several dysfunctions of nuclear receptors leading to the cancer

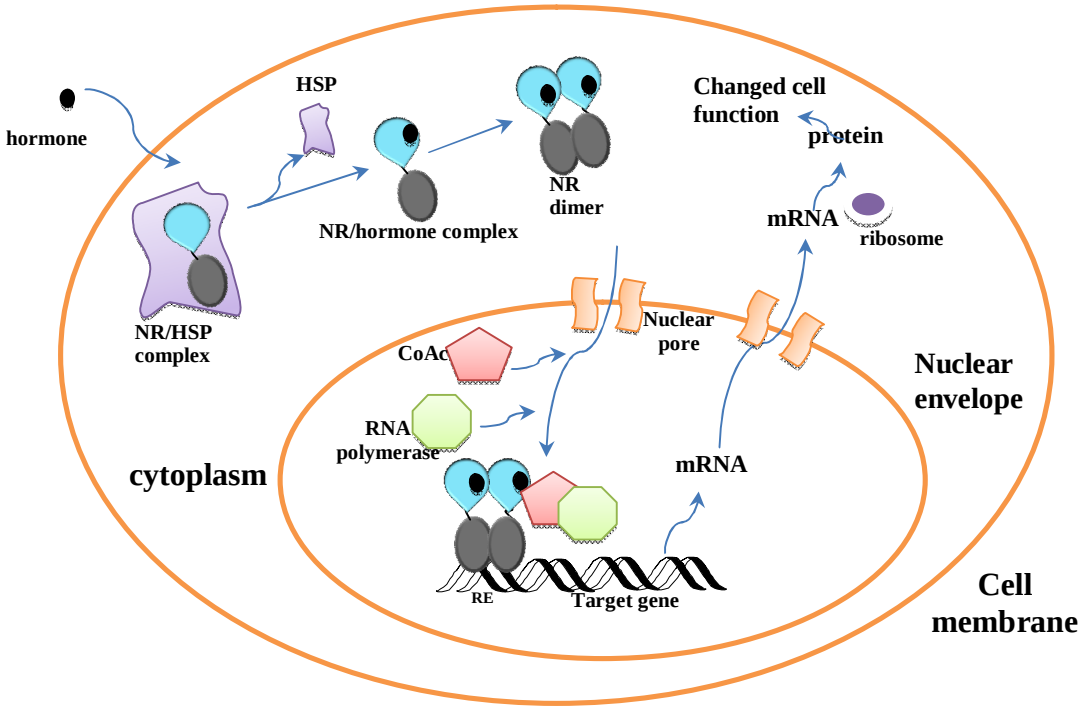

Figure 1.6 Transcriptional regulations by nuclear receptors.

and other diseases. Unfortunately, the binder protein has not been found to bind the surface of the BF-3 site [48].

These recent findings indicate that allosteric modulation of the nuclear receptor is essential for the proper function of the nuclear receptors and more work needs to be done to understand how this interaction directly and indirectly influences the transcription activation. Such knowledge would play a significant role in the development of the novel transcription modulators.

1.4 Diversity of Nuclear Receptor Ligands

Transcriptional regulation by nuclear receptors via binding small molecule ligands opens avenues for the development of various drugs for nuclear receptor related diseases, such as cancer and diabetes. Most of the synthetic ligands are based on natural ligands that bind and active NRs. Nuclear receptor ligands are mainly hydrophobic, small molecules, with structural diversity and also include retinoids and antibiotics (Figure 1.7). They also vary in size from 220 to 1600 angstrom [6, 49, 50]. However, the mean volume of endogenous ligands is 318 $Å^3$ (SD: 53 $Å^3$) and is conserved across nuclear receptors[50]. Interestingly, the ligands for nuclear receptors are evolved from the biomarkers for early microorganisms. For instance, okenane which is a derivative of carotenoid, the precursor to retinoic acid, was extracted from sedimentary rocks 1600 million years ago[51]. Thus, nuclear receptor ligands have origins much older than the nuclear receptors themselves. The high diversity of ligands allows for strong selectivity between superfamily of nuclear receptors. However, they differ in sensitivity. Steroids

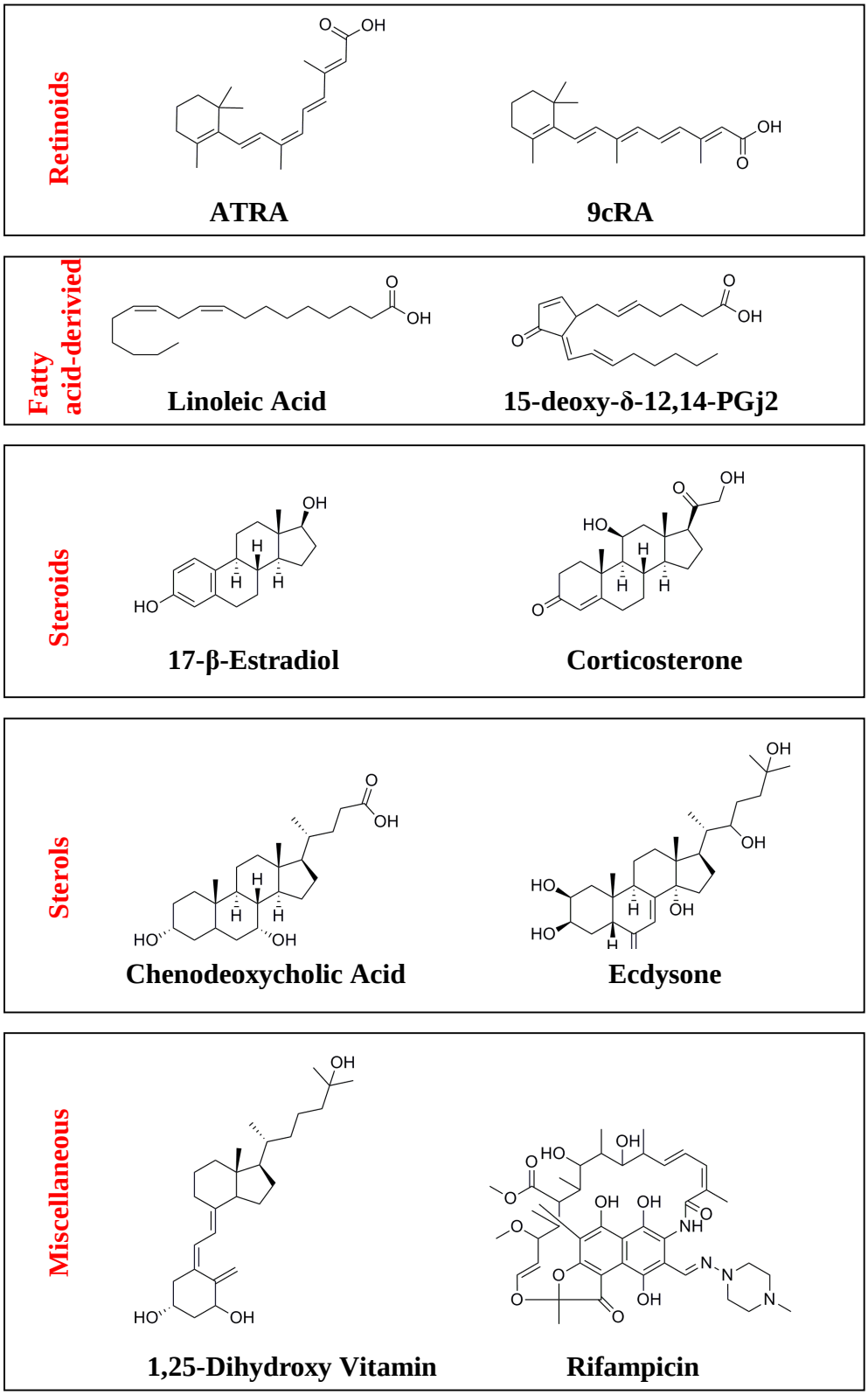

Figure 1.7 Structure of nuclear receptor ligands.

are able to give transcriptional response in nanomolar ligand concentration, but fatty acids need 100,000 times higher concentration than steroids to active PPARγ [5]. Thus, the receptor response is related to the concentration of these ligands in the human body.

Such diversity in shape, size and sensitivity has influence on the kind of response that ligands induce towards nuclear receptors. Based on the kind of transcriptional response, a few classes of ligands can be identified: agonists, inverse agonist, antagonist, partial antagonists, selective nuclear receptor modulators (SERMs) and selective nuclear receptors downregulators (SERDs) [52-54]. These ligand classes differ in influence on the position of the helix 12 and in creating interface with corepressor or coactivators. Understanding the correlation between the ligand structure and its effects on the transcriptional activity is crucial for creating the novel ligands that will induce the specific physiological response.

1.5 Detection of trafficking of nuclear receptors

Nuclear receptors are predominantly located in the nucleus, due to their ability to bind to the specific DNA sites and response elements and to modulate transcriptional response. However, some of nuclear receptors such as ER and GR are located in the nucleus as well as in the cytosol. In the cytoplasm they are complexed with the heat shock protein (HSP) and with the corepressors. As soon as the proper ligand binds the nuclear receptor, the HSP dissociates and the nuclear receptor is translocated from cytoplasm to the nucleus, where coactivator binding allows for the interaction of NR with the response elements and turns on the transcription of the specific gene [55]. Recent finding shows that some nuclear receptors such PPAR are shuttled between the nucleus

and the cytoplasm. This creates questions about trafficking and function of the nuclear receptors outside of the nucleus, especially that many NRs have been found in the membranes and in cellular organelles such us mitochondria [56, 57].

Thus, the nuclear receptor trafficking in the cell has been the subject of studies to understand the mobility of different subfamilies of NR between the cell compartments. To observe trafficking, nuclear receptors in the cell fluorescent marker have been used in previous studies. The most common method is the fusion of green fluorescent protein (GFP) to the nuclear receptor. Previously, this method has been reported successfully to visualize the NR in the cell [58, 59]. However, the bulky GFP protein could be responsible for disrupting interaction of nuclear receptor with coregulatory protein such as coactivators. Therefore, it can influence the mobility of NR in the cell and may not present the actual state of this receptor *in vivo*.

The nuclear receptor can also be visualized using the radiolabeled ligands. Previously, using this method, localization of ERα and TR has been reported [60, 61]. Due to the restrictions on using the radiolabeled compounds as a biosensor, the development of the fluorescent ligand has progressed. Recently NR ligands conjugated with fluorescent dye have been made to allow for the visualization of NRs *in vivo*. However, these conjugated ligands have shown significantly lower binding affinities [62-64].

These recent findings suggest that the development of novel fluorescent ligands is needed to study the nuclear receptor trafficking and to reveal the expression patterns in specific tissues. Such ligands will also aid in gaining detailed understanding of the interactions of NR with other proteins.

1.6 References

1. Gronemeyer, H., J.A. Gustafsson, and V. Laudet, *Principles for modulation of the nuclear receptor superfamily.* Nat Rev Drug Discov, 2004. **3**(11): p. 950-64.

2. Chambon, P., *The nuclear receptor superfamily: a personal retrospect on the first two decades.* Mol Endocrinol, 2005. **19**(6): p. 1418-28.

3. Evans, R.M., *The nuclear receptor superfamily: a rosetta stone for physiology.* Mol Endocrinol, 2005. **19**(6): p. 1429-38.

4. Novac, N. and T. Heinzel, *Nuclear receptors: overview and classification.* Curr Drug Targets Inflamm Allergy, 2004. **3**(4): p. 335-46.

5. Sladek, F.M., *What are nuclear receptor ligands?* Mol Cell Endocrinol, 2011. **334**(1-2): p. 3-13.

6. Benoit, G., M. Malewicz, and T. Perlmann, *Digging deep into the pockets of orphan nuclear receptors: insights from structural studies.* Trends Cell Biol, 2004. **14**(7): p. 369-76.

7. Markov, G.V., et al., *The evolution of the ligand/receptor couple: a long road from comparative endocrinology to comparative genomics.* Mol Cell Endocrinol, 2008. **293**(1-2): p. 5-16.

8. Moore, J.T., J.L. Collins, and K.H. Pearce, *The nuclear receptor superfamily and drug discovery.* ChemMedChem, 2006. **1**(5): p. 504-23.

9. Germain, P., et al., *Overview of nomenclature of nuclear receptors.* Pharmacol Rev, 2006. **58**(4): p. 685-704.

10. Giguere, V., *Orphan nuclear receptors: from gene to function.* Endocr Rev, 1999. **20**(5): p. 689-725.

11. Mukherjee, S. and S. Mani, *Orphan nuclear receptors as targets for drug development.* Pharm Res, 2010. **27**(8): p. 1439-68.

12. Shi, Y., *Orphan nuclear receptors in drug discovery.* Drug Discov Today, 2007. **12**(11-12): p. 440-5.

13. Baker, K.D., et al., *The Drosophila orphan nuclear receptor DHR38 mediates an atypical ecdysteroid signaling pathway.* Cell, 2003. **113**(6): p. 731-42.

14. Folkertsma, S., et al., *The nuclear receptor ligand-binding domain: a family-based structure analysis.* Curr Med Chem, 2005. **12**(9): p. 1001-16.

15. Mangelsdorf, D.J., et al., *The nuclear receptor superfamily: the second decade.* Cell, 1995. **83**(6): p. 835-9.

16. Aci-Seche, S., M. Genest, and N. Garnier, *Ligand entry pathways in the ligand binding domain of PPARgamma receptor.* FEBS Lett, 2011. **585**(16): p. 2599-603.

17. Szanto, A., et al., *Retinoid X receptors: X-ploring their (patho)physiological functions.* Cell Death Differ, 2004. **11 Suppl 2**: p. S126-43.

18. Egea, P.F., A. Mitschler, and D. Moras, *Molecular recognition of agonist ligands by RXRs.* Mol Endocrinol, 2002. **16**(5): p. 987-97.

19. Kliewer, S.A., B. Goodwin, and T.M. Willson, *The nuclear pregnane X receptor: a key regulator of xenobiotic metabolism.* Endocr Rev, 2002. **23**(5): p. 687-702.

20. Lehmann, J.M., et al., *The human orphan nuclear receptor PXR is activated by compounds that regulate CYP3A4 gene expression and cause drug interactions.* J Clin Invest, 1998. **102**(5): p. 1016-23.

21. Sonoda, J., L. Pei, and R.M. Evans, *Nuclear receptors: decoding metabolic disease.* FEBS Lett, 2008. **582**(1): p. 2-9.

22. McDonnell, D.P., E. Vegeto, and M.A. Gleeson, *Nuclear hormone receptors as targets for new drug discovery.* Biotechnology (N Y), 1993. **11**(11): p. 1256-61.

23. Soprano, D.R., P. Qin, and K.J. Soprano, *Retinoic acid receptors and cancers.* Annu Rev Nutr, 2004. **24**: p. 201-21.

24. Feng, J., et al., *Structural variants in the retinoid receptor genes in patients with schizophrenia and other psychiatric diseases.* Am J Med Genet B Neuropsychiatr Genet, 2005. **133B**(1): p. 50-3.

25. Sarachana, T., et al., *Sex hormones in autism: androgens and estrogens differentially and reciprocally regulate RORA, a novel candidate gene for autism.* PLoS One, 2011. **6**(2): p. e17116.

26. Folkertsma, S., et al., *A family-based approach reveals the function of residues in the nuclear receptor ligand-binding domain.* J Mol Biol, 2004. **341**(2): p. 321-35.

27. Greschik, H. and D. Moras, *Structure-activity relationship of nuclear receptor-ligand interactions.* Curr Top Med Chem, 2003. **3**(14): p. 1573-99.

28. Mascrez, B., et al., *Differential contributions of AF-1 and AF-2 activities to the developmental functions of RXR alpha.* Development, 2001. **128**(11): p. 2049-62.

29. Garza, A.S., et al., *Binding-folding induced regulation of AF1 transactivation domain of the glucocorticoid receptor by a cofactor that binds to its DNA binding domain.* PLoS One, 2011. **6**(10): p. e25875.

30. Garza, A.S., N. Ahmad, and R. Kumar, *Role of intrinsically disordered protein regions/domains in transcriptional regulation.* Life Sci, 2009. **84**(7-8): p. 189-93.

31. Rastinejad, F., *Retinoid X receptor and its partners in the nuclear receptor family.* Curr Opin Struct Biol, 2001. **11**(1): p. 33-8.

32. Haelens, A., et al., *The hinge region regulates DNA binding, nuclear translocation, and transactivation of the androgen receptor.* Cancer Res, 2007. **67**(9): p. 4514-23.

33. Melvin, V.S., et al., *The C-terminal extension (CTE) of the nuclear hormone receptor DNA binding domain determines interactions and functional response to the HMGB-1/-2 co-regulatory proteins.* J Biol Chem, 2002. **277**(28): p. 25115-24.

34. Sanchez-Pacheco, A., et al., *Residues K128, 132, and 134 in the thyroid hormone receptor-alpha are essential for receptor acetylation and activity.* Endocrinology, 2009. **150**(11): p. 5143-52.

35. Egea, P.F., B.P. Klaholz, and D. Moras, *Ligand-protein interactions in nuclear receptors of hormones.* FEBS Lett, 2000. **476**(1-2): p. 62-7.

36. Ekins, S., et al., *Challenges predicting ligand-receptor interactions of promiscuous proteins: the nuclear receptor PXR.* PLoS Comput Biol, 2009. **5**(12): p. e1000594.

37. Bourguet, W., et al., *Crystal structure of the ligand-binding domain of the human nuclear receptor RXR-alpha.* Nature, 1995. **375**(6530): p. 377-82.

38. Nagy, L., et al., *Mechanism of corepressor binding and release from nuclear hormone receptors.* Genes Dev, 1999. **13**(24): p. 3209-16.

39. Baniahmad, A., *Nuclear hormone receptor co-repressors.* J Steroid Biochem Mol Biol, 2005. **93**(2-5): p. 89-97.

40. Chandra, V., et al., *Structure of the intact PPAR-gamma-RXR- nuclear receptor complex on DNA.* Nature, 2008. **456**(7220): p. 350-6.

41. Hu, X. and M.A. Lazar, *The CoRNR motif controls the recruitment of corepressors by nuclear hormone receptors.* Nature, 1999. **402**(6757): p. 93-6.

42. Guenther, M.G., O. Barak, and M.A. Lazar, *The SMRT and N-CoR corepressors are activating cofactors for histone deacetylase 3.* Mol Cell Biol, 2001. **21**(18): p. 6091-101.

43. McInerney, E.M., et al., *Determinants of coactivator LXXLL motif specificity in nuclear receptor transcriptional activation.* Genes Dev, 1998. **12**(21): p. 3357-68.

44. Darimont, B.D., et al., *Structure and specificity of nuclear receptor-coactivator interactions.* Genes Dev, 1998. **12**(21): p. 3343-56.

45. Wolf, I.M., et al., *Coactivators and nuclear receptor transactivation.* J Cell Biochem, 2008. **104**(5): p. 1580-6.

46. Estebanez-Perpina, E., et al., *A surface on the androgen receptor that allosterically regulates coactivator binding.* Proc Natl Acad Sci U S A, 2007. **104**(41): p. 16074-9.

47. Nettles, K.W., et al., *Allosteric control of ligand selectivity between estrogen receptors alpha and beta: implications for other nuclear receptors.* Mol Cell, 2004. **13**(3): p. 317-27.

48. Buzon, V., et al., *A conserved surface on the ligand binding domain of nuclear receptors for allosteric control.* Mol Cell Endocrinol, 2012. **348**(2): p. 394-402.

49. Ingraham, H.A. and M.R. Redinbo, *Orphan nuclear receptors adopted by crystallography.* Curr Opin Struct Biol, 2005. **15**(6): p. 708-15.

50. Bogan, A.A., F.E. Cohen, and T.S. Scanlan, *Natural ligands of nuclear receptors have conserved volumes.* Nat Struct Biol, 1998. **5**(8): p. 679-81.

51. Brocks, J.J. and J. Banfield, *Unravelling ancient microbial history with community proteogenomics and lipid geochemistry.* Nat Rev Microbiol, 2009. **7**(8): p. 601-9.

52. Kieser, K.J., et al., *Characterization of the pharmacophore properties of novel selective estrogen receptor downregulators (SERDs).* J Med Chem, 2010. **53**(8): p. 3320-9.

53. Cosman, F. and R. Lindsay, *Selective estrogen receptor modulators: clinical spectrum.* Endocr Rev, 1999. **20**(3): p. 418-34.

54. Nettles, K.W. and G.L. Greene, *Nuclear receptor ligands and cofactor recruitment: is there a coactivator "on deck"?* Mol Cell, 2003. **11**(4): p. 850-1.

55. Kolodkin, A.N., et al., *Design principles of nuclear receptor signaling: how complex networking improves signal transduction.* Mol Syst Biol, 2010. **6**: p. 446.

56. Levin, E.R., *Membrane oestrogen receptor alpha signalling to cell functions.* J Physiol, 2009. **587**(Pt 21): p. 5019-23.

57. Yang, S.H., et al., *Mitochondrial localization of estrogen receptor beta.* Proc Natl Acad Sci U S A, 2004. **101**(12): p. 4130-5.

58. Hager, G.L., et al., *Trafficking of nuclear receptors in living cells.* J Steroid Biochem Mol Biol, 2000. **74**(5): p. 249-54.

59. Georget, V., et al., *Trafficking of androgen receptor mutants fused to green fluorescent protein: a new investigation of partial androgen insensitivity syndrome.* J Clin Endocrinol Metab, 1998. **83**(10): p. 3597-603.

60. Cunha Lima, S.T., et al., *Differential effects of TR ligands on hormone dissociation rates: evidence for multiple ligand entry/exit pathways.* J Steroid Biochem Mol Biol, 2009. **117**(4-5): p. 125-31.

61. Jonson, S.D. and M.J. Welch, *PET imaging of breast cancer with fluorine-18 radiolabeled estrogens and progestins.* Q J Nucl Med, 1998. **42**(1): p. 8-17.

62. Adamczyk, M., R.E. Reddy, and Z. Yu, *Synthesis of a novel fluorescent probe for estrogen receptor.* Bioorg Med Chem Lett, 2002. **12**(9): p. 1283-5.

63. Asai, D., et al., *Direct measure of fluorescence intensity for efficient receptor-binding assay: conjugates of ethinylcarboxyestradiol and 5(and 6)-carboxyfluorescein via alpha, omega-diaminoalkanes as a tracer for estrogen receptor.* J Biochem, 2008. **143**(6): p. 781-92.

64. Rickert, E.L., et al., *Synthesis and characterization of fluorescent 4-hydroxytamoxifen conjugates with unique antiestrogenic properties.* Bioconjug Chem, 2010. **21**(5): p. 903-10.

CHAPTER 2

GREEN FLUORESCENT CHROMOPHORES

2.1 Green Fluorescent Protein (GFP)

The green fluorescent protein (GFP) discovered in 1962 in the jellyfish *Auquorea victoria* is the most well known molecular imaging tool used in chemistry, biology and medicine [1]. However, 30 years after discovery of GFP, first cloning and *in vivo* expression of GFP (fluorescence displayed in bacteria and *C. elegans*) demonstrated that this protein can be used as a marker of gene expression and trafficking of protein in the cell [2, 3]. This finding made GFP one of the most powerful molecular biology tools. Now, GFP is being used as a fluorescent tag that can be fused to N or C terminal part of many proteins without disturbing their native functions (in most of the cases) [4, 5]. It has been shown to be successfully expressed in bacteria, yeast, zebrafish, plants and mammalian cells [6-8].

To date, there are over 200 solved crystal structures of GFP and GFP-like proteins which are fluorescent proteins from other marine organisms and numerous GFP mutants [9]. This large amount of data gave insight into structures and properties of GFP. GFP is composed of 238 residues and is folded into the 11-stranded β-barrel structure with single α helix that is positioned in the center of the barrel (Figure 2.1)[10]. These 11 strands of the sheet create almost symmetrical structure. Thus, the β-barrel constructed seems to create a protective environment for the chromophore which is positioned in the center of the barrel. The chromophore, 4-(p-hydroxybenzylidene)-5-imidazolinone (p-HBI) is formed by an autocatalytic, posttranslational cyclization and oxidation of the polypeptide

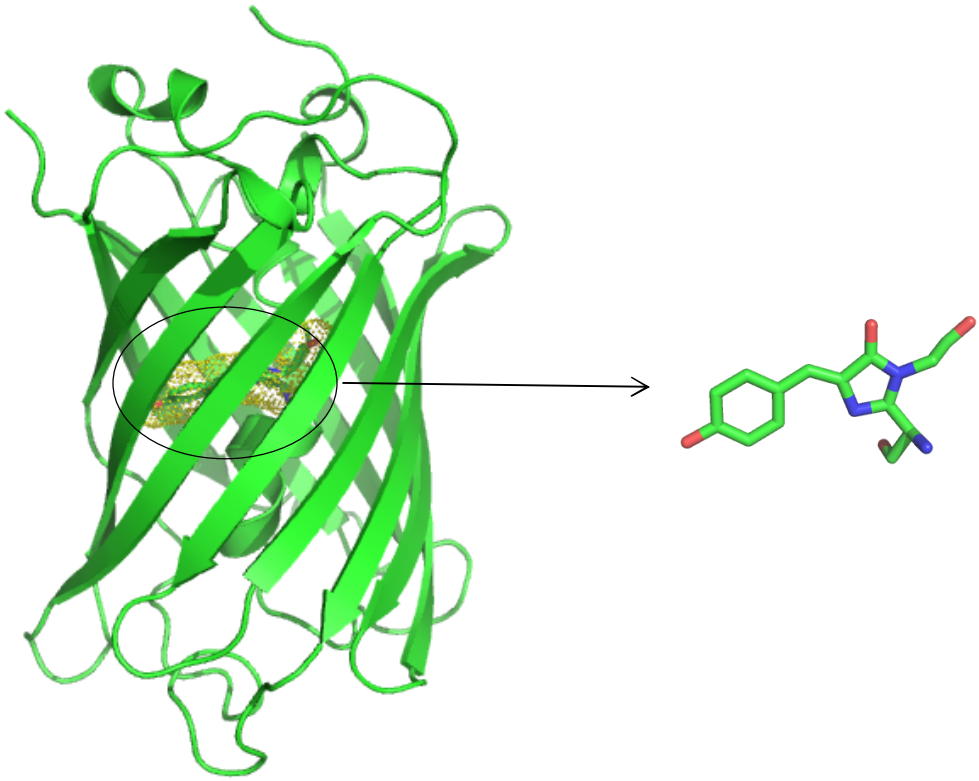

Figure 2.1 Structure of Green Fluorescent Protein (GFP).

backbone, involving Ser-65, Tyr-66 and Gly-67 residues (Figure 2.2) [11]. Chromophore, the component of GFP, which is responsible for the green fluorescence is protected from the solvent by short helices. However, several water molecules have been found also inside the barrel. They are responsible for creating hydrogen bonding network around chromophore which together with other amino acid side chains and hydrophobic contacts is crucial for photochemical properties of GFP [4]. This tightly constructed hydrogen bond network keeps the conjugated rings of chromophore in almost co-planar orientation and does not allow the rings to twist. Chromophore's *cis*-configuration is mainly responsible for the fluorescence of GFP [2].

The wild-type GFP chromophore exhibits two absorption peaks at 398 nm and 477 nm corresponding to the neutral form and the anionic form [12, 13]. The emission peak is at 508 nm. Photochemical properties of GFP change upon denaturation, GFP exhibits absorption maxima at 370 nm and an emission peak at 440 nm with loss of fluorescence quantum yield [12]. Photochemical properties of the protein can also be modified by point mutations. Many mutagenesis studies of GFP have shown that point mutations can change spectral response of chromophore [14, 15]. The change in position 65 from threonine to serine S65T creates GFP variant (eGFP) with enhanced fluorescence with absorption at a single peak of 484 nm and an emission maximum at 507.

Change of the protein microenvironment by introducing specific mutations not only creates enhanced fluorescence of GFP but also can create many fluorescent protein (FP) color variants. Thus, mostly random mutagenesis studies have developed different FP variants with wide range of emission spectra (Figure 2.3). Fluorescent proteins are divided into several classes based upon their emission spectrum. They include the blue

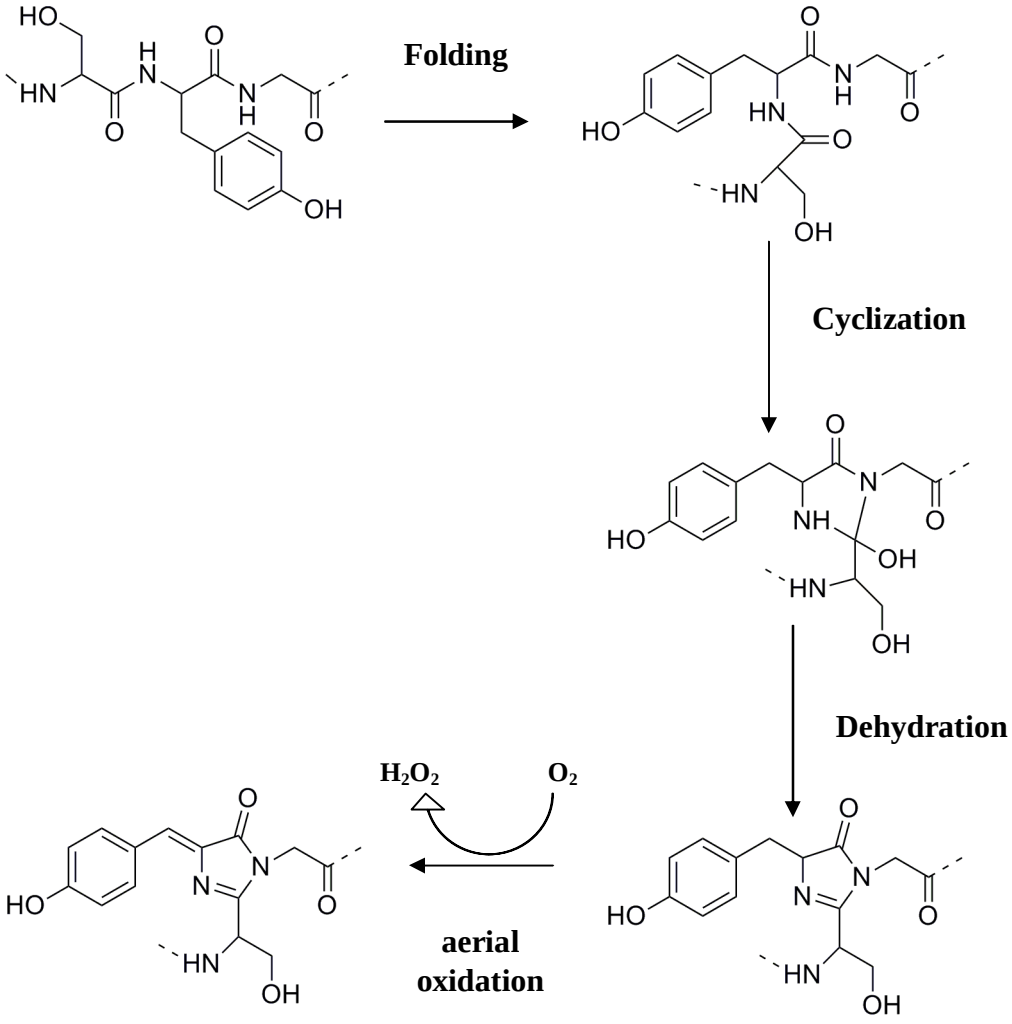

Figure 2.2 Posttranslational modifications leading to chromophore formation in GFP.

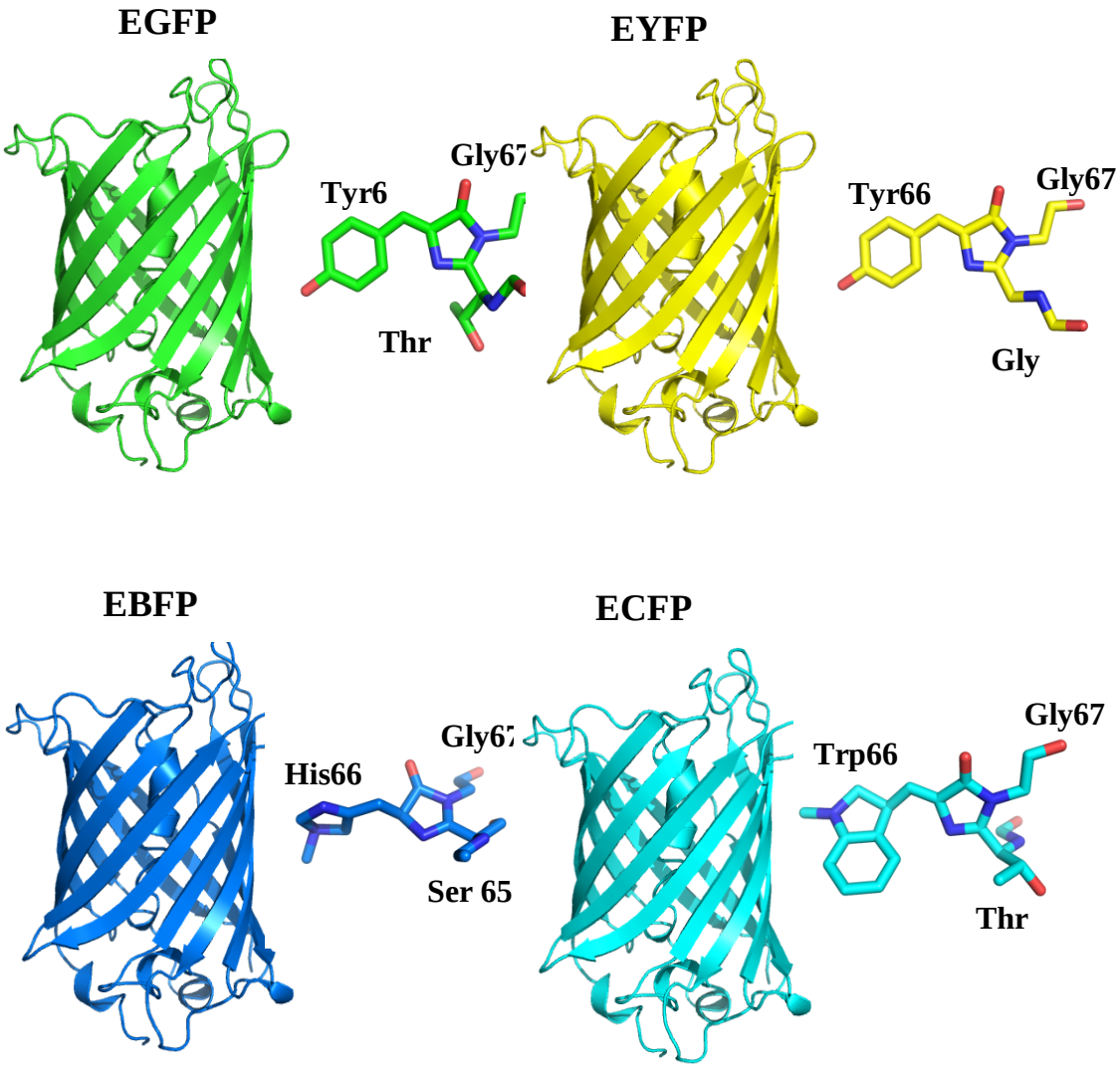

Figure 2.3 Variety of fluorescent proteins exhibiting different spectroscopic properties with their respective chromophores.

BFP with emission spectrum 440–470 nm, cyan CFP (471–500 nm), yellow YFP (521–550 nm), orange OFP (551–575 nm) and red RFP (576–610 nm) [16]. To receive significant change in emission spectrum, the core of chromophore has to be changed by mutagenesis. For instance, in case of BFP, replacement of the tyrosine at position 66 by histidine results in blue shifted emission spectrum, but also causes low fluorescence quantum yield [11].

The GFP and its variants' unique properties have revolutionized the study of cell biology. The number of applications of GFP as a fluorescent probe is growing continuously and brings opportunity to monitor the gene expression, as well as, to study function and localization of many proteins in the cell. However, GFP also has a limitation. GFP fused to the protein does not interact with the natural function of this protein in most of the cases. Some proteins, such as nuclear receptors change conformation upon binding and interact with many regulatory proteins. Thus, a bulky GFP can interfere with the protein and can disrupt the function of the nuclear receptors.

2.2 Synthesis of Arylmethyleneimidazolodinone (AMI)

The derivatives of chromophore have been designed based on arylmethyleneimidazolidinone (AMI). Based on the AMI core structure, a variety of chromophore analogs have been designed, to activate specific nuclear receptors, providing chromophore emission upon binding to the receptor's ligand binding domain (LBD). To achieve specificity of AMIs for particular nuclear receptors, side chains of the core of AMIs (R1 and R2) have been modified to incorporate various molecular

interactions, such as hydrogen bonding and hydrophobic contacts with the various residues in the ligand binding pocket.

Such a large number of AMI derivatives needed not only a quick and reliable synthesis method but also a method that will allow one to synthesize a variety of substituted imidazolinones which can provide efficiency, directness and a diversity of functional groups. Thus, the method developed by Dr. Anthony Baldridge (PhD., Georgia Tech, 2011) was based on the adaptation of methodology proposed previously by Bazureau and Grigg.

Synthesis of AMIs is carried out with three step synthesis (Figure 2.4) [17]. The first part of the synthesis requires production of iminoglycine methyl ester. It is produced from the reaction of ethyl acetimidate hydrochloride with glycine methyl ester hydrochloride. Next, the synthesis of 4-arylideneimidazolin-5-one, the Schiff base, is required. It is synthesized in high yields by condensation of aromatic an aldehydes and a primary amines. This step is significant for the development of AMI derivatives due to functional groups that are carried on both aromatic aldehydes and aliphatic amines. Both of these compounds are commercially available and bring opportunity to generate a variety of AMIs in a fast manner. The last part of the synthesis is 2+3 cycloaddition, which leads to creation of arylideneimidazolinones. In this reaction, the Schiff base provides the aromatic substituent, as well as the amide nitrogen of the imidazolinone, while the other component iminoglycine methyl ester contributes to all other atoms in the imidazolinone ring [17].

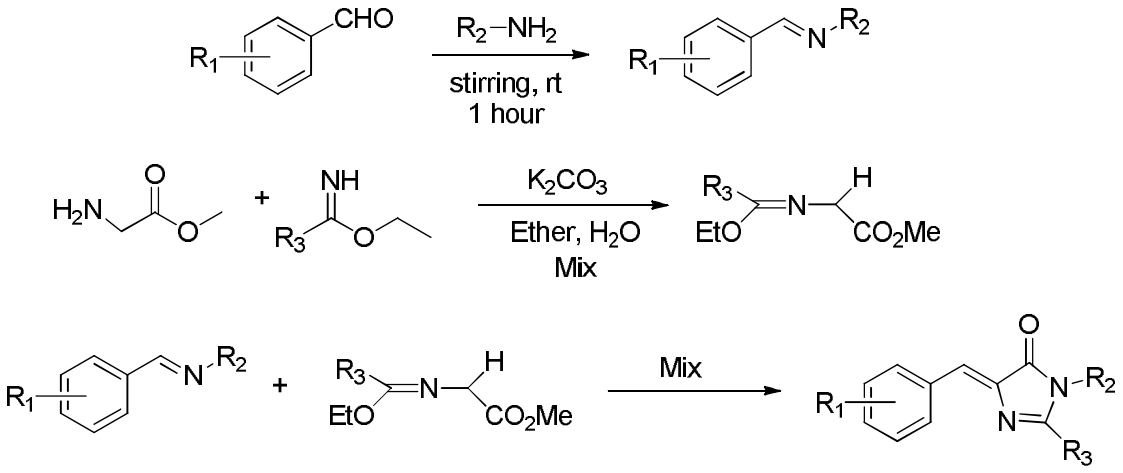

Figure 2.4 Synthetic scheme of the 2+3 cycloaddition.

2.3 Arylmethyleneimidazolidinone (AMI) Chromophore for various Proteins

The AMIs, synthetic compounds derived from the imidazolidinone chromophore of the green fluorescent protein (GFP) from *Aequorea victoria* are known to be weakly fluorescent [4]. The derivatives of AMI developed did not display enhanced fluorescence in the solution. The weak fluorescence is due to vibrational modes of the unbound chromophore. Previously, it has been stated that the high fluorescence of GFP chromophore is a result of the *cis* configuration and co-planar orientation of molecule inside the β-barrel [2]. Lack of the protein host increases conformational freedom of chromophore and results in the weak fluorescence. Thus, replacing the β-barrel with another host protein could increase the fluorescence quantum yield of synthesized AMI. Mimicking the β-barrel by binding the chromophore to the protein could restore fluorescence and open new avenues for synthesized AMIs to provide a very powerful method for protein analysis *in vitro* and *in vivo*. Previously, it has been reported that several AMIs are able to bind to human serum albumin (HSA) and enhanced the emission quantum yield significantly [18]. HSA is a blood plasma protein and is able to bind many different ligands due to its 12 ligand binding pockets. The group of ligands with long alkyl chain displays a significantly higher fluorescence quantum yield in comparison to the other members of the library of AMI derivatives. There is visibly clear correlation between length of the aliphatic chain and the fluorescence. The highest fluorescence quantum yield was displayed in case of hexyl and heptyl chain in comparison to the shorter alkyl chains. These results suggested that increasing hydrophobicity by incorporation of longer alkyl chain results in higher fluorescence level. The hydrophobic pocket of HSA creates a similar environment for AMI that the β-barrel created for the

chromophore. These findings are promising for the other proteins as well. Design and synthesis of AMI derivatives that can specifically bind to the chosen protein brings an opportunity to create fluorescent ligands for various proteins. These ligands differ from other known fluorescent molecules that display fluorescence only upon binding. Thus, they can be used as potential fluorescent probes for studying the mobility and trafficking of specific proteins in the cell.

2.4 References

1. Morin, J.G. and J.W. Hastings, *Energy transfer in a bioluminescent system.* J Cell Physiol, 1971. **77**(3): p. 313-8.

2. Sample, V., R.H. Newman, and J. Zhang, *The structure and function of fluorescent proteins.* Chem Soc Rev, 2009. **38**(10): p. 2852-64.

3. Prasher, D.C., et al., *Primary structure of the Aequorea victoria green-fluorescent protein.* Gene, 1992. **111**(2): p. 229-33.

4. Zimmer, M., *Green fluorescent protein (GFP): applications, structure, and related photophysical behavior.* Chem Rev, 2002. **102**(3): p. 759-81.

5. De Giorgi, F., et al., *Targeting aequorin and green fluorescent protein to intracellular organelles.* Gene, 1996. **173**(1 Spec No): p. 113-7.

6. Chalfie, M., et al., *Green fluorescent protein as a marker for gene expression.* Science, 1994. **263**(5148): p. 802-5.

7. Kahana, J.A., B.J. Schnapp, and P.A. Silver, *Kinetics of spindle pole body separation in budding yeast.* Proc Natl Acad Sci U S A, 1995. **92**(21): p. 9707-11.

8. Wang, S. and T. Hazelrigg, *Implications for bcd mRNA localization from spatial distribution of exu protein in Drosophila oogenesis.* Nature, 1994. **369**(6479): p. 400-03.

9. Ong, W.J., et al., *Function and structure of GFP-like proteins in the protein data bank.* Mol Biosyst, 2011. **7**(4): p. 984-92.

10. Yang, F., L.G. Moss, and G.N. Phillips, Jr., *The molecular structure of green fluorescent protein.* Nat Biotechnol, 1996. **14**(10): p. 1246-51.

11. Tsien, R.Y., *The green fluorescent protein.* Annu Rev Biochem, 1998. **67**: p. 509-44.

12. Bell, A.F., et al., *Probing the ground state structure of the green fluorescent protein chromophore using Raman spectroscopy.* Biochemistry, 2000. **39**(15): p. 4423-31.

13. Rajput, J., et al., *Photoabsorption studies of neutral green fluorescent protein model chromophores in vacuo.* Phys Chem Chem Phys, 2009. **11**(43): p. 9996-10002.

14. Brejc, K., et al., *Structural basis for dual excitation and photoisomerization of the Aequorea victoria green fluorescent protein.* Proc Natl Acad Sci U S A, 1997. **94**(6): p. 2306-11.

15. Jung, G., J. Wiehler, and A. Zumbusch, *The photophysics of green fluorescent protein: influence of the key amino acids at positions 65, 203, and 222.* Biophys J, 2005. **88**(3): p. 1932-47.

16. Pakhomov, A.A. and V.I. Martynov, *GFP family: structural insights into spectral tuning.* Chem Biol, 2008. **15**(8): p. 755-64.

17. Baldridge, A., et al., *Activation of fluorescent protein chromophores by encapsulation.* J Am Chem Soc, 2010. **132**(5): p. 1498-9.

18. Baldridge, A., et al., *Recapture of GFP chromophore fluorescence in a protein host.* ACS Comb Sci, 2011. **13**(3): p. 214-7.

CHAPTER 3

FLUOROPHORES AS LIGANDS FOR THE HUMAN ESTROGEN RECEPTOR ALPHA

3.1 Human Estrogen Receptor alpha

The estrogen receptor (ER) is a member of the NR superfamily and was among the first NRs identified [1]. Estrogen receptors which include two main subtypes, ERα and ERβ, play crucial roles in human body, such as differentiation and proliferation. The wide distribution of ERs in various human tissues, including bone, uterus, breast and brain, along with their significant role in gene expression, implicates this receptor in a number of diseases, including breast cancer, osteoporosis, cardiovascular diseases, multiple sclerosis and Alzheimer's disease [2-8]. Despite their similarity, both isotypes, ERα and ERβ, have different tissue distributions, ERα is prominently present in breast and uterus and ERβ is expresses highly in the prostate, salivary glands, testis, ovary and smooth muscles.

Endogenous estrogens, i.e., 17β-estradiol and its derivatives, are natural ligands for both isotypes [9]. 17 β-estradiol (E2) has higher affinity to ERα than ERβ (EC_{50} 0.018 and 0.039 nM, respectively) but ERβ is activated preferentially by phytoestrogens such as Genestein [10]. The differences in ligand preferences are in part due to different tissue distributions, but are also due to slight structural differences observed among the two isotypes, seen predominantly in the ligand binding domain [11]. ERα and ER β have about 58% sequence identity on an amino acid level in their LBD with only two amino acids differences in the ligand binding pocket [12].

Estradiol

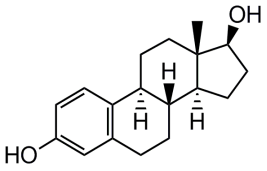

Bisphenol

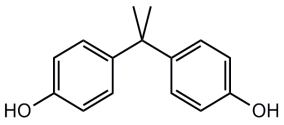

Resveratrol

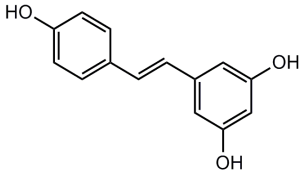

PPT

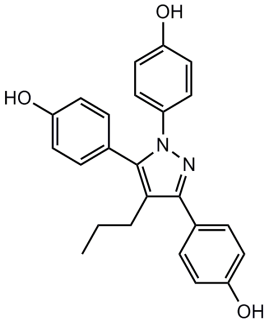

MPP

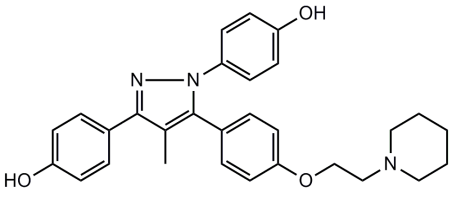

Tamoxifen

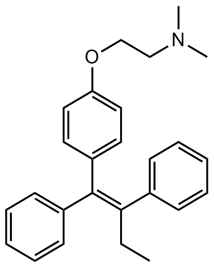

Figure 3.1 Various ligands for Estrogen Receptor α

ERα contains M421 and L384 which in ERβ corresponds to I373 and M336, respectively [13].

The most extensively studied estrogen receptor, ERα, binds a wide range of ligands such as bisphenol and resveratrol that activate ERα as well as tamoxifen, propylpyrazole triol (PTT) and methyl-piperidino-pyrazole (MPP) which act as selective estrogen receptor modulators (SERMs) activating ERα only in specific tissues due to availability of specific coactivators (Figure 3.1) [14-17]. However, many of the ERα ligands are derivatives of the ABCD steroidal ring system based on ERα natural ligand, 17β-estradiol. Recently, ligands with deconstructed ABCD ring system with A-CD ring have also been reported. Thus, large range of compounds which selectively activate ERα in different tissue, make challenge for developing novel ligands for ERα, and understanding structure - activation relationship is essential.

The ligand binding pocket (LBP) of the LBD of the ERalpha contributes to the selectivity and function of this receptor. The LBP formed by helices 3, 7 and 12, comprising a pocket with a volume of 450 $Å^3$, double the of volume of the 17β-estradiol ligand itself (Figure 3.2) [18]. In the binding of ERα ligand with a high affinity, involves primarily hydrophobic interactions, as well as polar contacts created by two hydroxyl groups 11 Å apart. Extensive mutagenesis studies of ERα showed importance of many other residues in contact with ligand, including essential hydrophobic amino acids which interact with hydrophobic core of ERα pharmacophore [18-20]. Thus it has essential role for ligand selectivity and sensitivity. One of them, the phenolic hydroxyl of the A ring in the ABCD steroidal ring system creates a hydrogen bond with two residues, glutamine

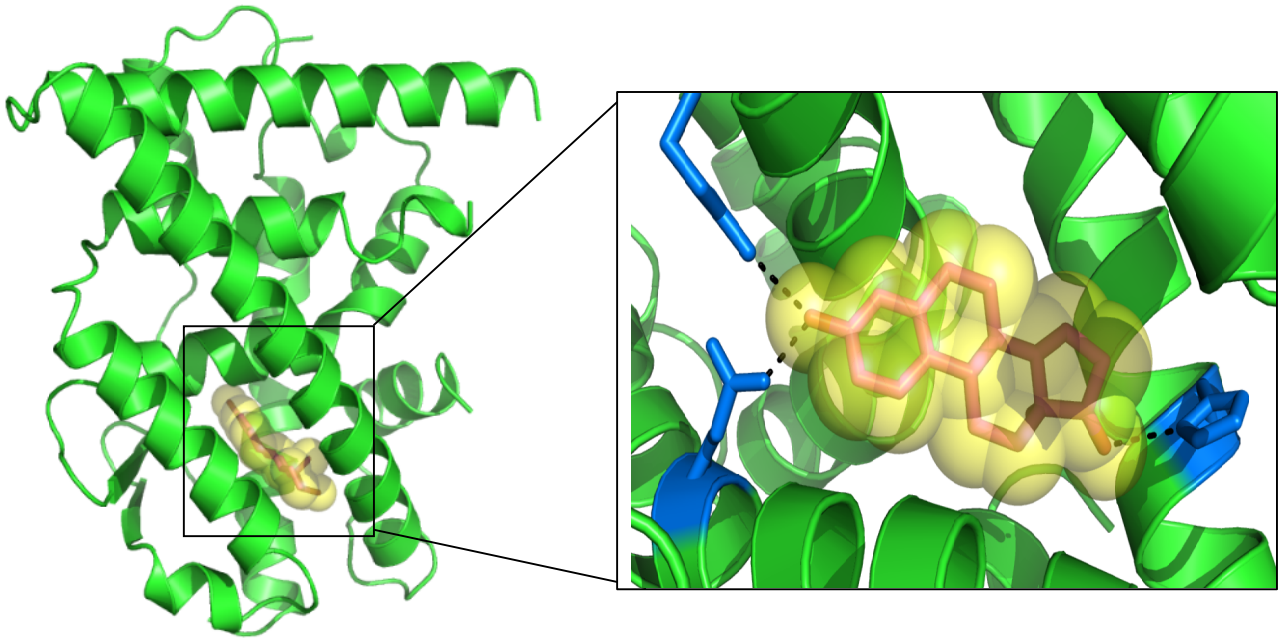

Figure 3.2 Crystal structure of the LBD of hERα with estradiol. The ligand is shown in red.

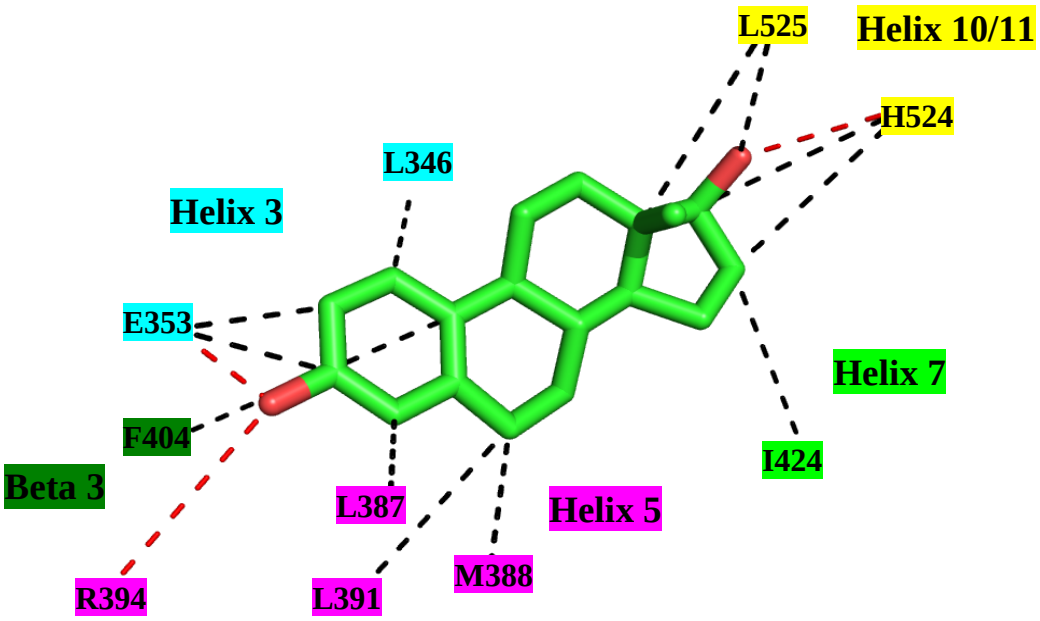

Figure 3.3 ERα ligand binding pocket. The ligand, 17β-estradiol, is shown in green and the residues in the ligand binding pocket of ERα are colored by their corresponding helix.

353 (E353) and arginine 436 (R346) as well as a water molecule. The other hydroxyl group is the 17β-hydroxyl group in the D ring of the steroidal hormone, which hydrogen bonds to histidine 524 (H524) [18]. However, this hydrogen bond contributes far less towards the affinity of the ligand for the pocket [9].

As most NRs, the ER α undergoes conformation change by binding to an agonist. Thus, recruitment of RNA polymerase eventually occurs through the interaction between the LBD and coactivator proteins which are involved in mediating those interactions. The estrogen receptors are known to interact with a number of coactivator proteins, such as p160 steroid receptor coactivator (SRC) family of coactivators, primarily SRC-1, -2, and –3 are required [21]. These coactivators interact with ERα LBD by coactivator binding site, known as LXXXLL NR box (L is leucine and X is any amino acid) created on the surface by active conformation of helix 12 [22]. However, this binding site is available for activator only in case of agonist binding. In case of antagonist, helix 12 does not display active conformation to enable in recruitment of coactivator.

3.2 hERα as a Drug Target for Discovery of Fluorescent Probes

As previously mentioned, the wide distribution of ERα in various human tissues implicates this receptor in a large number of diseases, including breast cancer, osteoporosis and cardiovascular diseases. To date, tamoxifen, the most widely used drug to treat breast cancer, is an ERα antagonist [23, 24]. Due to the success of this molecule and others which have served as antagonists to this receptor, and also play a critical role as chemotherapeutic agents, a keen interest lies in developing novel ligands for ERα, as well as other NRs, that could serve as potential drugs for a number of NR-related

diseases. Furthermore, some highly successful drugs, like tamoxifen, which are used in the treatment of the ER- positive breast cancer, face the issue of cells developing resistance, as noted in 40% of patients [25]. Thus identification of a novel class of small molecules as potential agonists or antagonists is a key step in developing new drugs that will enhance therapy for ER related diseases, and addressing the issue of resistance.

In addition to drug discovery, understanding the mobility patterns of the receptor *in vivo* can lead to early detection of several diseases, such as breast cancer. As with most of the steroidal subclass of nuclear receptors, ERα is translocated to the nucleus upon binding to a ligand. Thus estrogen receptor is prominently localized in nucleus [26]. However, recent studies showed the presence of ERα in cytoplasm, the function of which is unknown and others have reported a localization of ERα in the cell membrane [27]. These ERs localized outside of the nucleus interact with many cell signaling molecules and other factors such as epidermal growth factor receptor (EGFR) that it is known to play a role in tamoxifen resistance by phosphorylation of ERα [25, 28, 29]. However, a significant amount of work needs to be accomplished to understand ERα trafficking in cells and its role in nuclear and non-nuclear signaling. This could perhaps shed some light in early patterns of several nuclear receptor based diseases.

In recent years, the development of fluorescent probes has helped visualize the localization and trafficking of NRs inside cells. In particular, the use of the green fluorescent protein (GFP) from *Aequorea victoria* fused to specific nuclear receptors has provided a powerful method for detecting both function and mobility of NRs *in vivo* [30]. A disadvantage to fusion proteins with respect to NRs and to their LBD is the potential interference of a bulky fusion protein with coactivator proteins essential for

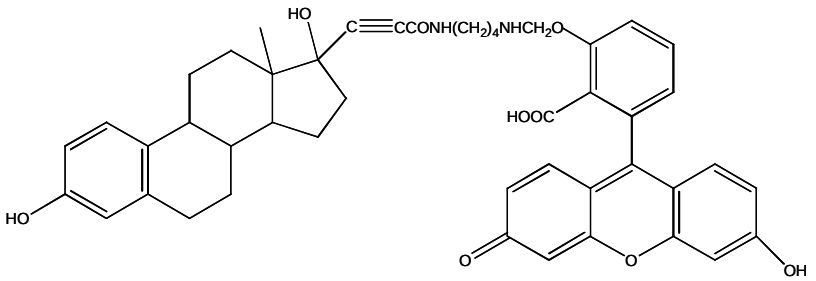

E2(4)cF

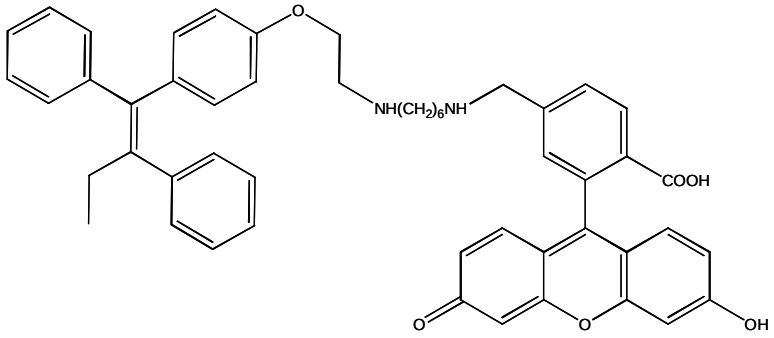

OHT-6C

Figure 3.4 The structures of fluorescent ligands for ERα.

transcriptional regulation. The presence of a bulky protein could hinder the conformational change or interface with surface protein – protein interactions necessary for the natural function of these receptors. More recently, studies have described various molecules that consist of a conjugate of the ligand and the fluorescent dye for ERα. In most cases the fluorescent conjugates are attached to well-known ERα ligands such as 17-β-estradiol (E2) or tamoxifen (Figure 3.4) [31-33]. However, the bulkiness of these conjugates decreases the affinity of these molecules for the receptor decreasing their potential as drugs due to their limited activation profile [34]. Thus, despite their visualization properties, these compounds are unable to serve as potential ligands for these receptors.

Thus, the characterization and development of potentially fluorescent small molecule ligands instead of the bulky GFP fusion protein or small molecule conjugates serves a two-fold advantage. Not only would these small molecules potentially serve as a new class of ligands for these receptors with activation profiles similar to other known ligands for these receptors, but the fluorescence capability of these small molecules would eliminate the bulkiness of a fusion protein that could distract the natural function of these proteins.

3.3 Fluorescent Protein Chromophore Design and Molecular Modeling for hERα

The ERα selective FP chromophores were rationally designed using the arylmethyleneimidazolidinone (AMI) core to resemble the ABCD ring system of steroids (Figure 3.5). As mentioned previously, most of the estrogen selective ligands are based on the classic steroid ring system. However, most of these compounds induce side effects

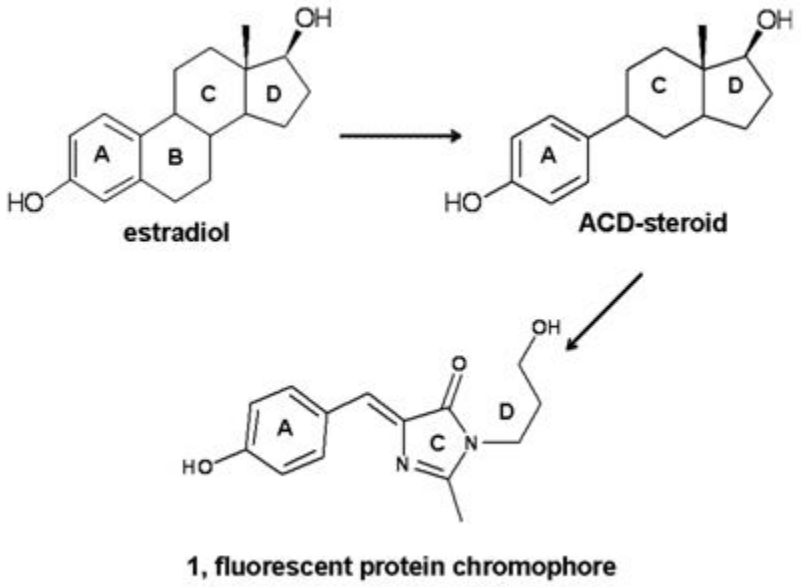

Figure 3.5 Creating chromophores for Estrogen Receptor α.

involving the increase of the risk cancer or vascular problems. Thus, development compounds with removed B – ring from ABCD steroid structures brought new avenue for novel selective ERα ligands. These compounds have shown to bind to receptor with similar affinity as estradiol. The A-CD ring system compounds could prevent formation of undesirable metabolites, ortho-quinones, which are linked to estrogen-related carcinogenicity [35, 36]. In addition removal of B-ring increases the compound flexibility.

By analyzing the base AMI structure, a resemblance was noted to the ACD core structure of several ER ligands. Thus, ER selective AMIs were designed to not incorporate at a B ring, by analogy to other known estrogen receptor agonists incorporating only the A-CD ring system [35, 37]. In analyzing the AMI core, a phenolic aryl group was retained to play a role analogous to the functionalized ring A of the steroid molecule and create crucial contacts with E353. The obligatory imidazolidinone group in the AMI structure was designed to mimic the C ring of a steroid molecule, and alkyl substituents around the heterocycle (R1) were employed to mimic for the absent steroidal D ring. A series of such derivatives was designed based on this core structure, with the addition of substituents to create potential ligands for ERα. The ability of the designed chromophores to mimic the overall interaction of the heterocyclic core of various ERα ligands was determined via molecular modeling. AMI 4 was docked into the crystal structure of the ERα ligand binding domain (1ERE) using AutoDock Vina, the software which predict of fit and interactions of small molecules with binding site of the protein [38]. It samples of different conformations of ligand in rigid binding site of receptor and scores them based on its algorithm function. Thus docked AMI was

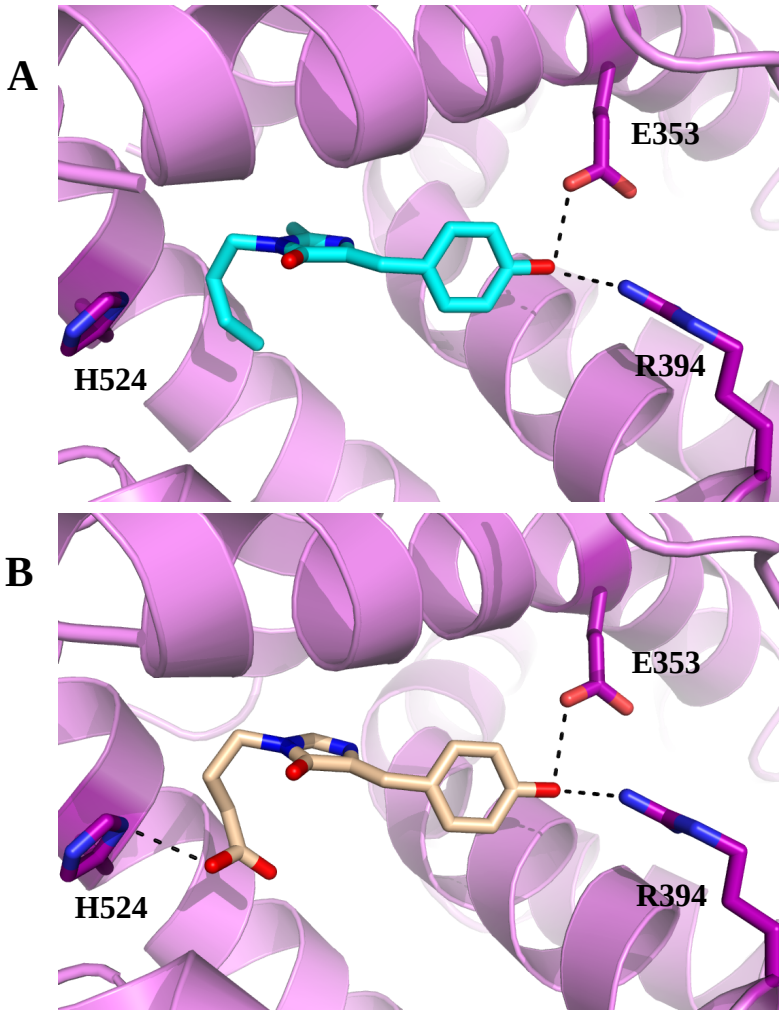

Figure 3.6 Structures of the AMIs ligands docked into the crystal structure of hERα (pdb:1ERE) using the software Autodock Vina. A) 4, B) 1

overlayed with crystal structure of estradiol and showed binding to ERα with favorable superimposition with estradiol. In addition, modeling showed that the phenolic group, superimposed on the A ring of estradiol (E2), created an analogous hydrogen bond with glutamate E353 and arginine R394 (Figure 3.6A), analogous to estradiol. It has been shown that these interactions are crucial for binding and activation of estrogen receptor by most of ligands. However, the same calculations failed to overlay the imidazolidinone ring of the AMI compound with the C ring of estradiol. This is probably due to free rotation between the phenyl and the imidazolindinone ring, which is crucial for the fluorescence of these AMIs, as previously reported [39, 40]. Based on the docking results and examination of known structures with ERα agonists, additional compounds were designed with potential hydrogen bonding between the ligand and the histidine at 524 (H524). Histidine H524 is known to form a hydrogen bond with the 17-β hydroxyl group on the D-ring of E2 (Figure 3.6B) [18]. From this, addition of a polar group such as the hydroxyl group as in compound 3 or a carboxyl group in compound 1 and 2 could provide the additional hydrogen bond, based on the *in silico* modeling results, increasing the probability of ligand binding and activation.

Despite the advantages of molecular modeling as a tool for visualizing protein-ligand interactions, such calculations are limited in elucidating the importance of specific substituents. Therefore, additional AMI molecules with various substituents were designed, synthesized, and tested based on chemical properties, such as hydrogen bonding and hydrophobicity, as well as shape and volume of these potential ligands (Table 3.1). The various activation profiles could indicate a correlation between the structures of moieties and ligand binding with ERα.

Table 3.1 Structures of AMIs

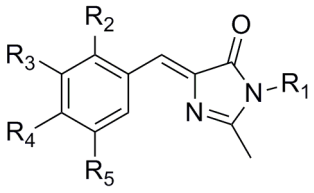

AMI	R_1	R_2	R_3	R_4	R_5
1	$C_3H_6CO_2H$	H	H	OH	H
2	$C_5H_{10}CO_2H$	H	H	OH	H
3	C_3H_6OH	H	H	OH	H
4	C_3H_7	H	H	OH	H
5	$C_3H_6CO_2H$	H	H	H	H
6	CH_3	H	H	CH_3	H
7	CH_3	H	H	H	H
8	CH_3	H	CH_3	OH	CH_3
9	CH_3	H	H	$N(Me)_2$	H
10	C_5H_{11}	OH	H	$N(Me)_2$	H

3.4 Evaluating Fluorogens via Chemical Complementation

Genetic selection system is powerful tool for protein engineering and drug discovery due to the possibility of evaluation the protein – small molecules interactions. Chemical complementation as genetic selection system in yeast is fast and feasible powerful tool for detection interactions between nuclear receptor and small molecules, ligands.

Chemical complementation is a semi high-throughput selection, where the survival of an engineered yeast (*Saccharomyces cerevisiae*) strain, PJ69-4A, is linked to the ability of a small molecule ligand to activate a nuclear receptor [41-43]. PJ69-4A contains Gal4 response elements (Gal4RE) controlling expression of the genetic selection genes, *HIS3* and *ADE2*, involved in the histidine and adenine biosynthetic pathway, respectively. Two fusion proteins consisting of the Gal4 DNA binding domain (GBD) fused to the ERα LBD (GBD: ERα LBD) is transformed into yeast along with the fusion protein of the NR coactivator fused to Gal4 activation domain (GAD). Upon ligand binding to the ERα LBD, the GBD: ERα LBD fusion binds to Gal4RE, recruiting the coactivator, the GAD fusion protein. Thus the GAD serves to recruit the yeast transcriptional machinery required to initiate transcription of the selection gene (*ADE2* or *HIS3*) [42]. Activation of the selection gene, such as the *HIS3* gene, enables the yeast strain to grow on media lacking histidine in the presence of the ligand (Figure 3.7). Thus, the survival of the yeast depends on the presence of the small ligand molecules.

Ten synthetic AMI ligands (Table 3) were tested in chemical complementation. The growth of the yeast strain PJ69-4A expressing fusion proteins GBD: ERαLBD and

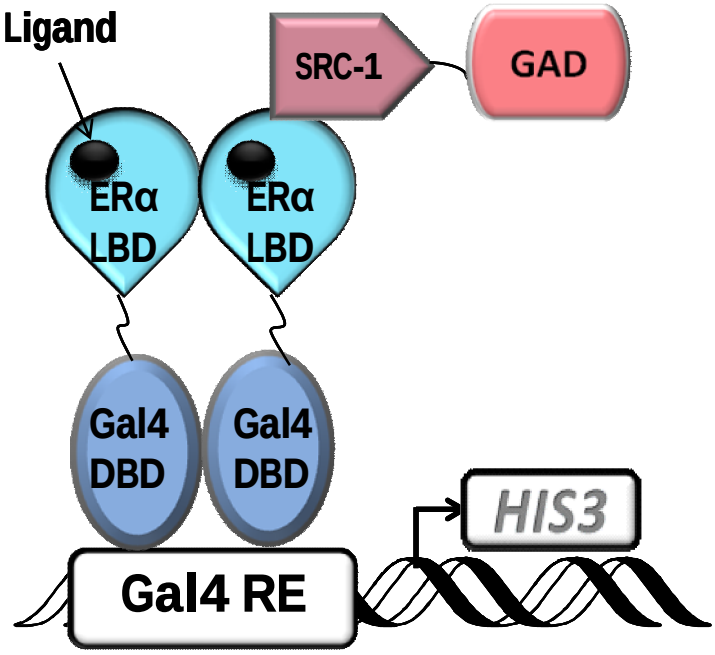

Figure 3.7 Scheme of chemical complementation assay.

SRC-1: GAD was observed in histidine selective media at (SC-HLW with 1 mM 3AT), containing 10 μM of AMI, and 3-amino-1,2,4-triazole (3AT), an inhibitor of imidazoleglycerol-phosphate dehydratase was added to reduce basal expression observed due to "leaky" *HIS3* gene [44]. As shown in Figure 3.8, yeast expressing Gal4 ligand independent factor displayed growth as expected. As a positive control, yeast expressing ERα, were incubated with 17-β estradiol (E2). As shown in Figure 3.8, ligand activated growth was observed with E2 and Gal4 as expected. AMI 1 and 2 also showed slight ligand activated growth (two-fold activation based on growth) and low sensitivity (EC_{50} >10μM) with ERα. However, most of the tested ligands did not induce growth in yeast, indicating that the ligand was unable to bind and activate the receptor, allowing the yeast to survive. This data indicated that designed AMI is able to bind and activate slightly ERα in yeast.

3.5 hERα activation by fluorogens in mammalian cells

To determine whether a similar trend in activation seen in yeast is observed in mammalian cells, the fluorogens were analyzed for activation and fluorescence in human embryonic kidney 293T cells (HEK293T). The Gal4 DNA binding domain fused to the ERα ligand binding domain (GBD: ERαLBD) was cloned into a mammalian expression vector (pCMX) containing a cytomegalovirus (CMV) promoter. Using a luciferase reporter gene assay, HEK293T cells were co-transfected with a reporter plasmid containing the Renilla luciferase gene under the control of Gal4 response elements. Cells were transfected with the two plasmids and various chromophores were added and tested

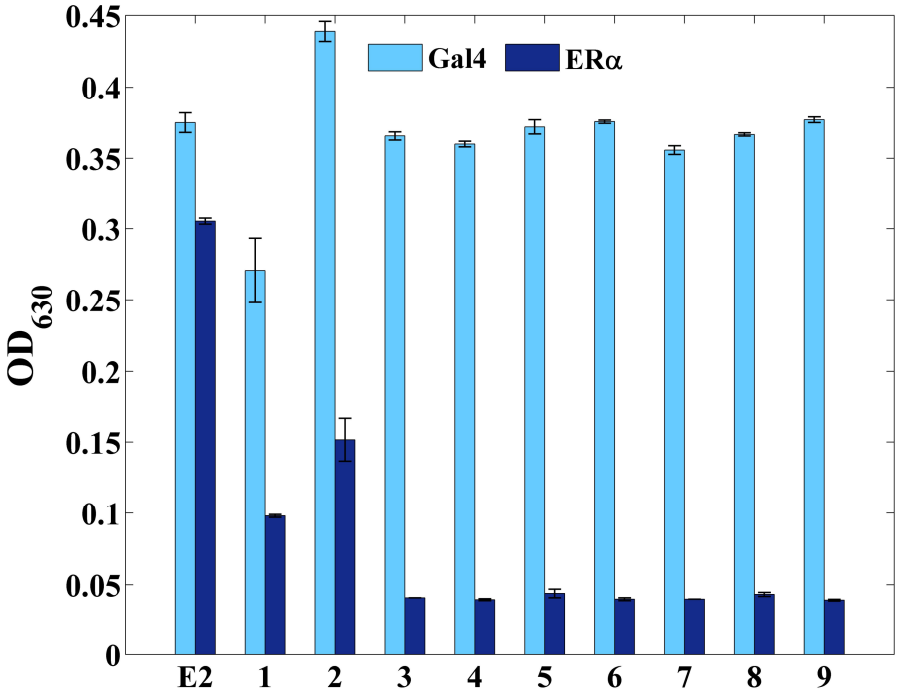

Figure 3.8 Chemical complementation in yeast. Results of chemical complementation in histidine selective media (-HLW) with 1mM 3-AT. The ligand concentration of 10 μM was used. Gal4 is a ligand independent transcription factor and is used as a positive control. ERα with estradiol (E2) is also used as a positive control.

for luciferase activity at concentration of 10 μM. Luciferase activity is an indicator of binding and activation of nuclear receptor by small molecule.

To evaluate interaction of AMIs with ERα in mammalian cells, library of synthesized AMIs was tested for ERα activation. Cells expressing receptor were incubated with 10 μM of a library of 46 AMIs and tested for luciferase activity. As a control, the receptor was tested with the E2 ligand, and as expected, ERα was activated by E2. As shown in Figure 3.9, AMI 1 and 2 activated ERα displaying 6-fold activation. However, there are few compounds, AMI 4, 49, 94 and 97 and 108 which activated ERα with 5 fold activation, in comparison to the 14-fold activation with E2. However, based on the previous results achieved in yeast, our studies were focused on AMI 1 and 2 and its derivatives.

The ten synthetic AMI chromophores were tested with ERα at a concentration of 10 μM or in the absence of ligand. The highest activation was observed with chromophores 1-4, 8 and 9 displaying an approximately 10-fold activation as shown in Figure 3.10A, in comparison to the 21-fold activation observed with E2. To determine the EC_{50} values of these compounds, a dose response curve was generated for each compound. As seen in Figure 3.10B, compounds 4, 8 and 9 showed the highest sensitivity with an EC_{50} of 3 μM whereas compounds 2, 3 and 4 displayed $EC_{50} > 3$ μM. Compounds 5, 6 and 7 showed no activation. Despite the fact that these compounds had a higher EC_{50} value and lower activation in comparison to ERα and estradiol (873 pM), compounds 4, 8 and 9 showed promise as starting points for a potentially a new class of ERα agonists.

A

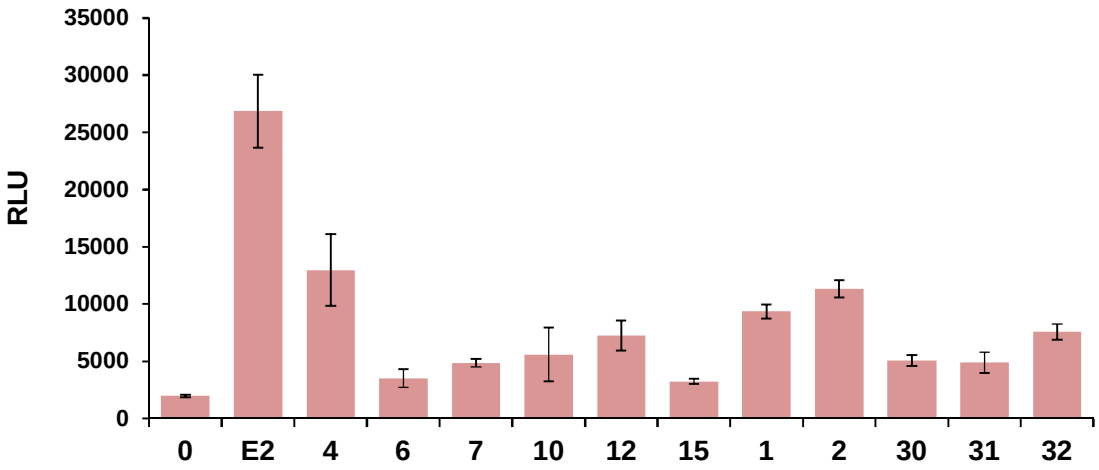

B

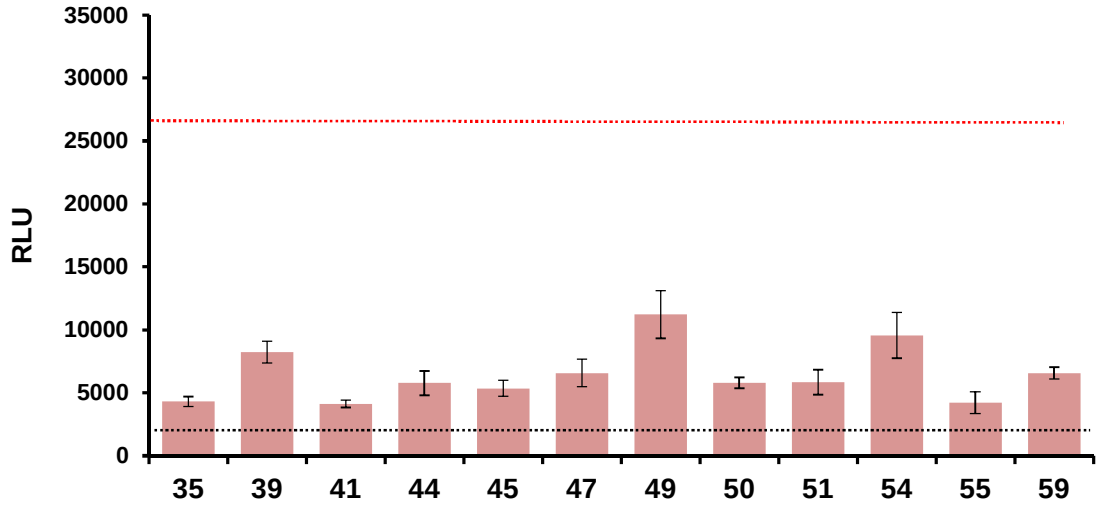

Figure 3.9 Activation profile of AMIs in ERα. Part I. ERα (GBD: ERαLBD) was transfected into HEK298T cells with p17*4TATALuc plasmid, a luciferase reporter gene under the control of Gal4 response elements and were incubated with 10 μM of ligand. Red line indicates the E2 activation level. Structures of all above the ligands are included in appendix.

A

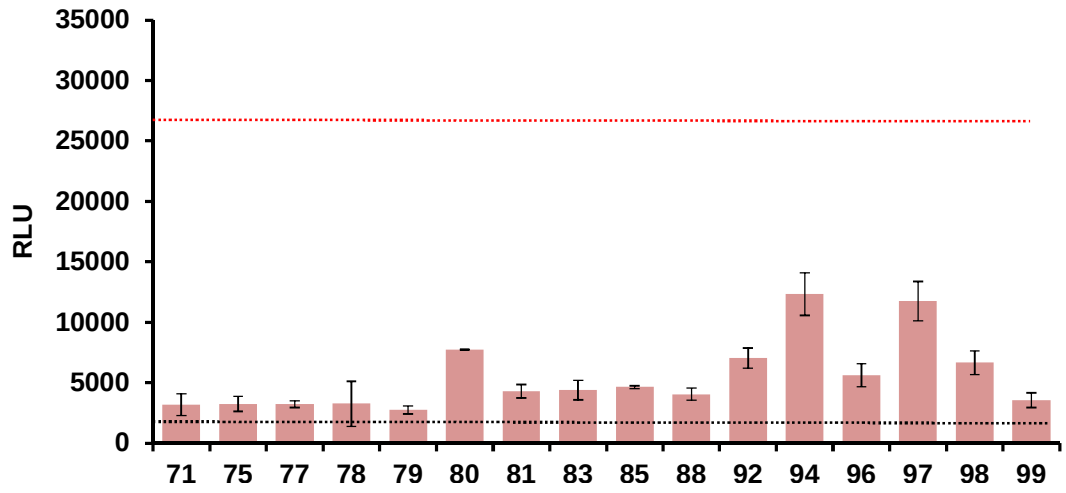

B

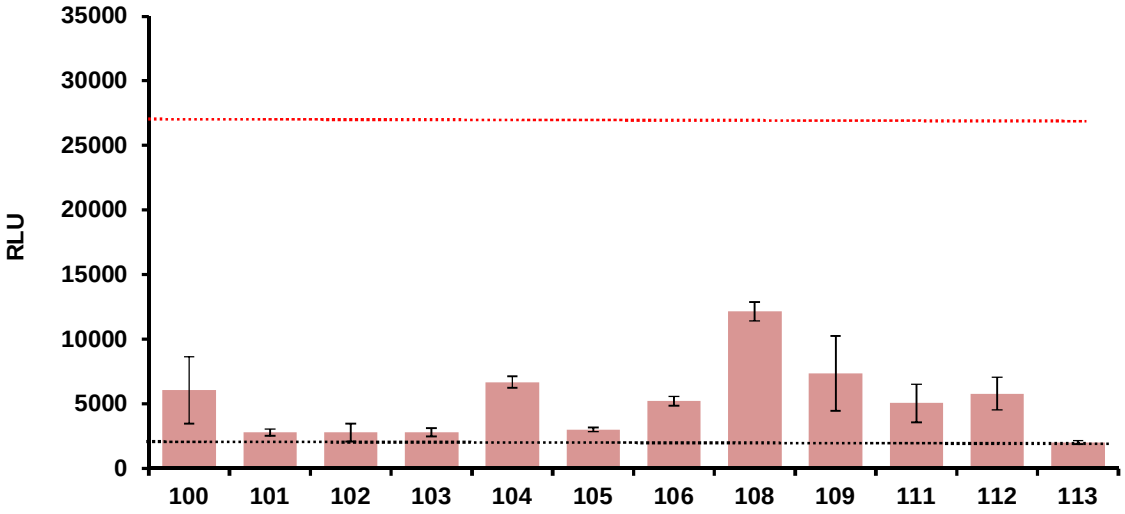

Figure 3.9 Activation profile of AMIs in ERα. Part II. ERα (GBD:ERαLBD) was transfected into HEK298T cells with p17*4TATALuc plasmid, a luciferase reporter gene under the control of Gal4 response elements and were incubated with 10 μM of ligand. Red line indicates the E2 activation level. Structure of all above ligands is included in appendix.

These results confirm initial hypothesis, based on molecular modeling, that a key moiety for binding of ERα LBD is the hydroxyl group of the phenyl ring of AMI, which could potentially form a hydrogen bond with E353 and R394. Compounds 5, 6 and 7, lacking a hydroxyl group at that position, did not display activation of the estrogen receptor. The importance of creating polar contacts with H524 has also been taken into account. Thus, the chromophores must include a substituent R_1 on the imidazolidinone ring. Hydrogen-bonding moieties on the alkyl group can potentially lead to an interaction with H524. However, such polar groups do not seem essential for activation. This is evident with 8, lacking this group, which displays the same sensitivity as 1 containing a carboxyl group at this position. This substitution activity is noted for 3 with a hydroxyl group and 1 and 2 with carboxyl groups, which show the same degree of activation. A main feature of chromophore design is that the length of the alkyl group has little influence on sensitivity. Chromophore 1, which lacks two carbons in the alkyl chain compared to 2, has only slightly higher activation than 2. Another factor that might contribute to increased sensitivity to ERα is the presence of substituents in positions R_3 and R_5. Conversely, with methyl groups in these positions, 8 shows higher sensitivity, similar to that of 1. These groups can possibly play a role in hydrophobic interactions with non-polar residues in the binding pocket. In addition, substitutions at these positions may reduce the flexibility between the phenyl and imidazolindinone rings that can lead to a more planar conformation of the chromophore, similar to the enforced conformation of estradiol and similar to the conditions found within the restrictive β-barrel of GFP.

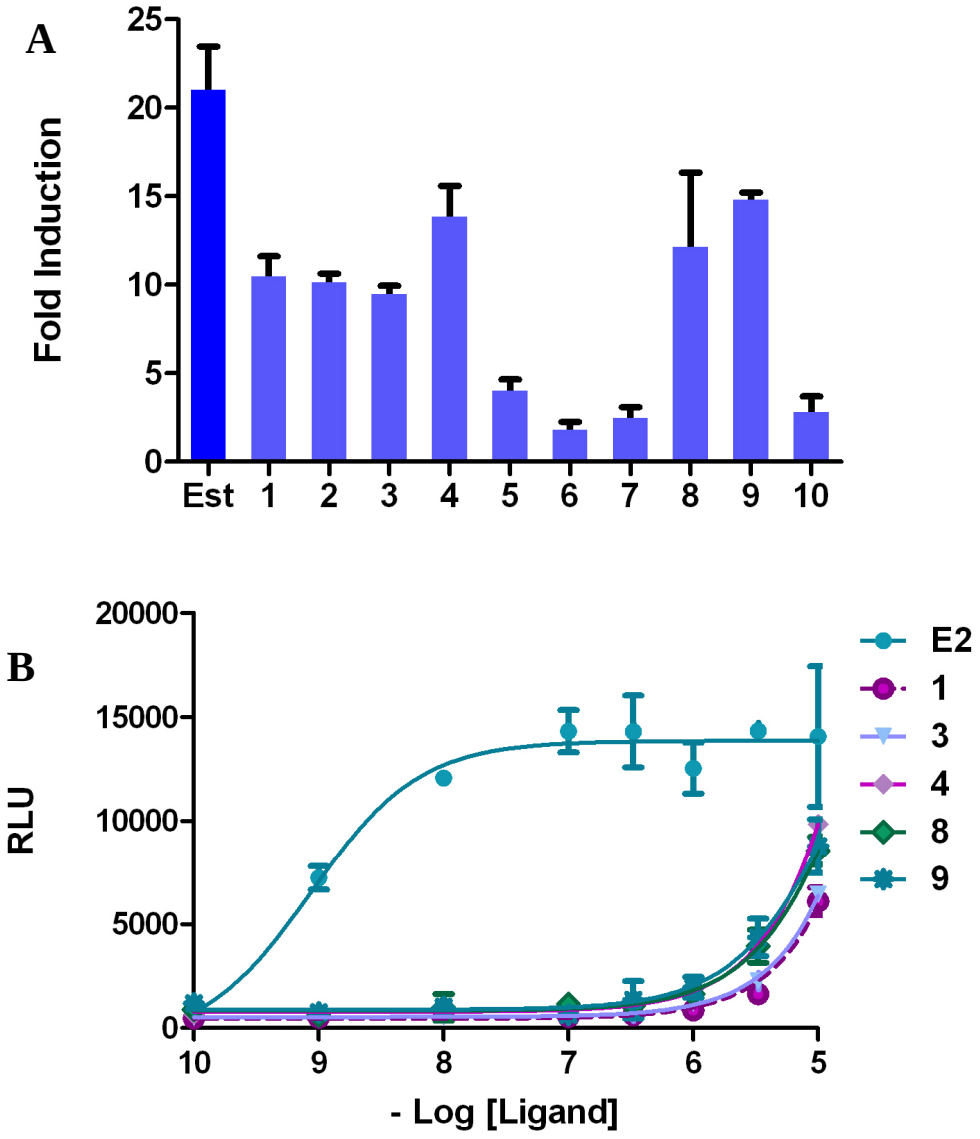

Figure 3.10 Activation profile of chromophores in mammalian cells (HEK293T), A. Relative inductions of ERα in the presence of 10μM of each ligand **B.** Dose response curves for the activation of ERα (Gal4DBD: ERαLBD) in response to various concentrations of 1,3, 4, 8, 9. Activity is measured in relative light units (RLU) derived from the measurement of luciferase activity and normalization against a β-galactosidase internal standard.

3.6 Visualization of hERα in yeast and in mammalian cells using Fluorescent Chromophores

As mentioned previously, a goal of developing AMIs as novel ligands was to determine if fluorescence would be observed upon binding to the NRs. The chromophores were tested for fluorescence in the presence of ERα in yeast and NIH3T3 mammalian cells. The chromophores were then tested in yeast for fluorescence, where yeast cells containing ER, along with the Gal4 control were exposed to the chromophores, along with estradiol as a negative control. In the presence of the ER and both chromophores AMI 1 and AMI 2, yeast cells displayed fluorescence, showing much higher in intensity with AMI 1 than with AMI 2 (Figure 3.11). The amount of fluorescence observed with AMI 2 was higher in comparison to cells containing ER and estradiol. As a method of assessing basal fluorescence, yeast cells containing the Gal4 protein, a ligand-independent yeast transcriptional factor, was visualized where no basal fluorescence was observed.

The next step was to determine whether a similar trend in activation and fluorescence seen in yeast would be observed in mammalian cells. Confocal microscopy was used to monitor cellular uptake and localization of the chromophores in the cell. The cells were transfected with the mammalian expression vector pCMXGhERLBD expressing Gal4DBD:ERαLBD fusion protein and incubated in media in each of the ten chromophores. To determine the amount of background fluorescence observed with cells and the compounds, a series of negative controls were employed. First, the NIH3T3 cells transfected with ERα were exposed either to no ligands or to estradiol alone, addressing

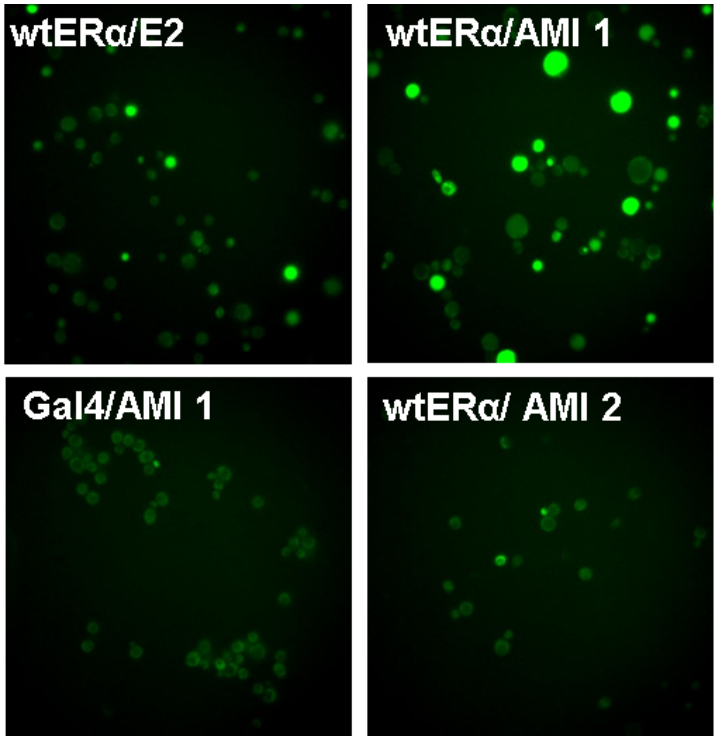

Figure 3.11 Imaging of yeast cells with the fluorescent chromophores. Yeast cells expressing ERα (Gal4DBD: ERαLBD) were incubated with 1 and 2. As a negative control cells lacking ERα were incubated with 2.

the basal fluorescence observed due to the cells and in the presence of ERα. Cells lacking ERα were also exposed to the AMI compounds, addressing the potential fluorescence due to non specific binding of the fluorophore to endogenous proteins.

As shown in Figure 3.12 slight basal fluorescence was observed in the case of one of the controls--cells lacking ERα and incubated with compound 10. In the presence of ERα, 6 of 10 of the chromophores showing activation displayed no fluorescence (data not shown). However in the case of compound 10, fluorescence was observed in the cytoplasm of the NIH3T3 cells, despite the absence of activation. Perhaps, this observation suggests that activation and fluorescence can be independent of each other.

In other words, these chromophores could serve as agonists that bind, activate and display fluorescence. Conversely, in other instances these compounds can bind and fluoresce but not activate, similar to a traditional antagonist. The localization of the observed fluorescence in the cytoplasm of the cell was also unexpected due to the fact that previous research and findings have shown ERα localizes to the nucleus in the presence of agonist or an antagonist [45]. However, Rickert et al have recently shown that OHT- derived conjugates display fluorescence in cytoplasm. It remains unexplained why these compounds are not able to be transported to nucleus [33].

3.7 Materials and Methods

Synthesis of ligands

Synthesis of the ligands was carried out using previously described synthetic methods in Chapter 2. For compounds 1-3 and 5 the Schiff base was obtained by

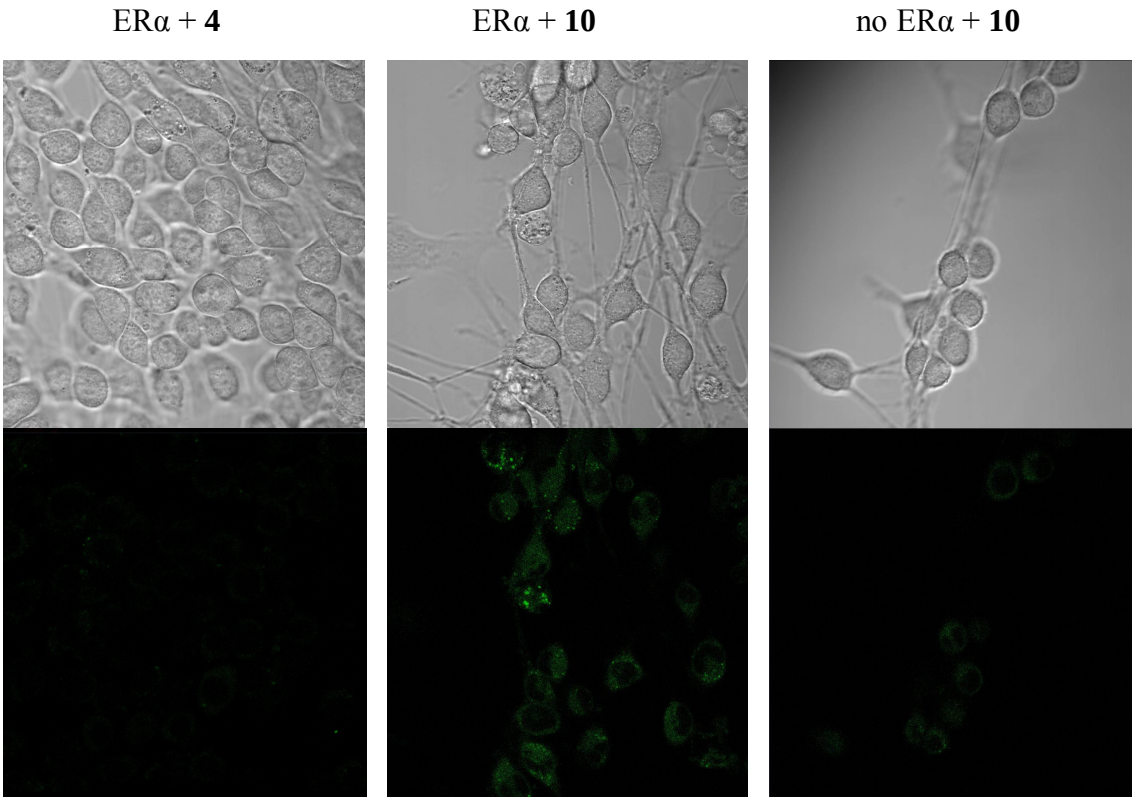

Figure 3.12 Imaging of NIH 3T3 cells with the fluorescent chromophores. Mammalian cells expressing ERα (Gal4DBD: ERαLBD) were incubated with 4 and 10. As a negative control cells lacking ERα were incubated with 10.

reacting the aromatic aldehyde (1eq), the primary amine (1eq) and sodium hydroxide (1.1eq) in 40.0 mL of MeOH at reflux for 4hr, followed by removal of solvent under reduced pressure to yield product. For 4 and 6-9 the aldehyde (1eq) and primary amine (1eq) were allowed to stir 12 h, yielding pure product. The imidate was prepared as previously described [46]. Imidazolidinones were synthesized by combining the corresponding Schiff base with the imidate and ~0.5mL of MeOH with stirring for 12 h which resulted in precipitate formation for 4 and 6-9. Solvent removal from compounds 1-3 and 5 under reduced pressure provided solid products as nearly pure materials. All products were further washed with cold Et_2O to yield the desired products as light yellow crystalline materials.

In Silico Docking Studies

Modeling of ligand–protein complexes was carried out with AutoDock Vina® using the estradiol–ERα ligand binding domain (pdb: 1ERE) crystal structure under standard parameters. The estrogen receptor was prepared for docking via UCSF CHIMERA, an interactive molecular graphics program, by removing the ligand and water molecules, adding polar hydrogens, and assigning Kollman united atom charges [47]. Ligands were created using ChemBioDraw Ultra 11.0 / ChemBio3D Ultra 11.0 (Cambridge Soft, USA) and were minimized using MMFF94 force field. Ligands were modified with the AutoDockTools by adding Gasteiger charges to set the partial charge of each atom [48]. The best docked ligand/receptor complexes were subjected to further studies.

Liquid quantification assay in yeast

Variants were tested in liquid quantification assays in 96-well plates with media lacking histidine, leucine, and tryptophan (SC-HLW), 0.1 mM 3AT, and with or without chromophores or 17β-estradiol at varying concentrations. Media and cells were added in a 4:1 ratio into 96-well plates. Plates were incubated at 30°C, with shaking at 170 rpm. Optical density (OD) readings at 630 nm were recorded at 0, 24, and 48 hours to measure growth density.

Cell culture

HEK293T cells (ATCC, USA) were transfected with the plasmid pCMXwthERαLBD. This plasmid contains the Gal4DBD (GBD) fused to the wild-type ERα ligand binding domain LBD (GBD:LBD fusion under the control of a cytomegalovirus (CMV) promoter). The reporter plasmid, p17*4TATAluc, contained the *Renilla* luciferase gene under the control of four Gal4 response elements located upstream from a minimal thymidine kinase promoter. The pCMXβgal, a plasmid containing the β-galactosidase gene under the control of the mammalian CMV promoter, was also used as an internal standard. Lipofectamine 2000 (Invitrogen, USA) was used as the cationic lipid and transfection experimental details are described in Taylor et al.[49] Ligands were added to the wells at various concentrations. Cells were harvested and analyzed for luciferase and β-galactosidase activity. All data points represent the average of triplicate experiments normalized against β-galactosidase activity.

Fluorescence Microscopy

Transfection of NIH3T3 cells was performed in a single plate with PolyFect (Qiagen, USA) transfection reagent according to the manufacturer's protocol. Plasmids pCMXwthERαLBD expressing Gal4DBD:ERαLBD fusion protein and mCherry-nuc as control were co-transfected into NIH3T3 cells. After 8 hours of transfection at 37˚C in humidified air with 5% CO_2, the media in the wells was removed and ligand (10mM) was added with the media to the wells. Cells were then subjected to microscopy after 30 hours of incubation. Samples were washed with 1X PBS and confocal imaging was performed using a Zeiss LSM 510 NLO w/META MPE confocal microscope (Carl Zeiss MicroImaging GmbH, Germany).

3.8 References

1. Katzenellenbogen, J.A. and B.S. Katzenellenbogen, *Nuclear hormone receptors: ligand-activated regulators of transcription and diverse cell responses.* Chem Biol, 1996. **3**(7): p. 529-36.

2. Khan, S.A., et al., *Estrogen receptor expression of benign breast epithelium and its association with breast cancer.* Cancer Res, 1994. **54**(4): p. 993-7.

3. Yager, J.D., *Endogenous estrogens as carcinogens through metabolic activation.* J Natl Cancer Inst Monogr, 2000(27): p. 67-73.

4. Lonard, D.M., R.B. Lanz, and B.W. O'Malley, *Nuclear receptor coregulators and human disease.* Endocr Rev, 2007. **28**(5): p. 575-87.

5. Mendelsohn, M.E., *Estrogen actions in the cardiovascular system.* Climacteric, 2009. **12 Suppl 1**: p. 18-21.

6. Bodhankar, S., et al., *Estrogen-induced protection against experimental autoimmune encephalomyelitis is abrogated in the absence of B cells.* Eur J Immunol, 2011. **41**(4): p. 1165-75.

7. Elloso, M.M., et al., *Suppression of experimental autoimmune encephalomyelitis using estrogen receptor-selective ligands.* J Endocrinol, 2005. **185**(2): p. 243-52.

8. Pike, C.J., et al., *Protective actions of sex steroid hormones in Alzheimer's disease.* Front Neuroendocrinol, 2009. **30**(2): p. 239-58.

9. Anstead, G.M., K.E. Carlson, and J.A. Katzenellenbogen, *The estradiol pharmacophore: ligand structure-estrogen receptor binding affinity relationships and a model for the receptor binding site.* Steroids, 1997. **62**(3): p. 268-303.

10. Meyers, M.J., et al., *Estrogen receptor-beta potency-selective ligands: structure-activity relationship studies of diarylpropionitriles and their acetylene and polar analogues.* J Med Chem, 2001. **44**(24): p. 4230-51.

11. Harris, H.A., J.A. Katzenellenbogen, and B.S. Katzenellenbogen, *Characterization of the biological roles of the estrogen receptors, ERalpha and ERbeta, in estrogen target tissues in vivo through the use of an ERalpha-selective ligand.* Endocrinology, 2002. **143**(11): p. 4172-7.

12. Waibel, M., et al., *Bibenzyl- and stilbene-core compounds with non-polar linker atom substituents as selective ligands for estrogen receptor beta.* Eur J Med Chem, 2009. **44**(9): p. 3412-24.

13. Koehler, K.F., et al., *Reflections on the discovery and significance of estrogen receptor beta.* Endocr Rev, 2005. **26**(3): p. 465-78.

14. Levenson, A.S., et al., *Resveratrol acts as an estrogen receptor (ER) agonist in breast cancer cells stably transfected with ER alpha.* Int J Cancer, 2003. **104**(5): p. 587-96.

15. Yang, M., et al., *Effects of bisphenol A on breast cancer and its risk factors.* Arch Toxicol, 2009. **83**(3): p. 281-5.

16. Stauffer, S.R., et al., *Pyrazole ligands: structure-affinity/activity relationships and estrogen receptor-alpha-selective agonists.* J Med Chem, 2000. **43**(26): p. 4934-47.

17. Davis, A.M., et al., *The effects of the selective estrogen receptor modulators, methyl-piperidino-pyrazole (MPP), and raloxifene in normal and cancerous endometrial cell lines and in the murine uterus.* Mol Reprod Dev, 2006. **73**(8): p. 1034-44.

18. Brzozowski, A.M., et al., *Molecular basis of agonism and antagonism in the oestrogen receptor.* Nature, 1997. **389**(6652): p. 753-8.

19. Lazennec, G., et al., *Mechanistic aspects of estrogen receptor activation probed with constitutively active estrogen receptors: correlations with DNA and coregulator interactions and receptor conformational changes.* Mol Endocrinol, 1997. **11**(9): p. 1375-86.

20. Pike, A.C., *Lessons learnt from structural studies of the oestrogen receptor.* Best Pract Res Clin Endocrinol Metab, 2006. **20**(1): p. 1-14.

21. Leo, C. and J.D. Chen, *The SRC family of nuclear receptor coactivators.* Gene, 2000. **245**(1): p. 1-11.

22. McInerney, E.M., et al., *Determinants of coactivator LXXLL motif specificity in nuclear receptor transcriptional activation.* Genes Dev, 1998. **12**(21): p. 3357-68.

23. Crosignani, P.G., et al., *Hormone replacement and the menopause: a European position paper. Writing Group on Women's Health of the Fondazione Giovanni Lorenzini Medical Science Foundation.* Eur J Obstet Gynecol Reprod Biol, 1997. **74**(1): p. 67-72.

24. Jordan, V.C., *Tamoxifen (ICI46,474) as a targeted therapy to treat and prevent breast cancer.* Br J Pharmacol, 2006. **147 Suppl 1**: p. S269-76.

25. Ring, A. and M. Dowsett, *Mechanisms of tamoxifen resistance.* Endocr Relat Cancer, 2004. **11**(4): p. 643-58.

26. Matsuda, K., et al., *Colocalization and ligand-dependent discrete distribution of the estrogen receptor (ER)alpha and ERbeta.* Mol Endocrinol, 2002. **16**(10): p. 2215-30.

27. Yang, Z., C.J. Barnes, and R. Kumar, *Human epidermal growth factor receptor 2 status modulates subcellular localization of and interaction with estrogen receptor alpha in breast cancer cells.* Clin Cancer Res, 2004. **10**(11): p. 3621-8.

28. Miyoshi, Y., et al., *Mechanisms of estrogen receptor-alpha upregulation in breast cancers.* Med Mol Morphol, 2010. **43**(4): p. 193-6.

29. Mendelsohn, M.E. and R.H. Karas, *Rapid progress for non-nuclear estrogen receptor signaling.* J Clin Invest, 2010. **120**(7): p. 2277-9.

30. Htun, H., et al., *Direct visualization of the human estrogen receptor alpha reveals a role for ligand in the nuclear distribution of the receptor.* Mol Biol Cell, 1999. **10**(2): p. 471-86.

31. Adamczyk, M., R.E. Reddy, and Z. Yu, *Synthesis of a novel fluorescent probe for estrogen receptor.* Bioorg Med Chem Lett, 2002. **12**(9): p. 1283-5.

32. Asai, D., et al., *Direct measure of fluorescence intensity for efficient receptor-binding assay: conjugates of ethinylcarboxyestradiol and 5(and 6)-carboxyfluorescein via alpha, omega-diaminoalkanes as a tracer for estrogen receptor.* J Biochem, 2008. **143**(6): p. 781-92.

33. Rickert, E.L., et al., *Synthesis and characterization of fluorescent 4-hydroxytamoxifen conjugates with unique antiestrogenic properties.* Bioconjug Chem, 2010. **21**(5): p. 903-10.

34. Christoph, S. and F.J. Meyer-Almes, *Novel fluorescence based receptor binding assay method for receptors lacking ligand conjugates with preserved affinity: study on estrogen receptor alpha.* Biopolymers, 2003. **72**(4): p. 256-63.

35. Asim, M., et al., *Deconstructing estradiol: removal of B-ring generates compounds which are potent and subtype-selective estrogen receptor agonists.* Bioorg Med Chem Lett, 2009. **19**(4): p. 1250-3.

36. Rivera-Portalatin, N.M., et al., *Comparison of estrogen-derived ortho-quinone and para-quinol concerning induction of oxidative stress.* J Steroid Biochem Mol Biol, 2007. **105**(1-5): p. 71-5.

37. Wright, J.S., et al., *A-CD estrogens. I. Substituent effects, hormone potency, and receptor subtype selectivity in a new family of flexible estrogenic compounds.* J Med Chem, 2011. **54**(2): p. 433-48.

38. Trott, O. and A.J. Olson, *AutoDock Vina: improving the speed and accuracy of docking with a new scoring function, efficient optimization, and multithreading.* J Comput Chem, 2010. **31**(2): p. 455-61.

39. Enoki, S., et al., *Acid denaturation and refolding of green fluorescent protein.* Biochemistry, 2004. **43**(44): p. 14238-48.

40. Martin, M.E., F. Negri, and M. Olivucci, *Origin, nature, and fate of the fluorescent state of the green fluorescent protein chromophore at the CASPT2//CASSCF resolution.* J Am Chem Soc, 2004. **126**(17): p. 5452-64.

41. Azizi, B., E.I. Chang, and D.F. Doyle, *Chemical complementation: small-molecule-based genetic selection in yeast.* Biochem Biophys Res Commun, 2003. **306**(3): p. 774-80.

42. Schwimmer, L.J., et al., *Creation and discovery of ligand-receptor pairs for transcriptional control with small molecules.* Proc Natl Acad Sci U S A, 2004. **101**(41): p. 14707-12.

43. Baker, K., et al., *Chemical complementation: a reaction-independent genetic assay for enzyme catalysis.* Proc Natl Acad Sci U S A, 2002. **99**(26): p. 16537-42.

44. Struhl, K. and R.W. Davis, *Production of a functional eukaryotic enzyme in Escherichia coli: cloning and expression of the yeast structural gene for imidazole-glycerolphosphate dehydratase (his3).* Proc Natl Acad Sci U S A, 1977. **74**(12): p. 5255-9.

45. Miksicek, R.J., *In situ localization of the estrogen receptor in living cells with the fluorescent phytoestrogen coumestrol.* J Histochem Cytochem, 1993. **41**(6): p. 801-10.

46. Lerestif, J.M., Tetrahedron Lett, 1995. **51**: p. 6757-6774.

47. Pettersen, E.F., et al., *UCSF Chimera--a visualization system for exploratory research and analysis.* J Comput Chem, 2004. **25**(13): p. 1605-12.

48. Sanner, M.F., *Python: a programming language for software integration and development.* J Mol Graph Model, 1999. **17**(1): p. 57-61.

49. Taylor, J.L., et al., *Characterization of a molecular switch system that regulates gene expression in mammalian cells through a small molecule.* BMC Biotechnol, 2010. **10**: p. 15.

CHAPTER 4

FLUOPHORES AS LIGANDS FOR THE PREGNANE X RECEPTOR

4.1 Pregnane X Receptor (PXR)

The pregnane X receptor (PXR; gene designation NR1I2) is a member of the nuclear receptor superfamily and is expressed in liver and intestine [1, 2]. PXR regulates the expression of number of enzymes involved in xenobiotic metabolism and transport of various drugs, endogenous substances and environmental toxins [3, 4]. PXR is involved in the regulation of several cytochrome P450s, and one of its main targets is cytochrome P450 monooxygenase 3A4 (CYP3A4), which has a major role in the biotransformation of drugs and catalyzes the metabolism of 60% of all drugs that are in use, such as contraceptive steroids, immunosuppressive agents and some antibiotics [5]. In addition to regulation of the CYP3A4 gene, PXR regulates the expression other target genes, including glutathione *S*-transferases, sulfotransferases, uridine 5′-diphosphate glucuronosyltransferases (UGTs) and drug transporters such as P-glycoprotein and multi-drug resistance-associated proteins 2 and 3 [6-8]. This nuclear receptor has been implicated in various physiological and pathophysiological processes, such as glucose and bone homeostasis, lipid metabolism, inflammatory response and apoptosis in cancer [9-12].

Structurally, similar to other NRs, PXR contains both DNA-binding domain (DBD) and ligand binding domain (LBD) connected by a flexible hinge region [13]. The PXR DBD is highly conserved with 95% amino acid identity in nuclear receptor superfamily [14]. As with other nuclear receptors, PXR forms a heterodimer partner with

the retinoid X receptor (RXR). However, the PXR LBD is highly divergent across species, compared to other nuclear receptors. The LBD between mammalian and non-mammalian PXR sequences, shares only approximately 50% identity on the amino acid level and 80% between mammalians PXR [15, 16]. The human PXR LBD, similar to other nuclear receptors is arranged into three-layered α helical sandwich with five stranded anti-parallel β- sheets, unique to PXR (Figure 4.1) [17]. These extended β – sheets has been shown to take a crucial role in mediating dimerization and even more importantly, contributes to the binding capabilities of this receptor in comparison to other nuclear receptors [18].

Several crystal structures of PXR with different ligands bound to the PXR LBD revealed unique ligand binding pocket. The large, hydrophobic and flexible PXR ligand binding pocket is able to accommodate a wide range of ligands, expanding to 1200 $Å^3$. This pocket size accommodates the binding of ligands varying in mass from 232 Daltons (Da) of phenobarbital to 823 Da of rifampicin [16, 19, 20]. The promiscuity of this receptor is in part due to the fact that structurally this receptor contains additional β-sheets, allowing for a larger binding pocket in relation to other nuclear receptors. The PXR ligand binding pocket besides the flexibility is also mostly hydrophobic. Of the 28 residues present in the ligand binding pocket (LBP), 20 of these residues are hydrophobic, contributing largely to its ability to bind and activate in response to hydrophobic ligands [21]. Many of the PXR ligands contain a partition coefficient in range logP 3.5 – 10, indicating the hydrophobic character of ligands [19].

Flexibility, hydrophobicity and the additional two β- strands are major factors which contribute to promiscuity of PXR and allow for binding a large range of ligands.

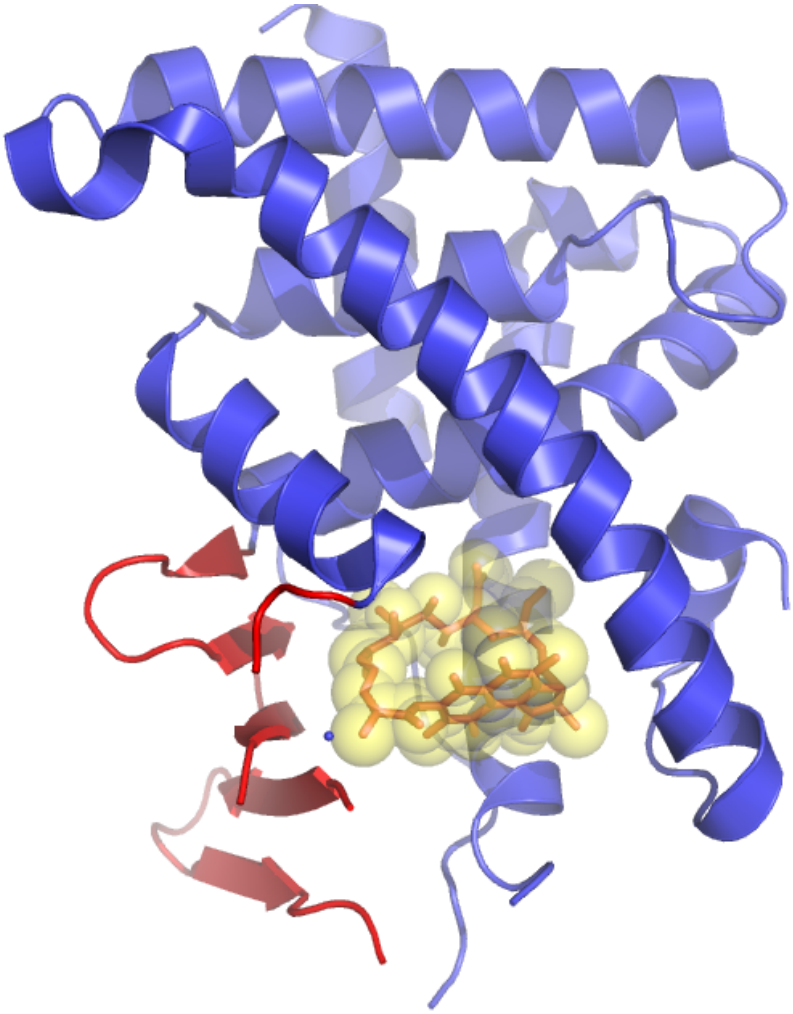

Figure 4.1 Crystal structure of PXR LBD with rifampicin (Pdb:1SKX). B-stands are shown in red and rifampicin is shown in orange with yellow space filling.

However, PXR's promiscuity is also in part contributed to a flexible loop that is connected to ligand binding pocket by a nonsolvent – accessible pore. This flexible loop allows for the opening of the pocket to accommodate larger compounds, such as the antibiotic rifampicin [17, 21]. This is particularly important since PXR serves as axenobiotic sensor. This receptor is known to bind a number of structurally diverse ligands, such as the cholesterol-lowering drug SR12813, anticancer compounds, herbal components (e.g. St. John's Wort), plant extracts and HIV protease inhibitors (e.g. indinavir and ritonavir) (Figure 4.2) [22-25]. The PXR activation by above mentioned drugs implies that this nuclear receptor in clinically important for drug-drug interactions (Figure 4.3). For example, use of St. John's Wort causes upregulation of cytochrome P450 due to PXR activation, which in turn reduces the serum levels of several drugs including antiviral indinavir, immunosuppressant ciclosporin and oral contraceptives [26-28]. Despite its promiscuous behavior, a certain amount of specificity is also observed in the binding properties of this receptor. Specific atoms are known to influence the binding and activation properties of this receptor, often referred to as direct promiscuity.

4.2 Evaluating Fluophores Interaction with the PXR in mammalian cells

As previously described in Chapter 3, the goal of this work is development of novel ligands based on the structure of the chromophore of the green fluorescent protein (GFP), the arylmethyleneimidazolodinone (AMI), for various nuclear receptors with fluorescence ability. Successfully, we have developed novel AMIs for estrogen receptor α. To date, there is lack of fluorescent ligands for PXR which will be able to fluorescence upon binding to receptor and be use for trafficking PXR in the cell. In addition

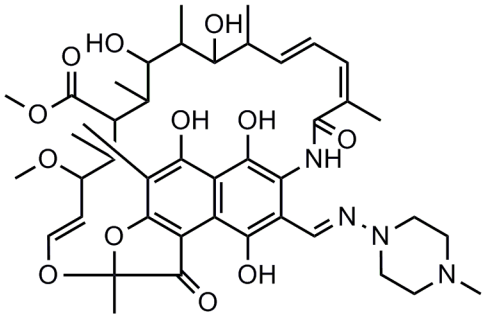

Rifampicin
823 Da

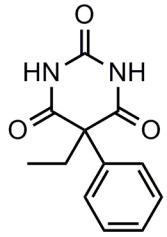

Phenobarbital
232 Da

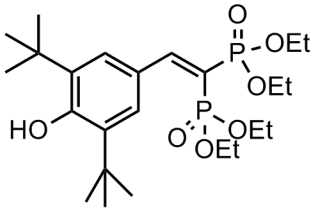

SR12813
504 Da

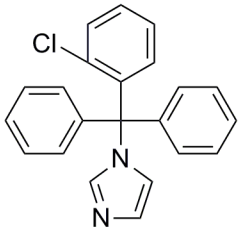

Clotrimazole
345 Da

Figure 4.2 Various sizes and shapes of PXR agonists.

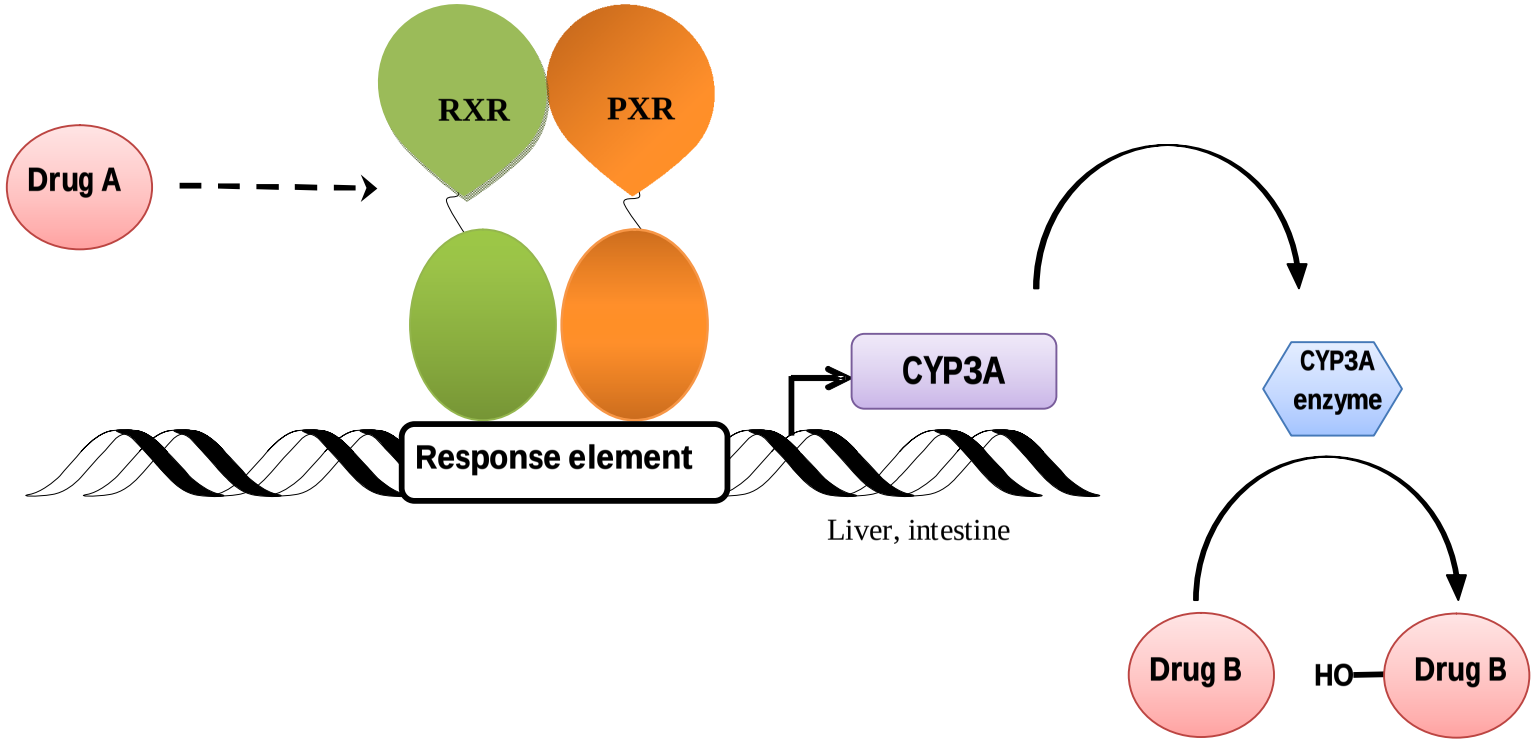

Figure 4.3 The molecular basis of a drug–drug interaction. The heterodimer PXR/RXR regulates the expression of the *CYP3A* gene (violet) in the liver and intestine. Drug A binds to PXR and induces expression of the CYP3A enzyme (blue), then metabolize drug B, which is a substrate for CYP3A.

development of specific ligands for PXR could be beneficial for treatment PXR related diseases. Based on these previous results we decided to evaluate interaction of AMIs with the pregnane x receptor. It had been shown that PXR is activated by several ERα ligands, such as 17-β estradiol and tamoxifen, and because of their similar ligand binding profiles, the thought was that certain AMIs that activate ER, could potentially activate PXR. In addition to being potential ligands, AMIs are designed to fluoresce upon binding PXR, leading potentially to the development of the first fluorescent ligands, serving as a powerful visualization tool for this receptor *in vivo*. Human embryonic kidney 293T cells (HEK293T) were used to determine the activity of the AMIs with PXR in vivo. The cells were transfected with a mammalian expression vector (pCMX) containing the Gal4 DNA binding domain fused to the PXR ligand binding domain (GBD:PXRLBD). The cells were also co-transfected with a reporter plasmid, which contained a luciferase reporter gene assay under the control of Gal4 response elements. Transfected cells were incubated with the AMI derivatives at 10 μM and tested for activation by measuring luminescence. In the presence of ligand binding to the receptor, the interaction of the Gal4 DBD with Gal4 response element, allows for luciferase expression, hence leading to luminescence.

As shown in Figure 4.4, cells expressing PXR are able to active this receptor in the presence of the rifampicin, the known PXR ligand which was used as a control. However, ERα AMIs, numbered 1 through 9, derivatives did not display any activation with PXR as we expected. However, these results confirmed that the AMI compounds selectively activated ERα.

Next, we decided to determine if modifications to the AMI core could lead to the development of potential ligands for PXR. Thus, a library of synthesized AMIs derivates

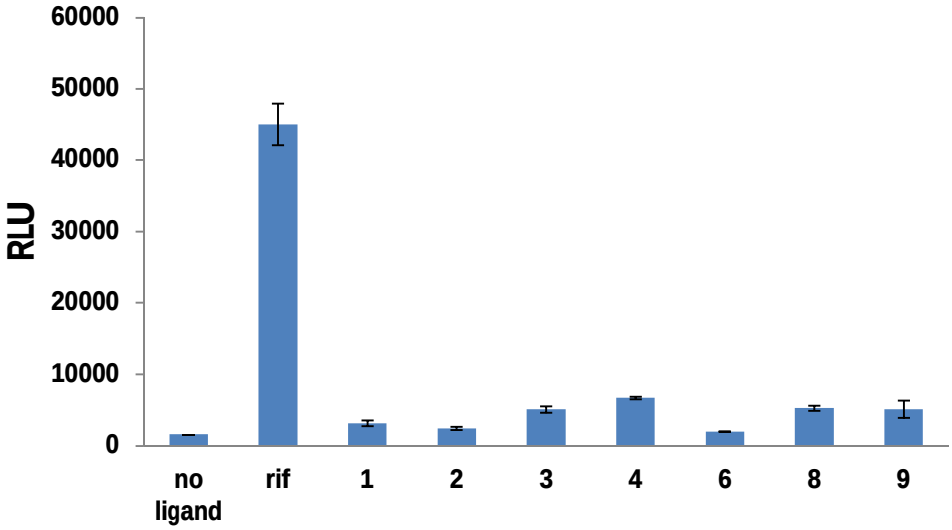

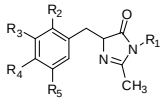

AMI	R_1	R_2	R_3	R_4	R_5
1	$C_3H_6CO_2H$	H	H	OH	H
2	$C_5H_{10}CO_2H$	H	H	OH	H
3	C_3H_6OH	H	H	OH	H
4	C_3H_7	H	H	OH	H
6	CH_3	H	H	CH_3	H
8	CH_3	H	CH_3	OH	CH_3
9	CH_3	H	H	$N(Me)_2$	H

Figure 4.4 Activation profile of ER AMI to test for PXR activation. HEK298T cells were transfected with plasmid expressing hybrid (GBD:PXR) and reporter plasmid. Rifampicin used as a control. Luciferase assay in the presence of 10 µM ligand.

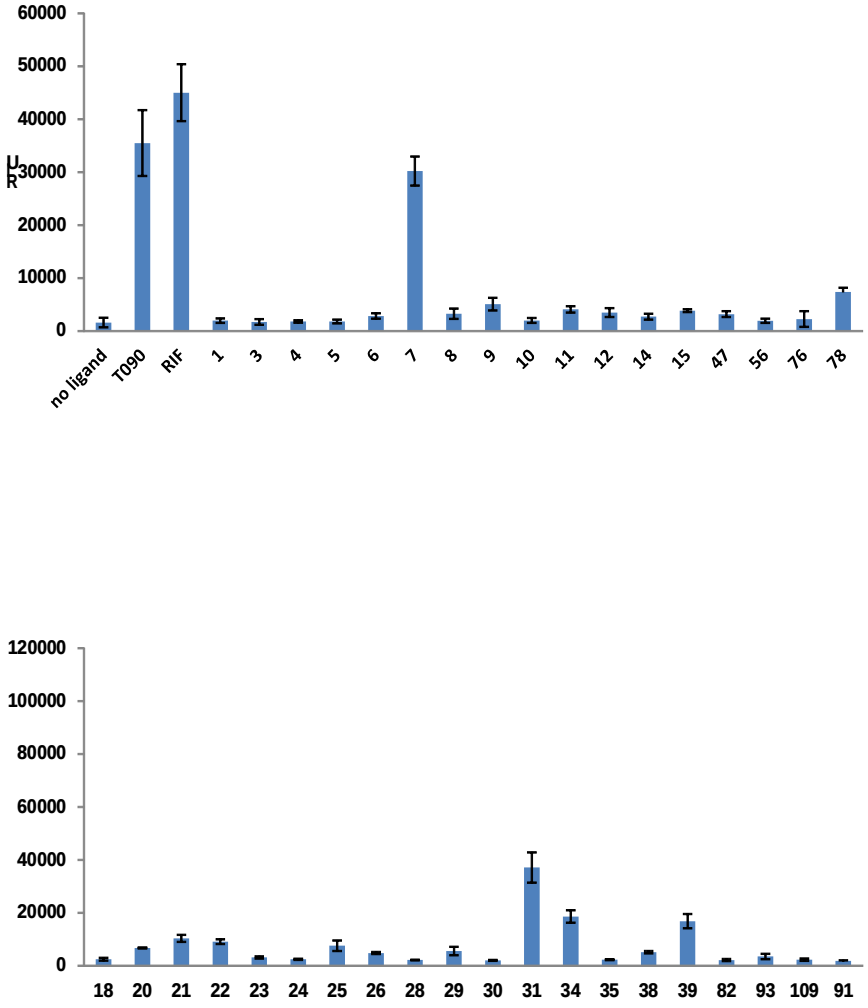

Figure 4.5 Activation profile of 60 AMIs in PXR. Part I. PXR (GBD:PXRLBD)was transfected into HEK298T cells with p17*4TATALuc plasmid, a luciferase reporter gene under the control of Gal4 response elements and were incubated with 10 μM of ligand. Structure of all above ligands are included in appendix.

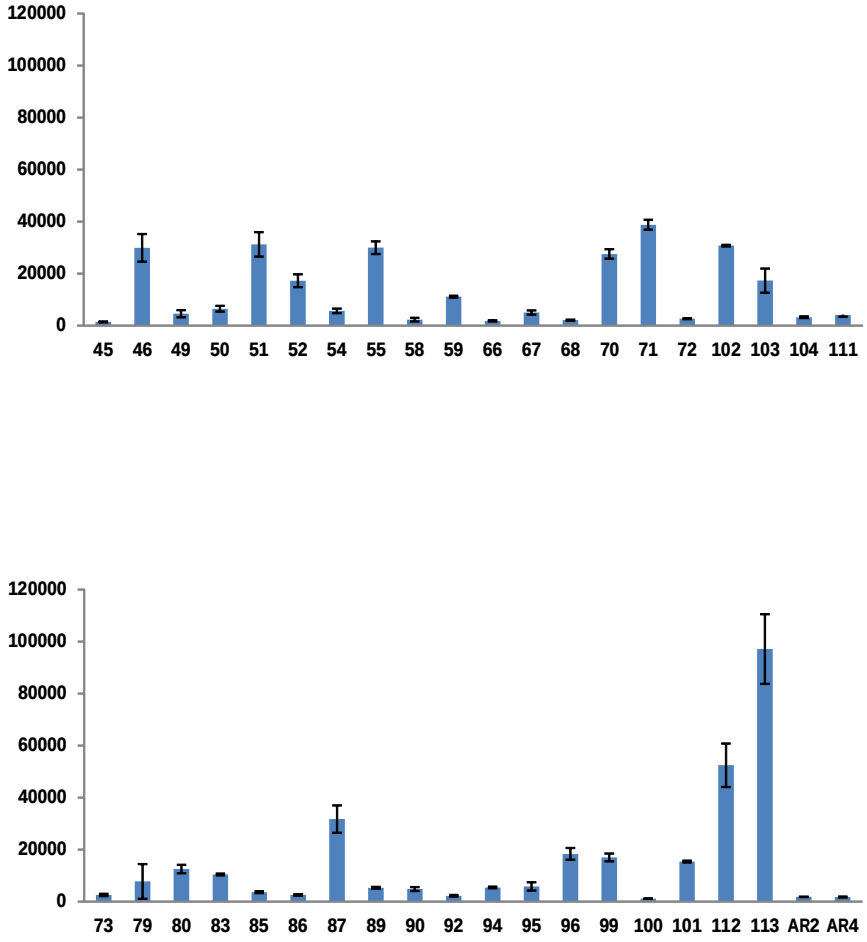

Figure 4.5 Activation profile of 60 AMIs in PXR. Part II. PXR (GBD:PXRLBD)was transfected into HEK298T cells with p17*4TATALuc plasmid, a luciferase reporter gene under the control of Gal4 response elements and were incubated with 10 μM of ligand. Structure of all above ligands are included in appendix.

tested in HEK293T cells as described above. As shown in Figure 4.5 rifampicin and T0901317 served as controls, since these two ligands were previously shown to activate PXR and this was consistent with our results as these compounds both display 90 and 64 fold activation, respectively. Of the 60 compounds shown, 17 compounds displayed activity with PXR. Some of these compounds have showed similar activity of 70 – 100 fold activation in comparism to rifampicin and T090 (90 and 64 fold activation, respectively), the known PXR activators.

4.3 Analysis of PXR activation by AMIs

The results that were obtained through screening the AMI library indicated that several of these AMIs could serve as agonists for PXR. In certain instances, as seen with AMI 112 and 116 the fold activation observed with these molecules were higher than that observed with rifampicin. Furthermore, in looking closer at the structure of these compounds, the AMIs could be grouped based on their chemical properties forming four main groups, refereed to as groups A-D, as shown in Figure 4.6 and in Table 4.1.

These groups indicate a specific preference of the receptor for a variety of substituents on the core of the AMI structure. Two of these groups, A and B, are characterized by diethylamine group at position R_4 that seems to have a direct effect on increase the activation level. The highest activation level is achieved by group A (AMI 1-8) which has additional hydroxyl group at position R_2 on the core of the AMI structure. Interestingly, in comparing this group of compounds to group B (AMI 9-12), we are able to see that the lack of the hydroxyl group seems to be causing a two fold decrease in activation, as observed with group B ligands.

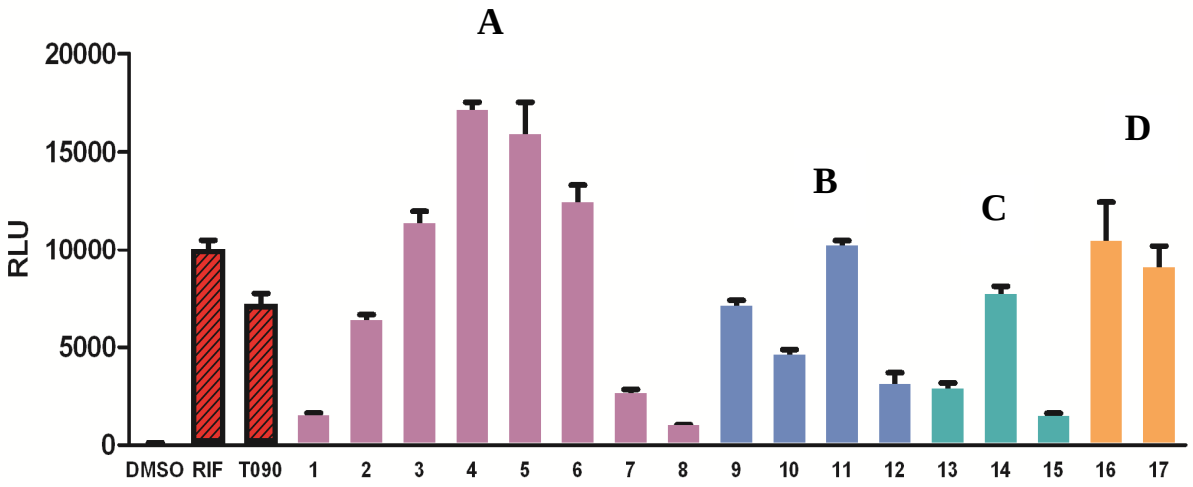

Figure 4.6 Activation profile of PXR with various AMIs. AMIs were categorized on 4 classes based structure similarity. Group A is presented in purple, group B in blue, group C in turquoise and group D in orange. HEK293T cells were transfected with a luciferase reporter gene and expression plasmid encoding fusion of Gal4DBD and LBD of PXR. Transfected cells were treated with 10 µM compounds for 30h. Rifampicin (RIF) and T090 were used as references. DMSO is used as a negative control.

Table 4.1. Structures of Fluorescent Protein Chromophores

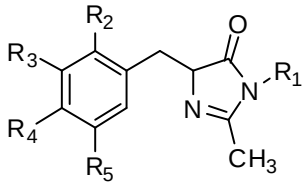

Compound	R_1	R_2	R_3	R_4	R_5
1A	CH_3	OH	H	$N(Et)_2$	H
2A	C_3H_7	OH	H	$N(Et)_2$	H
3A	C_5H_{11}	OH	H	$N(Et)_2$	H
4A	C_6H_{13}	OH	H	$N(Et)_2$	H
5A	C_7H_{15}	OH	H	$N(Et)_2$	H
6A	C_8H_{17}	OH	H	$N(Et)_2$	H
7A	$C_{10}H_{21}$	OH	H	$N(Et)_2$	H
8A	$C_3H_6CO_2H$	OH	H	$N(Et)_2$	H
9B	C_3H_7	H	H	$N(Et)_2$	H
10B	C_5H_{11}	H	H	$N(Et)_2$	H
11B	C_6H_{13}	H	H	$N(Et)_2$	H
12B	*i*-C_3H_7	H	H	$N(Et)_2$	H
13C	CH_3	Br	H	H	H
14C	C_3H_7	Br	H	H	H
15C	C_3H_7	Cl	H	H	H
16D	CH_3	H	$C(CH)_3$	OH	$C(CH)_3$
17D	CH_3Bz	H	$C(CH)_3$	OH	$C(CH)_3$

To further analyze the individual compounds in each of the groups, each of the AMIs were further tested in a dose-response fashion for activation with PXR. To determine the sensitivity of these derivatives a subset of the best activators of PXR were tested for their efficacy in a dose-response assay, with AMI concentrations ranging from 10 nM to 10 μM, in order to calculate EC_{50} values, the effective concentration required to reach 50% of maximum activation. As shown in Figure 4.7B, most of the compounds displayed a sensitivity profile between 3-7 μM, comparable to that of rifampicin ($EC_{50} \approx$ 1.3 μM). Thus, these AMI derivatives are similar in sensitivity but show higher activation levels than rifampicin, making these compounds a novel and potential class of PXR agonists.

The activation observed with the various AMI derivatives can be correlated with the presence of certain R-groups around the core structure of the molecule. In particular, the size of the alkyl chain at position R_1 seems to have a direct effect on the activation level. As observed with AMI derivatives 1-8, a variety of alkyl chain sizes produced activation profiles similar or greater than rifampicin ($EC_{50} \approx 1.3$ μM, 100 fold activation), but the hexyl chain (AMI 4) displayed the greatest activation with a 180-fold activation and an EC_{50} value of 6.3 μM. This observation confirms the promiscuous and shape-sensitive nature of the PXR. As indicated previously, the activation profiles of these AMI derivatives provides some insight into the structure/function relationship between PXR and different ligands. First, the presence of a diethylamino group at R_3 position, as seen in AMI (1-8), seems to be important for activation since AMIs, which lacks this functional group at R_3 position, displays no activation. In addition, hydrophobic contacts between the ligand and the receptor seem to be required for obtaining maximal activation,

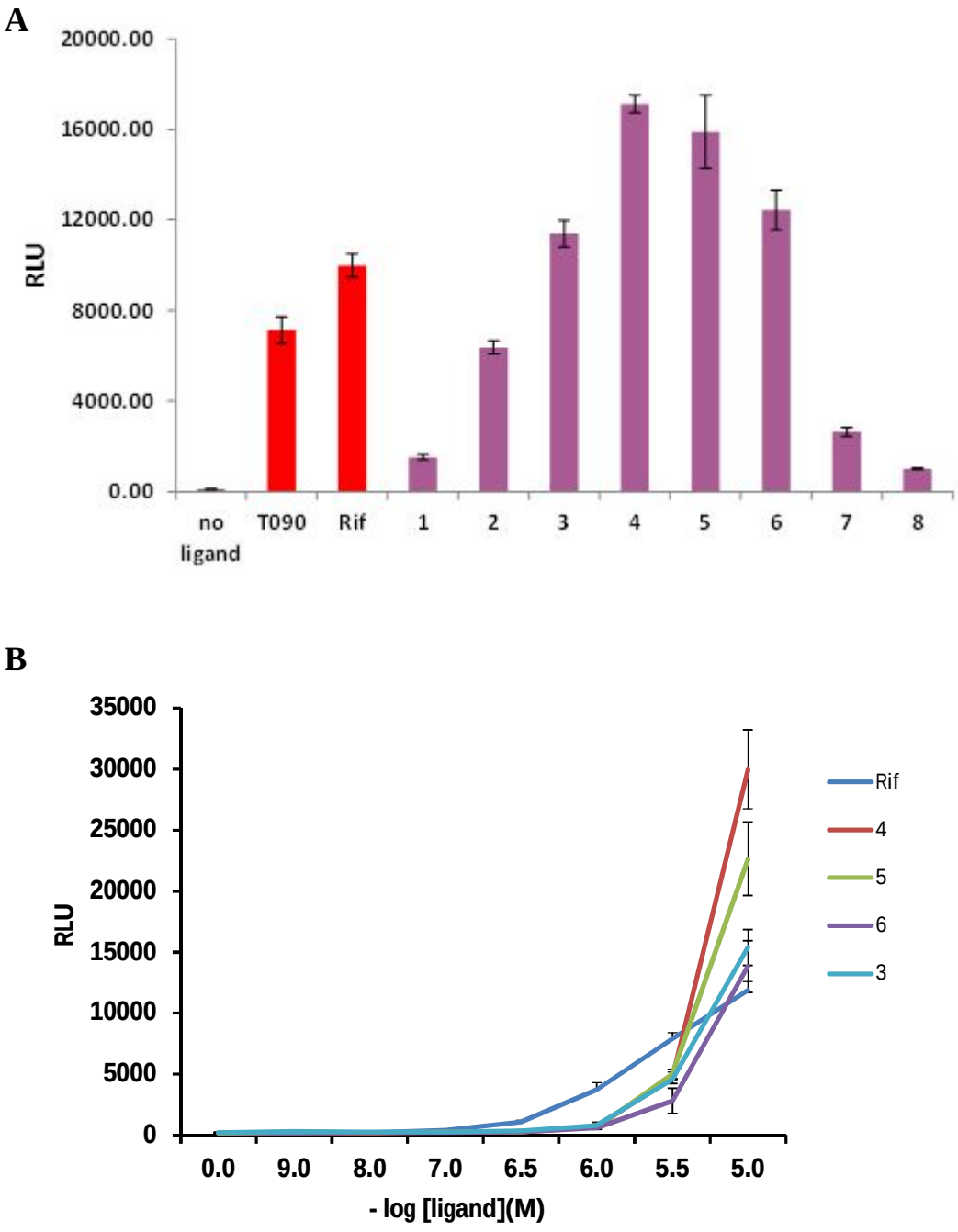

Figure 4.7 Activation profile of class A of AMIs. A. PXR (GBD:PXRLBD) transfected into mammalian cells HEK298T and incubated with 10µM ligand **B.** Dose response of the best AMIs and Rifampicin with PXR.

but within the limits imposed by the volume of the alkyl chain. The activation observed with AMI 4**,** with six carbons, was almost twice that of rifampicin (Eff_{4} = 172%) as shown in Table 4.2, while larger and smaller alkyl groups produced lower activation. Compounds 5 and 6 (Eff_5 = 159%, Eff_6 = 125%) display slightly lower fold activation compared to 4 differing by one or two carbons in the alkyl chain. However, the compound 2 displays almost one third of fold activation reached by 4. These results suggest that optimal length of alkyl chain for activation is six carbons to obtain maximal activation with PXR. More than eight carbons in this position lead to a drastic decrease in the activation, as seen in the case of chromophore 7 (Eff_7 = 26%). The presence of a methyl group does not lead to activation as seen with compound 1. This suggests that probably alkyl group takes place in creating of key hydrophobic contacts in the binding pocket. This hydrophobic volume effect is reminiscent of other volume-sensitive effects on AMI fluorescence within hydrophobic cavities and human serum albumin (HSA) earlier reported in literature. It has been shown that increased length of alkyl chain of AMIs had additional effect not only on binding but also on fluorescence level [31-33]. Finally, the differences in activation for AMI 2 and AMI 8, which differ only by the presence of a terminal carboxyl group, emphasize the importance of hydrophobicity.

The activity observed with group B of the AMIs derivatives displays a significantly lower activation profile when compared with group A described above. As seen in Figure 4.8 AMI (9-12) obtain the highest activation level in case of compound 11 (Eff = 103%, EC_{50}= 5.4 μM) same as in group A compound 6 (Eff = 172%, $EC_{50} \approx 5$ μM)). Both of these AMIs have the hexyl chain in position R_1. These results suggest that

Table 4.2. Biological activities of RARα agonists and their selected physical/chemical properties. Rifampicin (Rif) was used as reference and set to 100% efficacy at concentration of 10 µM. Strong PXR activators (activation higher than rifampicin) are indicated in red color, moderate activators in green color and weak activators in black.

Compound	Eff (%)	EC_{50} (µM)	MW (Da)	logP	MolSurf (Å^2)
Rif	100±5	1.3	823	3.85	1198
1A	15±8	5.4	287.36	1.77	442
2A	64±4	5	315.4	2.64	506
3A	114±5	5.6	343.46	3.53	567
4A	172±2	6.3	357.5	3.98	596
5A	159±10	5.9	371.5	4.42	626
6A	125±7	5	385.5	4.87	656
7A	26±7	6.4	413.6	5.76	722
8A	10±3	6	359.4	1.77	543
9B	71±4	5.9	315	2.64	506
10B	46±6	3	343.5	3.53	567
11B	103±2	5.4	357.5	4.28	587
12B	31±19	3.4	313.4	3.31	524
13C	29±11	4.5	279	2.02	302
14C	77±5	4.3	307.2	2.9	365
15C	15±9	3	262.7	2.73	362
16D	105±19	5.1	328.4	4.03	547
17D	91±12	5.8	404.5	5.76	654

A

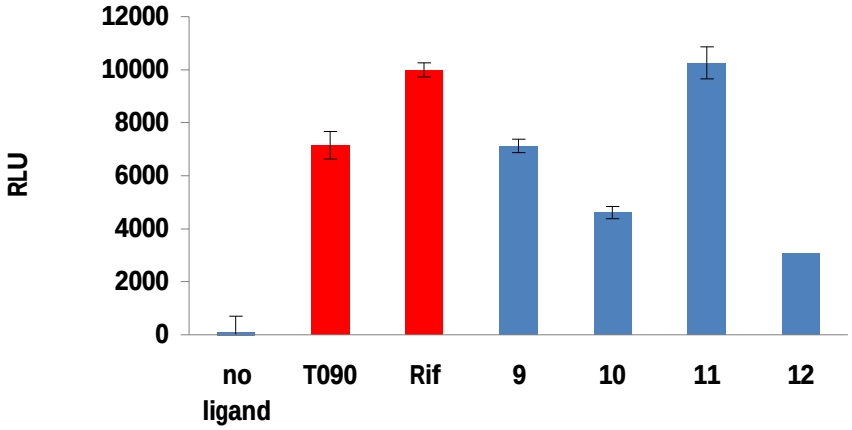

B

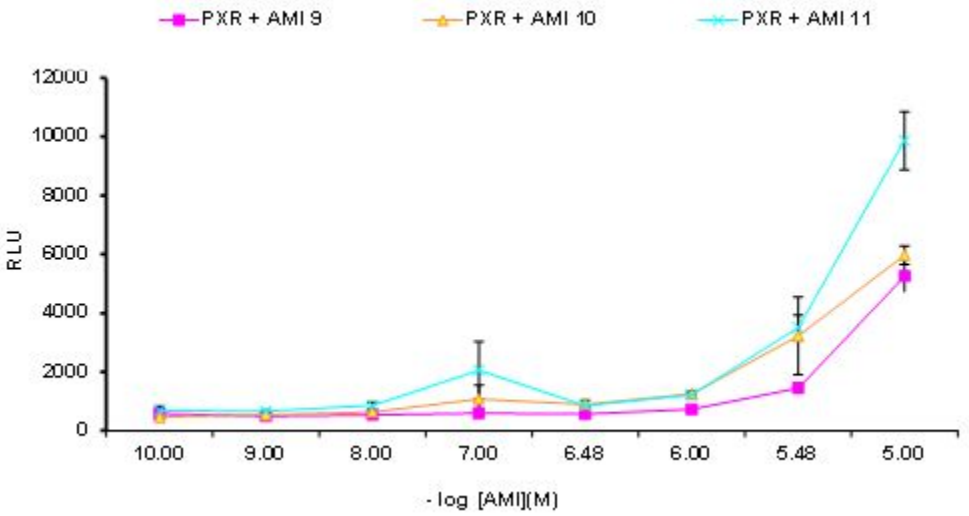

Figure 4.8 Activation profile of class B of AMIs. A. PXR (GBD:PXRLBD) transfected into mammalian cells HEK298T and incubated with 10 µM ligand **B.** Dose response of the best AMIs with PXR

optimal length of alkyl chain for activation is six carbons to obtain maximal activation in group A as in group B. Perhaps the hexyl chain creates optimal hydrophobic contacts in the pocket, higher or lower number of the carbons in the alkyl chain does not allow for AMI to obtain specific conformation to get higher fold activation. Same as in group A, the decreased number of carbons caused significant lower activation level in compound 9 and 10. This suggests that hydrophobic volume of AMIs is important for activation level. This data indicates that hydroxyl group at position R_2 of AMI core is crucial for receiving higher activation. The most probably this polar group is responsible for creating contact with one of the polar residues in the ligand binding pocket. When looking at groups C and D which contain completely different substituents on the core of the AMI structure, there are varying results observed. Group C includes three compounds that have halogens incorporated in the AMI core. Previously, several ligands with halogen moieties such as metachlor, oxadiazon and propiconazole were reported to be PXR agonists [34]. As observed in Figure 4.9, the highest level of activation was achieved by compound 14 which has bromine in position R_2 of the AMI core. In addition, the data suggests again that length of alkyl chain in position R_1 is significant for activation level. Compound 13 (Eff = 29%, EC_{50}= 4.5 μM) shows two-fold decrease in activation in comparison to compound 14 (Eff = 77%, EC_{50}= 4.3 μM). However, presence of chlorine in same position results in decreased activation as seen in AMI 15 (Eff = 15%, EC_{50}= 3 μM)). The most probable cause of this behavior is the difference in the sizes of chlorine and bromine atoms and difference in electrostatic surface potential which could influence the interaction of a ligand with the PXR ligand binding pocket.

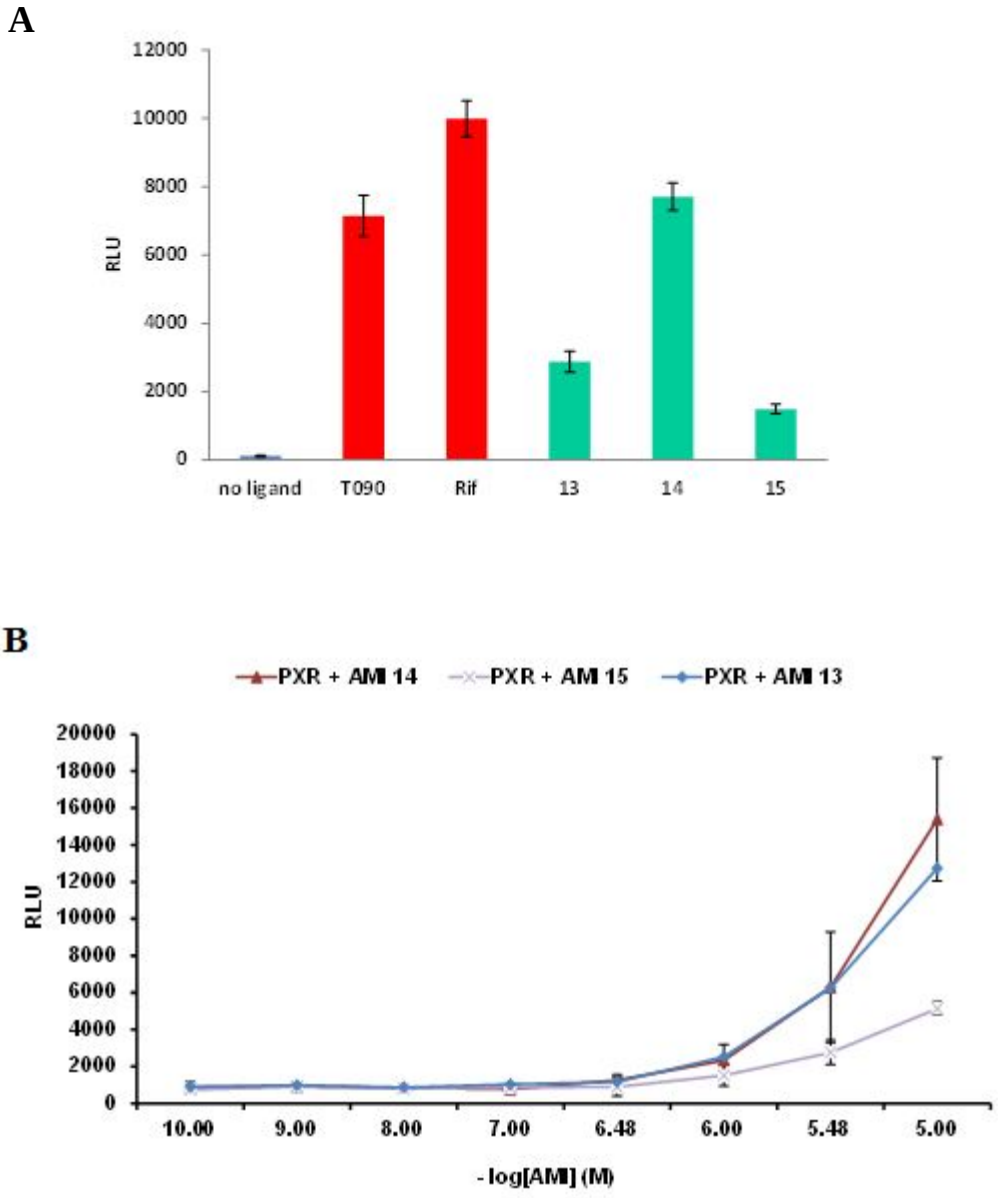

Figure 4.9 Activation profile of class C of AMIs. A. PXR (GBD:PXRLBD) transfected into mammalian cells HEK298T and incubated with 10µM ligand **B.** Dose response of the best AMIs with PXR

However, the best compound AMI 14 shows only 45% of activation achieved by the best AMI PXR activator, AMI 4.

In Group D, two compounds showed activity with PXR. The structures of these AMIs are interesting due to the presence of the 2,6-di-tert-butylphenol moiety, which is present in the SR12813 (EC_{50} = 200 nM), the cholesterol lowering drug known to activate PXR (Figure 4.10) [17, 35]. As seen in Figure 4.11 compound 16, the best activator of group D displays activation level similar to rifampicin (Eff_{16} =105%, Eff_{rif} = 100%). However, compound 17, which has additional moiety, the benzene in position R_1, displayed the reduced activation (Eff_{17} = 91%) in compare with 16 (Eff_{16} =105%). These results suggest that moiety of known well agonists can be successfully incorporated into the core of AMI and show comparable activation.

The differences in activation profiles with PXR and the various AMI groups indicate that the length of the alkyl chain and activation show a correlation. In addition to the length of the alkyl chain, the presence of the 2,6-di-tert-butylphenol moiety seemed to show activation and different chain length, potentially could display higher activation than rifampicin. Thus AMIs 130, 131 and 132 were synthesized with three, five and six carbons in alkyl group in position R_1, respectively. As shown in Figure 4.12 AMI 130 has similar sensitivity as rifampicin. AMI 131, 132 and 17 has higher sensitivity than rifampicin. Particularly, AMI 131 has similar profile as AMI 17 but it has slightly higher sensitivity. As predicted, length of the alkyl chain has influence on activation. The highest sensitivity was obtained with AMI 131 which has five carbons in the alkyl chain. Again obtained data indicates that length of the alkyl chain is important for activation.

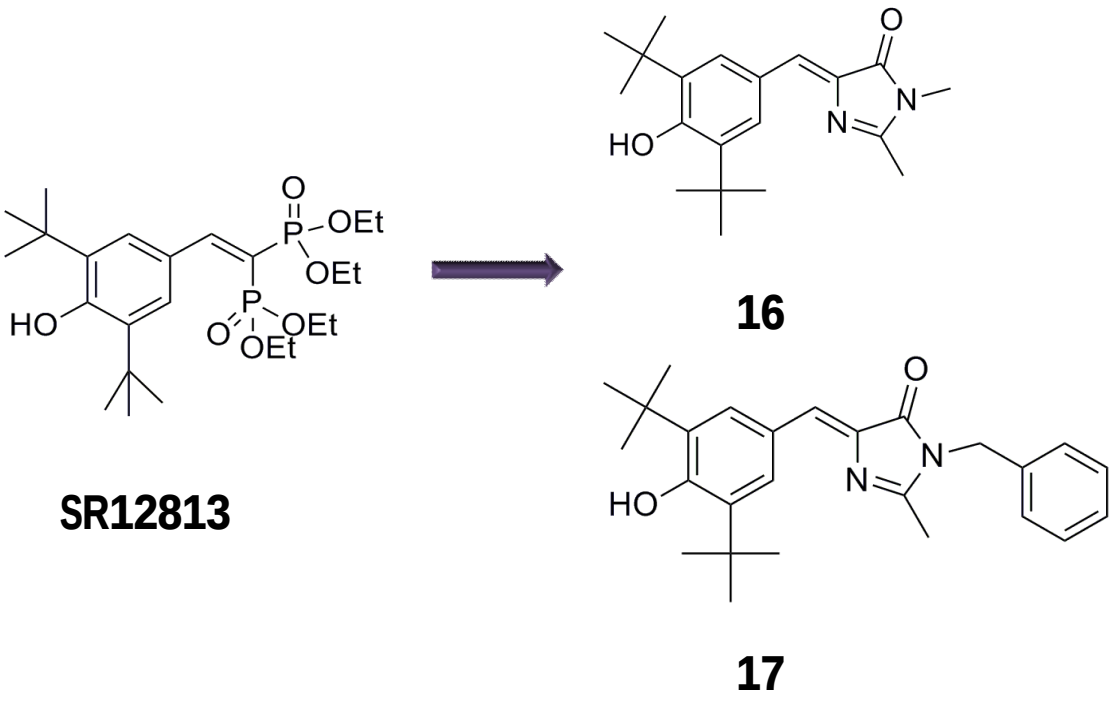

Figure 4.10 Design of PXR AMI based on ligand SR12813. Presence of the common 2,6-di-tert-butylphenol moiety, which is main part of SR12813 and AMI 16-17

A

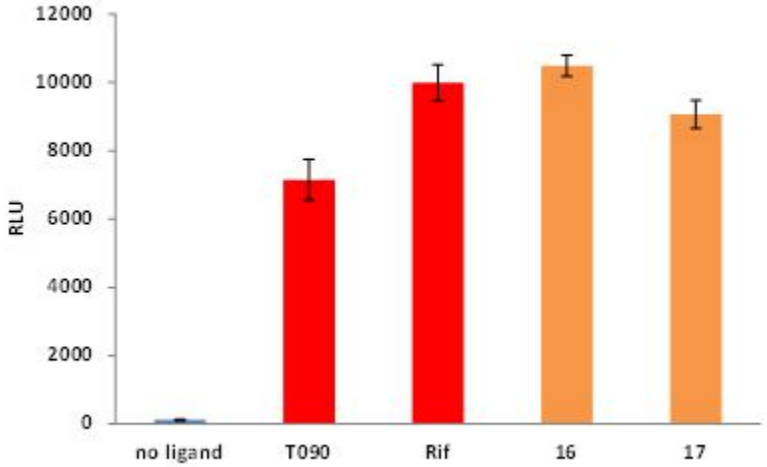

B

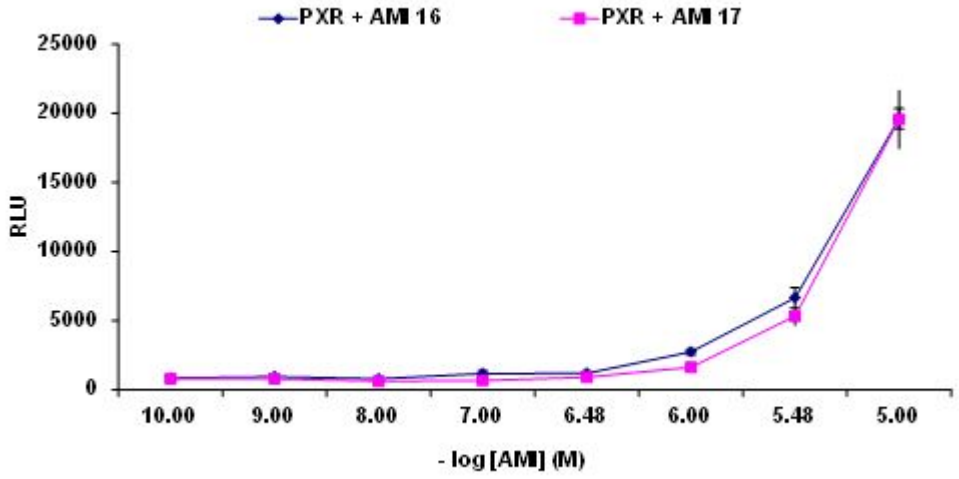

Figure 4.11 Activation profile of class D of AMIs. A. PXR (GBD:PXRLBD) transfected into mammalian cells HEK298T and incubated with 10µM ligand **B.** Dose response of the best AMIs with PXR

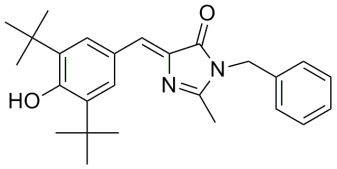

AMI 17

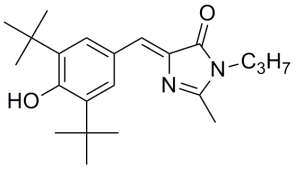

AMI 130

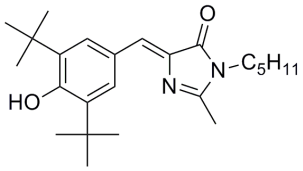

AMI 131

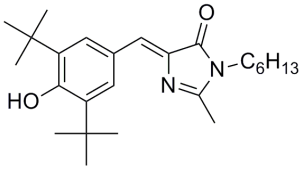

AMI 132

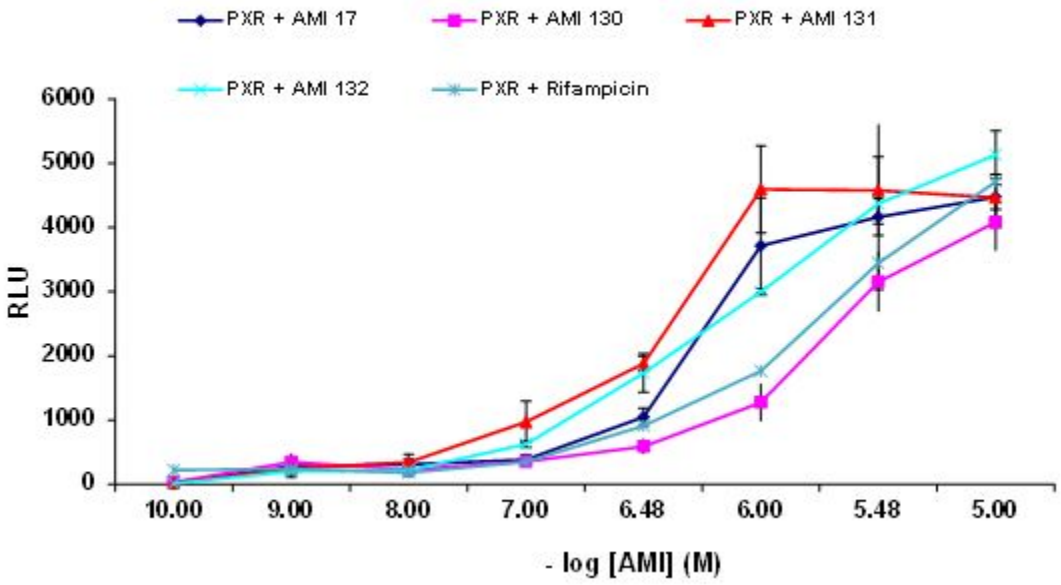

Figure 4.12 Activation profile of class D of AMIs. PXR (GBD:PXRLBD) transfected into mammalian cells HEK298T and incubated with wide range of concentration of AMIs.

Thus, hydrophobicity increased with length of the alkyl chain and volume is essential for PXR ligands to achieve activation.

The above results show activation of PXR by AMI compounds in cell culture using GBD:PXRLBD construct, containing the Gal4 DNA binding domain fused to the PXR ligand binding domain. However, this fusion is not present in the human body and potential activators for PXR as potential drugs should be also tested in their natural state. In the human body, PXR forms heterodimer with the retinoid x receptor α (RXR α). To confirm that PXR AMIs can act as agonists, full length PXR and RXR were tested for activation using AMI 3. The HEK298T cells were transfected with the plasmids containing full length RXR (pCMXRXR) and full length PXR (pCMXPXR), both under the control of a cytomegalovirus (CMV) promoter. The pLucPXRRE plasmid containing PXR response elements controlling expression of luciferase was used in the transfection. As seen in Figure 4.13a AMI 3 is able to activate full length of PXR with RXR with same fold activation as rifampicin. However, fold activation of AMI 3 is slightly lower in comparision to fusion of GBD:PXRLBD (Figure 4.13b). Lower activation can be due to different interaction of Gal4 DBD with Gal4 response element versus PXRDBD and PXR response elements. However, these results are promising and show that PXR/RXR heterodimer can be activated by AMIs.

In conclusion, we demonstrated novel PXR ligands based on the structure of AMI core. These four groups of compounds are potential PXR agonists and some of them display higher activation level in comparision with known PXR ligand, rifampicin. The most important feature of these compounds is an alkyl group that probably takes place in creating key hydrophobic contacts in the binding pocket. As previously reported,

A

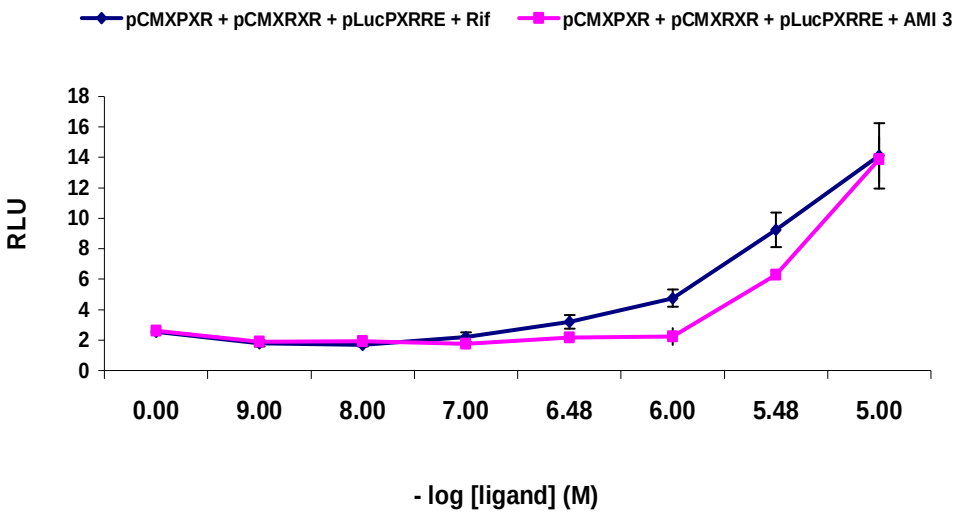

B

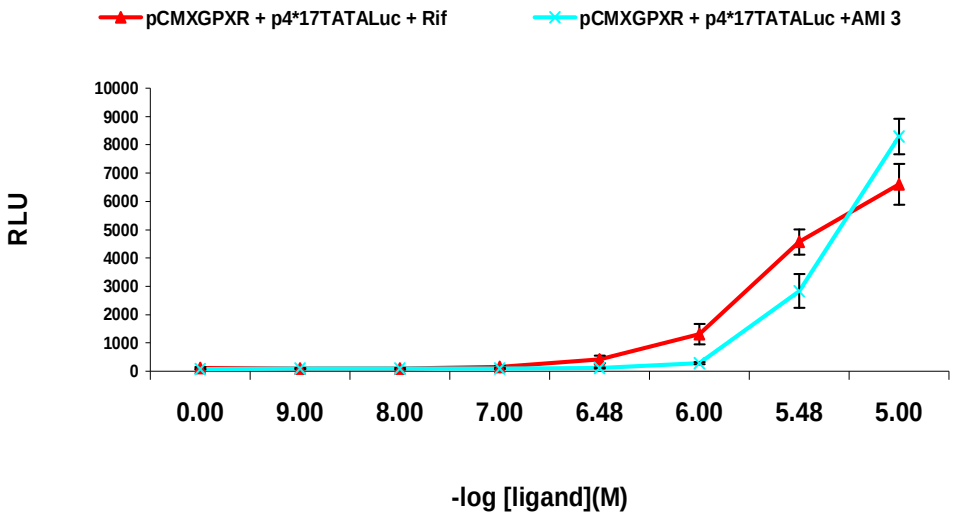

Figure 4.13 Activation profile of heterodimer PXR with AMI 3. **A.** HEK298T cells transfected with full length of PXR and full length of RXR with PXR response elements, **B.** HEK298T cell transfected with fusion GBD:PXR and luciferase gene reporter.

most of PXR ligands are hydrophobic with logP (3.5-10) [18]. Calculation of the logP of PXR AMIs showed that it varies between 3.5 and 5 (Table 4.2). However, the compounds that do not activate this nuclear receptor displayed the logP below 3. These results indicate importance hydrophobicity of the AMI for the PXR activation. However, specific polar groups are significant to achieve enhanced activation as in case of group A of AMIs. Similar to that observed between logP and activation level, a correlation was found in the size of molecular surface and activation. Molecular surface of the best PXR AMI agonist has a size of 550-650 $Å^2$ and decreases to 300-500 $Å^2$ in the case of AMIs that do not activate PXR. It suggests that volume of the ligand is important to achieve optimal contact with residues in the ligand binding pocket. Despite that fact that PXR ligand binding pocket is flexible and is able to accommodate ligands of different size and shape, in case of AMI, molecular surface below 500 $Å^2$ cause that activation level is significantly decreased.

4.4 Molecular modeling of Fluophores

In order to determine whether, AMIs are able to activate PXR due to the specific hydrophobic and polar contacts or ligand shape and volume, molecular modeling of AMIs into ligand binding domain of PXR was performed. Modeling was performed with AutoDock Vina, using crystal structure of ligand binding domain of PXR with SR12813 (PDB:1NRL) [36].

Four identified classes of PXR AMIs were docked into the crystal structure of PXR LBD bound to SR12813 after previous removal of the ligand. This crystal structure was chosen based on the size of the ligand bound into PXR. As mentioned previously, PXR LBD is highly flexible and modeling AMI into LBD bound with large ligand such

as rifampicin will not give expected results. Thus AMIs were docked into crystal structure of PXR LBD with ligand of similar size to AMIs. As seen in Figure 4.14A the modeled AMI 4 into structure of LBD of PXR, binds in position of SR12813 inside of ligand binding pocket as other fluophores. However, the AMI 1 is located in the opposite orientation as seen with AMI 4 and SR12813 (Figure 4.14b). This result is not surprising, since AMI 1 does not activate PXR and AMI 4 is the best agonist between all tested fluophores. In case of others AMIs from group A, data indicates importance of length of alkyl chain for activation. These theoretical models show that increase number of the carbons in alkyl chain create significant increase of space in LBP which could create steric clashes (Figure 4.14c). However, too short alkyl chain can lead to a decrease in hydrophobic contacts of ligand with residues in LBP and this leads to lower activation. The experimental and theoretical data indicates that six carbon chain is optimal for getting the highest PXR activation.

To determine the importance of hydroxyl group in position R_2 of AMI core in the class A of AMIs, we compare the modeled AMI 4 with AMI 11 which differs only by hydroxyl group. As seen in Figure 4.15A, AMI4 is able to create the hydrogen bond with serine S247, which lacks in case of AMI 11. It has been known that S247 is significant for interaction with SR12813 [35]. We have shown that group A which differs from group B only about the presence of hydroxyl group give much higher activation than group B. Thus this theoretical model implicated hydroxyl group to be involved in increasing activation level.

To further investigation of binding of class D of AMIs, AMI 16 was modeled into PXR LBD (Figure 4.15B). The 2,6-di-tert-butylphenol moiety of AMI 16 overlay in same

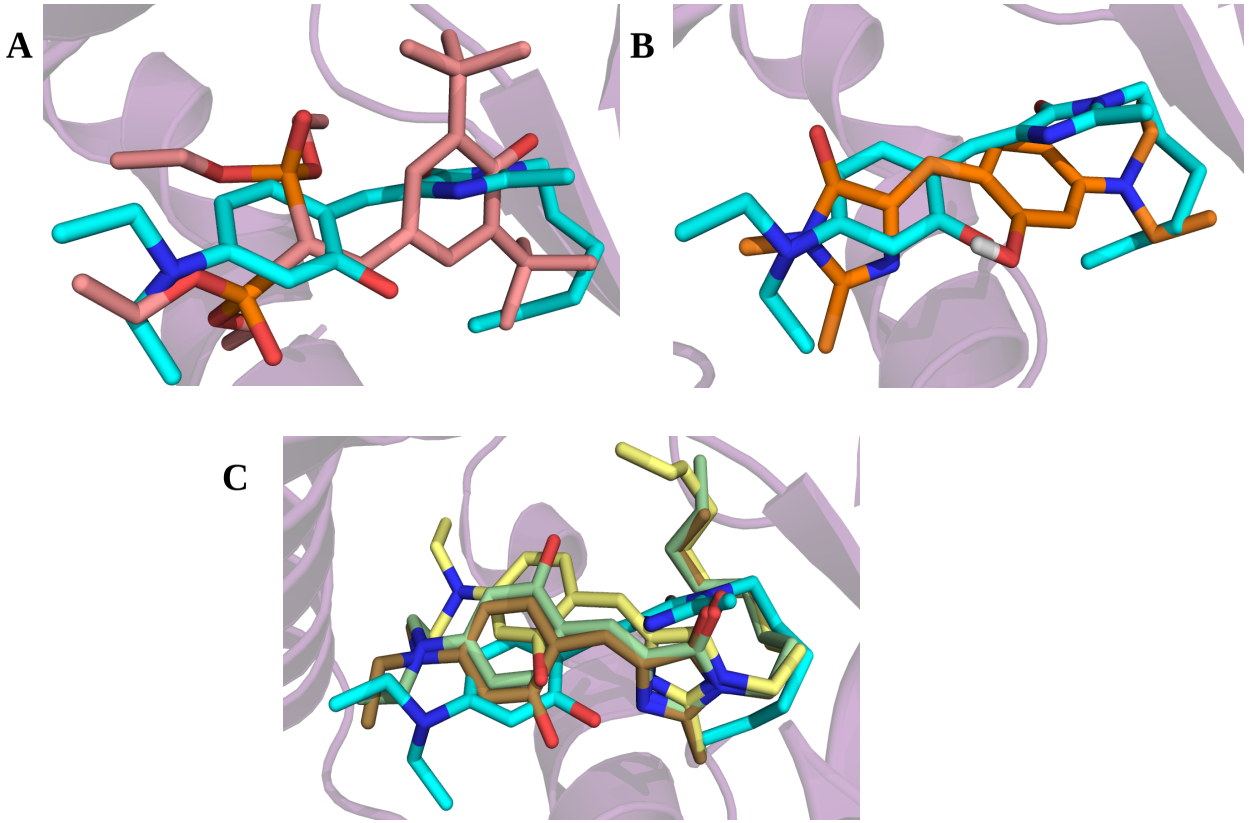

Figure 4.14 Modeling of PXR LBD crystal structure with the AMIs. A. Overlay of docked AMI 4 (blue) with SR12813(pink), **B.** Overlay of docked structure of AMI 1 (orange) with docked structure of AMI 4 (blue), **C.** Overlay of docked structures of AMI 4, 5, 6, 7

A

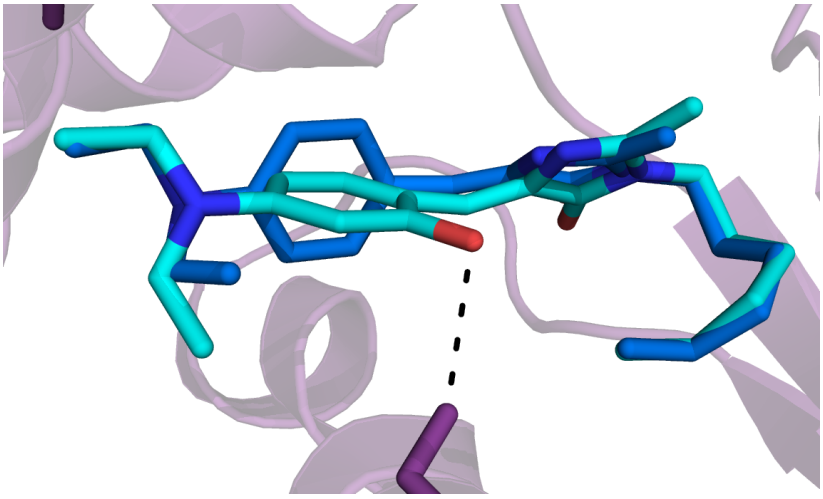

B

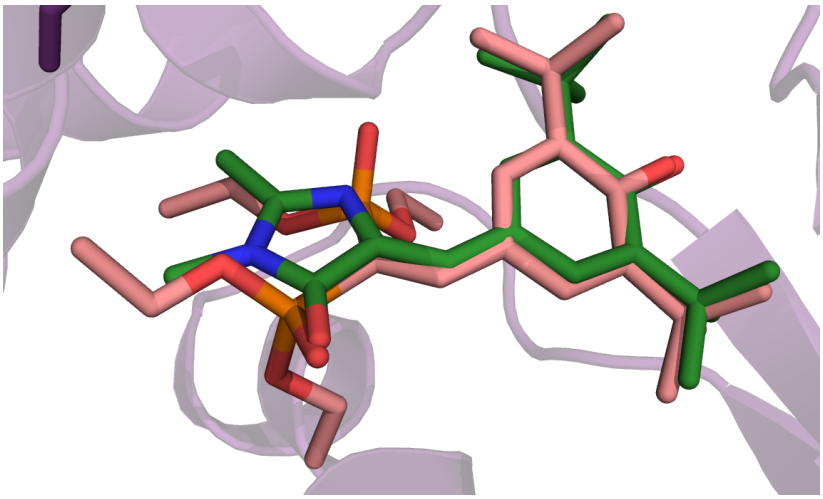

Figure 4.15 Modeling of PXR LBD crystal structure. A. Overlay of docked structure of AMI 4 (blue) and 11 (dark blue), **B.** Overlay of the docked structure of AMI 16 (green) with crystal structure of SR12813 (pink)

position as in SR12813, producing the binding energies of -9.4 kcal/mol; the lowest binding energy received from modeling of AMIs. These results indicate that class D of AMIs is able to bind in similar manner as SR12813. It correlates to data achieved previously, where AMI 16 and 17 are found to activate PXR in similar level as other known PXR activators.

Knowledge gained from modeling of binding AMI into ligand binding domain of PXR implicates the hydrophobicity, volume and hydrogen bonding essential for activation. Although these theoretical models provide important highlights into understanding "behavior" of AMIs inside of the binding pocket of PXR, this knowledge needs to be carefully adapted to future designing of PXR ligands. Flexible nature of PXR LBD creates a challenge for molecular modeling of this nuclear receptor [19, 37-39]. Thus, comprehensive analysis of binding and activation of PXR AMIs will be essential for developing novel classes of PXR agonists.

4.5 Visualization of PXR in mammalian cells using Fluophores

The goal of this work is development a novel PXR agonists, which will be able to "turn on" fluorescence in the presence of the PXR. As discussed in Chapter 2, AMIs that acts as agonist, are hypothesized to bind to the LBP of nuclear receptors by mimicking the effects of the β-barrel and restore the fluorescence by rigidifying the flexible fluophore.

In order to determine whether PXR AMIs are not only able to act as agonists but also display fluorescence upon binding, AMIs were tested for fluorescence using confocal microscopy. NIH3T3 cells were transfected with full length of PXR and RXR

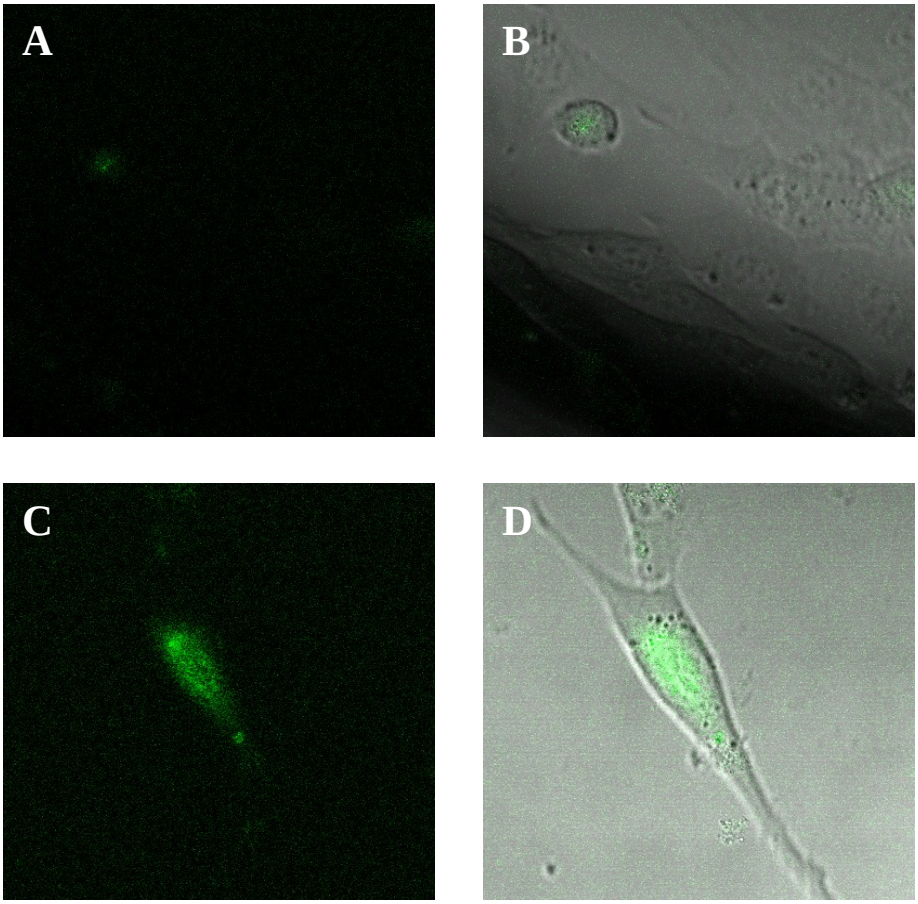

Figure 4.16 Confocal microscopy with AMI 3. NIH3T3 cells incubated with AMI 3, **A.** and **B.** NIH3T3 cells without expressed PXR, **C.** and **D.** NIH3T3 cells transformed with PXR/RXR, **C.** and **D.** Cells image with overlay cells in DIC.

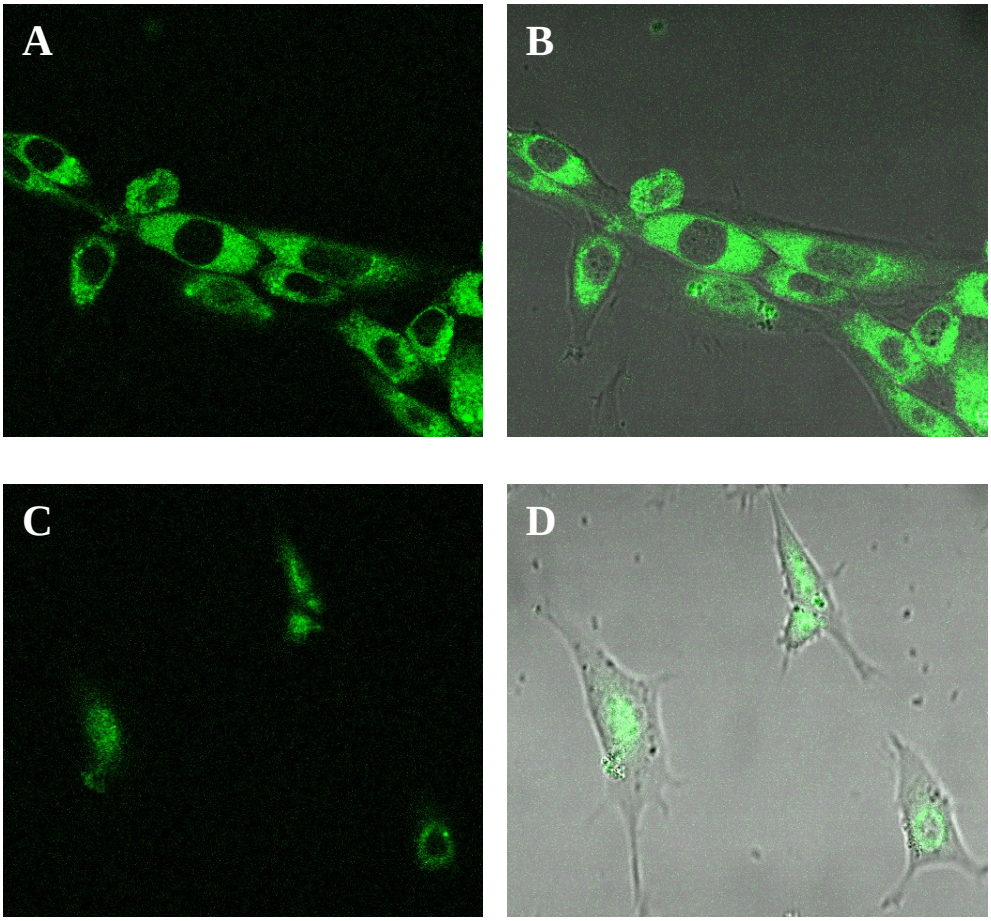

Figure 4.17 Confocal microscopy with AMI 4. NIH3T3 cells incubated with AMI 4, **A.** and **B.** NIH3T3 cells without expressed PXR, **C.** and **D.** NIH3T3 cells transformed with PXR/RXR, **C.** and **D.** Cells image with overlay cells in DIC.

and cells were incubated with10 μM of the ligand for six hours. As shown in Figure 4.17 and 4.18, the cells in the presence of the AMI 3 and 4 and the PXR displayed localized fluorescence. The cells which were expressing PXR/RXR and incubated with AMI 3 did not display high background fluorescence in comparision to cells without the receptors. However, the cells expressing receptors display fluorescence localized in the nucleus. These finding are not surprising due to overexpression of PXR in the nucleus. However, AMI 4 shows fluorescence in the cytoplasm without expression of the PXR. It means that AMI 4 is responsible for non specific binding in the cytoplasm of the cell. Surprisingly, when cells are expressing PXR/RXR heterodimer, localization of fluorescence is changed. Fluorescence is observed in the nucleus instead of the cytoplasm. These findings indicate that AMI 4 is able to bind and fluoresce upon binding to receptor. Probably, after binding receptor is moving to nucleus. These results are promising to show that AMIs are not only able to bind and active PXR but also they display fluorescence upon binding. Furthermore, more studies are needed to determine the correlations between fluorescence and activation. Some of fluophore agonists did not display fluorescence upon binding, when others as AMI 3 and 4 did. Comprehensive studies of fluorescence *in vitro* and *in vivo* and crystallography will be necessary to understand the correlations between fluorescence, binding and activation. These data will allow for the design of more specific AMIs which will be able to act as fluorescent agonists.

4.6. Summary

The goal of this work was developing novel PXR agonists based on arylmethyleneimidazolidinone (AMIs) core, which will be able to fluoresce upon

binding. Successfully, four classes of PXR ligands were discovered. Experimental studies and theoretical modeling provided insight into the correlation between structure of AMIs and activation level. The data implicated the importance of length of alkyl chain in R_1 position of AMI core. The six carbon chain is optimal to get the highest activation level. Besides hydrophobicity, the importance of hydroxyl group in R_2 position of the AMI core was discussed. Absence of this moiety causes a significant decrease in activation. Additionally, we have explored the effect of the 2,6-di-tert-butylphenol moiety, main part of SR12813 in AMI core for activation level. Incorporation of this moiety into the AMI core leads to activation comparable to that of rifampicin, the known PXR agonist.

Hence, part of the goal was to determine if these novel PXR agonists are able to "turn on" fluorescence upon binding, AMIs were tested in NIH3T3 cells using confocal microscopy. We have found that AMI 3 and 4 displays fluorescence upon binding PXR in cells. These results show that AMIs can be potentially used as fluorescence probes to detect PXR cell trafficking. However, more extensive studies need to be done to understand complexity of correlation between binding, activation and fluorescence of these ligands. This knowledge will be necessary to develop more sensitive PXR ligands with enhanced fluorescence upon binding to the receptor.

4.7 Materials and Methods

Ligands

Rifampicin (MW=823 g/mol) was purchased from Sigma (St. Louis, MO). Compounds were synthesized by Dr. Anthony Baldridge. Synthesis of AMI compounds 1-7, 9 was carried out by a 2+3 cycloaddition of the corresponding aromatic Schiff base

with the imine ester as described in Chapter 2. Schiff bases were prepared by reaction of the aromatic aldehyde (1eq) with the corresponding primary alkyl amine (1eq) according to the literature. The imine ester was prepared according to literature. Compound 8 was prepared using the corresponding aromatic aldehyde (1eq), aminobutanoic acid (1eq), and sodium hydroxide (1eq).

10 mM stocks of each ligand were dissolved in80% ethanol: 20% DMSO and stored at 4 °C.

Transfection in 3T3 cells

HEK293T cells (ATCC, USA) were transfected with the plasmid pCMXPXRLBD. This plasmid contains the Gal4DBD (GBD) fused to the wild-type PXR ligand binding domain LBD (GBD:LBD fusion under the control of a cytomegalovirus (CMV) promoter). The reporter plasmid, p17*4TATAluc, contained the *Renilla* luciferase gene under the control of four Gal4 response elements located upstream from a minimal thymidine kinase promoter. The pCMXβgal, a plasmid containing the β-galactosidase gene under the control of the mammalian CMV promoter, was also used as an internal standard. Lipofectamine 2000 (Invitrogen, USA) was used as the cationic lipid. Ligands were added to the wells at various concentrations. Cells were harvested and analyzed for luciferase and β-galactosidase activity. All data points represent the average of triplicate experiments normalized against β-galactosidase activity.

***In silico* Docking Studies**

Molecular modeling was performed as described in Chapter 3.

Fluorescence Microscopy

Confocal microscopy were performed as described in Chapter 3

4.8 References

1. Lehmann, J.M., et al., *The human orphan nuclear receptor PXR is activated by compounds that regulate CYP3A4 gene expression and cause drug interactions.* J Clin Invest, 1998. **102**(5): p. 1016-23.

2. Kliewer, S.A., et al., *An orphan nuclear receptor activated by pregnanes defines a novel steroid signaling pathway.* Cell, 1998. **92**(1): p. 73-82.

3. Rosenfeld, J.M., et al., *Genetic profiling defines the xenobiotic gene network controlled by the nuclear receptor pregnane X receptor.* Mol Endocrinol, 2003. **17**(7): p. 1268-82.

4. Maglich, J.M., et al., *Nuclear pregnane x receptor and constitutive androstane receptor regulate overlapping but distinct sets of genes involved in xenobiotic detoxification.* Mol Pharmacol, 2002. **62**(3): p. 638-46.

5. Nebert, D.W. and F.J. Gonzalez, *P450 genes: structure, evolution, and regulation.* Annu Rev Biochem, 1987. **56**: p. 945-93.

6. Xie, W., et al., *Orphan nuclear receptor-mediated xenobiotic regulation in drug metabolism.* Drug Discov Today, 2004. **9**(10): p. 442-9.

7. Staudinger, J.L., et al., *Regulation of drug transporter gene expression by nuclear receptors.* Drug Metab Dispos, 2003. **31**(5): p. 523-7.

8. Kast, H.R., et al., *Regulation of multidrug resistance-associated protein 2 (ABCC2) by the nuclear receptors pregnane X receptor, farnesoid X-activated receptor, and constitutive androstane receptor.* J Biol Chem, 2002. **277**(4): p. 2908-15.

9. Moreau, A., et al., *Xenoreceptors CAR and PXR activation and consequences on lipid metabolism, glucose homeostasis, and inflammatory response.* Mol Pharm, 2008. **5**(1): p. 35-41.

10. Zhou, C., et al., *Mutual repression between steroid and xenobiotic receptor and NF-kappaB signaling pathways links xenobiotic metabolism and inflammation.* J Clin Invest, 2006. **116**(8): p. 2280-2289.

11. Verma, S., M.M. Tabb, and B. Blumberg, *Activation of the steroid and xenobiotic receptor, SXR, induces apoptosis in breast cancer cells.* BMC Cancer, 2009. **9**: p. 3.

12. Tabb, M.M., et al., *Vitamin K2 regulation of bone homeostasis is mediated by the steroid and xenobiotic receptor SXR.* J Biol Chem, 2003. **278**(45): p. 43919-27.

13. Carnahan, V.E. and M.R. Redinbo, *Structure and function of the human nuclear xenobiotic receptor PXR.* Curr Drug Metab, 2005. **6**(4): p. 357-67.

14. Jones, S.A., et al., *The pregnane X receptor: a promiscuous xenobiotic receptor that has diverged during evolution.* Mol Endocrinol, 2000. **14**(1): p. 27-39.

15. Ekins, S., et al., *Evolution of pharmacologic specificity in the pregnane X receptor.* BMC Evol Biol, 2008. **8**: p. 103.

16. Kliewer, S.A., B. Goodwin, and T.M. Willson, *The nuclear pregnane X receptor: a key regulator of xenobiotic metabolism.* Endocr Rev, 2002. **23**(5): p. 687-702.

17. Watkins, R.E., et al., *The human nuclear xenobiotic receptor PXR: structural determinants of directed promiscuity.* Science, 2001. **292**(5525): p. 2329-33.

18. Noble, S.M., et al., *Human PXR forms a tryptophan zipper-mediated homodimer.* Biochemistry, 2006. **45**(28): p. 8579-89.

19. Ekins, S., et al., *Challenges predicting ligand-receptor interactions of promiscuous proteins: the nuclear receptor PXR.* PLoS Comput Biol, 2009. **5**(12): p. e1000594.

20. Moore, L.B., et al., *Pregnane X receptor (PXR), constitutive androstane receptor (CAR), and benzoate X receptor (BXR) define three pharmacologically distinct classes of nuclear receptors.* Mol Endocrinol, 2002. **16**(5): p. 977-86.

21. Ngan, C.H., et al., *The structural basis of pregnane X receptor binding promiscuity.* Biochemistry, 2009. **48**(48): p. 11572-81.

22. Mani, S., et al., *Activation of the steroid and xenobiotic receptor (human pregnane X receptor) by nontaxane microtubule-stabilizing agents.* Clin Cancer Res, 2005. **11**(17): p. 6359-69.

23. Moore, L.B., et al., *St. John's wort induces hepatic drug metabolism through activation of the pregnane X receptor.* Proc Natl Acad Sci U S A, 2000. **97**(13): p. 7500-2.

24. Mu, Y., et al., *Traditional Chinese medicines Wu Wei Zi (Schisandra chinensis Baill) and Gan Cao (Glycyrrhiza uralensis Fisch) activate pregnane X receptor and increase warfarin clearance in rats.* J Pharmacol Exp Ther, 2006. **316**(3): p. 1369-77.

25. Dussault, I., et al., *Peptide mimetic HIV protease inhibitors are ligands for the orphan receptor SXR.* J Biol Chem, 2001. **276**(36): p. 33309-12.

26. Biswas, A., et al., *Elucidating the 'Jekyll and Hyde' nature of PXR: the case for discovering antagonists or allosteric antagonists.* Pharm Res, 2009. **26**(8): p. 1807-15.

27. Staudinger, J.L., X. Ding, and K. Lichti, *Pregnane X receptor and natural products: beyond drug-drug interactions.* Expert Opin Drug Metab Toxicol, 2006. **2**(6): p. 847-57.

28. Willson, T.M. and S.A. Kliewer, *PXR, CAR and drug metabolism.* Nat Rev Drug Discov, 2002. **1**(4): p. 259-66.

29. Chen, Y. and D. Nie, *Pregnane X receptor and its potential role in drug resistance in cancer treatment.* Recent Pat Anticancer Drug Discov, 2009. **4**(1): p. 19-27.

30. Sane, R.S., et al., *Role of human pregnane X receptor in tamoxifen- and 4-hydroxytamoxifen-mediated CYP3A4 induction in primary human hepatocytes and LS174T cells.* Drug Metab Dispos, 2008. **36**(5): p. 946-54.

31. Baldridge, A., et al., *Activation of fluorescent protein chromophores by encapsulation.* J Am Chem Soc, 2010. **132**(5): p. 1498-9.

32. Baldridge, A., et al., *Steric and electronic effects in capsule-confined green fluorescent protein chromophores.* J Am Chem Soc, 2011. **133**(4): p. 712-5.

33. Baldridge, A., et al., *Recapture of GFP chromophore fluorescence in a protein host.* ACS Comb Sci, 2011. **13**(3): p. 214-7.

34. Lemaire, G., et al., *Identification of new human pregnane X receptor ligands among pesticides using a stable reporter cell system.* Toxicol Sci, 2006. **91**(2): p. 501-9.

35. Watkins, R.E., et al., *Coactivator binding promotes the specific interaction between ligand and the pregnane X receptor.* J Mol Biol, 2003. **331**(4): p. 815-28.

36. Trott, O. and A.J. Olson, *AutoDock Vina: improving the speed and accuracy of docking with a new scoring function, efficient optimization, and multithreading.* J Comput Chem, 2010. **31**(2): p. 455-61.

37. Xiao, L., et al., *Evaluation of in vitro PXR-based assays and in silico modeling approaches for understanding the binding of a structurally diverse set of drugs to PXR.* Biochem Pharmacol, 2011. **81**(5): p. 669-79.

38. Xue, Y., et al., *Crystal structure of the PXR-T1317 complex provides a scaffold to examine the potential for receptor antagonism.* Bioorg Med Chem, 2007. **15**(5): p. 2156-66.

39. Kortagere, S., et al., *Hybrid scoring and classification approaches to predict human pregnane X receptor activators.* Pharm Res, 2009. **26**(4): p. 1001-11.

40. Rickert, E.L., et al., *Synthesis and characterization of fluorescent 4-hydroxytamoxifen conjugates with unique antiestrogenic properties.* Bioconjug Chem, 2010. **21**(5): p. 903-10.

CHAPTER 5

FLUOROPHORES AS LIGANDS FOR THE RETINOIC ACID RECEPTOR ALPHA

5.1 Retinoic Acid Receptor α (RARα)

Retinoids are a class of polyisoprenoids that are the natural or synthetic derivatives of vitamin A [1, 2]. These small molecules are significant for embryonic development and play essential role in physiological functions, such as differentiation, homeostasis, cell growth, carcinogenesis and apoptosis[3, 4]. Their function is linked to the binding to retinoic acid receptors (RARs) and retinoid x receptors (RXRs). These receptors are members of steroid/thyroid hormone nuclear receptor superfamily and function as ligand dependent transcription factors involved in regulating gene networks that control cell growth, differentiation and death. As a member superfamily of nuclear receptors, RAR is a ligand dependent transcription factor with common structure to all nuclear receptors, including N-terminal activation function AF-1, DNA binding domain DBD and C-terminal ligand binding domain LBD (Figure 5.1) [5]. The natural ligand of RAR is all-*trans* retinoic acid (ATRA). RAR and RXR form non – permissive heterodimers, which need RXR ligand 9 - *cis* retinoic acid to respond to RAR's ligands [6]. A number of synthetic ligands are used as therapeutic agents for many RAR-related diseases, such as tazarotene, AGN195183, R667 and tretinoin (Figure 5.2) [7]. However, some retinoids that are pan-specific for all RAR isotypes, are also toxic, as in the case of ATRA. This ligand is a successful drug for acute promyelocytic leukemia (APL), but also increases the level of serum and causes bone toxicity [8, 9]. Therefore, the discovery of

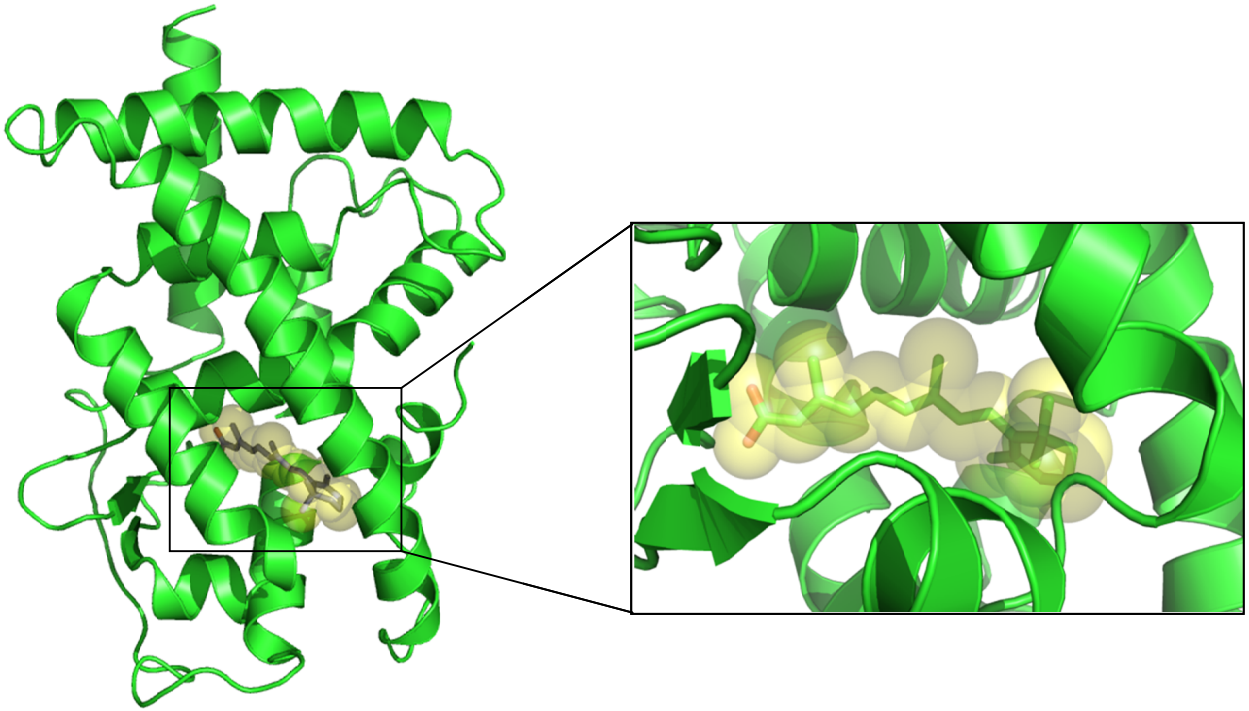

Figure 5.1 Crystal structure of the LBD of RAR*α* with all-*trans* retinoic acid. The ligand is shown in yellow space filling.

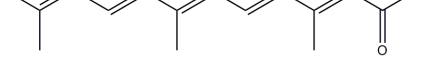

All-trans retinoic acid

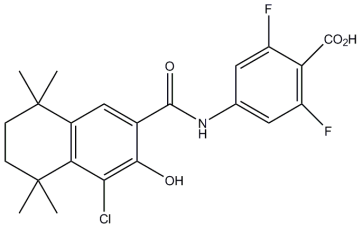

AGN 195183

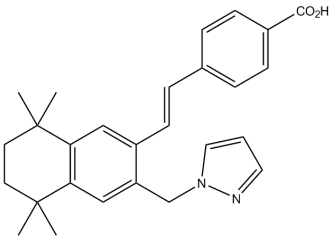

R667

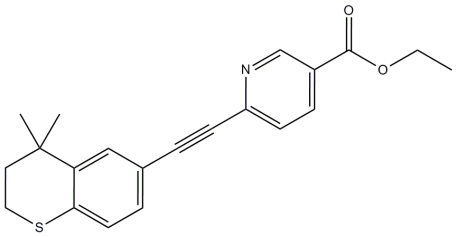

Tazarotene

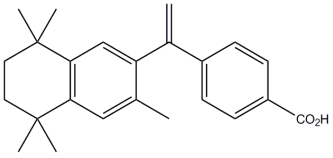

Bexarotene

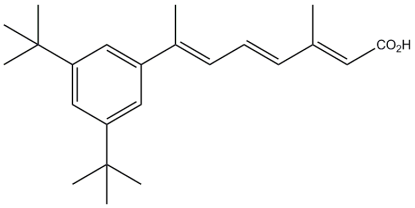

LGD 1550

Figure 5.2 RAR ligands which are approved for therapy.

RAR isotype-selective modulators are essential for developing therapeutics with decreased number of significant side effects.

Retinoic acid receptor has three isotypes known as α, β and γ [10-12]. They are encoded by separate, highly conserved genes, resulting in each isotypehaving a unique function [8]. RARα is predominatnly involved in skin differentiation, hence its involvement in acute promyelocytic leukemia (APL) by unregulated differentiation of leukemic cells [13, 14]. RARβ is responsible for embryogenesis and is also known as a suppressor of growth of different cell types and is silenced in various cancers [15]. On the other hand, RARγ is implicated in many skin diseases such as a skin cancer, acne and also in photoaging [16-18].

The ligand binding pocket of all RAR isotypes is predominantly hydrophobic. The hydrophobic ring of the retinoid is accommodated inside the ligand binding pocket in such way to create contacts with helix 11. However, the other side of the retinoid which contains polar groups interacts with helix 3 and helix 5. The RAR isotypes differ about 51 amino acids in the LBD [19]. However, these isotypes differ in only about three residues in ligand binding pocket. RARα and RARβ diverge by only one residue in helix 3 (S232 in RARα, A225 in RARβ). However, RARβ and RARγ differ by two residues, one in helix 5 (I263 in RARβ, M272 in RARγ) and other in helix 11 (V398 in RARβ, A397 in RARγ) [19-21]. As with most nuclear receptors, there is a lack of a deeper understanding of the mobility and trafficking of these receptors. Specific questions regarding the mobility of these receptors within the cell still exist, especially in relation to their function as transcription factors. Furthermore, understanding the trafficking of these receptors upon binding of agonist or antagonists, and on a time dependent scale can

provide insight into the natural function of these proteins, as well as their role in the various diseases. Using techniques, such as fluorescence, can be used as powerful tools for investigating RAR function *in vivo*. In particular, fluorescent probes were reported based on the hydrophobic ring of the retinoid ligand and a fluorescent dansyl moiety (tetrahydrotetramethylnaphatalenyl). These probes were designed to bind RARα and display fluorescence. As shown in Figure 5.3, these designed compounds DAM-3, ADAM-3 and DAM-15 were built based on the core of known RARα ligands AM580 and AM80, where binding studies were shown that these compounds were able to bind to the receptor. The use of the tetrahydrotetramethylnaphatalenyl moiety allowed for these probes to have a high binding affinity for the receptor. However, the dansyl moiety, which is responsible for the fluorescence, is bulky and is positioned outside of the ligand binding pocket. The location of this moiety on the surface of the protein could influence the natural function of these receptors and their interactions with other transcription factors. Activation profiles on these compounds were not reported, and this is most likely due to the fact that the bulky nature of the dansyl moiety and its location on the surface of the protein, disrupted the natural function of these receptors and prevented the specific interactions with coactivators and other transcriptional regulators. Due to their implications in several diseases, and the success of both RAR agonists and antagonists as therapeutics towards these various diseases, discovering potential new ligands for these receptors are greatly beneficial. In addition to discovering a potential new class of ligands for these receptors, if these molecules have the ability to fluoresce upon binding to the receptor, they could serve as potential probes for analyzing the mobility of RAR in cells. Thus, the goal of this work is the development of fluorescent ligands for RARα, which

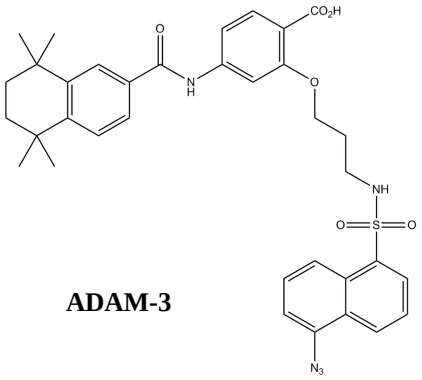

ADAM-3

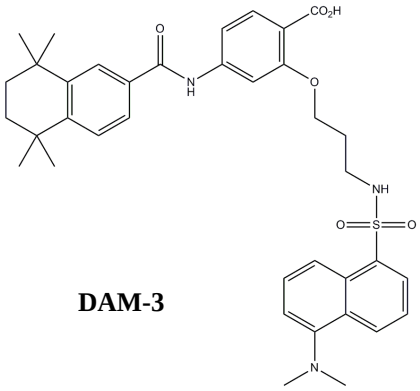

DAM-3

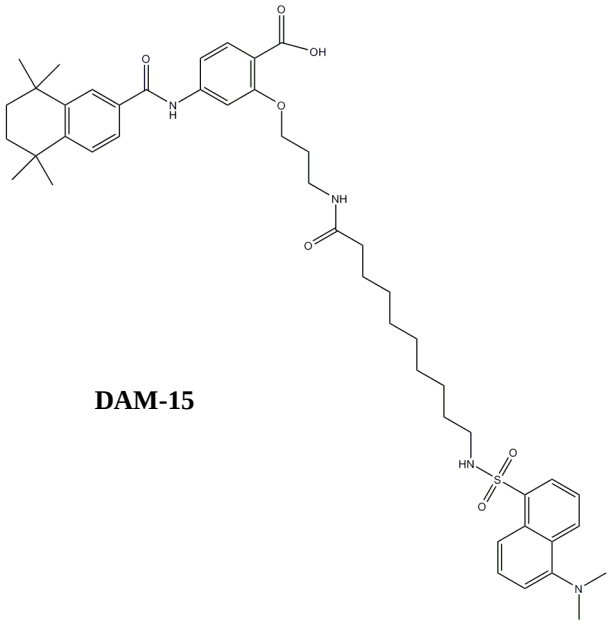

DAM-15

Figure 5.3 Structure of the fluorescent probes for RARα.

will be able to exhibit fluorescence upon the binding to the receptor. As previously described in Chapter 3 and 4, the goal of this work is development of fluophores based on the arylmethyleneimidazolodinone (AMI), the GFP chromophore for various nuclear receptors.

5.2 Fluophores Design for RARα

Analysis of known RARα ligands and properties of the ligand binding pocket of this receptor led us to design the RARα ligands based on AMI core. Incorporation of known retinoid moiety into AMI core could provide an opportunity to develop novel RARα agonists which will bind and activate the receptor and also fluoresce upon binding. Thus, our design of RARα AMI was subjected to molecular modeling to determine possible interactions of AMI with LBP.

5.2.1 Molecular Modeling of Designed RARα AMI

To determine if AMIs were a potential class of ligands for RARα, the core AMI molecule was modeled into the crystal structure of RARα LBD using modeling program Autodock Vina. As shown in Figure 5.4B, AMI-1 was modeled inside the ligand binding pocket. However, upon superimposition with the ligands of the solved crystal structures, DAM-3 or all-*trans* retinoic acid, the AMI derivatives did not occupy the entire volume in comparison to those ligands. In particular, the hydrophobic part of the RARα pocket seemed void, perhaps eliminating the hydrophobic contacts necessary for the receptor/ligand interactions. Structural studies of known RARα ligands, had previously shown that these hydrophobic contacts, especially the hydrophobic ring system of the ligands with helix 11, were critical for agonistic function, hence why most RAR agonists

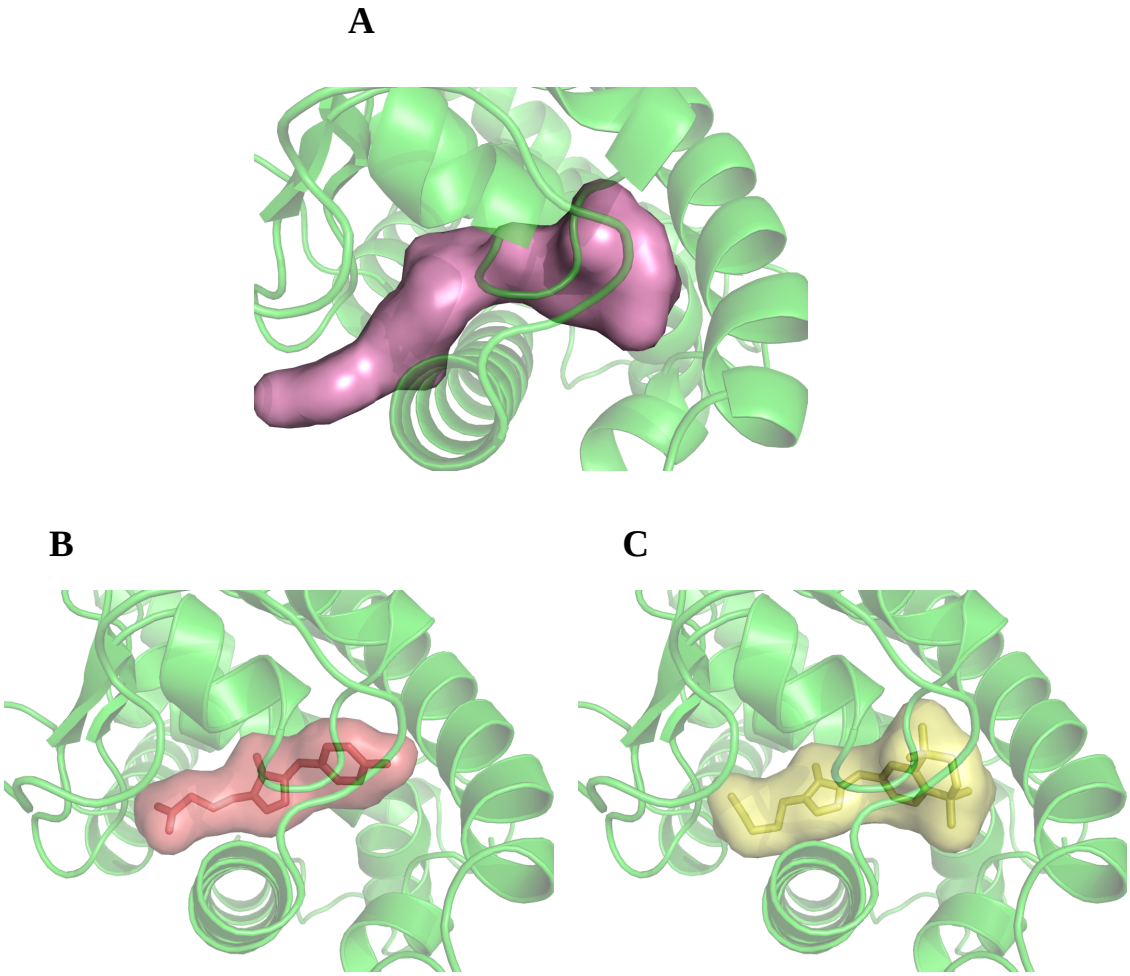

Figure 5.4 Modeling of RARα LBD crystal structure with the DAM-3 and AMIs. **A** Docked structure of DAM-3, represented in space filling, **B.** Docked structure of AMI-1 (red) **C.** Docked structure of AMI-2

are designed based on tetrahydrotetramethylnaphatalenyl moiety, which is able to fill the hydrophobic part of the pocket. In addition to the hydrophobic contacts, several hydrogen bonds are present that need to be maintained to fill the requirement as a RAR ligand. The hydrogen bonds exist between a few residues in the end of the ligand binding pocket, close to the surface of the protein and carboxylate moiety of the ligand. It has been previously shown that a water molecule and the side chains of arginine R278 and serine S289 create a hydrogen bonding network with the carboxylate moiety of the ligand [22, 23]. Based on this knowledge, an AMI derivative (AMI-2) was designed to incorporate tetrahydrotetramethylnaphatalenyl moiety as part of its core and carboxylic acid on the alkyl chain to create interaction with polar residues in the end of the pocket (Figure 5.5).

AMI-2 was modeled into the RARα ligand binding pocket and as shown in Figure 5.4C a similar conformation is observed with this AMI derivative and other known RAR ligands. The hydrophobic part of the pocket is able to accommodate the tetrahydrotetramethylnaphatalenyl moiety of new AMI (AMI-2) in similar manner as DAM-3. The modeling data also suggested that the designed AMI-2 is able to create hydrogen bonding with R278 and S289 by carboxylate group in R_1 position of AMI core (Figure 5.6). These results indicated that AMI-2 should be able to bind RARα. To validate this theoretical study, AMI-2 was synthesized using method described previously in Chapter 2.

5.2.2 Evaluation of Designed RARα AMI in Chemical Complementation

With the same methodology that was described previously for hERα and PXR, AMI-2 was tested for activation with RAR, first in yeast. Chemical complementation was used. Two plasmids pGBDRARα, carrying the Gal4DBD fused to the RARα LBD and

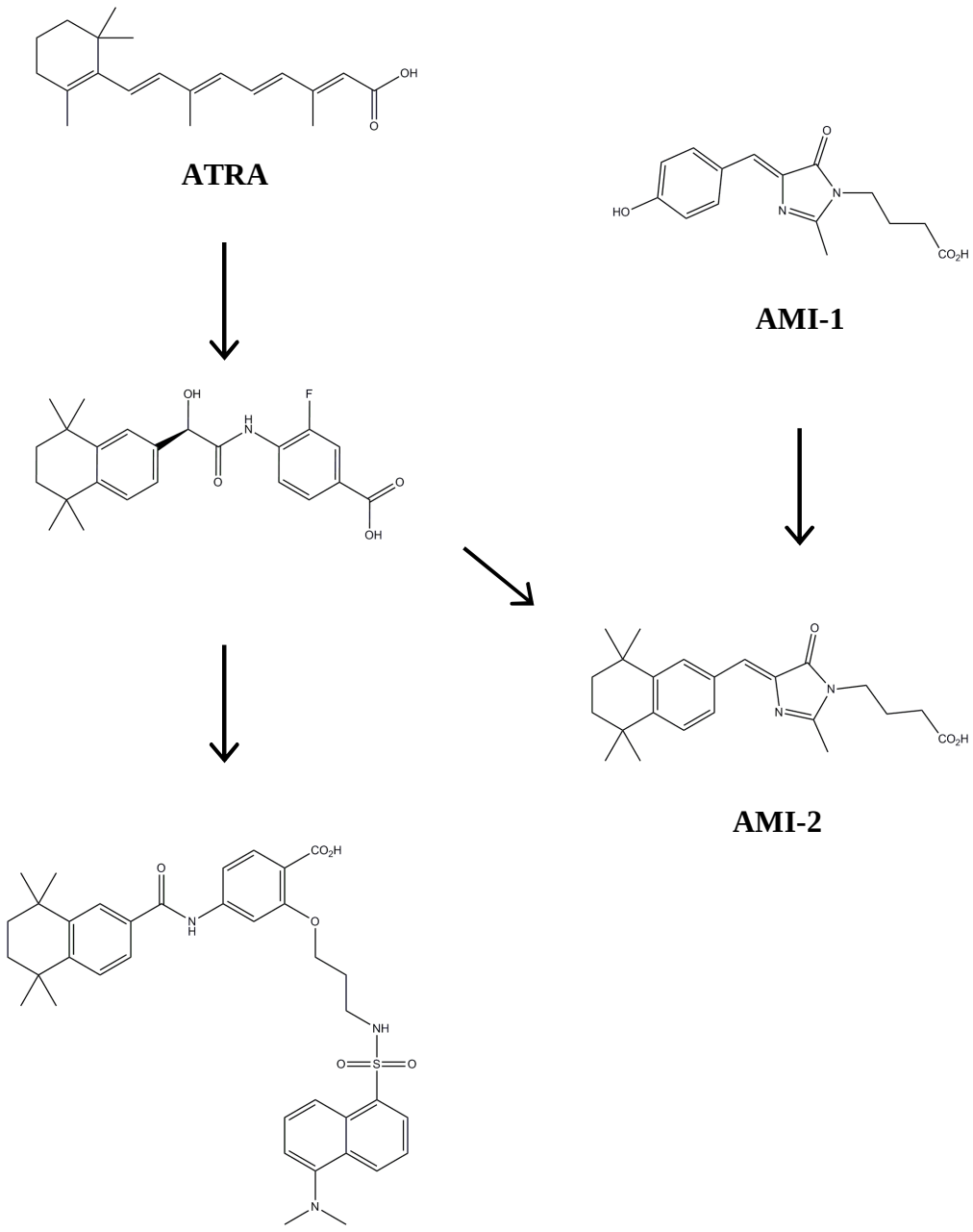

Figure 5.5 Scheme of design strategy for RARα selective AMI

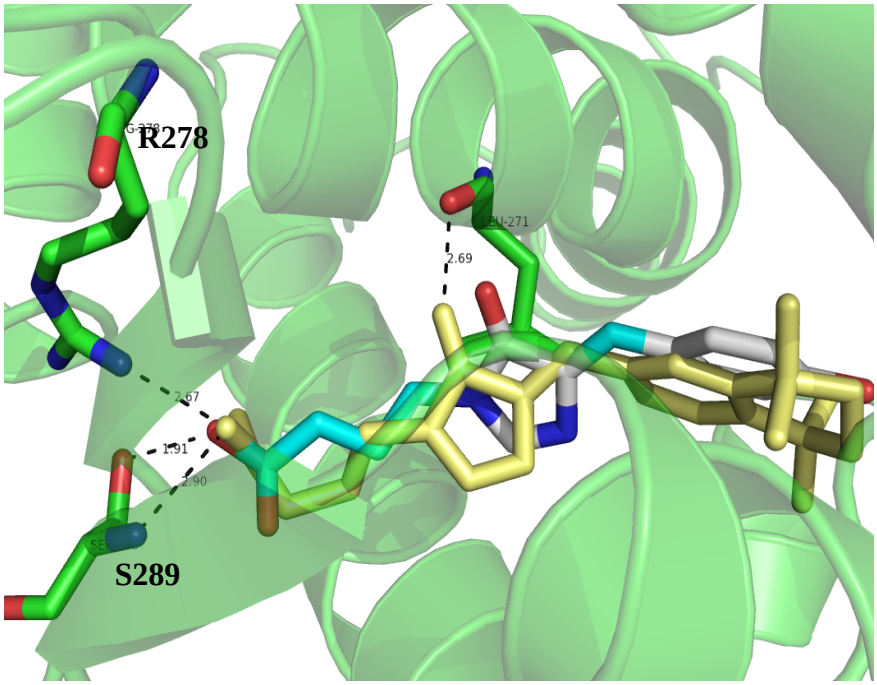

Figure 5.6 Modeling of RAR LBD crystal structure with the AMI-2.

pGAD10BAACTR containing GAD10AD fused to coactivator ACTR were co-transformed into the PJ69-4A yeast strain. Liquid quantitation assays of chemical complementation was used for testing activation profile of novel AMI as previously was it described in Chapter 3. In 96 well plate, yeast expressing RARα were growing in adenine selective media without the ligand as well as with varying concentration of the AMI.As a positive control, the Gal4, ligand independent yeast transcription factor was used. Yeast expressing RARα were also tested with its natural ligand ATRA to validate the assay. After 48 h incubation at 30°C, the yeast ligand activated growth which is linked to activation RARα was detected by reading optical density at wavelength 630 nm.

As expected, the yeast with Gal4 displayed growth in selective media with and without the ligand. The ligand activated growth was observed with ATRA as seen in Figure 5.7.When the AMI was tested for activation with RAR, no ligand activated growth was observed. This result was quite surprising due to the fact that the modeling of the AMI into the binding pocket seemed promising. However, the modeling presents only theoretical position of ligand in the pocket and this representation maybe not be accurate. This AMI could indeed activate the other isotypes of RAR, beta or gamma, since these isotypes do slightly vary in their ligand preferences.

5.3 Screening of Library of Fluophores using chemical complementation

As previously mentioned in Chapter 3 and 4 several specific AMIs were identified to activate ERα and PXR. Besides activation these novel compounds were able to display fluorescence upon binding receptor. The same library of AMI derivatives was tested for activation with RARα, in the chemical complementation;liquid assay was used. Yeast

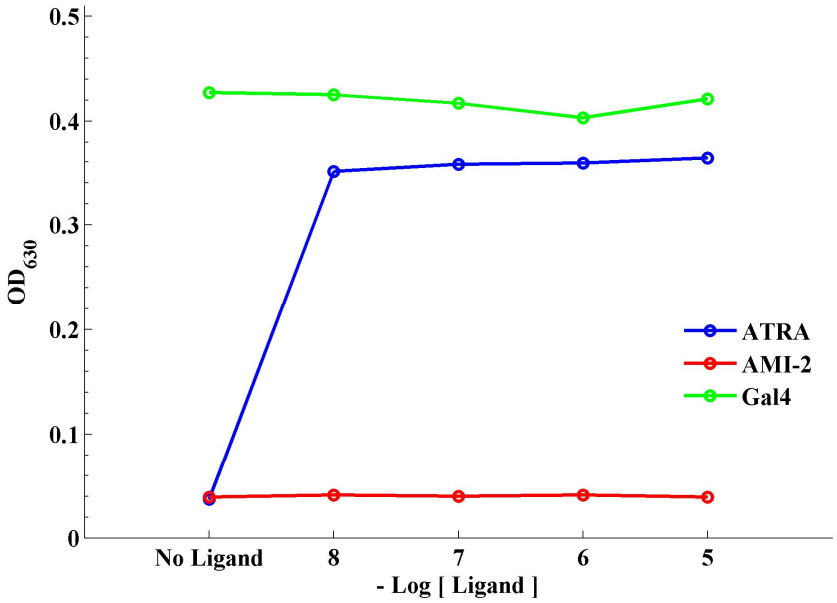

Figure 5.7 Activation profile of RARα with designed AMI-2. ATRA and Gal4 are used as positive controls.

expressing RARα were tested with library of AMI including 10 μM of 95 ligands and with its natural ligand, ATRA. The 96 well plates, with the PJ69-4A yeast strain expressing nuclear receptor and coactivator were incubated at 30 ℃ by 48h.

Of the 95 compounds tested, four showed ligand activation growth. AMI 42, 85 and 109, as well as all-*trans* retinoic acid displayed 17 fold activation,. However, AMI 100 showed slightly lower response with 14 fold activation (Figure 5.8). Figure 5.9 presents the structure of four AMIs, potentially novel class of RAR agonists. Three of four ligands share similar structure. They have incorporated a biphenyl moiety in the AMI core. These initial results were surprising due to the lack of the tetrahydrotetramethylnaphatalenyl moiety, which is normally present in many RAR ligands and is responsible for creating hydrophobic contacts in ligand binding pocket. However, AMI 42 displays totally different structure from other 3 ligands. To evaluate the interactions of these compounds with RARα, AMIs were subjected to further testing.

Overall, the screening of AMI library using chemical complementation assay in yeast led to discovery of the few RARα ligands.

5.4. Evaluation of Fluophores interactions with RARα in yeast

To determine the sensitivity of these compounds for the receptor, a dose response assay was performed in yeast. The ligands were tested with RARα at varying ligand concentrations, ranging from 1 nM to 10 μM. As a control, ATRA was used also at varying concentrations.

As expected ATRA, the natural ligand of RAR showed activation in all tested concentrations. As shown in Figure 5.10 three AMI compounds displayed activation with RARα, as seen with AMI 100 and 109 at 100 nM with EC_{50} 200 and 350 nM,

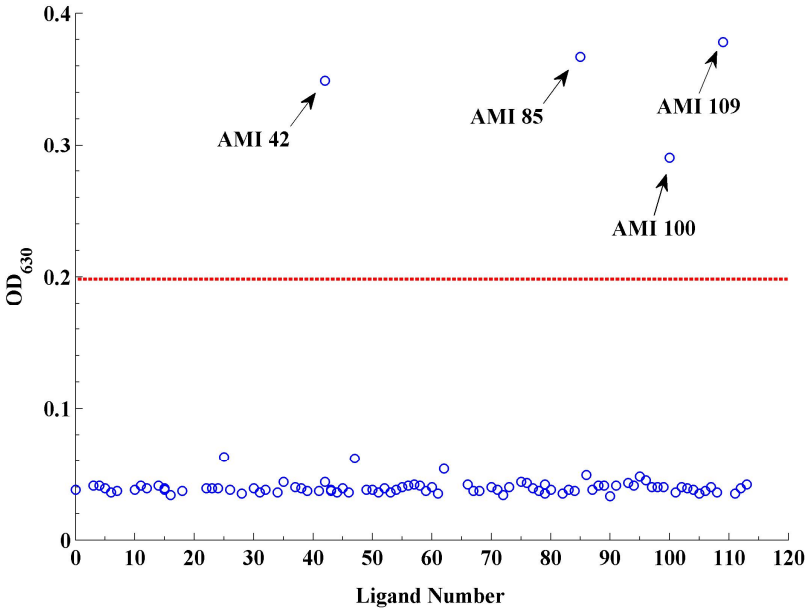

Figure 5.8 Nuclear receptor screening using chemical complementation in yeast. Library of 95 AMIs was tested with yeast expressing RARα

respectively based on growth with a relatively similar fold activation. AMI 85 showed decreased sensitivity in comparison to AMI 100 and 109 with an ~EC_{50} >10 μM. AMI 42 did not display ligand activation growth.

In looking at the structure of these molecules, the lack of activation observed with AMI-42 was not surprising due to the differences in the structure of this AMI derivative in comparison to the other compounds. However, the remaining three compounds that showed activation with RARα, all have a similar structure, incorporating a biphenyl group into AMI core. In doing a literature analysis, there had been reports were ligands based on the alkylbiphenyls has been reported to activate RARα [24, 25]. Specifically, novel RARβ agonists that were designed based on the biphenyl groups were reported. Derivatives of the 4'octyl-4-biphenylcarboxylic acid were synthesized with different length of the alkyl chain [24, 25]. The number of the carbons in the alkyls chain had been shown to have influence on activation level. Increasing length of alkyl chain showed increased in transcriptional activity. There is possibility that AMIs are able to activate RARα due to the presence of biphenyl. Based on hydrophobicity of the ligand binding pocket, probably incorporated to AMI biphenyl with alkyl chain is able to create hydrophobic contacts in the LBP.

The same trend and observations were present with these AMIs. In the case of AMI 85, in which the replacement of the alkylbenzene group with an alkoxybenzene group, a decrease in sensitivity was observed. This is expected due to the increased hydrophobicity of the phenyl groups, confirming the importance of the hydrophobic nature of compounds that are desgined as agonists for the RARs. In addition to the alkylbiphenyl, the length of the alkyl groups was crucial for activation level. AMI 109

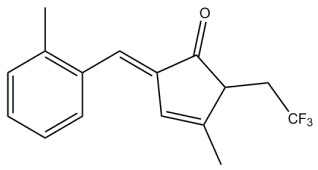

42

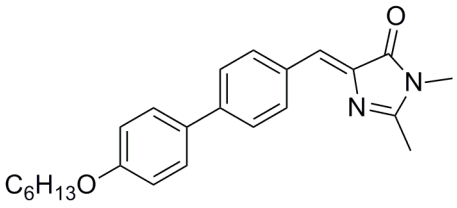

100

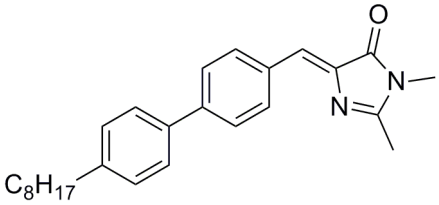

109

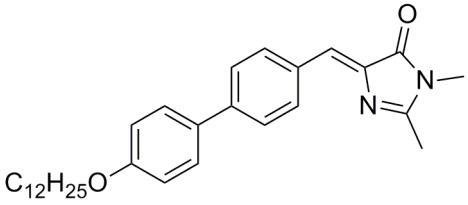

92

Figure 5.9 Structures of potential AMI agonist for RARα

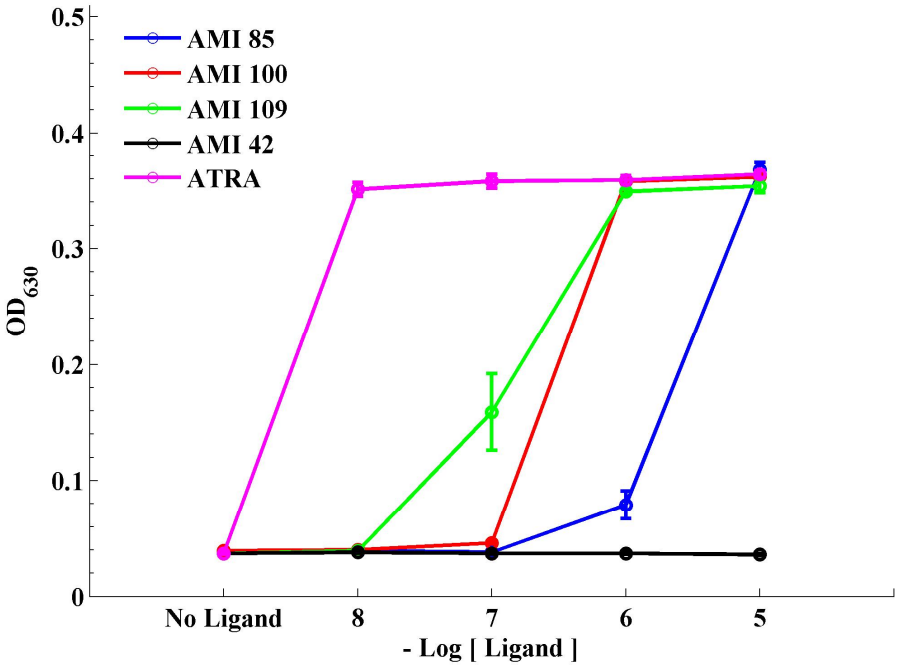

Figure 5.10 Activation Profile of RARα AMIs in yeast

with five carbons in its alkyl group displayed a higher sensitivity in comparison to chromophore 100 with eight carbons in this position.

To further analyze the importance of the number of carbons in the alkyl group and correlating this relationship with activation, several additional RARα agonists with shorter alkyl chains were designed and synthesized. Based on the previous results (Figure 5.10) which indicated that the highest ligand activated growth was displayed with a pentyl chain (AMI 109) and that increasing the number of the carbons decreased activation level, the upper end of the range had been determined to be five carbons. However, the lower end of the range was yet to be determined, as well as whether an alkyl chain even needed to be present in order to get any activation. Therefore, AMI 129 with a propyl group was synthesized and AMI 153 which lacked an alkyl chain was also synthesized. The question of the hydrophobicity was also evaluated, where the hydrophobicity was increased with AMI 92 where a twelve carbon alkoxyl chain was synthesized (Table 5.1). These compounds were then tested in yeast once again using the liquid quantitation assay of chemical complementation as described previously.

As shown in Figure 5.11 novel ligands for RARα were not able to display higher activation than AMI 109 (EC_{50}= 220 nM) . Several conclusions were made. First decreasing the number of carbons of the alkyl chain perhaps failed to create sufficient contacts with the residues in the pocket. AMI 129 containing propyl group has EC_{50} of 160 nM in comparism to AMI 100 (EC_{50}= 280 nM) with octyl chain indicating that the presence of the alkyl group is necessary for sensitivity with the receptor. This was further confirmed when AMI 153 was tested, and the lack of the alkyl group in this compound lead to much much higher EC_{50}, (EC_{50}= 3 μM) in comparison to the other AMI

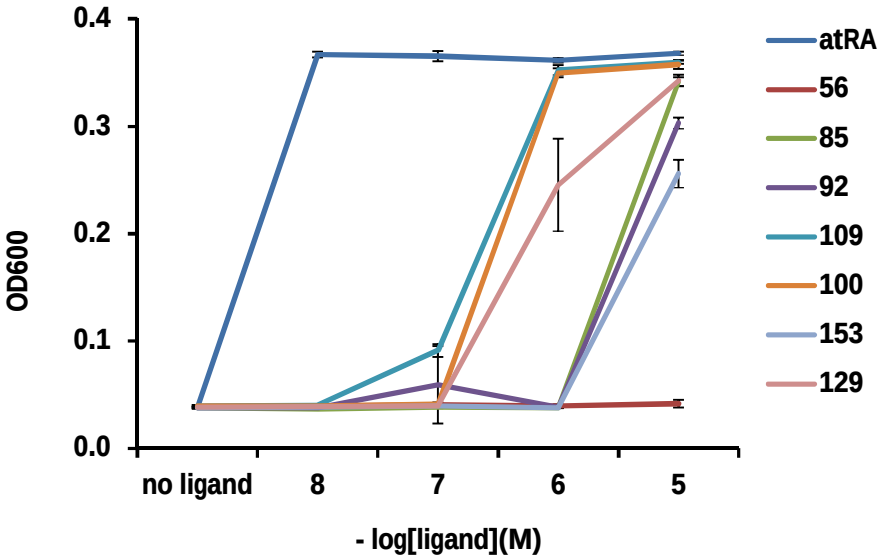

Figure 5.11 Activation Profile of various RARα AMIs.

Table 5.1 Structures of the RARα AMI agonists

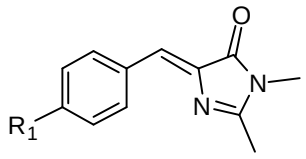

AMI	R_1
56	H
153	Ph
129	Ph-C_3H_7
109	Ph-C_5H_{11}
100	Ph-C_8H_{17}
85	OC_6H_{13}
92	$OC_{12}H_{25}$

derviatives. These results indicate that pentyl chain seems to provide the ideal interactions that are necessary from the group of compounds that have been synthesized. The hydrophobic nature of the compounds seems to once again play a profound role in the sensitivity that is observed. AMI 92 (EC_{50}= 3 μM), which contains the twelve carbon alkoxyl chain, shows comparable activation to AMI 153 (EC_{50}= 3 μM), but these compounds show reduced activation in comparison the the compounds containing the alkyl chains. Therefore, the decrease in activation by introducing a polar group to the end of the alkyl chain reduces the hydrophobic nature of these compounds as expected.

5.5 Molecular Modeling of Fluophores

To gain further insight into the differences in the contacts that are created between the receptor and these derivatives, the AMIs were docked into the ligand binding pocket of RARα using AutoDock Vina. The crystal structure of the RARα LBD with BMS961 was used for modeling due to the similar size of the ligands (PDB:4LBD) [26]. The AMIs that were tested for activation in yeast were all docked and the results of the docking was analyzed.

As shown in Figure 5.12 all of the ligands were modeled into the ligand binding pocket and were superimposable with the BMS961 ligand. Interestingly, the alkyl chain superimposed directly onto the position of the tetrahydrotetramethylnaphatalenyl moiety of the BMS961 ligand, which suggests that the main function of the alkyl chain is satisfying the necessary hydrophobic interactions in that part of the binding pocket, as seen in the case of the pentyl chain of AMI 109. This could also perhaps explain why AMI 153, which lacks the alkyl chain, did not display any activity. It is unable to fulfill those necessary contacts which is generally filled by the the

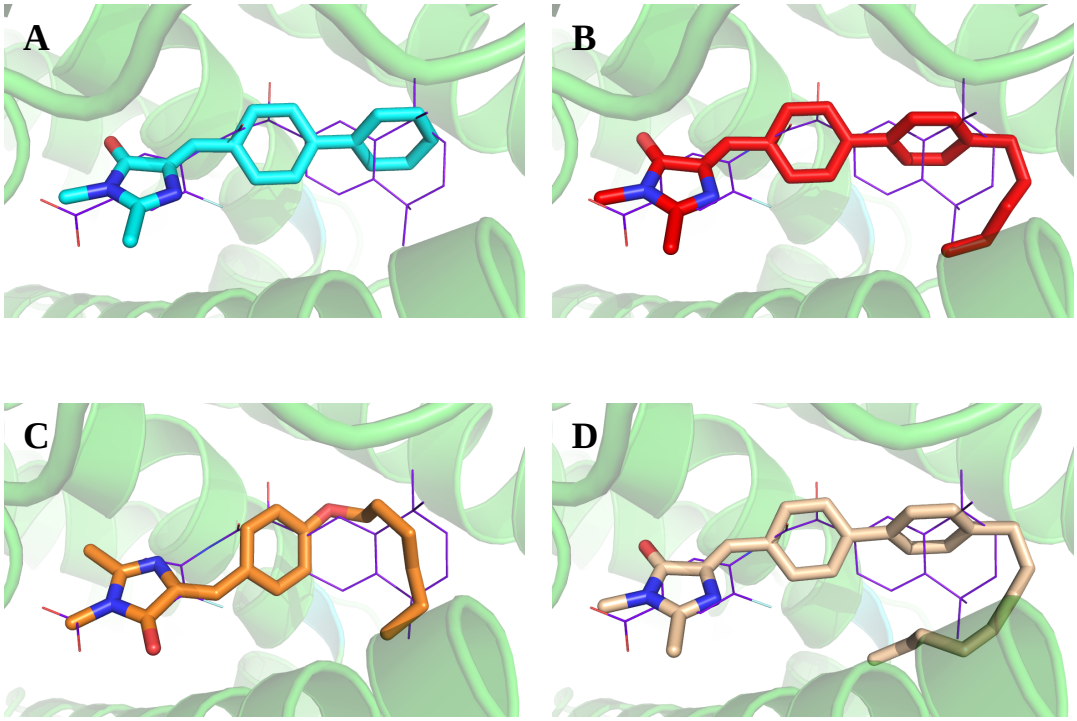

Figure 5.12 Modeling of RAR LBD crystal structure, BMS961 (purple) is used for overlay with docked structure, **A.** AMI 153, **B.** AMI 109, **C.** AMI 85, **D.** AMI 100

tetrahydrotetramethylnaphatalenyl moiety or alkyl chain as it is in case of AMIs. On the other hand, in the presence of an alkoxyl chain, there was a shift in the position of these ligands, indicating a plausible reason for the decreased sensitivity that is observed with the presence of the alkyoxy chain.

Hence, the experimental and computational data corroborate the hypothesis that interaction between the alkyl chain of the AMI and hydrophobic part of the ligand binding pocket is essential for activation. Thus, incorporation of the alkylbenzene moiety into AMI core can benefit in discovery novel potential RARα agonists and can replace of position of the tetrahydrotetramethylnaphatalenyl moiety as a major building block of the RAR ligand. This could provide a new structural base for developing novel RAR ligands, and perhaps even a new class of drugs for RAR- based disease.

5.6 Visualization of RARα in yeast

As described in previous chapter, the part of the goal of this work was development of the novel ligands which will not be only potential nuclear receptor agonists but also will be able to fluoresce upon binding into receptor.

The AMIs that were tested for activation were also tested for fluroscence in yeast. The plasmid pGBDRARα, contained the Gal4DBD fused to the RARα LBD was co-transformed with pGAD10BAACTR containing GAD10AD fused to coactivator ACTR into the PJ69-4A yeast strain. Yeast expressing RARα, were incubated in adenine selective media with AMI at 30 °C. After 48h of incubation, yeast were washed to remove any remaining media. As a control, yeast lacking the plasmid pGBDRARα were incubated with AMIs to detect the any background fluorescence.

As shown in Figure 5.13 yeast expressing the RARα and incubated only with AMI 100 and 109 displayed the fluorescence. Yeast without RARα shows slight background fluorescence due to the known auto fluorescence that exists with yeast..An interesting fact that was observed is that only the AMI derivatives that contain an alkyl chain showed any fluorescence (AMI 100 and 109). AMIs with alkoxyl chain did not display fluorescence. Again, in looking back at the modeling that was observed, this could perhaps conclude that for fluroscence, a certain conformation must be adopted. Since the conformation of the alkyoxy compounds was different in the binding pocket in comparison to the alkyl chains, this suggests that alkyl chain adopts the preferable conformation for "turning on" fluorescence. Further structural analysis, such as obtaining a crystal structure, needs to be obtained.

5.7 Summary

In addition to ERα and PXR, we have discovered novel AMI agonists for RARα. These initial studies had shown that incorporation of biphenyl group into AMI core is able to create affinity of AMI to RARα. However, to enhance this activity introduction of the alkyl chain is necessary. The pentyl chain of AMI 109 creates significant contacts in hydrophobic part of the pocket. Decreasing or increasing the number of the carbons in the alkyl chain lead to significant undesired change in EC_{50}. Additionally, the replacement of the alkyl by alkoxyl chain leads to decreasing activation.

Furthermore, AMI 100 and 109 displayed fluorescence in yeast, indicating that these molecules could indeed be fluorogens for RARα, which could provide a powerful mechanism for analyzing cell trafficking and mobility of these receptors.

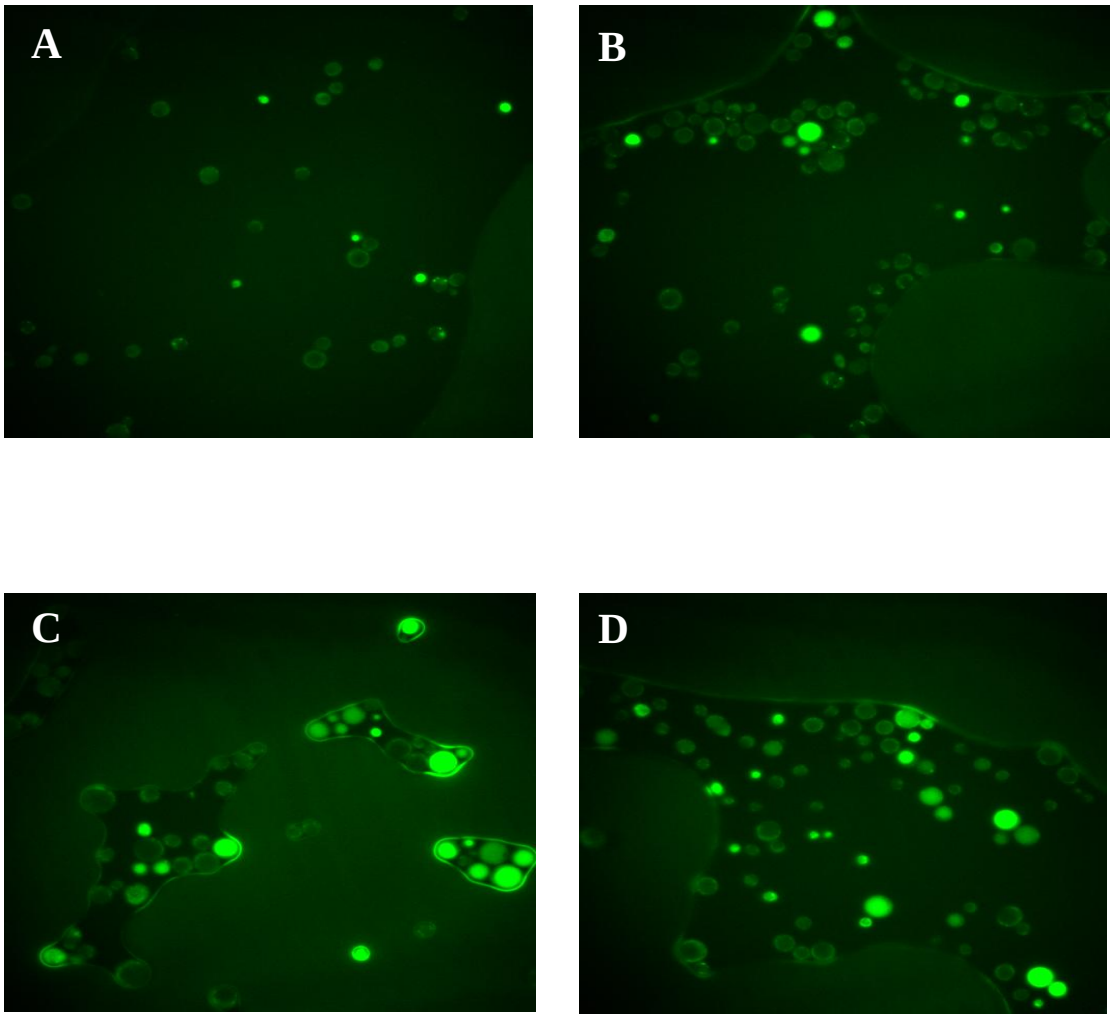

Figure 5.13 Fluorescence microscopy of RARα AMIs in yeast. Yeast expressing RARα (C and D) or Gal4 (A and B) were incubated with various AMIs. A.and C (109), B and D (100).

5.8 Materials and Methods

Ligands

9-*cis* retinoic acid (MW=300.44 g/mol) was purchased from ICN Biomedicals (Aurora, OH), T0901317 (481.3 g/mol) from Cayman Chemicals (Ann Arbor, MI), all-*trans* retinoic acid (MW=300.44 g/mol) from Biomol Inc (Plymouth Meeting, PA), lithocholic acid from MP Biomedicals, LLC (Solon, OH).

The library of AMIs was synthesized by Dr. Anthony Baldridge. Method of synthesize was described previously in Chapter 2.

Yeast transformation

The plasmids pGBDRARα, pGBDRXRα, pGBDERα, pGBDrERβ, pGBDLXRβ, pGBDVDR, pGBDCAR, pGBDFXR and pGBDPPARγ and coactivator plasmids pGADACTR or pGADSRC-1were transformed in the PJ69-4A strain using the TRAFCO yeast transformation protocol. The transformation mixture was placed onto nonselective plates (SC-LW). Plates were incubated at 30 °C for 3 days.

Liquid Quantitation Assay

Colonies from the yeast transformation were grown overnight in nonselective media SC-LW, at 30 °C, shaking at 300 rpm. Yeast were pelleted by centrifugation and resuspended in selective media SC-ALW with 10 µM or a range of ligand concentration and placed in 96-well plates. Plates were then incubated at 30 °C, shaking at 170 rpm for 48 hours. After 0, 24, and 48 hours optical density readings were taken at a 630 nm wavelength.

In silico Docking Studies

Molecular modeling was performed as described in Chapter 3.

Fluorescence Microscopy

The PJ69-4A strain expressing RARα was incubated in selective media SC-ALW with RARα AMIs, at 30 °C, shaking at 300 rpm. After incubation yeast were pelleted by centrifuging and resuspended in distill steril water. Cells were again centrifuged and resuspended in water. Next the cell were displayed under fluorescent microscope and analyzed for green fluorescence.

5.9 References

1. Tang, X.H. and L.J. Gudas, *Retinoids, retinoic acid receptors, and cancer.* Annu Rev Pathol, 2011. **6**: p. 345-64.

2. Theodosiou, M., V. Laudet, and M. Schubert, *From carrot to clinic: an overview of the retinoic acid signaling pathway.* Cell Mol Life Sci, 2010. **67**(9): p. 1423-45.

3. Altucci, L. and H. Gronemeyer, *The promise of retinoids to fight against cancer.* Nat Rev Cancer, 2001. **1**(3): p. 181-93.

4. Germain, P., et al., *Overview of nomenclature of nuclear receptors.* Pharmacol Rev, 2006. **58**(4): p. 685-704.

5. de Lera, A.R., et al., *Design of selective nuclear receptor modulators: RAR and RXR as a case study.* Nat Rev Drug Discov, 2007. **6**(10): p. 811-20.

6. Forman, B.M., et al., *Unique response pathways are established by allosteric interactions among nuclear hormone receptors.* Cell, 1995. **81**(4): p. 541-50.

7. Altucci, L., et al., *RAR and RXR modulation in cancer and metabolic disease.* Nat Rev Drug Discov, 2007. **6**(10): p. 793-810.

8. Busby, S.A., et al., *Identification of a novel non-retinoid pan inverse agonist of the retinoic acid receptors.* ACS Chem Biol, 2011. **6**(6): p. 618-27.

9. Simoni, D., *Retinoic acid and analogs as potent inducers of differentiation and apoptosis. New promisingchemopreventive and chemotherapeutic agents in oncology.* Pure Appl. Chem, 2001. **73**(9): p. 1437-1444.

10. Petkovich, M., et al., *A human retinoic acid receptor which belongs to the family of nuclear receptors.* Nature, 1987. **330**(6147): p. 444-50.

11. Brand, N., et al., *Identification of a second human retinoic acid receptor.* Nature, 1988. **332**(6167): p. 850-3.

12. Krust, A., et al., *A third human retinoic acid receptor, hRAR-gamma.* Proc Natl Acad Sci U S A, 1989. **86**(14): p. 5310-4.

13. Fenaux, P., Z.Z. Wang, and L. Degos, *Treatment of acute promyelocytic leukemia by retinoids.* Curr Top Microbiol Immunol, 2007. **313**: p. 101-28.

14. Raelson, J.V., et al., *The PML/RAR alpha oncoprotein is a direct molecular target of retinoic acid in acute promyelocytic leukemia cells.* Blood, 1996. **88**(8): p. 2826-32.

15. Widschwendter, M., et al., *Methylation and silencing of the retinoic acid receptor-beta2 gene in breast cancer.* J Natl Cancer Inst, 2000. **92**(10): p. 826-32.

16. Nagpal, S., et al., *Negative regulation of two hyperproliferative keratinocyte differentiation markers by a retinoic acid receptor-specific retinoid: insight into the mechanism of retinoid action in psoriasis.* Cell Growth Differ, 1996. **7**(12): p. 1783-91.

17. Spanjaard, R.A., et al., *Specific activation of retinoic acid receptors (RARs) and retinoid X receptors reveals a unique role for RARgamma in induction of differentiation and apoptosis of S91 melanoma cells.* J Biol Chem, 1997. **272**(30): p. 18990-9.

18. Wang, Z., et al., *Ultraviolet irradiation of human skin causes functional vitamin A deficiency, preventable by all-trans retinoic acid pre-treatment.* Nat Med, 1999. **5**(4): p. 418-22.

19. Gehin, M., et al., *Structural basis for engineering of retinoic acid receptor isotype-selective agonists and antagonists.* Chem Biol, 1999. **6**(8): p. 519-29.

20. Ostrowski, J., et al., *Serine 232 and methionine 272 define the ligand binding pocket in retinoic acid receptor subtypes.* J Biol Chem, 1998. **273**(6): p. 3490-5.

21. Alvarez, S., et al., *Retinoid receptor subtype-selective modulators through synthetic modifications of RARgamma agonists.* Bioorg Med Chem, 2009. **17**(13): p. 4345-59.

22. Klaholz, B.P., A. Mitschler, and D. Moras, *Structural basis for isotype selectivity of the human retinoic acid nuclear receptor.* J Mol Biol, 2000. **302**(1): p. 155-70.

23. Renaud, J.P., et al., *Crystal structure of the RAR-gamma ligand-binding domain bound to all-trans retinoic acid.* Nature, 1995. **378**(6558): p. 681-9.

24. Lund, B.W., et al., *Discovery of a potent, orally available, and isoform-selective retinoic acid beta2 receptor agonist.* J Med Chem, 2005. **48**(24): p. 7517-9.

25. Lund, B.W., et al., *Design, synthesis, and structure-activity analysis of isoform-selective retinoic acid receptor beta ligands.* J Med Chem, 2009. **52**(6): p. 1540-5.

26. Trott, O. and A.J. Olson, *AutoDock Vina: improving the speed and accuracy of docking with a new scoring function, efficient optimization, and multithreading.* J Comput Chem, 2010. **31**(2): p. 455-61.

CHAPTER 6

FLUOPHORES AS LIGANDS FOR THE RETINOID X RECEPTOR AND OTHER NUCLEAR RECEPTORS

6.1 Retinoid X Receptor alpha

Besides the RAR, retinoid signaling pathway is mediating, by other retinoid receptors, such as the retinoid X receptor (RXR) [1]. The RXR is involved in regulation of organogenesis, cell proliferation and differentiation[1-3]. RXR has three subtypes, RXRα, β and γ which are coded by separate genes. Thus, distribution of the isotypes is tissue specific. RXRα is expressed dominantly in liver, skeletal muscles and skin and the RXRβ is found in major physiological systems. RXRγ is mainly expressed in central nervous system and heart [4-7]. Due to their role in various regulation pathways RXR is involved in many diseases such as type I diabetes, schizophrenia, autism and immune disorders [8-10].

All RXR subtypes are activated by selective retinoids, known as rexinoids [11]. The endogenous ligand of RXRα is 9-*cis* retinoic acid (9cRA). However, there are other rexinoids that are known to activate RXR, such as docosahexaenoic acid, phytanic acid and linoleic acid [7, 12]. Other studies have suggested that 9cRA is not natural ligand due to the presence other ligands in mammalian tissues. However, 9cRA is the most potent natural RXRα ligand with an EC_{50} of 1.7 nM. RXRα is also activated by many synthetic ligands such as targretin, LG100268 and BMS649 (Figure 6.1).

One of the unique functions of RXR is that it serves as heterodimer partner for many NR including the RAR, vitamin D receptor (VDR), thyroid hormone receptor

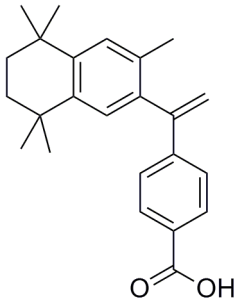

Targretin

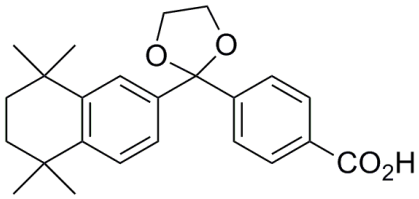

BMS649

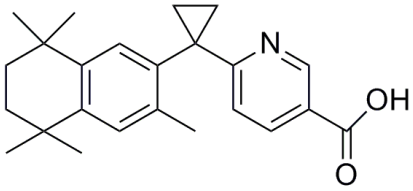

LG100268

Figure 6.1 Natural and synthetic structures of the RXRα ligands

(TR), the peroxisome proliferators-activated receptor (PPAR), the liver X receptor (LXR) and the farnesoid X receptor (FXR) [13-18]. These heterodimer partners can be non-permissive such as VDR and TR, which their ligands are mainly responsible for transactivation, and that both ligands are needed for the maximal activation to be observed. There are also conditionally permissive partners, in which the RXR ligand alone had only a minimal effect on activation and its partner's ligand enhances induced transactivation. They can also be permissive, in which, either the RXR ligand or the partner's ligand induce the maximal activation; however when both ligands are present an additive approach is observed. RXR has also been shown to form homotetramers in cancer cells [19].

The crystal structure of RXRα was the first structure of a nuclear receptor that was solved, revealing details of the structure of the ligand binding domain (LBD) [20]. More recently, the RXRα LBD in an apo (unligated) form and holo (with ligand) conformation has been determined. Detailed information about structure of the LBD and molecular recognition of ligands by RXRα was revealed. The volume of the ligand binding pocket was determined to be between 470 to 530 $Å^3$ in which ~80% of the ligand binding pocket is occupied by the ligand [12, 21]. As with most nuclear receptors, the RXRα LBD consists of 12 α-helices and a β-sheet between helices H5 and H6 that are arranged in an anti-parallel helical sandwich, creating a hydrophobic ligand binding pocket (Figure 6.2) [20]. The most flexible part of the LBD is helix 12where ligand binding induces a conformational change in the position of helix 12, creating a binding surface for interactions between the nuclear receptor and the coactivator proteins. The

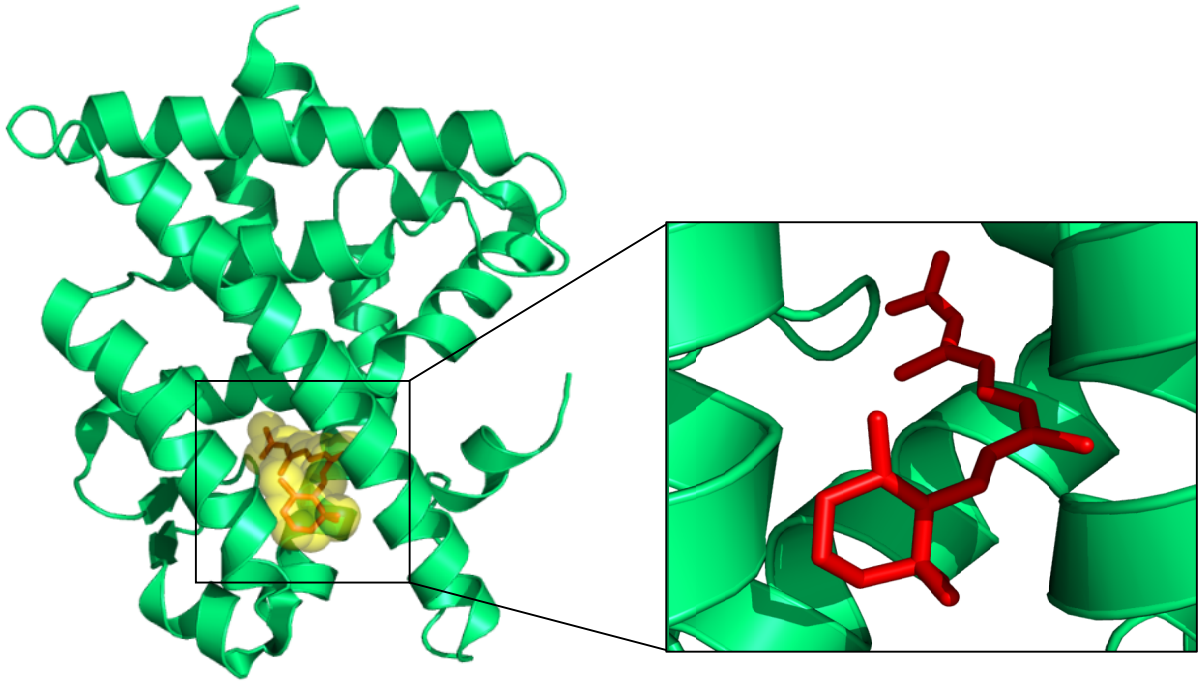

Figure 6.2 Crystal structure of the LBD of RXRα with 9-*cis* retinoic acid. The ligand is shown in yellow space filling.

recruitment of these coactivators eventually leads to the initiation of transcription [22, 23].

Unlike steroid receptors, which upon the ligand binding translocate from cytoplasm to nucleus, RXR is mainly located in nucleus independently on the presence of the ligand [24, 25]. Recent studies have highlighted the cytoplasmic function of the RXR, where the role of the receptor has been extended to biological processes, such as apoptosis and inflammation through the cross-talking with other signal transduction pathways [26]. For example, RXR has been thought to take the role of in shuttling the orphan nuclear receptor, TR3, from nucleus to cytoplasm, allowing TR3 to interact with the mitochondrial protein, Bcl-2, to promote apoptosis [27]. However, more information regarding the expression patterns and trafficking profile of this receptor have yet to be determined.

6.2 Evaluation of Fluophores for RXRα in Yeast and in Mammalian Cells

As described in previous chapters the goal of this work was development of fluorescent ligands which will be able to act as agonists or antagonists for various nuclear receptors, with the ability to fluorescence upon binding to the receptor. The successfully we have been able to developed AMIs for the ERα, PXR and RARα.

Due to the similarity between the RAR and RXR in terms of structure, the library of AMIs that were tested with RARα were also tested with RXR. In addition because of the dimerization capability of this receptor, developing an AMI, which will be able to bind, activate and fluoresce in the presence of the RXR, could provide opportunity

visualizing trafficking and molbility patterns of not only this receptor, but of other nuclear receptors that form partners with this receptor.

The library of AMI derivativeswas screened using chemical complementation system in yeast for evaluation of interactions of AMIs with RXRα. However, none of these ligands were able to induce ligand activated growth with RXRα. Based on these results, a library of AMIs was synthesized based on known RXRα ligands. The AMIs were modified based on the addition of polar groups, such as carboxyl groups which are present in most RXRα ligands. The shape of the ligand was taken in to account, accommodating the properties of the ligand binding pocket. As result, two ligands, AMI S1 and S2 were chosen and analyzed (Figure 6.3). Due to their similarity in chemical properties and shape to the RXR ligand, 9cRA, these two compounds were expected to activate the receptor.

To gain further insight into ability of possible interaction of these ligands with RXRα, AMI S1 and S2 were tested using liquid quantitation assay of chemical complementation in yeast. As described in previous chapters, the plasmid, pGBDRXRαLBD, was cotransformed with coactivator plasmid pGADACTR into yeast strain PJ69-4A. Yeast cells containing both plasmids were placed in the 96 well plates in selective media (-ALW) and incubated at 30 ℃ for 48h. As a control, yeast expressing ligand independent transcription factor, Gal4, was used. As shown in Figure 6.4 ligand activated growth was observed with RXR and 9cRA, as expected and the Gal4 wells showed growth independent of ligand. However, no ligand activated growth was observed for RXRα in adenine selective media with AMI S1 and S2. To investigate whether similar activation profiles of AMI S1 and AMI S2 would be present in the

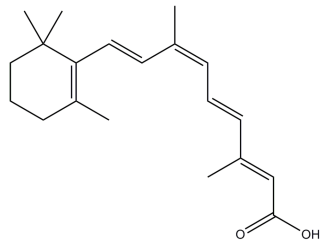

9cRA

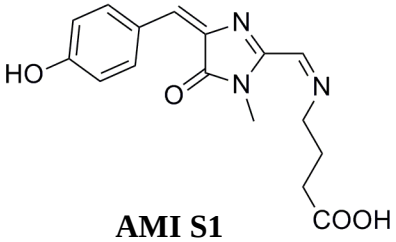

AMI S1

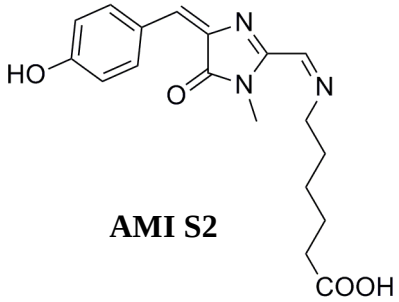

AMI S2

Figure 6.3 Structures of RXRα AMIs, AMI S1 and AMI S2 based on the 9cRA structure.

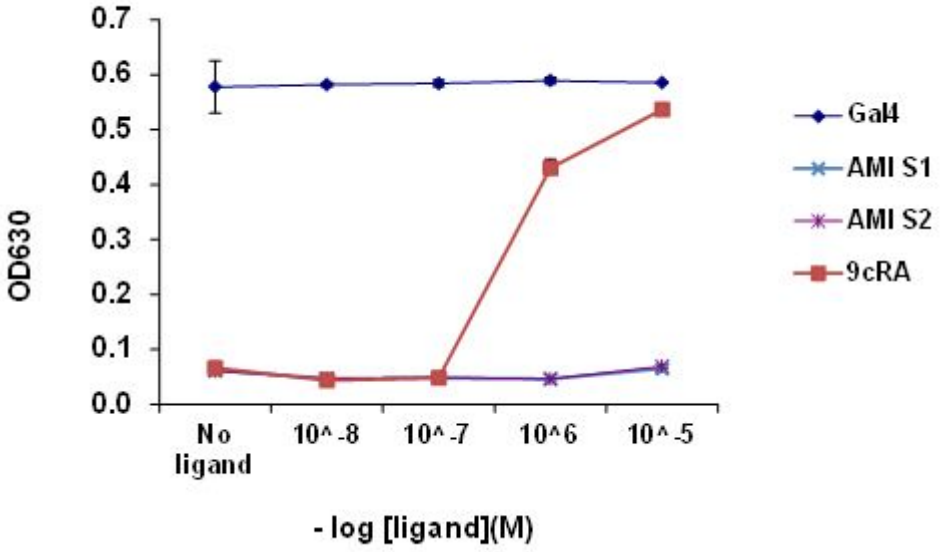

Figure 6.4 Activation Profile of AMI S1 and S2 with RXRα. Gal4 – ligand independent transcription factor, used as positive control.

mammalian cells, the compounds designed were tested for activation in the mammalian cells. HEK293T cells were transfected with a mammalian expression vector pCMXRXRαLBD containing the Gal4 DNA binding domain fused to the RXR ligand binding domain and transfected cells were incubated with the various concentration of AMIs and tested for activation. Using a luciferase reporter gene under the control of Gal4 response elements, ligands AMI S1 and S2 did not display luciferase activation, whereas RXRα with 9cRA showed activity (EC_{50}= 500 nM) (Figure 6.5). These results conformed that AMI S1 and S2 do not activate RXRα. One of our interests was to determine whether these derivatives were able to bind to the receptor. These receptor - AMIs pairs were tested for their ability to fluoresce.

6.3 Visualization of RXRα in Yeast and in Mammalian Cells

In order to determine if AMI S1 and S2 are able to bind and fluoresce in the presence of the RXRα, these compounds were tested for fluorescence in yeast. The strain PJ69-4A yeast was co-transformed with plasmid pGBDRXRα and pGADACTR. Yeast expressing RXRα, were incubated in yeast selective media with AMI at 30 °C. After 48h of incubation, yeast were washed to remove any remaining media. As a control, yeast lacking the plasmid pGBDRARα were incubated with AMIs to detect the any background fluorescence. To determine if interaction of the tested AMIs are specific, yeast expressing RXRα were incubated with AMI 2, the ERα agonist and 9cRA, the natural RXRα ligand.

As shown in Figure 6.6 yeast expressing only Gal4 and incubated with AMI S1 as well as with S2 did not display any fluorescence, displaying no basal fluroscence.

However, cell expressing RXRα fluoresce only in the presence AMI S2. On other hand, the yeast expressing RXRα incubated with 9cRA or AMI2, a known ERα agonist,did not

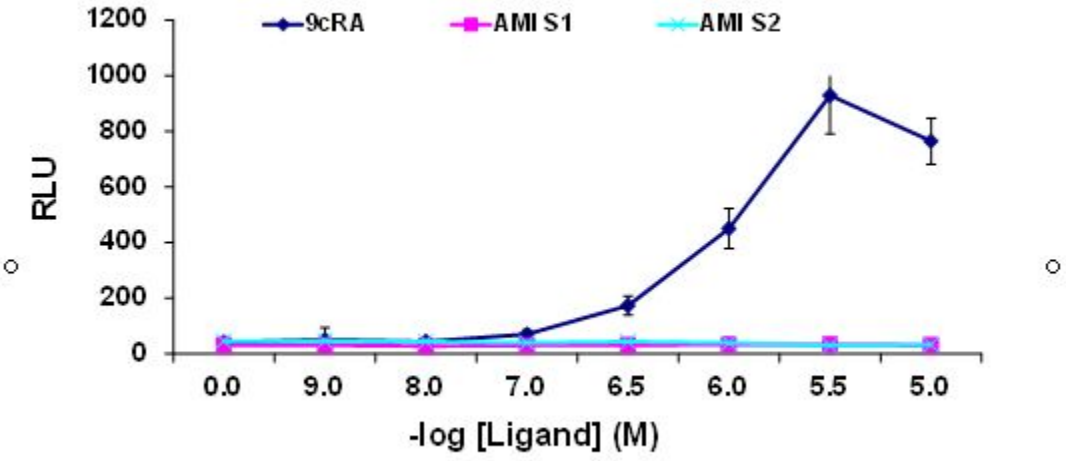

Figure 6.5 Activation profile of RXRα with AMI S1, S2 and 9cRA in mammalian cells.

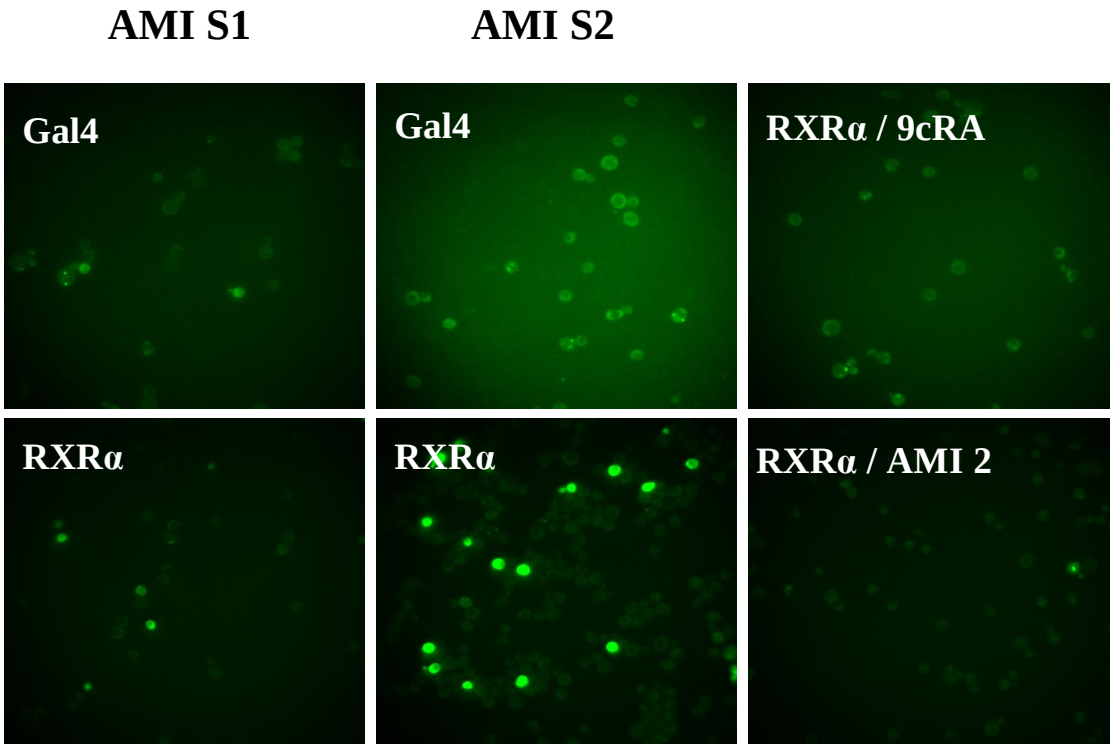

Figure 6.6 Fluorescence microscopy of RXRα AMIs in yeast. Yeast expressing RXRα or Gal4 were incubated with various AMIs, AMI S1, AMI S2 and AMI 2.

display fluorescence. These results corroborate the hypothesis that AMI S2 is able to bind and fluoresce in the presence of the RXRα and displayed fluorescence is specific only to cells which express the receptor, Therefore, although activation was not observed with this ligand receptor pair, the AMI derivative seems to be able to bind to the receptor, and upon binding, fluorescence is observed.

To confirm the results which were obtained in yeast, fluorescence of AMI S1 and S2 was evaluated in mammalian cells. The NIH3T3 cells were transfected with the mammalian expression vector pCMXGRXRLBD expressing Gal4DBD:RXRαLBD fusion protein and incubated in media with S1 and S2. To determine the amount of background fluorescence observed with cells and the compounds, the NIH3T3 cells transfected with RXRα were exposed to 9cRA and AMI2 (ERα agonist) as well as cells lacking RXRα were also exposed to the AMI compounds.

As shown in Figure 6.7 in the presence of RXRα, 9cRA and AMI2 displayed no fluorescence. Also cell lacking RXRα do not fluorescence after incubation with S1 or S2. However in the case of compound AMI S2, fluorescence was observed in the NIH3T3 cells expressing RXRα, despite the absence of activation. Slight fluorescence was observed with the S1 chromophore. The pattern of fluorescence displayed with the S1 chromophores showed speckles of fluorescence localized around the nucleus, whereas the S2 chromophore displayed an intense bright light spanning the entire nuclear area. The most probably, S1 is not able to bind RXRα and compound is not able to be transfer to nucleus. However, S2 after binding to RXRα is transferred to nucleus. These

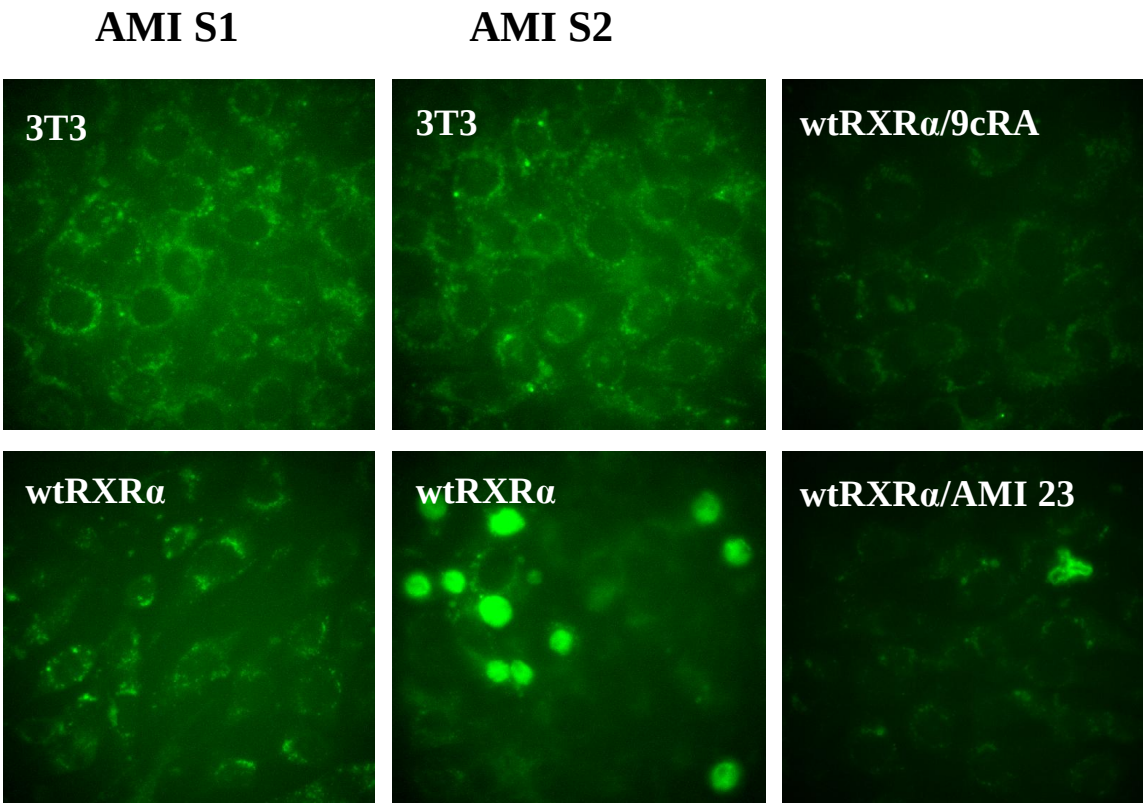

Figure 6.7 Fluorescence of mammalian cells. NIH3T3 cells transfected with RXRα or without transfection were incubated for 24 h with AMI S1and S2, AMI 2 and 9cRA

observations suggest like in case of ERα described in Chapter 3 that activation and fluorescence can be independent of each other.

6.3.1 Evaluation of AMI interactions with RXRα

Previously, studies had shown that water molecules present in a ligand binding pocket of a protein, have been shown to play a part in modifying the shape and flexibility of the binding pocket, improving the steric complementarities between the protein and the ligand, thus playing a significant role in the protein-ligand interactions [28]. This importance is based on their ability to mediate the interactions between the ligand and the protein by forming hydrogen bonded network that stabilizes protein-ligand complex [29, 30].

To date, there are four crystallographic structures of RXR ligand binding domain with bound to 9cRA, the docosahexaenoic acid (HXA), synthetic compound BMS 649 and to 3-(2'-propoxy)-tetrahydronaphtyl cinnamic acid (3TN) [11, 12, 21]. There are several water molecules that are conserved in all four structures of RXR, and a water molecule displaced by some of the four ligands, which were identified by superimposing the structures of the same protein complexed with the different ligands using Relibase [31]. Analysis of the conserved water molecules in all four x-ray structures of RXR showed that there is a conserved hydrogen bond network, involving several buried water molecules that bridge the polar atoms of the ligand to the backbone and/or the side chain groups of the protein. However, the comparison of all the water-mediated interactions shows that some of them are common to all the structures of the RXR ligand binding pockets. We noticed that the carboxylate group from all the ligands participates in a water-mediated hydrogen bond

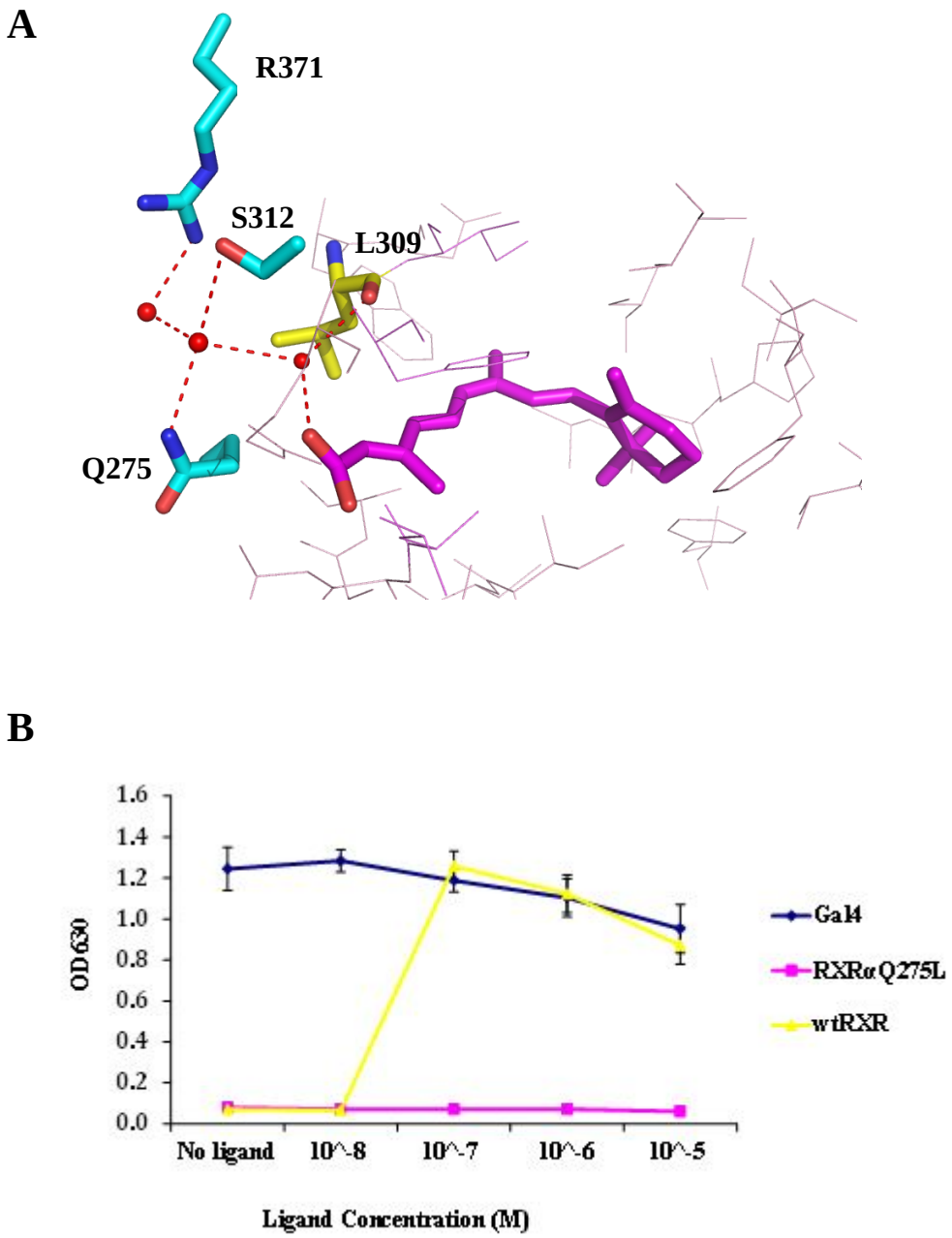

Figure 6.8 RXRαQ275L variant. A. Water mediated interaction between RXR residues and 9cRA. **B.** Selection assay for yeast growth in presence of 9cRA

network involving the backbone carbonyl group of Leu309 and the side chains of Arg371 and Gln275 (Figure 6.8A). However, the side chain of Ser312 is also connected with carboxylate group of the ligand by water mediated hydrogen bond network as it is in the case of RXR bound to 9cRA and HXA. By using these observations we proposed to design a RXR mutant, which carried single mutation that could disrupt the water-mediated interaction between the ligand and the protein.

In order to confirm the binding of AMI in the ligand pocket of RXR and displayed fluorescence, due to interaction of the AMI S2 with RXRα, engineering of RXRα variant could bring the insight into specific interactions between the ligand and the receptor.. We hypothesized that introducing specific mutations can lead to a disruption a water-mediated interaction between the ligand and the protein. Using site-directed mutagenesis, residue Q275 was mutated to leucine to determine whether replacing polar with non polar can disturb the water mediated interaction by eliminating the hydrogen bonding and lead to decrease of affinity to ligand.

The Q275L RXRα variant was transformed with coactivator plasmid into PJ69-4A yeast strain and tested using chemical complementation. As shown in Figure 6.8B ligand activated growth was observed only in case of yeast expressing wtRXR with an EC_{50} value of 500 nM. As expected, RXRα variant did not display ligand activated growth probably due to disturbed water mediated interaction with carboxyl group of 9cRA. Thus we hypothesized that this variant will have also disturbed interactions with AMI S2, which could lead to lack of fluorescence. Furthermore, RXRαQ275L variant was transformed into PJ69-4A along with coactivator plasmid. After incubation cells were washed and tested for fluorescence by using fluorescence microscope. As shown in

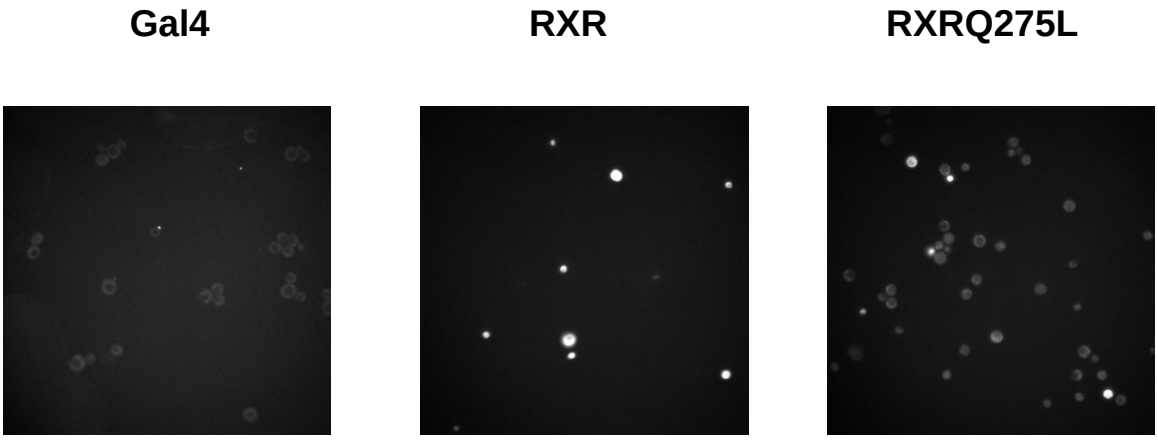

Figure 6.9 Fluorescence microscopy of RXR variant . Yeast expressing, Gal4, RXRα and RXRαQ275L were incubated with AMI S2.

Figure 6.9 yeast expressing RXRαQ275L variant did not fluoresce with AMI S2 in compare to yeast expressing RXRα which display fluorescence. RXRαQ275L variant, used as a negative control. This indicated that the AMI mediated fluroscence was due to the binding of the AMI inside the pocket, and upon disrupting key contacts in the pocket, such as the hydrogen bonding network, the AMI derivative is no longer able to bind inside the pocket. Thus, fluroscence is not observed.

6.4 Molecular Modeling of Fluophores.

Molecular modeling was used to gain insight into conformation of AMIs inside the RXRα ligand binding domain. Thus, modeling was performed with AutoDock Vina, using crystal structure of the ligand binding domain of RXR with 9cRA (PDB:1FBY). AMI S1 and S2 were docked into the RXRαLBD. As shown in Figure 6.10 both AMIs are able to bind inside the ligand binding pocket. Superimposition of the AMI S1 and S2 with 9cRA shows that these compounds are able to adopt a similar conformation to natural ligand of RXRα. They display the shape of 9cRA inside the ligand binding pocket. Based on the theoretical positions of AMIs in the ligand binding pocket is difficult conclude why only AMI S2 is able to “turn on” fluorescence upon binding. It is possible that longer chain in case of AMI S2 provides a more hydrophobic environment and allowing for a tighter interaction between the receptor and the ligand.

6.5. Evaluation of AMIs for other NRs using Chemical Complementation

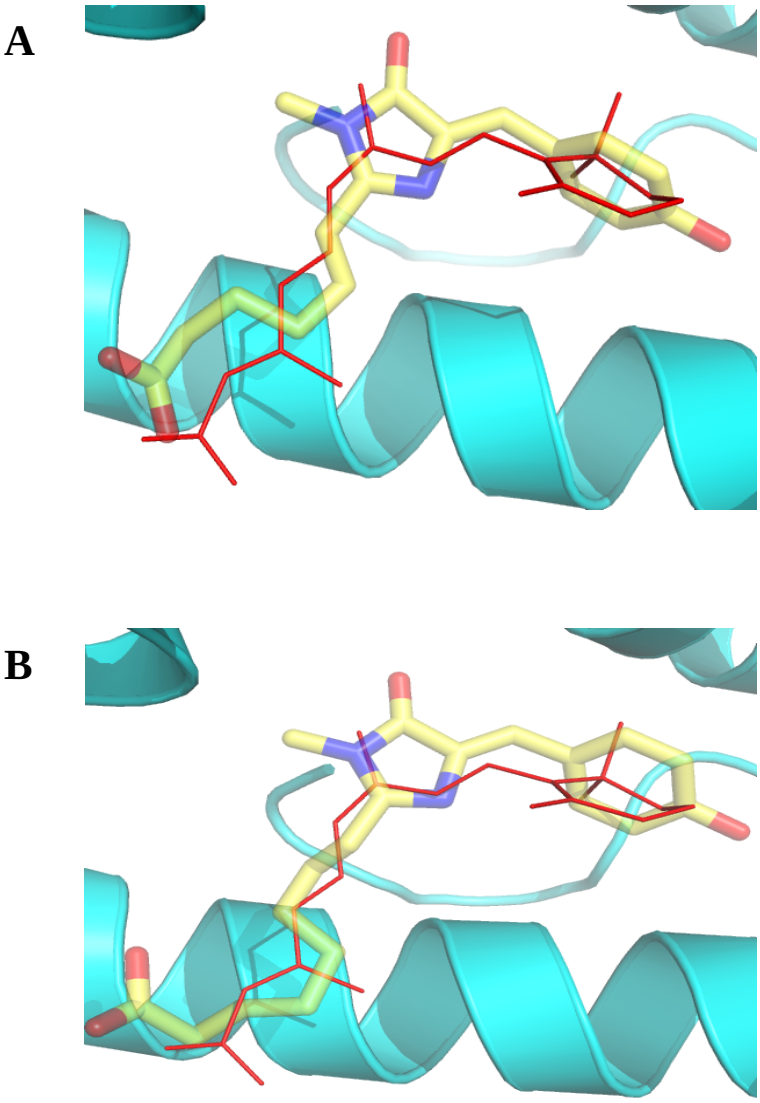

Figure 6.10 Modeling of AMI S1 (A) and S2 (B) in binding pocket of RXRα with overlay of 9cRA.

To determine whether library of AMI derivatives are able to activate other nuclear receptors, chemical complementation assay was used using a liquid quantitation assay of chemical complementation, allows for a quick and easy method for deciphering receptor/ligand interactions. The following receptors were tested for activation with the AMI derivatives: rat estrogen receptor β (rERβ), vitamin D receptor (VDR), liver X receptor (LXRβ), retinoid X receptor α (RXR α), constitutive androstane receptor (CAR), Farnesoid X receptor (FXR) and peroxisome proliferator-activated receptor γ (PPARγ). LXRβ, RXR, CAR, FXR and PPARγ were tested in adenine or histidine selective media. Due to the known leaky of expression of the *HIS3* gene, 3-amino-1,2,4-triazole 3-AT (3-AT) the an inhibitor of imidazoleglycerol-phosphate dehydratase was used to reduce background.

Each of the nuclear receptors was tested with library of AMI including 95 ligands and with natural or synthetic ligand. Thus, rERβ were tested with 17-βestradiol, RXR with 9-*cis* retinoic acid, VDR with lithocholic acid and LXR with T0901317. CAR, FXR and PPARγ were previously shown to be constitutively active nuclear receptors in yeast, where an endogenous ligand is perhaps binding to these receptors and activating them. This is not surprising due to similarity with the metabolites that are present in both yeast and mammalian systems. However, we decided to test against the library of AMIs to determine whether AMIs are able to serve as potential antagonists for these receptors.

The 96 well plates, with the PJ69-4A yeast strain expressing nuclear receptor and coactivator were incubated at 30 °C by 48h. Ligand activated growth was not observed in case of 96 well plates with yeast expressing VDR, LXRβ, rERβ and RXR as shown in Figure 6.11. As expected, the plates with yeast expressing CAR, FXR and PPARγ have

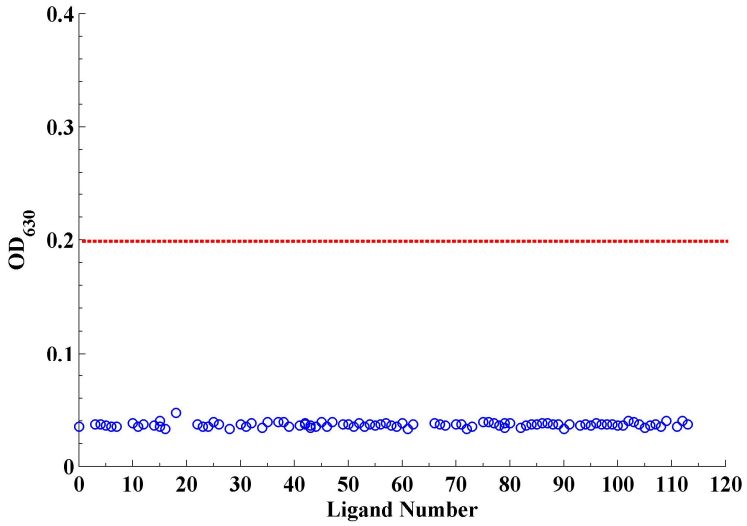

Figure 6.11 Nuclear receptor screening using chemical complementation in yeast. Library of 95 AMIs was tested with yeast expressing rERβ, VDR, LXRβ, RXRα. Red line shows expected ligand activated growth. None of the ligands show ligand activated growth with tested nuclear receptors.

showed constitutive growth. Overall, the screening of AMI library using chemical complementation assay in yeast did not show ligand activated growth with other nuclear receptors. In spite of lack of discovery novel AMIs for other nuclear receptors, these results indicated that AMIs which previously showed activation for ERα, PXR and RARα are specific for these nuclear receptors.

6.6 Summary

As discussed in previous chapters, we discover several AMIs which besides displaying fluorescence in the presence of the receptors they also act as agonists for ERα, PXR and RARα. Here we presented the discovery of AMI S2 which is able to bind to RXRα and fluoresce upon binding. Discovery of this compound, which fluoresces in the presence of the RXRα but does not activate is extremely important because it can serve as potential antagonist for RXRα. However, they can also be used as a potential fluorescent probes for traffic this receptor in the cell.

On the other side these results provide opportunity for development of novel AMIs which will not only able to bind and fluoresce but also activate RXRα.

6.7 Materials and Methods

Ligands

9-*cis* retinoic acid (MW=300.44 g/mol) was purchased from ICN Biomedicals (Aurora, OH), all-*trans* retinoic acid (MW=300.44 g/mol) from Biomol Inc (Plymouth Meeting, PA).

The library of AMIs was synthesized by Dr. Anthony Baldridge. Method of synthesize was described previously in Chapter 2.

Site-Directed Mutagenesis

Mutation Q273L was introduced into the yeast expression plasmid, pGBDRXRα by using PCR (Stratagene, Santa Clara, CA) with specific mutagenic primers (Operon, Huntsville, AL) and DpnI digestion. Plasmid carried mutation was purified using the QIAprep® Spin Miniprep Kit (Qiagen, Valencia, CA).

Yeast transformation

The plasmids pGBDRXRα and coactivator plasmids were transformed in the PJ69-4A strain using the TRAFCO yeast transformation protocol. The transformation mixture was placed onto nonselective plates (SC-LW). Plates were incubated at 30 °C for 3 days.

Liquid Quantitation Assay

PJ69-4A expressing RXRα was grown overnight in nonselective media SC-LW, at 30 °C, shaking at 300 rpm. Yeast were pelleted by centrifugation and resuspended in selective media SC-ALW with 10 μM or a range of ligand concentration and placed in 96-well plates. Plates were then incubated at 30 °C, shaking at 170 rpm for 48 hours. After 0, 24, and 48 hours optical density readings were taken at a 630 nm wavelength.

***In silico* Docking Studies**

Molecular modeling was performed as described in Chapter 3.

Fluorescence Microscopy

The PJ69-4A strain expressing RARα was incubated in selective media SC-ALW with RARα AMIs, at 30 °C, shaking at 300 rpm. After incubation yeast were pelleted by centrifuging and resuspended in distill steril water. Cells were again centrifuged and resuspended in water. Next the cell were displayed under fluorescent microscope and analyzed for green fluorescence.

Confocal microscopy was performed as described in Chapter 3.

6.8 References

1. Mangelsdorf, D.J., et al., *Nuclear receptor that identifies a novel retinoic acid response pathway.* Nature, 1990. **345**(6272): p. 224-9.

2. Mangelsdorf, D.J., et al., *Characterization of three RXR genes that mediate the action of 9-cis retinoic acid.* Genes Dev, 1992. **6**(3): p. 329-44.

3. Szanto, A., et al., *Retinoid X receptors: X-ploring their (patho)physiological functions.* Cell Death Differ, 2004. **11 Suppl 2**: p. S126-43.

4. Yu, V.C., et al., *RXR beta: a coregulator that enhances binding of retinoic acid, thyroid hormone, and vitamin D receptors to their cognate response elements.* Cell, 1991. **67**(6): p. 1251-66.

5. Fleischhauer, K., et al., *Isolation of a full-length cDNA clone encoding a N-terminally variant form of the human retinoid X receptor beta.* Nucleic Acids Res, 1992. **20**(7): p. 1801.

6. Nohara, A., J. Kobayashi, and H. Mabuchi, *Retinoid X receptor heterodimer variants and cardiovascular risk factors.* J Atheroscler Thromb, 2009. **16**(4): p. 303-18.

7. Dawson, M.I. and Z. Xia, *The retinoid X receptors and their ligands.* Biochim Biophys Acta, 2012. **1821**(1): p. 21-56.

8. Feng, J., et al., *Structural variants in the retinoid receptor genes in patients with schizophrenia and other psychiatric diseases.* Am J Med Genet B Neuropsychiatr Genet, 2005. **133B**(1): p. 50-3.

9. Miyazaki, S., et al., *Nuclear hormone retinoid X receptor (RXR) negatively regulates the glucose-stimulated insulin secretion of pancreatic ss-cells.* Diabetes, 2010. **59**(11): p. 2854-61.

10. Chow, E.K., B. Razani, and G. Cheng, *Innate immune system regulation of nuclear hormone receptors in metabolic diseases.* J Leukoc Biol, 2007. **82**(2): p. 187-95.

11. Nahoum, V., et al., *Modulators of the structural dynamics of the retinoid X receptor to reveal receptor function.* Proc Natl Acad Sci U S A, 2007. **104**(44): p. 17323-8.

12. Egea, P.F., A. Mitschler, and D. Moras, *Molecular recognition of agonist ligands by RXRs.* Mol Endocrinol, 2002. **16**(5): p. 987-97.

13. Berrodin, T.J., et al., *Heterodimerization among thyroid hormone receptor, retinoic acid receptor, retinoid X receptor, chicken ovalbumin upstream promoter transcription factor, and an endogenous liver protein.* Mol Endocrinol, 1992. **6**(9): p. 1468-78.

14. Bugge, T.H., et al., *RXR alpha, a promiscuous partner of retinoic acid and thyroid hormone receptors.* EMBO J, 1992. **11**(4): p. 1409-18.

15. Kliewer, S.A., et al., *Retinoid X receptor interacts with nuclear receptors in retinoic acid, thyroid hormone and vitamin D3 signalling.* Nature, 1992. **355**(6359): p. 446-9.

16. Ziouzenkova, O. and J. Plutzky, *Retinoid metabolism and nuclear receptor responses: New insights into coordinated regulation of the PPAR-RXR complex.* FEBS Lett, 2008. **582**(1): p. 32-8.

17. Kassam, A., et al., *Retinoid X receptor (RXR) agonist-induced antagonism of farnesoid X receptor (FXR) activity due to absence of coactivator recruitment and decreased DNA binding.* J Biol Chem, 2003. **278**(12): p. 10028-32.

18. Yue, L., et al., *Ligand-binding regulation of LXR/RXR and LXR/PPAR heterodimerizations: SPR technology-based kinetic analysis correlated with molecular dynamics simulation.* Protein Sci, 2005. **14**(3): p. 812-22.

19. Lefebvre, P., Y. Benomar, and B. Staels, *Retinoid X receptors: common heterodimerization partners with distinct functions.* Trends Endocrinol Metab, 2010. **21**(11): p. 676-83.

20. Bourguet, W., et al., *Crystal structure of the ligand-binding domain of the human nuclear receptor RXR-alpha.* Nature, 1995. **375**(6530): p. 377-82.

21. Egea, P.F., et al., *Crystal structure of the human RXRalpha ligand-binding domain bound to its natural ligand: 9-cis retinoic acid.* EMBO J, 2000. **19**(11): p. 2592-601.

22. Ito, M., et al., *Ab initio fragment molecular orbital study of molecular interactions between liganded retinoid X receptor and its coactivator: roles of helix 12 in the coactivator binding mechanism.* J Phys Chem B, 2007. **111**(13): p. 3525-33.

23. Zhang, J., X. Hu, and M.A. Lazar, *A novel role for helix 12 of retinoid X receptor in regulating repression.* Mol Cell Biol, 1999. **19**(9): p. 6448-57.

24. Georget, V., et al., *Trafficking of the androgen receptor in living cells with fused green fluorescent protein-androgen receptor.* Mol Cell Endocrinol, 1997. **129**(1): p. 17-26.

25. Htun, H., et al., *Visualization of glucocorticoid receptor translocation and intranuclear organization in living cells with a green fluorescent protein chimera.* Proc Natl Acad Sci U S A, 1996. **93**(10): p. 4845-50.

26. Han, Y.H., et al., *A unique cytoplasmic localization of retinoic acid receptor-gamma and its regulations.* J Biol Chem, 2009. **284**(27): p. 18503-14.

27. Cao, X., et al., *Retinoid X receptor regulates Nur77/TR3-dependent apoptosis [corrected] by modulating its nuclear export and mitochondrial targeting.* Mol Cell Biol, 2004. **24**(22): p. 9705-25.

28. Li, Z. and T. Lazaridis, *Water at biomolecular binding interfaces.* Phys Chem Chem Phys, 2007. **9**(5): p. 573-81.

29. Pastor, M., G. Cruciani, and K.A. Watson, *A strategy for the incorporation of water molecules present in a ligand binding site into a three-dimensional quantitative structure--activity relationship analysis.* J Med Chem, 1997. **40**(25): p. 4089-102.

30. Barillari, C., et al., *Classification of water molecules in protein binding sites.* J Am Chem Soc, 2007. **129**(9): p. 2577-87.

31. Gunther, J., et al., *Utilising structural knowledge in drug design strategies: applications using Relibase.* J Mol Biol, 2003. **326**(2): p. 621-36.

CHAPTER 7

ENGINEERING NUCLEAR RECEPTORS TOWARDS FLUOROPHORES

7.1 Engineering Nuclear Receptors to bind Fluophores

As discussed in the previous chapters, the main goal of this work was the development of fluorogens to bind and activate various nuclear receptors. AMIs were characterized for ERα, RARα, PXR and RXRα. In most cases, the approach taken for discovering these novel AMIs required some modeling, and eventually the screening of small libraries of AMI derivatives. However, often times there seemed to be a lack of a correlation between the modeling results obtained and the activation profile of these compounds with various nuclear receptors. Another approach taken to gain insight into the structure function relationship between the AMI derivatives and nuclear receptors is by engineering the receptors to bind novel small molecules. By engineering nuclear receptors, the opportunity to gain further insight into interaction between the ligand and receptor is provided. In addition to the structural information gained through this process, engineering receptors to bind novel small molecules can also be used in a series of applications, ranging from gene therapy applications to biosensors.

To date, engineering nuclear receptors such as RARα, RXRα and ERα have been reported. Some of these studies were directed towards alanine scanning mutagenesis of the residues inside the ligand binding pocket to investigate their specific role in ligand binding [1-4]. However, mutagenic studies were also focused on creating orthogonal ligand-receptor pairs, in which mutated receptor is activated by novel ligand, and no

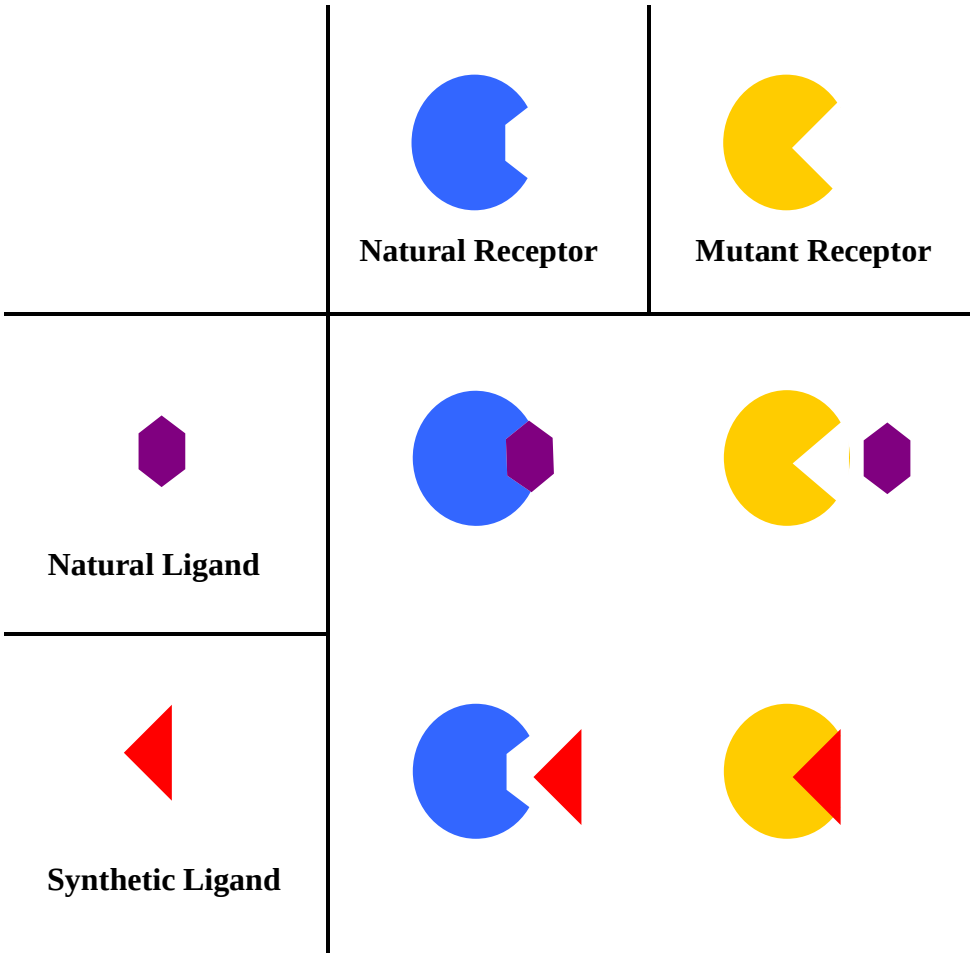

Figure 7.1 Receptor – ligand orthogonal pair. Wild-type receptor is able to respond to natural ligand but not to synthetic ligand. Engineered receptor is able give response to synthetic ligand but losing affinity to natural ligand.

longer is activated by natural ligand (Figure 7.1) [5-7]. These engineered receptor ligand pairs are used in a variety of applications, such as in molecular switches for gene therapy [5, 7]. All of these studies generated mutations in only the LBD of these receptors using a rational design approach to the types of mutations that were made, where specific residues were selected. For instance, RXRα variants were generated that were no longer activated by the wild-type ligand, 9cRA, but activated in response to a synthetic ligand LG335. This synthetic ligand shows minimal activity with the wild-type receptor. The RXR variants receptor had four mutations, I268A, I310A, F313A, and L436F which were localized inside the binding pocket [8]. Using this methodology relies heavily on understanding the structure/function relationship between the ligand and the receptor. Also, by limiting the mutations to the residues in the binding pocket, very little is understood about the effects of the secondary residues that surround the binding pocket. Thus, a part of our goal was to explore the possibility to engineer a receptor to bind and activate in response to an AMI derivative, that the wild-type receptor had shown no activity with. However, to explore the impact of the residues in the entire ligand binding domain, random mutagenesis was employed, which had been previously used to generate VDR variants [9, 10].

7.2 Random Mutagenic Approach: Error –Prone PCR Libraries for VDR, LXRα, RXRα and ERα

Initially, the VDR, LXRα, RXRα and ERα were subjected to random mutagenesis. The nuclear receptors were chosen based on a number of different reasons. Our lab had previously obtained VDR variants that were discovered through random

mutagenesis to show activation in response to a novel ligand, therefore this receptor was used. LXR was chosen as a target due to the lack of mutagenic work that has been performed with this receptor. The RXRα was used because of the fact that AMI S1 and S2, two of the derivatives designed for this receptor, did not show activation with the wild-type receptor. Our goal was to be able to discover a variant capable of showing activation with these two derivatives. On the other hand, ERα was subjected to random mutagenesis due to previous discovery of AMIs for this receptor. Engineering of wild-type ERα could present an opportunity to enhance activation with AMIs or discover a variant showing activity with other AMIs derivatives.

Libraries of variants were subjected to selective pressure using chemical complementation, where variants activated by specific AMI. To engineer these variants, epPCR was performed by two different approaches. The first method involved using Taq polymerase and modifying the conditions of the PCR reaction to enhance the error-rate. Concentrations of manganese (II) chloride ($MnCl_2$) with addition of magnesium (II) chloride ($MgCl_2$) replace the $MgCl_2$ that is needed by the Taq polymerase to function. Replacing the magnesium with managanese, still allows for the polymerase to function, but not with a very high efficiency. To modulate the affinity of the enzyme various concentrations of $MnCl_2$ were used (20 – 400 μM). The second approach used an engineered polymerase, mutazyme, was used. This commercial enzyme is a mutated polymerase, which introduces mutations more frequently than Taq polymerase and does not require manipulation of epPCR condition. Each of epPCR products (insert cassettes) were used to create libraries of variants for each nuclear receptor.

To create library, the nuclear receptor insert cassette along with background plasmid (eg. pGBDhERαbackground) were transformed into yeast strain PJ69-A containing fusion protein GAD:coactivator. The background plasmid, contain the Gal4 DNA binding domain fused to part of NR LBD, along a random sequence introducing multiple STOP codons, was used to decrease appearance of wild-type nuclear receptor in library. However, insert cassette contained ends complementary to the specific region of digested background plasmid, allowing for homologous recombination to take place between the insert cassette with mutations and the digested background plasmid and create expression plasmid containing Gal4DBD fused to nuclear receptor variant's LBD. The library of variants was transformed into yeast and plated onto non-selective agar plates (SC-LW) lacking leucine and tryptophan to select the GAD:Coactivator plasmid (leucine marker) and Gal4DBD:LBD expressing plasmid (tryptophan marker). These plates were also used to determine whether homologous recombination had occurred and to determine transformation efficiency. Yeast were also plated on selective agar plates (SC–ALW) lacking leucine and tryptophan, as well, as adenine or histidine, and containing different AMIs at concentration of 10 μM. As discussed in Chapter 3, the selective plates were lacking adenine or histidine due to presence of the genes *ADE* or *HIS3* in PJ69-A which were involved in biosynthetic pathway of adenine or histidine production. Activation of this selection gene, such as the *HIS3* gene, which was under control of Gal4 response element enables the yeast strain to grow on media lacking histidine in the presence of the AMI. Thus, the survival of the yeast expressing specific variant of nuclear receptor depends on the presence of the small ligand molecules (Figure 7.2).

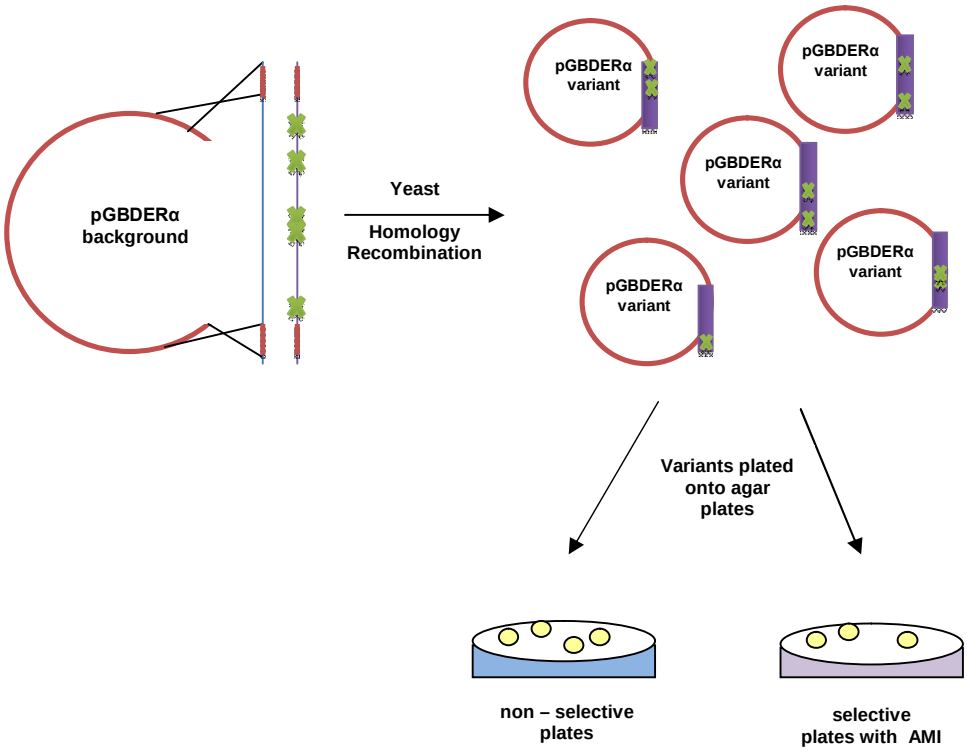

Figure 7.2 Generation of libraries of ERα variants in yeast. The library cassette is transformed into PJ69-A yeast strain along with background plasmid which contains the homology regions with cassettes. Cassettes contain the random mutations which were generated by error – prone PCR. Through homologous recombination, library of ERα variants were created.

7.2.1 Results of Error-Prone Libraries

As shown in Table 7.1, for each receptor, a similar library size in the range of 10^3 - 10^4 variants was obtained and transformation efficiency in range of $10^4 – 10^5$ cfu/μg VC was observed. Despite of large number of created variants, no ligand activated variants were observed with the VDR, RXRα and LXR libraries. However, the ERα libraries resulted in several dozen potential ligand activated variants for specific AMIs.

Most of variants were tested for ligand activated growth by streaking out onto non –selective (SC-LW), selective (SC-ALW) and ligand (SC-ALW +AMI) plates. Most of variants display growth on selective plates SC –ALW, which indicated that they are constitutively active, growing without the presence of ligand. This could indicate two possibilities: (1) these variants are binding an endogenous ligand, or (2) that these variants have structural modifications that enable the active of the receptor to become independent of the presence of ligand. However, the most surprising aspect of this is that these variants did not grow on selective plates with the AMI ligands, suggesting that perhaps these AMI compounds are acting as antagonists, ligands that bind but do not activate these receptors. To determine activation the profile of the obtained variants, several from each library were sequenced and retransformed to yeast for further testing. As shown in Table 7.2 most of the sequenced variants displayed single or double mutations and most of the mutations were outside of the ligand binding pocket. Both the mutazyme and *Taq* libraries produced a similar mutational diversity and number of mutations per gene.

To confirm the activation profile of sequenced variants, variants were tested in liquid quantitation assays in chemical complementation. Each variant was tested with

Table 7.1 Transformation results for VDR, LXR and ERα libraries.

Library name	Polymerase	Library Size	Transformation Efficiency (cfu/μg VC)
VDR_1	*taq*	1.3×10^4	1.8×10^5
VDR_2	mutazyme	4.4×10^3	4.6×10^4
LXR_1	*taq*	4.0×10^3	5.5×10^4
LXR_2	mutazyme	1.5×10^3	1.6×10^4
ERα_1	*taq*	1.8×10^4	2.4×10^5
ERα_2	mutazyme	1.1×10^4	1.1×10^5

Table 7.2 Sequencing results for ERα libraries.

Taq polymerase		Mutazyme	
Nonselective Variants			
ER1	L372H, L508P, K520E	**ER1**	V478A, Q498K
ER3	W383R, L403P,Q414L		
Selective Variants			
4_9	L507F, E561stop,Y582H	**4_1**	D374Q, N439K,M490L,Y537S
4_23	wtER	**4_15**	L320stop,V478A
24_9	E380D	**24_5**	P406H,K416I
24_12	H567L	**12_9**	wtER
12_8	N348S,G442R	**14_20**	H373N, L462P, N519I, Y537C
12_9	wtER	**23_9**	K520R
9_8	wtER	**23_31**	I487V

natural ligand of ERα, 17-β estradiol and various AMI derivatives. As seen in Figure 7.3 and Figure 7.4, most of the variants were constitutively active, displaying growth without ligand as also in the presence of the AMI and 17-β estradiol. Interestingly, one of these variants (23_9) has a single mutation, K520R. However, besides constitutively active variants, two non-functional variants were obtained.

Finally, besides the constitutively active and non-functional variants, one of the variants (24_9) obtained displayed ligand activated growth in the presence of the AMI 24 with a 5-fold activation in comparison to 8-fold activation with 17-β estradiol. Thus, the engineered variant showed to be activated by AMI 24. However, this ligand showed previously slight growth and low sensitivity (EC_{50} > 10mM) with wild-type ERα.

7.3 Testing E380D variant in chemical complementation

Variant 24_9, which contained a single point mutation at position 380 (E380D), showed a novel activation profile with AMI-24. In comparison to the activity with wild-type ER, this variant showed an increase in the fold activation from two to five fold with AMI 24. Due to the similarity between AMI 24 and AMI 23, which lacks two carbons in the alkyl chain compared to AMI 24, this ligand was also tested in yeast for activation with E380D variant. As shown in Figure 7.5B AMI 23 shows activation with the ERαE380D variant, at a relatively low activation (3-fold activation) and with an EC_{50}> 10 μM. ERαE380D variant enhances activation about three fold compared with wild-type ERα. Despite the fact that the ERαE380D variant shows activation with AMI 23 and 24, this variant shows the same activation profile with 17-β estradiol as the wild-type

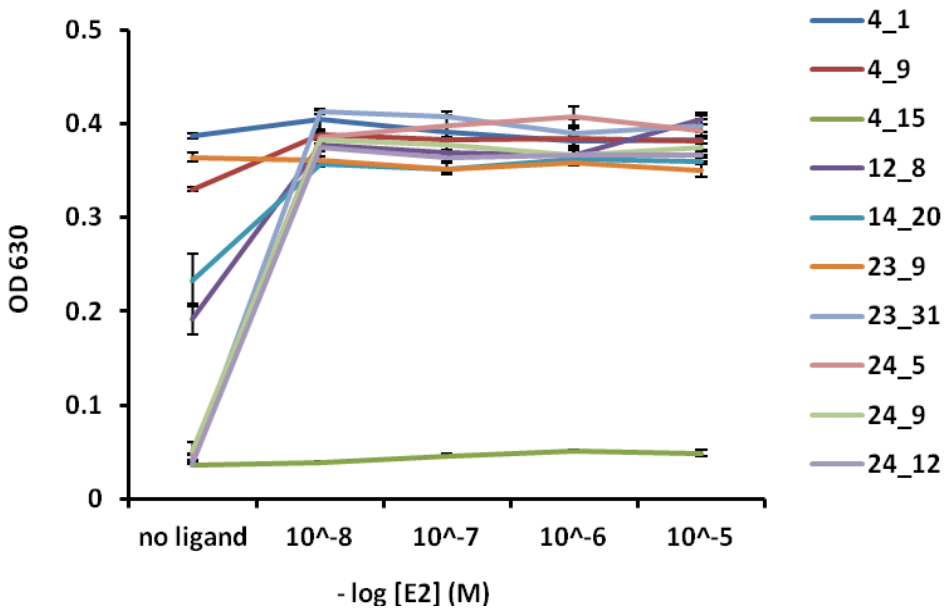

Figure 7.3 Ligand activated growth profiles of ERα variants with 17-β Estradiol.

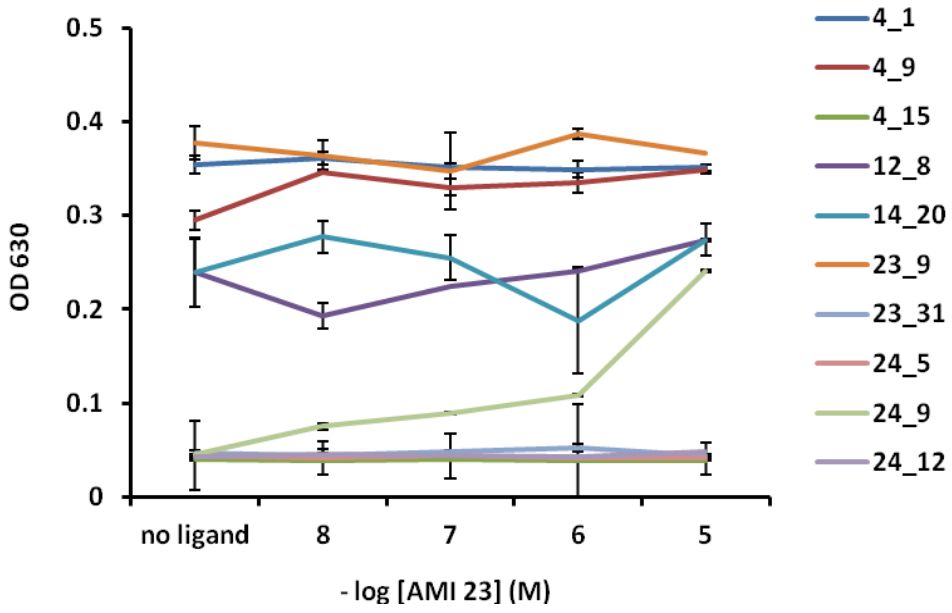

Figure 7.4 Ligand activated growth profiles of ERα variants with AMI 23.

A

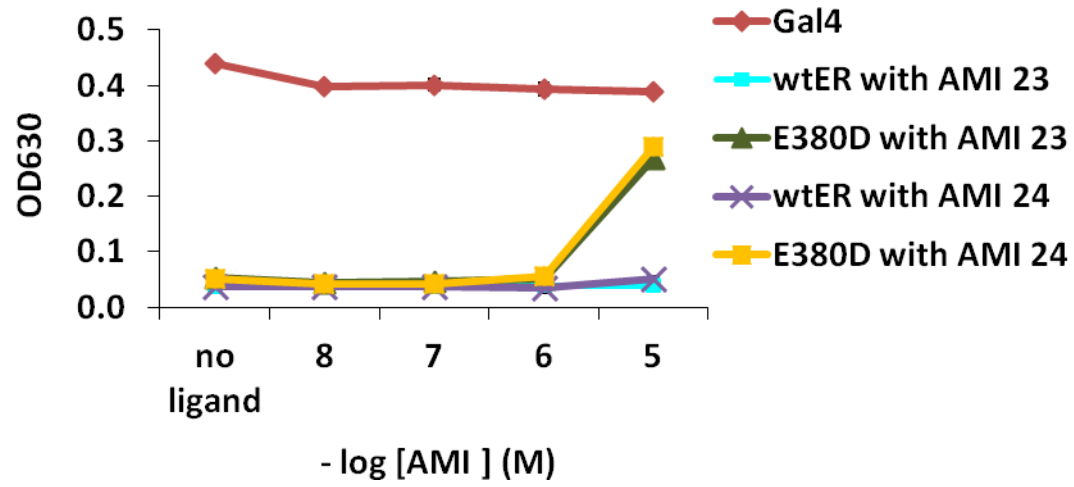

B

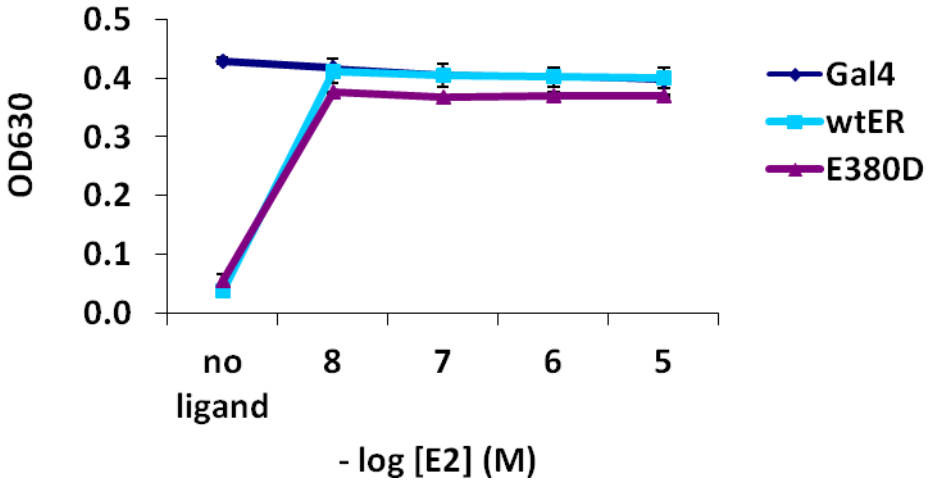

Figure 7.5 Ligand activated growth profiles of wtERα and E380D variant. Receptors were tested with **A.** AMI 23 and 24, **B.**17-β Estradiol,

receptor (Figure 7.5A). Thus, this mutation does not have effect on binding and activation by 17-β estradiol.

Due to the ability of E380D variant to enhance activation of ERα with AMI 23 and 24, we hypothesized that this mutation would also be able to display activation with other AMI derivatives which are similar in their structure to AMI 23 and 24. Thus, a variety of AMIs with different position of hydroxyl group on AMI core and lack of carboxyl group on alkyl chain of fluophore, were tested for activation E380D variant as well as with wild-type ERα. However, from all of the AMI derivatives that were tested, none of these compounds showed activation with the E380D variant or the wild-type receptor (Figure 7.6). This indicated that this variant did display specificity toward these two AMI derivatives, but others that were very similar in structure failed to activate the receptor.

7.3.1 Influence of E380D variant on interaction with coactivators

To understand impact of E380D mutation on activation, the importance of this residue was further explored. As previously mentioned, residue E380 is localized out side of the ligand binding pocket and it is not in direct contact with ligand. This glutamate is positioned on helix 5 and pointed outward toward the solvent (Figure 7.7). Previous studies indicated that E380 is part of a cluster of 16 amino acid residues which create a binding groove for coactivators (Figure 7.8). The crystal structure of ERα with a coactivator peptide containing the traditional LXXLL motif of coactivator SRC-1 reveals a hydrophobic surface used for interaction between the coactivator and nuclear receptors. Previous work had shown that this residue plays an important part in the interaction

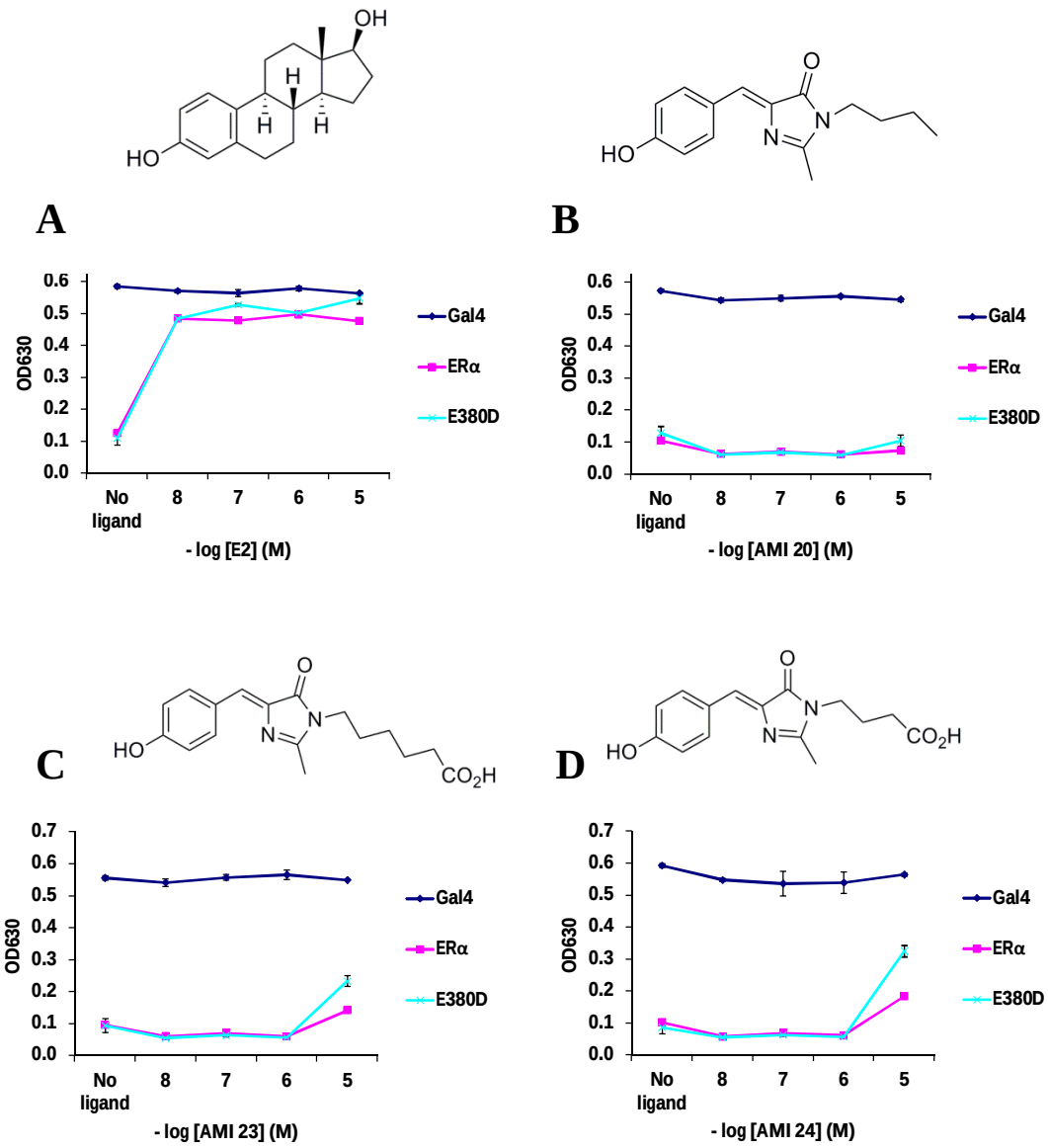

Figure 7.6 Ligand activated growth profiles of E380D variant. **Part I.** Engineered variant was tested with **A.** 17-β Estradiol, **B.** AMI 20, **C.** AMI 23, **D.** AMI 24,

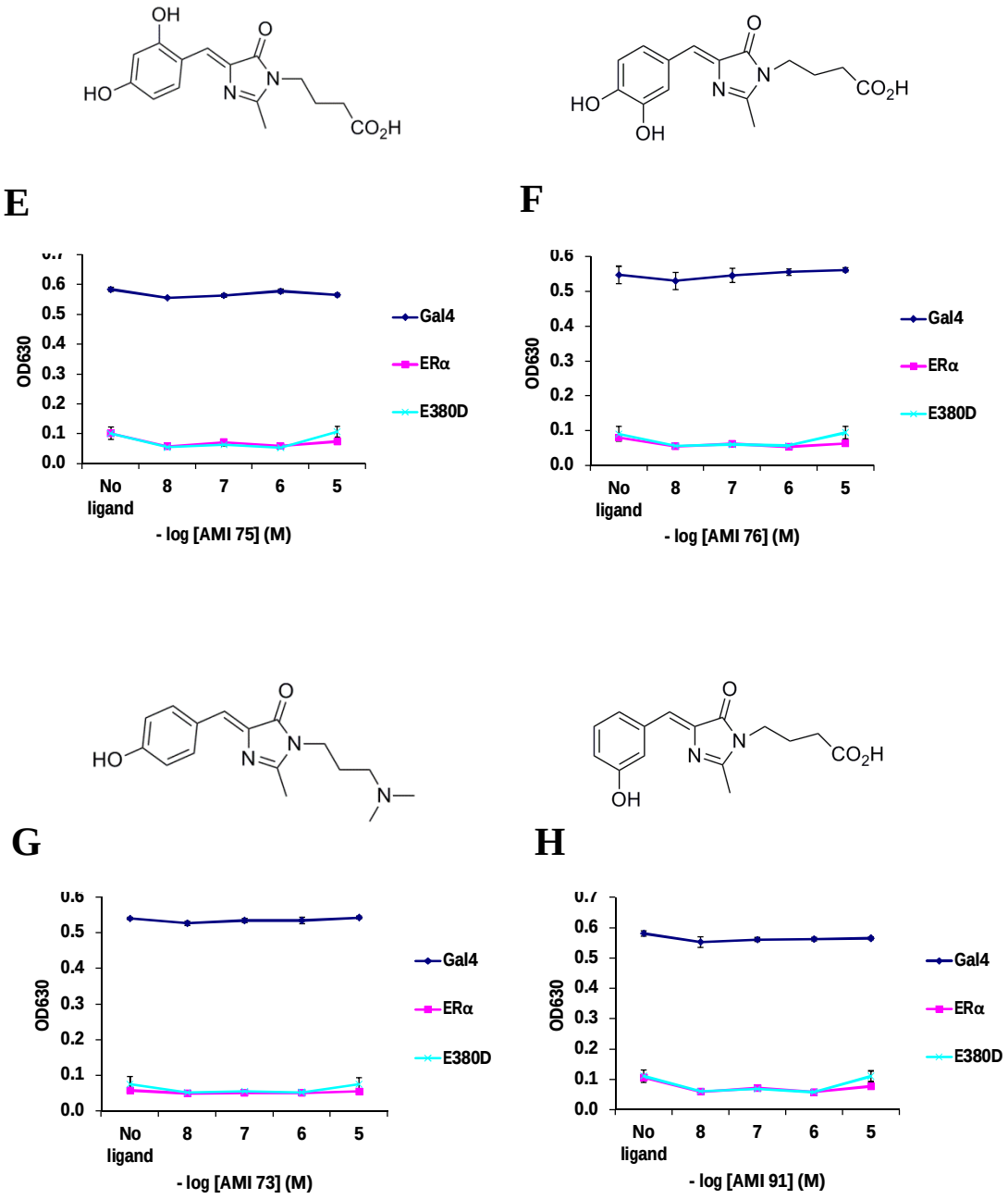

Figure 7.6 Ligand activated growth profiles of E380D variant. Part II. Engineered variant was tested with **E.** AMI 75, **F.** AMI 76, **G.** AMI 73, **H.** AMI 91

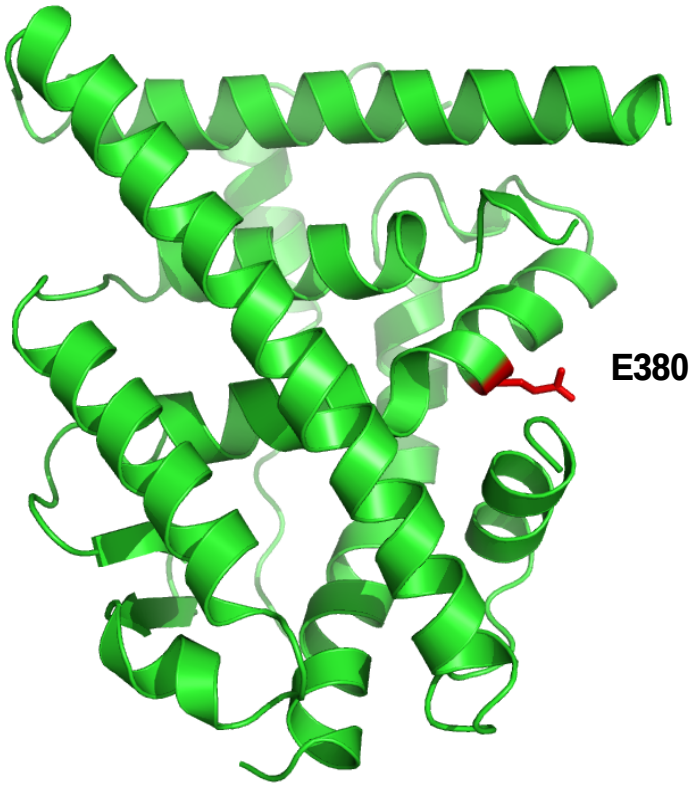

Figure 7.7 Crystal structure of ERα. Residue E380D is shown in red (pdb: 1ERE).

between nuclear receptor, coactivator and corepressor [13]. Changing of E380 to an alanine has been reported to abolish interaction with several peptides mimicking coactivators, and corepressors [14]. Other mutagenic work also showed that the E380Q variant is constitutively active. This mutation is able to modulate non-direct interactions with the coactivator without the presence of the ligand [15]. Furthermore, E380, the negatively charge residue shows conservation only within this subclass of nuclear receptors (Figure 7.9). As shown in Figure 7.9 alignment E380 with many nuclear receptors shows that glutamate is present only in case of ERα and ERβ and in other nuclear receptor subfamilies the positively charge lysine and arginine is present in this position. It the same time, other residues which together with E380 create coactivator binding site are conserved hydrophobic residues across all nuclear receptors. This indicates that perhaps the residue E380 is important for distinguishing between the different coactivators for the various nuclear receptors [13]. In the fact, subfamilies of nuclear receptors use different types of coactivators for activation. For instance, the steroid receptor subfamily interacts with SRC-1 class of coactivators, whereas the retinoid receptors preferentially bind the SRC-3 coactivators [16, 17].

The presence of an amino acid residue in which the side chain is shorter by one carbon and that the overall charge remains the same between these residues makes the presence of an aspartate to a glutamate at position 380 a very conservative change. The observed enhanced activation could be due to coactivator binding with a higher affinity.

To test this hypothesis and determine whether the presence of this mutation influences coactivator recruitment, chemical complementation with two different coactivators was performed. The E380D variant was tested with steroid receptor

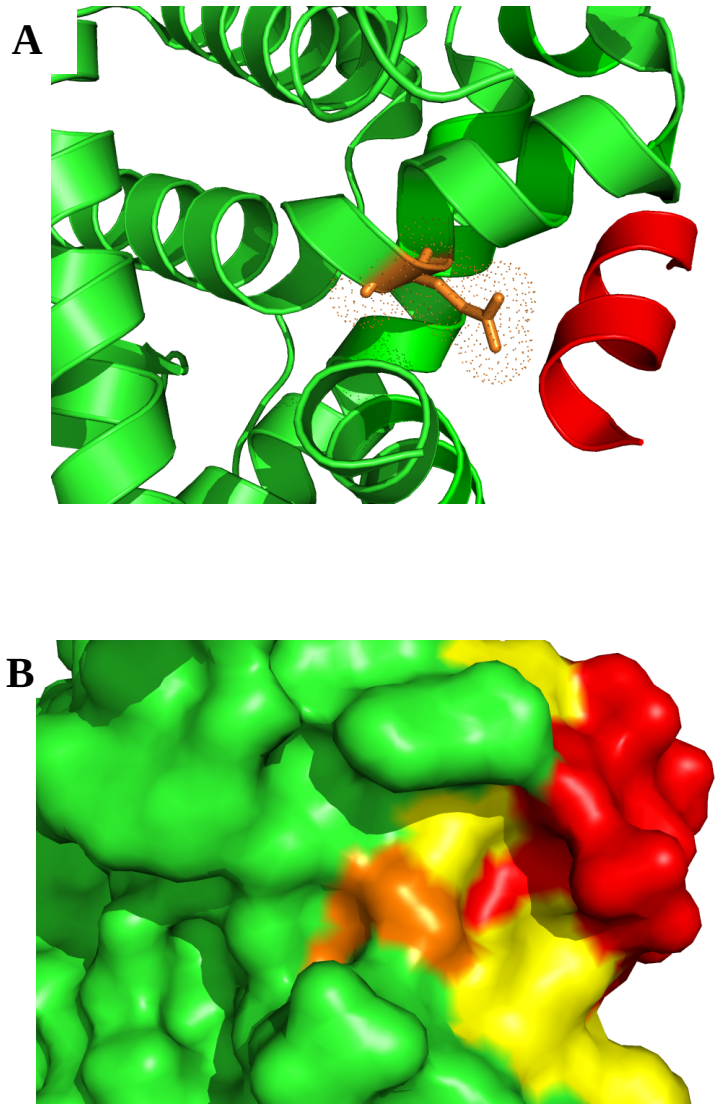

Figure 7.8 Interaction of residue E380 with coactivator. A. Position of E380 residue with coactivator, **B.** Coactivator binding site (yellow) with E380 residue (orange) and coactivator (red). Shown in space filling (pdb: 1GWR).

	Helix5/Helix6						
AR	A	V	I	Q	Y	S	W
ERα	H	L	L	E	C	A	W
ERβ	R	L	L	E	S	C	W
FXR	A	L	L	K	G	S	A
GR	T	L	L	Q	Y	S	W
LXRα	A	L	L	K	T	S	A
PPARγ	T	L	L	K	Y	G	V
RXRα	I	L	L	R	A	G	W
RARα	T	L	L	K	A	A	C
TRβ	I	L	L	K	G	C	C
VDR	V	L	L	K	S	S	

Figure 7.9 Sequence alignment part of Helix 5 and 6 in nuclear receptors. Alignment was made with selected nuclear receptors. Localization of residue E380 is highlighted. This residue is conserve between classes of NR eg. ERα and ERβ

coactivator-1 (SRC-1) and the activator for thyroid hormone and retinoid receptor (ACTR as also known as SRC-3). In addition, coactivators containing three of five LXXLL motifs from the SRC-1 and ACTR proteins (called SRC-1fragment, ACTR fragment, respectively) were tested as well.

As shown in Figure 7.10 the E380D variant shows a coactivator preference. E380D variant is activated at a concentration of 10 mM of AMI 23 and 24 in the presence of the SRC-1 protein and the SRC-1 fragment, which contains three LXXLL motifs. The SRC-1 fragment displays two-fold lower activation in compare to the full SRC-1 protein with both AMI 23 and 24, as well with 17β-estradiol. Influence of coactivators on E380D variant activation with 17β-estradiol differs from wild-type ERα. In case of wild-type receptor SRC-1 and SRC-1fragment coactivators has similar activation profile. However, in the presence of coactivator ATCR fragment, E380D variant has increased basal activity and displays constitutive activity with coactivator ACTR. ACTR coactivator does not cause the wild-type receptor to become constitutively active as was observed with the E380D variant, but does increase the basal activity.

As mentioned previously E380 has been shown to be involved in coactivator binding, but has also been implicated in creating a surface for antagonistic activity. To gain further insight into the importance of E380D, and the ability of the variant to modulate interaction with antagonists, ERα and the E380D variant were tested for interactions with tamoxifen and DY-001-148, known ERα antagonists and drugs against breast cancer (Figure 7.11). Using chemical complementation, yeast expressing E380D variant and wild-type receptor were incubated in the presence of the 0.1 nM 17β-estradiol and a range of concentrations of the tamoxifen or DY-001-148 and tested for induced

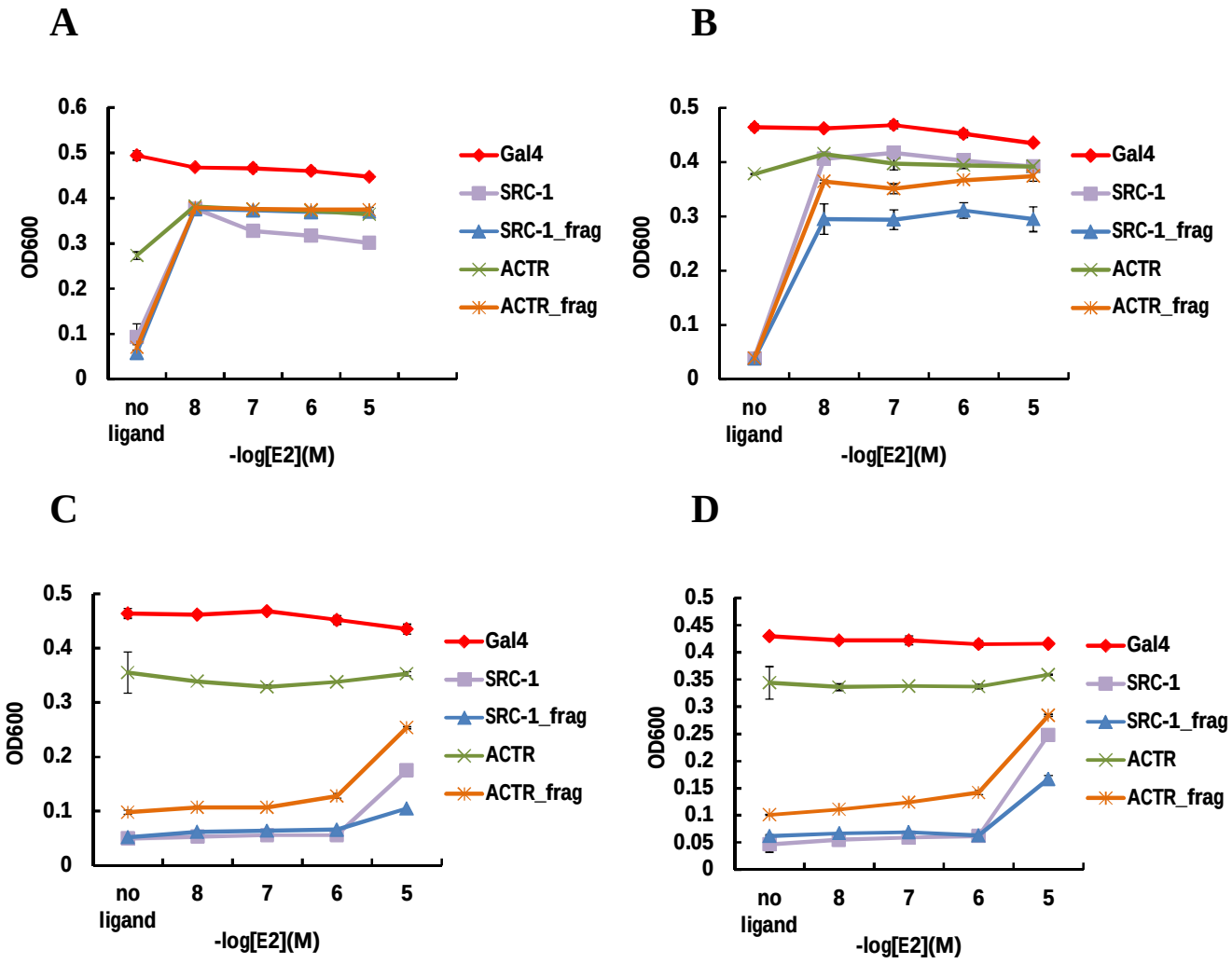

Figure 7.10 Ligand activated growth profiles of E380D variant and wtERα with different coactivators A. wtERα with 17-β Estradiol, **B.** E380D variant with 17-β Estradiol, **C.** AMI 1, **D.** AMI 2,

A

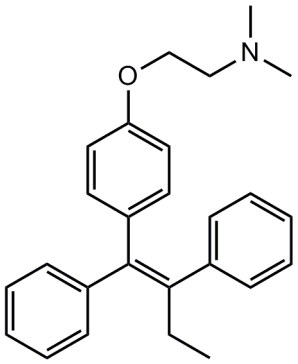

B

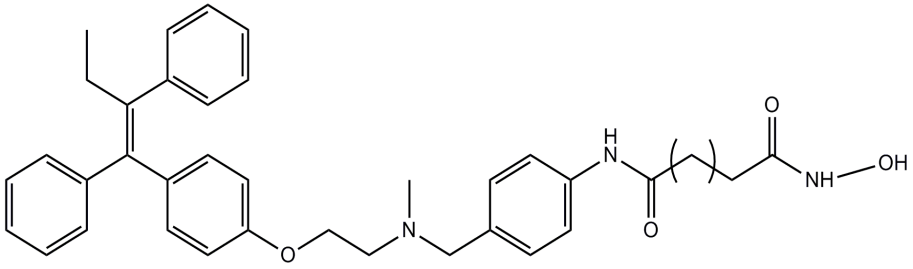

Figure 7.11 ERα antagonists. A. Tamoxifen, **B.** DY-001-148

inhibition of yeast growth by antagonists. Antagonists are able to bind and displace the agonist, 17-β-estradiol, preventing transcription to occur and decrease the growth observed as a result of agonist activity. As shown in Figure 7.12 both antagonists were able to displace 17β-estradiol and decrease estradiol induced growth in 10 μM of antagonist in case of wild-type estrogen receptor. However, in case of E380D variant only, compound DY-001-148 was able to act as an antagonist. Tamoxifen was not able to displace 17β-estradiol and inhibit ligand activated growth. These results indicate that probably this mutation influences the interaction with coactivators and corepressors, thus it can enhance activation with AMIs as well as modulate interactions with antagonists.

7.4 Testing E380D variant in mammalian cells

To verify whether the E380D variant displays the same activation level in yeast as in mammalian cells, variant containing Gal4DBDfused to ERαLBD was cloned into mammalian expression plasmid pCMX which has CMV promoter. The constructed plasmid was cotrasfected into HEK298T cells with plasmid containing Gal4 response elements controlling luciferase expression.

Interestingly, E380D variant did not display a similar activation profile with AMI 23 and 24 in mammalian cells as it has been shown in yeast. As shown in Figure 7.13 the tested variant does not display significant activation level compared to wild-type receptor. As previously described in Chapter 3 the AMI 23 and 24 activate the wild-type ERα with EC_{50} > 3 μM. Based on the yeast data, we hypothesized that E380D variant will be able to enhance the activation of ERα with AMIs. However, these results show that the introduced mutation decreased activation with AMIs as well 17β-estradiol,

indicating that perhaps E380D mutation is not able to allow for proper interaction with coactivators

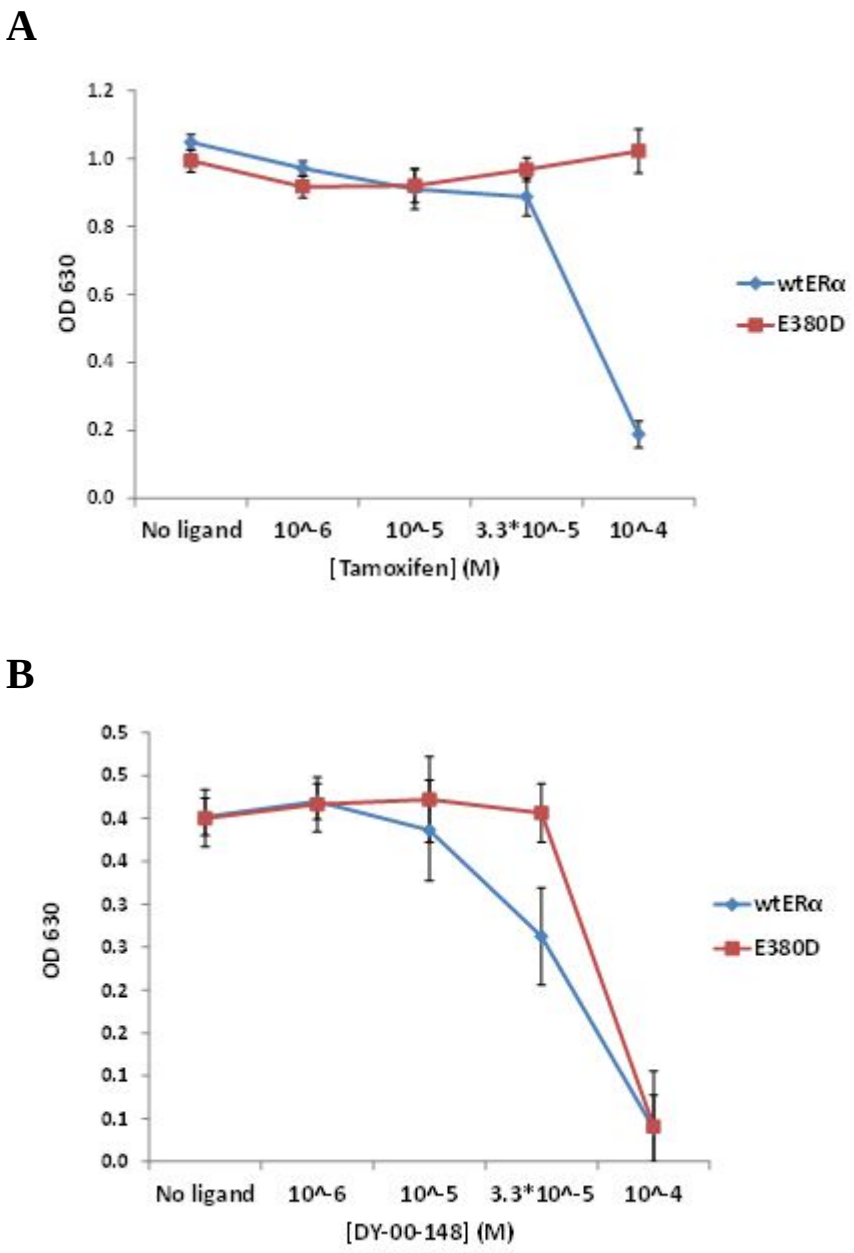

Figure 7.12 Inhibition of estrogen receptor alpha by A. Tamoxifen, B. DY-001-148. Cells were incubated with 0.1 nM of 17-β estradiol and range of concentration of antagonists.

A

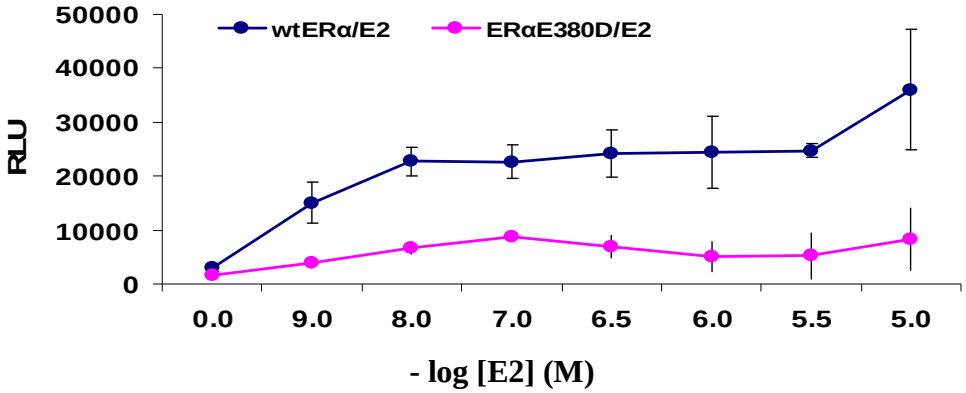

B

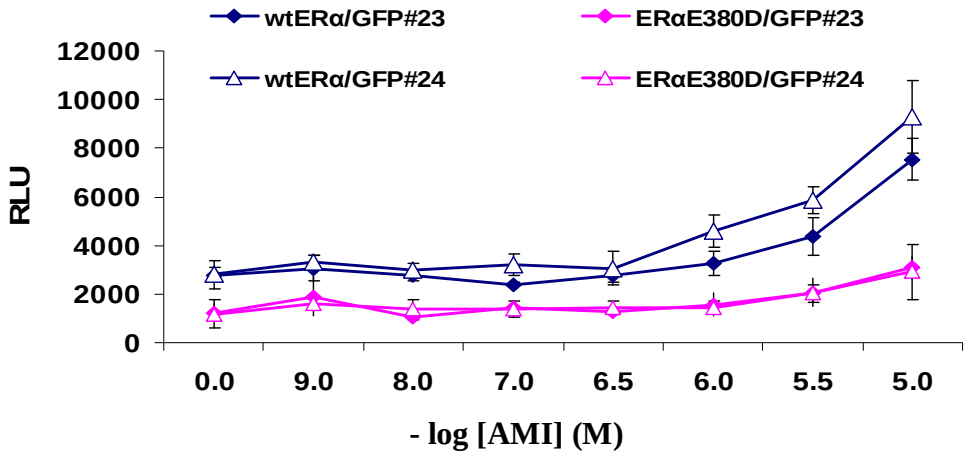

Figure 7.13 Activation profile of E380D variant in mammalian cells. Cells expressing wtERα or E380D variant were incubated with **A.** 17β-estradiol, **B.** AMI 23 and AMI 24.

in mammalian cells. Different expression pattern of coactivators in mammalian cells than in yeast could be responsible for discrepancy between yeast and mammalian data.

7.5 Influence of E380D mutation on Fluophores Fluorescence.

To determine whether E380D mutation of ERα was able to adopt a conformation optimal for fluorescence after binding the AMIs, the E380D variant and wild-type ERα were transformed into yeast. Yeast expressing the variant and wild-type receptor were incubated in yeast selective media with 10 μM AMI. To determine the amount of background fluorescence observed with cells and the compounds, various negative controls were employed. First, yeast transformed with ERα were exposed to the ligands or to estradiol alone, and as a control, were not exposed to any of the AMI derivatives to check for the basal fluorescence. Also, to determine the background fluorescence due to non-specific binding of the fluorophore to endogenous proteins, cells lacking ERα were exposed to the AMI compounds.

As shown in Figure 7.14 slight basal fluorescence was observed in the case of yeast expressing ERα and incubated with estradiol. However, yeast expressing Gal4 and incubated with AMI 23 did not display any fluorescence. It indicates lack of background fluorescence that could be due to AMI non-specific interactions with other proteins in cell. E380D variant that was incubated with AMI 23, displayed fluorescence in yeast. However, wild-type ERα showed a lack of fluorescence with this ligand. Another ligand which actives the receptor, AMI 24, indicated similar fluorescence level in E380D variant as well as ERα.

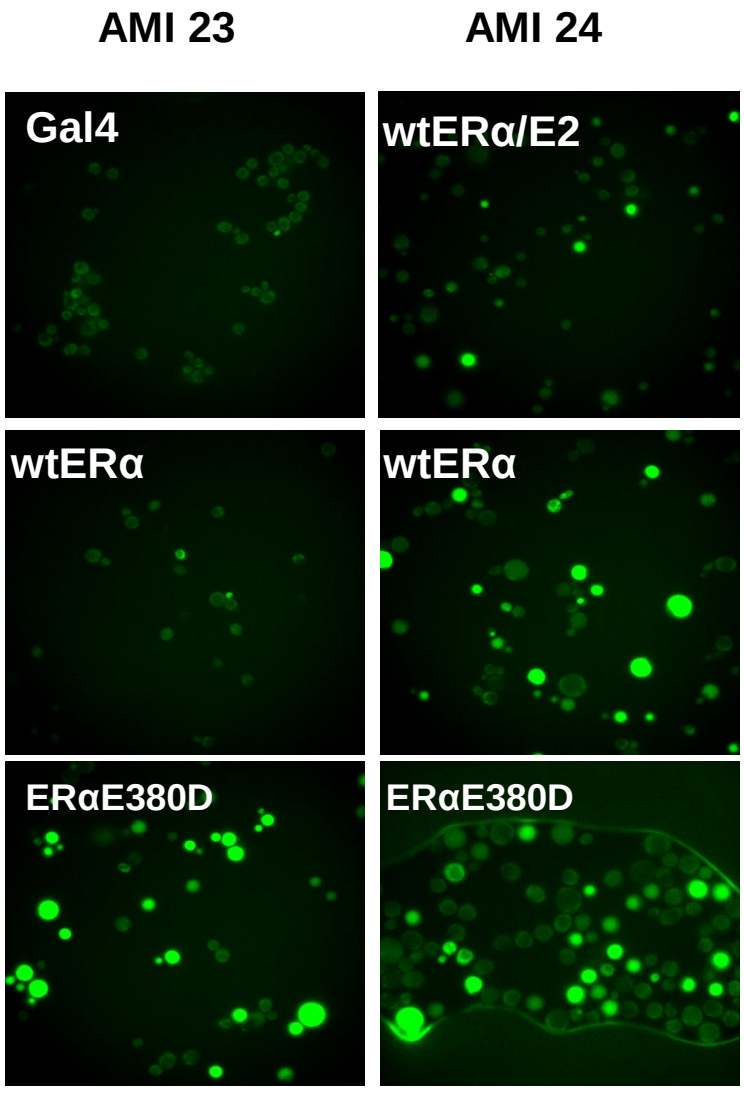

Figure 7.14 Fluorescence studies of wtERα and E380D variant in yeast. Yeast expressing wtERα or E380D were incubated with AMI 23 and 24. Yeast with Gal4 and expressed wtERα incubated with E2 were used as a negative control.

The fluorescence data provided surprising insights into the influence of this mutation on fluorescence. Looking at the position of E380D in the LBD, the presence of the fluorescence upon binding is probably related to the interaction of this residue with coactivator. Interaction of ERα variant with coactivator perhaps allows for conformational change of AMI to turn on fluorescence. These results open new avenues for engineering nuclear receptors which will be able to turn on fluorescence of AMIs upon binding. Extensive mutagenic studies could potentially help to understand what interactions between protein and ligand are important to enhance ligand fluorescence. The gained knowledge could be applied towards development of novel fluophores.

To determine whether results obtained in yeast with E380D variant were consistent in mammalian cells, an expression mammalian plasmid caring the E380D variant was transfected into NIH3T3 cells and HEK298T cells. Cells expressing wild-type ERα or E380D variant were incubated with AMI 23 and 24 and tested for fluorescence using confocal microscopy. To detect any basal fluorescence from AMIs, cells not expressing ERα were incubated with AMIs as well. As expected, cells did not present significant basal fluorescence (Figure 7.15 and Figure 7.16). Cells containing ERα and E380D variant displayed fluorescence which seems to be localized in the nucleus of the cells. This finding is consistent with the known localization of the ligand after ligand binding.

The fluorescence data which has been obtained in mammalian cells showed that this E380D variant is able to enhance fluorescence. However, due to lack of activation of this variant by AMIs in mammalian cells questions if fluorescence visible

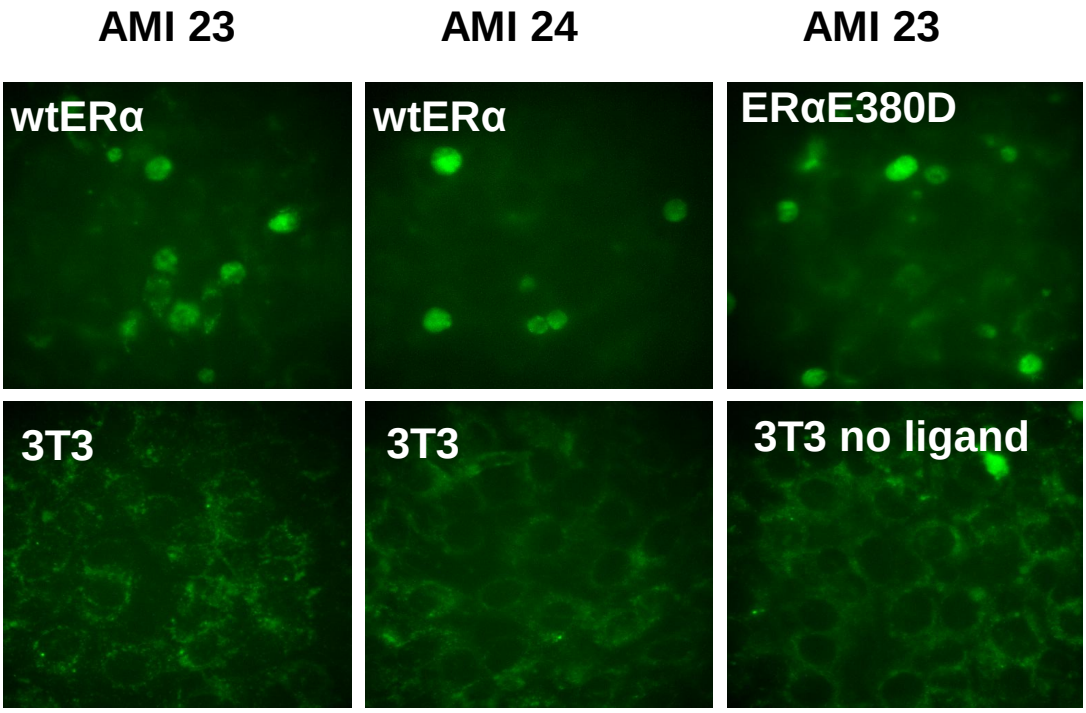

Figure 7.15 Fluorescence studies of wtERα and E380D variant in mammalian cells NIH3T3. Cells expressing wtERα or E380D were incubated with AMI 23 and 24. Cells without expressed receptor were used as a negative control.

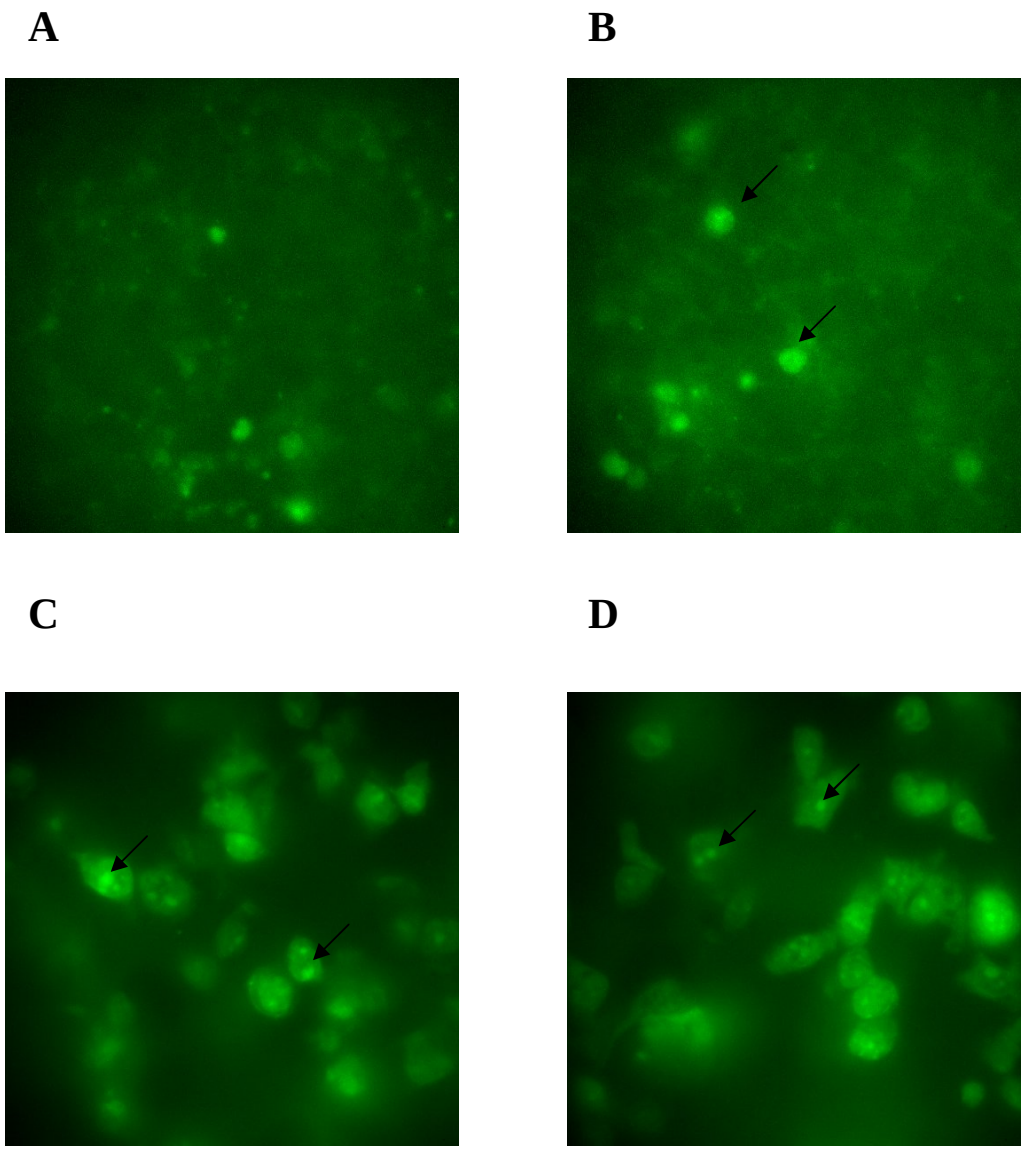

Figure 7.16 Fluorescence studies of wtERα and E380D variant in mammalian cells HEK298T. Cells expressing wtERα (**A**, **B**) or E380D (**C**, **D**) were incubated with AMI 23. Arrows indicated fluorescent spots (nucleus) in cells

in the nucleus is actually linked to activation. These results indicated that AMI 23 is able to bind and activate E380D variant in yeast but does not display activation in mammalian cells.

Perhaps, AMI 23 is able to bind E380D variant which is transferred to the nucleus upon binding. However, possible distracted interaction of variant with coactivator does not allow for activation but allows for displaying fluorescence. These findings could provide insight into correlations between binding, activation and fluorescence and also open new avenues for engineering nuclear receptors to active and enhance fluorescence by novel ligands.

7.6 Extensive Engineering of Estrogen Receptor α

The first attempt to create an ERα library resulted in the E380D variant which was able to enhance activity with AMI in yeast. This discovery led us to explore whether the power of selection in chemical complementation will be able to receive more engineered variants able to be activated by various AMIs. Thus random mutagenesis by error-prone PCR was used to generate ERα libraries. However, as mentioned previously error-prone PCR required the use of Taq polymerase. To generate specific mutation rates, a range of $MnCl_2$ (20 – 400 μM) was used to amplify the ERαLBD gene. The created insert cassettes were transformed into PJ69-A yeast strain along with digested background plasmid pGBDERαbackground and plasmid expressing coactivator pGBDSRC-1 and plated on non-selective plates (-LW) and selective plates with 10 μM of ligand. After 4 days of incubation at 30 °C a library of size 2×10^4 was obtained. 100 colonies were picked, retransformed and tested for constitutive activity by streaking on adenine selective and non-selective plates. Most streaking variants were constitutively

active. However, a few did not grow on adenine selective plates and they were selected for further testing in liquid quantitation assays.

Variants were tested for ligand activated growth with various AMIs which were used for creating libraries. None of these variants displayed ligand activated growth with AMIs but they were functional variants as determined by activation with estradiol. Interestingly, one of these variants ER32 which had five mutations (T347A, F367Y, R436R, L489M, L504P, and L541M) displayed ligand activated growth at 100 nM with estradiol (Figure 7.17). This variant was not activated by AMIs but its decreased sensitivity towards 17β-estradiol makes it as a potential variant to engineer orthogonal ligand – receptor pair.

7.6.1 Creating Second Generation ERα Variants.

To increase sensitivity of the E380D variant, it was used as a template for further engineering using random mutagenesis. In addition, to obtain orthogonal receptor, the ER32 variant was also subjected to engineer to obtain activity with AMIs and further lose affinity to 17β-estradiol. Thus, both variants were used as templates for error-prone PCR and, as described above, the insert cassette which obtained by PCR and transformed into PJ69-A along with background plasmid and plated on non-selective and selective plates. Additionally, a library based on wild-type ERα was also generated. 100 variants were picked and tested for constitutive activity. 13 variants which did not display constitutive activity have been sequenced and selected for further testing in liquid quantitation assays (Table 7.3). Variants were tested for ligand activated growth with AMI 23 and estradiol. Interestingly, variant NCC4 which is a first generation of wild-type ERα displayed ligand activated growth with AMI 23 at 10 μM (Figure 7.18). However, ligand activated

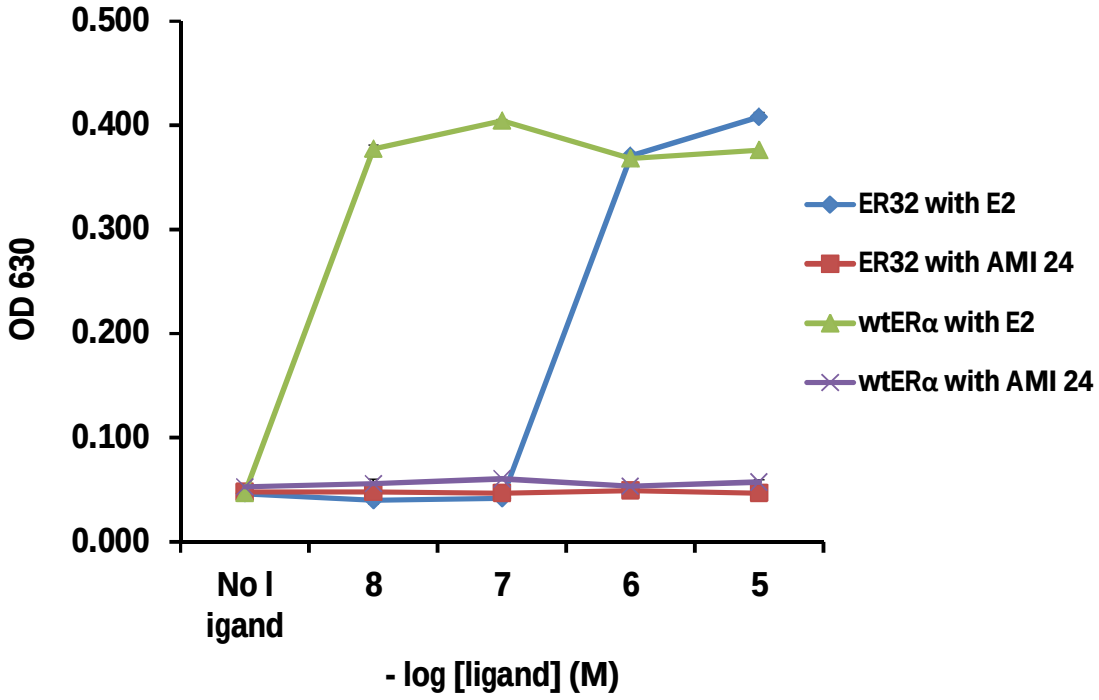

Figure 7.17 Ligand activated growth of wtERα and ER32 variant. Engineered ER32 variant were tested with 17-β Estradiol and AMI 24.To compare activation profile, wtERα was tested as well.

Table 7.3 Sequencing result for second generation of ERα variants.

	Template	Mutations
NCC1	E380D	NCC7
NCC2	wtER	S338R, G366D, M396V, A405S, C457W, D473E, V533E, D545Y
NCC3	wtER	wtER
NCC4	wtER	M396R, M437L, S456S, L525L
NCC5	E380D	F404F, M437L, Q441R, K449I, Y521C
NCC6	E380D	L310V, V364A, H377Y, M396I, A405A, H488Del, L454Del
NCC7	E380D	S329Y, L384P, I389I, F404L, I451T, L489R, S512S
NCC9	E380D	Q314P, N407S, I487I
NCC10	E380D	E380D
NCC11	ER32	ER32
NCC12	ER32	Y328F, V392I
NCC13	ER32	L319M, Q375R
NCC14	ER32	Q375R

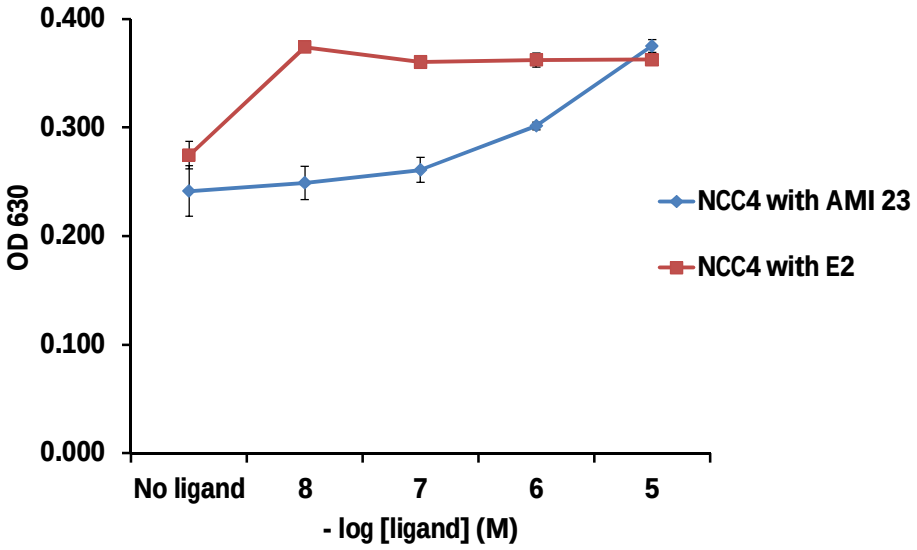

Figure 7.18 Ligand activated growth of NCC4 variant. Engineered variant were tested with 17-β Estradiol and AMI 23.

growth with AMI 23 as well as estradiol have high basal. Two mutations of NCC4, M396R and M437L may have allowed for conformational change of ERα to be activated by AMI 23. However, this conformational change makes the variant be in partly active state resulting in constitutive activity.

Library of second generation of variants did not create any variants activated by AMI. However, some of the second generation of ER 32 variants displayed decreased sensitivity toward 17β-estradiol compare to ER32. Variant NCC14, which has an additional mutation (Q375R) than the five mutations of ER32, shows ligand activated growth with 17β-estradiol at 10 μM, thus decreasing about 100 folds in sensitivity (Figure 7.19). Surprisingly, the NCC7 variant which is a second generation of E380D variant, displayed the same activation profile as NCC14. This variant, having an additional five mutations (E380D S329Y, L384P, F404L, I451T, and L489R) showed ligand activated growth with 17β-estradiol at 10 μM. However, these mutations inhibited activation with AMI 23, as was obtained with the E380D variant. These results indicated that additional five mutations to E380D restrained activation with AMI and decreased sensitivity towards estradiol due to perhaps their influence on folding of protein which does not allowed for proper interaction with coactivators and then activation.

Unfortunately, none of the second generation variants were the orthogonal variants are able to bind AMI but not to 17β-estradiol. Only one variant NCC4, was able to be activated with AMI 23 but it has high basal which makes it a potential engineered receptor with novel function.

7.6.2 Creating Second and Third Generation ERα Variants.

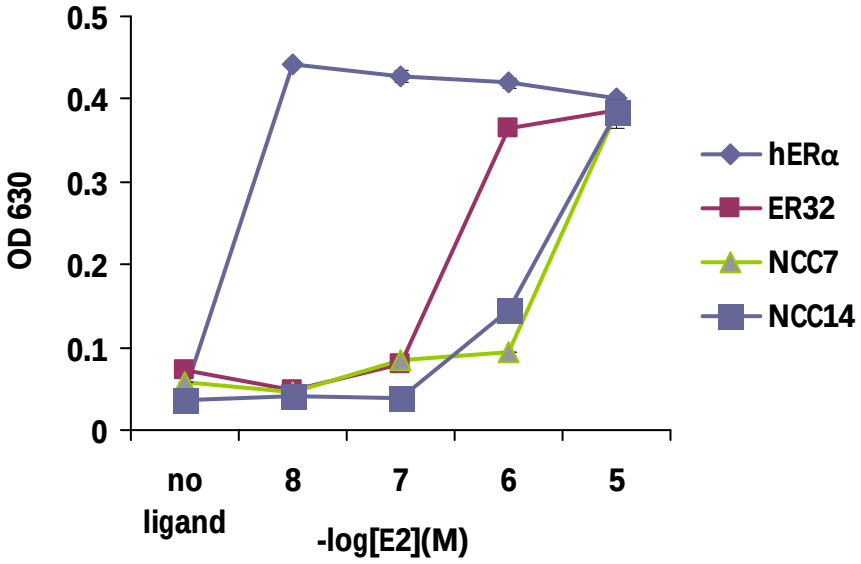

Figure 7.19 Ligand activated growth of variants with decreased response on 17β - estradiol. Engineered variants, NCC7 and NCC14 were tested with 17-β Estradiol. To compare activation profiles of tested variants, ligand activated growth of ER32 and wtERα.

An attempt to create a variant which capable of being activated by AMI required that we create another range of variants. The sixteen variants which were obtained from the previous libraries as a first or second generation of variants were used a template for next round of error-prone PCR. The 120 ng of each cassette obtained by error – prone PCR was transformed into PJ69-A yeast strain along with ERα background plasmid. After four days of incubations, a transformation efficiency of 5.2×10^4 was obtained, creating library size of about 5.5×10^3. One hundred of the variants were tested for constitutive activity by streaking out on selective and nonselective agar plates as mentioned previously. 30% of the tested variants did not display constitutive activity and their activation profile was tested using liquid quantitation assays with 17β-estradiol and a mix of eight derivatives of AMIs at 10 μM which were used as a selective pressure to drive the libraries. As shown in Figure 7.20 most of the variants displayed ligand activated growth with 17β-estradiol. However, several of variants showed ligand activated growth with AMIs 10 μM. All of the 16 assayed variants were sequenced and tested with each one of eight AMIs to find which AMIs was able to activate variants (Figure 7.21). Interestingly, sequencing results showed a high diversity (Table 7.4). Obtained variants were the next generations of the E380D, ER32, 12_8, NCC5, 24_5 and NCC13 variants. Additional mutations generated variants with new functions. The ER8GFP11 and ERL19 variants showed ligand activated growth with AMI 73 and 81. AMI 81 with ER8GFP11 variant had 6 fold activation versus 5 fold activation with ERL19. The other AMI that activates only ER8GFP11 is AMI 73 with 4 fold activation. These results are surprising due to the structures of the AMIs. AMI 73 and 81 differ

significantly in structure. AMI 73 has a similar structure to AMI 23 and 24, ERα activators with hydroxyl group on AMI core. However, AMI 73 has a dimethylamine

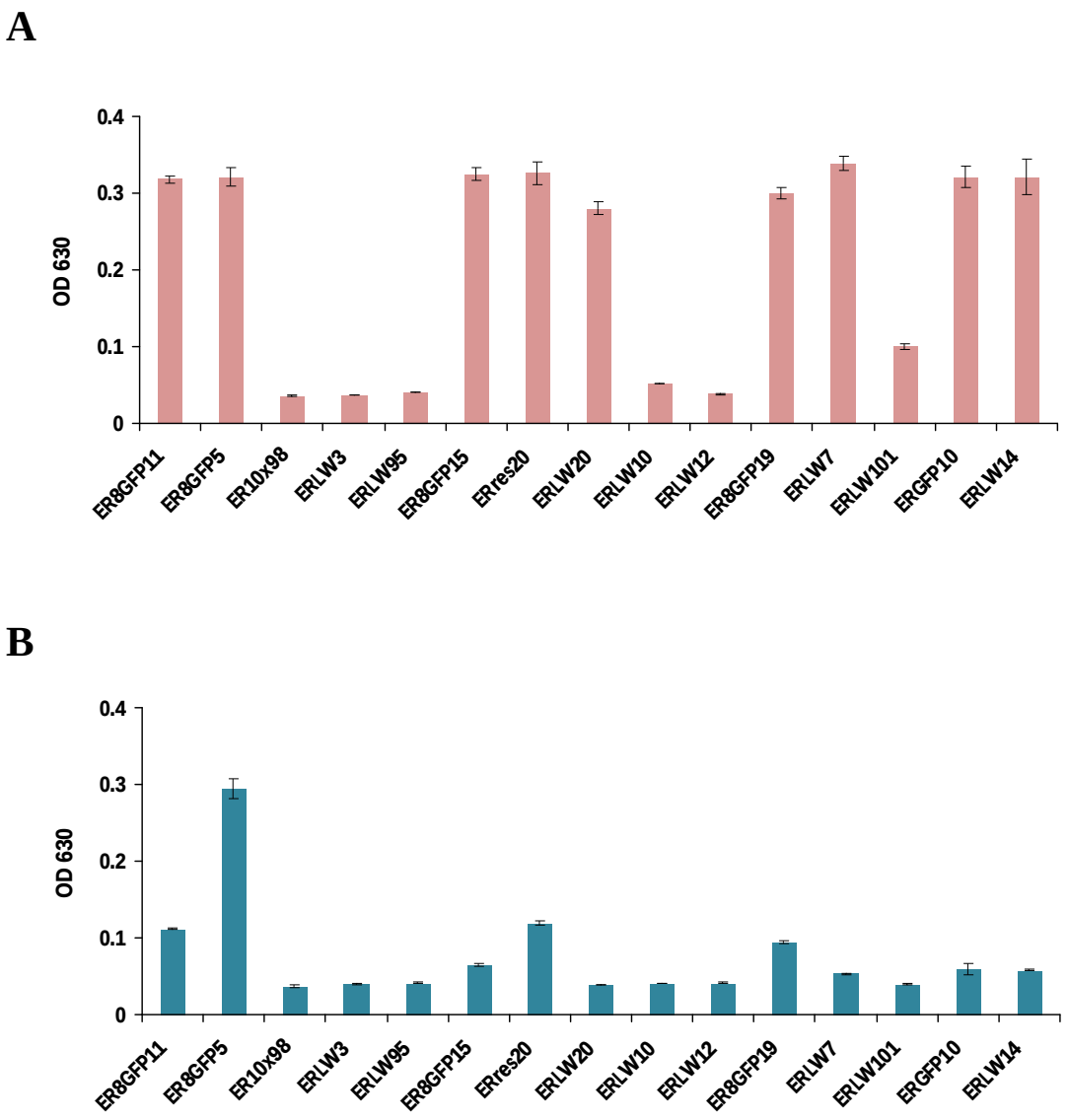

Figure 7.20 Ligand activated growth of second and third generation variants. Engineered variants were tested with **A.** 17-β Estradiol, and **B.** AMIs. Ligand activated growth were tested at 10 μM of ligand.

Table 7.4 Sequencing results for second and third generation of ERα variants.

	Template	Mutations	Activation
ER8GFP5	E380D	E380D, **L384P, G442R, L525L, L579stop**	**C.A.**
ERLW95	NCC5	E380D, F404F, M437L, K449I, Y521C, **L319M**	**EST**
ER8GFP19	12_8	N348S, G442R, **L387L K302K**	**EST, 10-5 GFP**
ERres20	12_8	N348S, G422R	**EST, 10-5 GFP**
ERLW3	ER32	T347A, F367Y, R436R, L489M, L504P,L541M **L509P**	**NA**
ERLW12	ER32	T347A, F367Y, R436R, L489M, L504P, L541M, **M396R, S456S, L486S**	**NA**
ERLW20	?	E339V, M396R, M337L, S456S, G521G, L525L	**EST (10^-7)**
ERLW7	24_5	P406H, K416I	**EST**
ER8GFP15	E380D	E380D, **R335R**	**EST, 10^-5 GFP**
ER8GFP10	E380D	E380D	**EST, 10^-5 GFP**
ERL19	12_8	N348S, G442R, **L354L, K416Q, T431I**	**EST, 10-5 GFP**
ER98LW10x	?	V376D	**NA**
ERLW101	NCC13	L319M, T347A, F367Y, R436R, L489M, L504P, L541M, **E471G**	**EST (10^-5 slight)**
ERLW14	12_8	N348S, G442R, **N519S**	**NA**
ER8GFP11	12_8	N348S, G442R, **L453L**	**EST, 10-5 GFP**
ERLW10		N383stop	**NA**

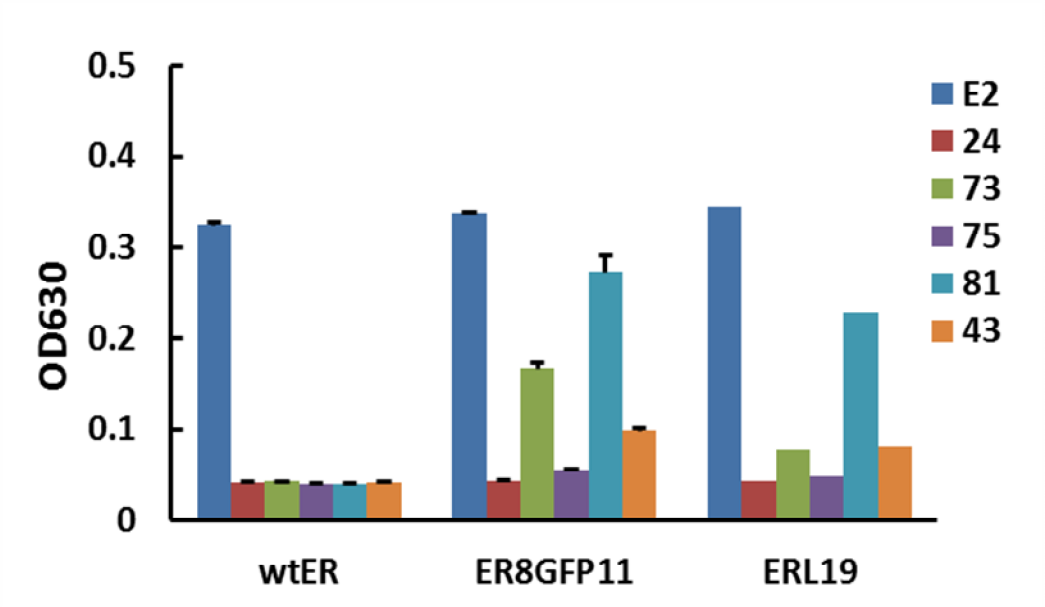

Figure 7.21 Ligand activated growth of ER8GFP11 and ERL19 variants. Engineered variants were tested with set of AMIs which was used for creation of library.

in stead of a carboxylic acid as in AMI 23 or 24. On the other hand, AMI 81 which has incorporated tetrahydrotetramethylnaphatalenyl moiety in AMI core differs substantially from AMIs that activate ERα.

Responsible for achieving novel functions are mutations of 12_8 variant which was used as template for creating next generation variants ER8GFP11 and ERL19. Variant 12_8, which was obtained in the first ERα library, was not tested for activation with AMI 81 and 73 previously. Sequencing results have shown that variant ER8GFP11 has the same mutations as the 12_8 variant with an additional silent mutation at L453. However, variant ERL19 is a second generation of the 12_8 variant with two additional mutations, K416Q and T431I (Figure 7.22).

Based on activation profiles of both variants, mutations of 12_8 (ER8GFP11) variant seems to be implicated in novel function of these variants. Thus, previous mutagenesis studies have shown that residue N348 stabilizing the ligand bound conformation of LBD by forming hydrogen bond with Y537 [18, 19]. However, residue G442 which is localized in helix eight is not close position to ligand binding pocket [19]. It has been shown that this residue takes place in contact with helix 1 and it is responsible for altering helix-helix interactions. Other mutagenesis studies have shown mutation G442V increased sensitivity to testosterone [20]. These previous studies indicate that obtained mutations perhaps stabilizing interactions in the ligand binding domain.

The additional mutations K416Q and T431I which are present in the ERL19 variant seem not to be essential for activation. This variant displays similar activation profile with its parent variant 12_8. However, activation with AMI 73 is decreased.

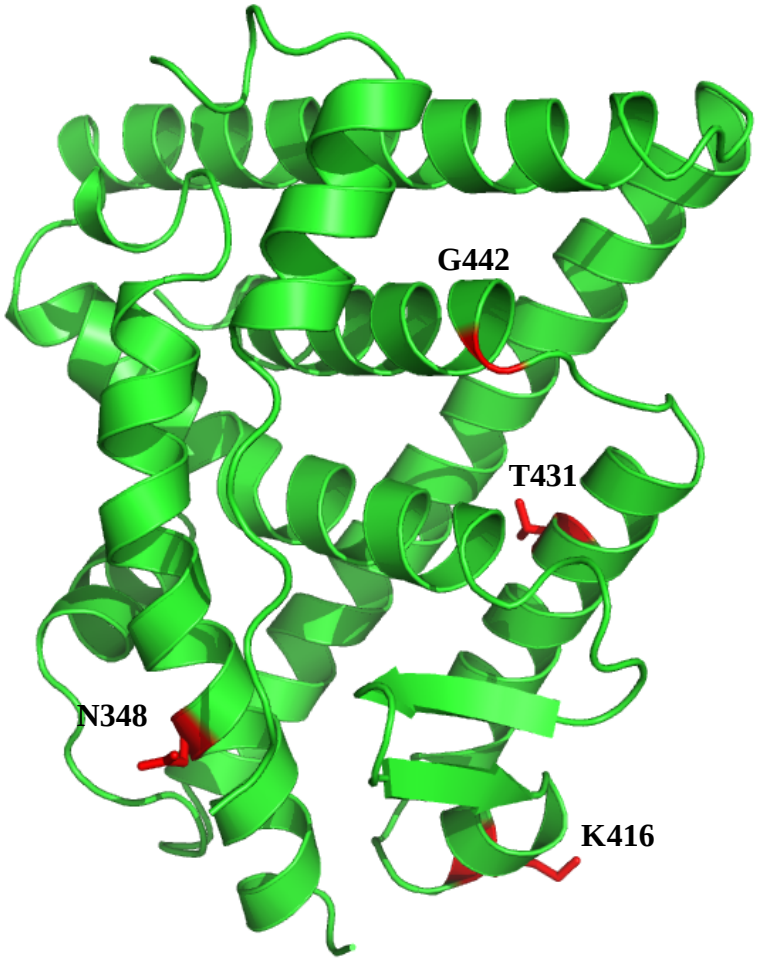

Figure 7.22 Crystal structure of ERα. Residues of variants ER8GFP11 and ERL19 are selected at crystal structure of ERα (shown in red), pdb: 1ERE.

The role of these residues for ligand binding have not been established and more mutagenesis studies need to be done to understand their role.

7.7 Summary

The analysis of presented evolved ERα variants provided new insights into the molecular basis of ERα ligand specificity. Obtained variants have shown novel function toward activation by AMIs. Besides the novel functions, which were presented in the case of ERL19 and ER8GFP11 variants, enhanced activation was also achieved as shown in E380D variant. This variant was not only able to enhance activation with AMI 23 and 24, which bind ERα, but also enhance fluorescence levels of AMIs in yeast as well as mammalian cells. These results demonstrate that directed evolution of nuclear receptors may be beneficial towards creating novel variants with abilities to activate various ligand.

Unfortunately, we were not able to engineer an orthogonal estrogen receptor which was activated by AMI but that lost affinity to 17β-estradiol. However, variants with decreased affinity to its natural ligand were obtained. They can be used for further engineering to create an orthogonal receptor-ligand pair.

In total, this insight can be applied toward engineering estrogen receptors using a random mutagenesis approach as well as by rational mutagenesis to enhance activation achieved by engineered variants.

7.8 Materials and Methods

Ligands

17-β estradiol (MW= 272.4 g/mol) was purchased from MP Biomedicals (Aurora, OH). The library of AMIs was synthesized by Dr. Anthony Baldridge. Method of synthesize was described previously in Chapter 2. 10 mM stocks of all ligands were made with 80 % ethanol: 20 % dimethyl sulfoxide (DMSO) and stored at 4 °C.

Plasmid constructions

The pGBDERαLBD , and pGBDERαbackground plasmid were constructed previously. Also coactivators plasmids pGAD10BALXXLLSRC-1, pGAD10BASRC-1, pGAD10BALXXLLACTR and pGAD10BAACTR were cloned before.

The created variant E380D was cloned into mammalian expression plasmid pCMX.

Error – Prone PCR

The ERαLBD was amplified using pGBDERαLBD as the template DNA for error – prone PCR random mutagenesis using 0.5 µM of each ERPCR1For 5’ GGT CAA AGA CAG TTG ACT GTA TCG C 3’ and ERPCR8Rev 5’ GCC TCC CCC GTG ATG TAA ATA CT 3’ primers (Operon). In addition to primers PCR solution consist contained 500 µM dNPTs, 7 nM MgCl2, 250 ng of template DNA, 1x *Taq* buffer, and *Taq* polymerase (Promega Bio-Tek) with varied concentrations of MnCl2 or Mutazyme polymerase (Stratagene). The PCR program was run with following steps 95 °C for 1 minute, 95 °C for 30 seconds, 55 °C for 30 seconds, 72 °C for 1 minute, which were repeated 20 times

and followed by 72 °C for 4 minutes. The created cassettes were purified using the QIAprep® Spin Miniprep Kit (Qiagen). To create second and third generation of the variants, previous parents' variants were used as template for amplification error –prone PCR.

Yeast Transformation – Libraries Creation

Each ERα Library was created using 10 μg of the full insert cassette and 0.3 μg of the yeast expression background plasmids which were transformed into PJ69-A strain by using TRAFCO yeast transformation protocol. Transformation mix was plated on non-selective (SC-LW) and selective (SC-ALW) agar plates. Selective plates contained 10 μM of selected AMIs. Plates were incubated at 30 °C by 3-4 days. Based on the number of colonies on non-selective plates library size and transformation efficiency was calculated.

Liquid Quantitation Assays

Obtained variants were rescue for pGBD plasmid which carried mutated ERα gene and sent for sequencing (Operon). Sequenced transformants were re-transformed into PJ69-A yeast strain and selected for further testing using liquid quantitation assay in chemical complementation. Transformants were incubated in non-selective media at 30 °C overnight and shaken at 300 rpm. Variants after removing media and washing in distillated water were resuspended in selective media (SC-ALW) with concentration range of various AMIs in 96-well plates. Plates were incubated at 30 °C by 48 hours and

shaken at 170 rpm. Ligand activated growth was tested by taking reading of optical density at 630 nm of wavelength after 0, 24 and 48 hours of incubation.

Fluorescence Microscopy

The PJ69-4A strain expressing ERα was incubated in selective media SC-ALW with AMIs, at 30 °C, shaking at 300 rpm. After incubation yeast were pelleted by centrifuging and resuspended in distill sterile water. Cells were again centrifuged and resuspended in water. Next the cell were displayed under fluorescent microscope and analyzed for green fluorescence.

Confocal microscopy was performed as described in Chapter 3.

7.9 References

1. Yamamoto, K., et al., *Alanine scanning mutational analysis of the ligand binding pocket of the human Vitamin D receptor.* J Steroid Biochem Mol Biol, 2007. **103**(3-5): p. 282-5.

2. Yamada, S. and K. Yamamoto, *Ligand recognition by vitamin D receptor: total alanine scanning mutational analysis of the residues lining the ligand binding pocket of vitamin D receptor.* Curr Top Med Chem, 2006. **6**(12): p. 1255-65.

3. Fagart, J., et al., *Antagonism in the human mineralocorticoid receptor.* EMBO J, 1998. **17**(12): p. 3317-25.

4. Ekena, K., et al., *Different residues of the human estrogen receptor are involved in the recognition of structurally diverse estrogens and antiestrogens.* J Biol Chem, 1997. **272**(8): p. 5069-75.

5. Doyle, D.F., et al., *Engineering orthogonal ligand-receptor pairs from "near drugs".* J Am Chem Soc, 2001. **123**(46): p. 11367-71.

6. Shi, Y. and J.T. Koh, *Functionally orthogonal ligand-receptor pairs for the selective regulation of gene expression generated by manipulation of charged residues at the ligand-receptor interface of ER alpha and ER beta.* J Am Chem Soc, 2002. **124**(24): p. 6921-8.

7. Taylor, J.L., et al., *Characterization of a molecular switch system that regulates gene expression in mammalian cells through a small molecule.* BMC Biotechnol, 2010. **10**: p. 15.

8. Schwimmer, L.J., et al., *Creation and discovery of ligand-receptor pairs for transcriptional control with small molecules.* Proc Natl Acad Sci U S A, 2004. **101**(41): p. 14707-12.

9. Castillo, H.S., et al., *The role of residue C410 on activation of the human vitamin D receptor by various ligands.* J Steroid Biochem Mol Biol, 2012. **128**(1-2): p. 76-86.

10. Ousley, A.M., et al., *A human vitamin D receptor mutant activated by cholecalciferol.* J Steroid Biochem Mol Biol, 2011. **125**(3-5): p. 202-10.

11. Lundberg, K.S., et al., *High-fidelity amplification using a thermostable DNA polymerase isolated from Pyrococcus furiosus.* Gene, 1991. **108**(1): p. 1-6.

12. Pritchard, L., et al., *A general model of error-prone PCR.* J Theor Biol, 2005. **234**(4): p. 497-509.

13. Ko, L., et al., *Ser-884 adjacent to the LXXLL motif of coactivator TRBP defines selectivity for ERs and TRs.* Mol Endocrinol, 2002. **16**(1): p. 128-40.

14. Heldring, N., et al., *Identification of tamoxifen-induced coregulator interaction surfaces within the ligand-binding domain of estrogen receptors.* Mol Cell Biol, 2004. **24**(8): p. 3445-59.

15. Lazennec, G., et al., *Mechanistic aspects of estrogen receptor activation probed with constitutively active estrogen receptors: correlations with DNA and coregulator interactions and receptor conformational changes.* Mol Endocrinol, 1997. **11**(9): p. 1375-86.

16. McInerney, E.M., et al., *Determinants of coactivator LXXLL motif specificity in nuclear receptor transcriptional activation.* Genes Dev, 1998. **12**(21): p. 3357-68.

17. Xu, J., et al., *The steroid receptor coactivator SRC-3 (p/CIP/RAC3/AIB1/ACTR/TRAM-1) is required for normal growth, puberty, female reproductive function, and mammary gland development.* Proc Natl Acad Sci U S A, 2000. **97**(12): p. 6379-84.

18. Herynk, M.H. and S.A. Fuqua, *Estrogen receptor mutations in human disease.* Endocr Rev, 2004. **25**(6): p. 869-98.

19. Eng, F.C., et al., *Probing the structure and function of the estrogen receptor ligand binding domain by analysis of mutants with altered transactivation characteristics.* Mol Cell Biol, 1997. **17**(8): p. 4644-53.

20. Chen, Z., et al., *Directed evolution of human estrogen receptor variants with significantly enhanced androgen specificity and affinity.* J Biol Chem, 2004. **279**(32): p. 33855-64.

APPENDIX A

EVALUATION OF AMI FOR LXRB IN MAMMALIAN CELLS

In Chapter 3, it was shown that the discrepancy between the activation profile of ERα in yeast and mammalian cells. These results indicated that NR activation tested using mammalian assay can provide more information than chemical complementation. Thus, LXRβ was subjected to test its activation profile with library of AMIs in mammalian cells. The HEK298T cells were co-transfected with the mammalian expression vector pCMXGLXRβLBD expressing Gal4DBD:LXRβLBD fusion protein and vector carrying Gal4 response element under luciferase promoter. Cells were incubated in media with library of 60 compounds of AMIs. As a control, cells were incubated with known LXRβ ligand, T090. As shown in Figure 6.12 LXRβ was not activated by any AMI compounds. These results indicated that AMI core is not suitable for activation of LXRβ.

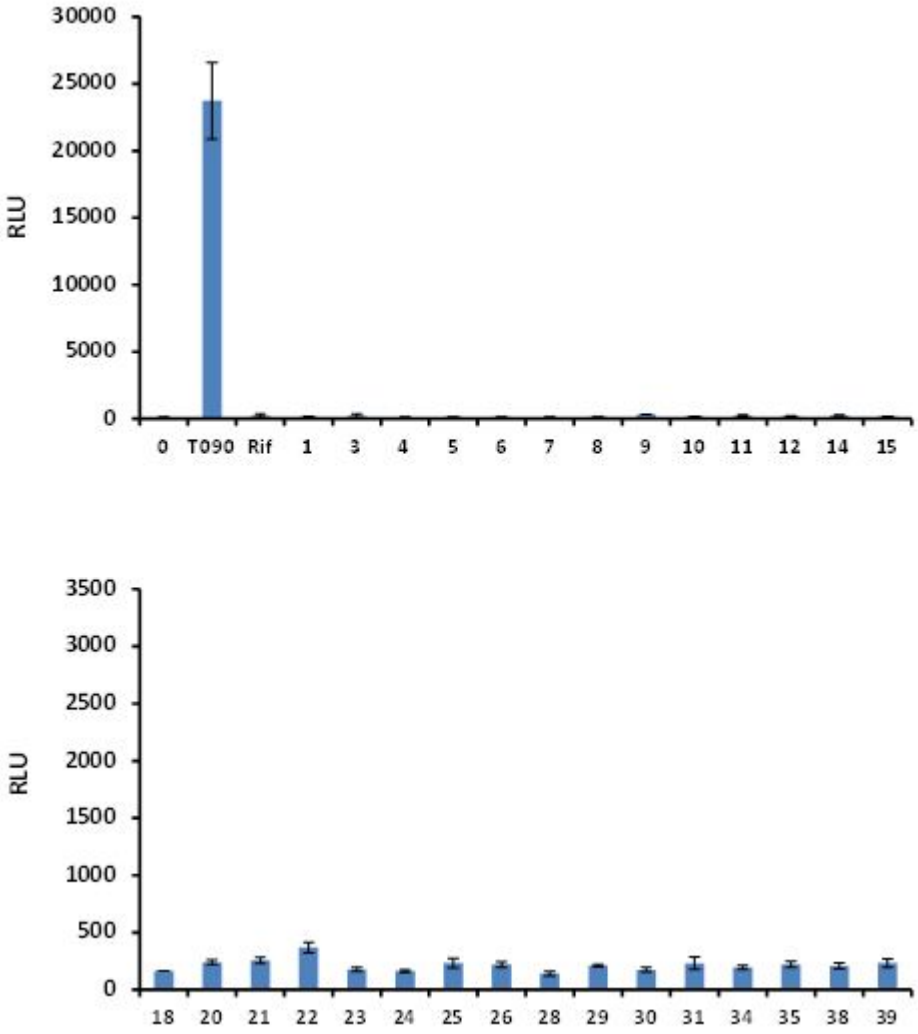

Figure A.1. Activation profile of 60 AMIs in LXRβ. Part I. LXRβ (GBD: LXRβLBD) was transfected into HEK298T cells with p17*4TATALuc plasmid, a luciferase reporter gene under the control of Gal4 response elements and were incubated with 10 μM of ligand. Structures of all above ligands are included in appendix.

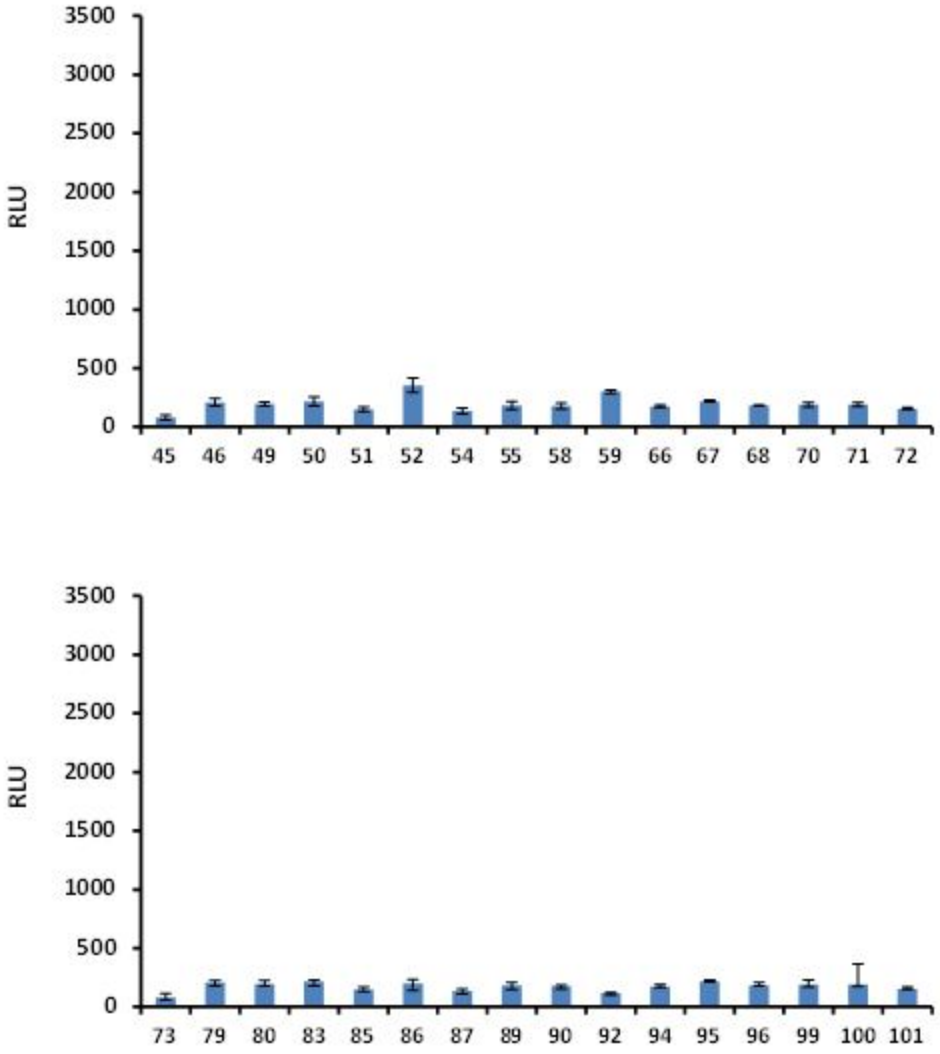

Figure A.1. Activation profile of 60 AMIs in LXRβ. Part II. LXRβ (GBD: LXRβLBD) was transfected into HEK298T cells with p17*4TATALuc plasmid, a luciferase reporter gene under the control of Gal4 response elements and were incubated with 10 μM of ligand. Structures of all above ligands are included in appendix.

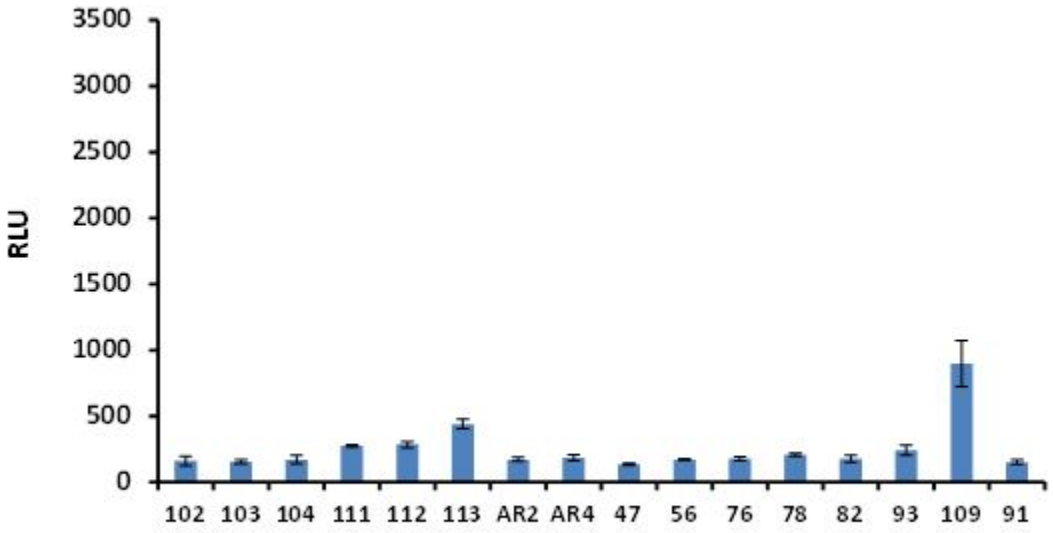

Figure A.1 Activation profile of 60 AMIs in LXRβ. Part III. LXRβ (GBD: LXRβLBD) was transfected into HEK298T cells with p17*4TATALuc plasmid, a luciferase reporter gene under the control of Gal4 response elements and were incubated with 10 μM of ligand. Structures of all above ligands are included in appendix.

APPENDIX B

LIBRARY OF AMI DERIVATIVES

Table B.1 Library of AMI derivatives.

#	R1	R2	R3	R4	#	R1	R2	R3	R4
1	4-Me	H	Me	Me	**89**	3,5-Me 4-OH	H	Me	Me
2	3-OMe	H	Me	Me	**90**	3-F	H	Me	Me
3	3-OH	H	Me	Me	**91**	3-OH	H	C3CO2H	Me
4	2,3-OMe	H	Me	Me	**92**	4-OC12H25	H	Me	Me
5	4-NO2	H	Me	Me	**93**	4-OMe	H	Me	Me
6	2,5-OMe	H	Me	Me	**94**	2-OMe	H	Me	Me
7	3,5-t-Bu 4-OH	H	Me	Me	**95**	4-OMe	H	n-Pr	Me
8	4-CO2H	H	Me	Me	**96**	4-Cl	H	n-Pr	Me
9	4-N(Me)2	H	Me	Me	**97**	4-Br	H	Me	Me
10	2-F	H	Me	Me	**98**	2-OMe	H	n-Pr	Me
11	4-OBz	H	Me	Me	**99**	2-Br	H	Me	Me
12	2,4,5-OMe	H	Me	Me	**100**	4-PhC8H17	H	Me	Me
13	2-pyridyl-4-OH	H	Me	Me	**101**	4-Br	H	n-Pr	Me
14	4-OH	H	Me	Me	**102**	2-Br	H	n-Pr	Me
15	2-Me	H	Me	Me	**103**	3-F	H	n-Pr	Me
16	4-CN	H	Me	Me	**104**	3-Cl	H	Me	Me
17	4-N(Et)2	H	Me	Me	**105**	3-OMe	H	n-Pr	Me
18	4-OH	H	n-Pr	Me	**106**	Benzyl	H	n-Pr	Me
19	4-OH	H	n-Pn	Me	**107**	3-OH	H	C3CO2H	Me

Table B.1 continued

20	4-OH	H	n-Bu	Me	**108**	Benzyl	H	C3CO2H	Me
21	4-Me	H	n-Pr	Me	**109**	4-PhC5H11	H	Me	Me
22	4-N(Me)2	H	n-Pr	Me	**110**	4-i-Pr	H	Me	Me
23	4-OH	H	C3CO2H	Me	**111**	3,4-Me	H	Me	Me
24	4-OH	H	C5CO2H	Me	**112**	2-OH 4-N(Et)2	H	n-Pn	Me
25	1-naphthyl	H	Me	Me	**113**	2-OH 4-N(Et)2	H	n-heptyl	Me
26	4-Et	H	Me	Me	**114**	2-OH 4-N(Et)2	H	n-Pr	Me
27	3-Me	H	Me	Me	**115**	4-N(Et)2	H	n-hexyl	Me
28	2,4-Me	H	Me	Me	**116**	2-OH 4-N(Et)2	H	n-hexyl	Me
29	2-quinoline	H	Me	Me	**117**	2-OH	H	n-Pr	Me
30	2,5-Me	H	Me	Me	**118**	3-Cl	H	n-Pr	Me
31	1-naphthyl	H	Et	Me	**119**	2-OH 4-N(Et)2	H	Dodecyl	Me
32	4-i-Pr	H	n-Pr	Me	**120**	2-OH 4-N(Et)2	H	Octyl	Me
33	4-N(Me)2	H	n-Bu	Me	**121**	4-i-Bu	H	C3CO2H	Me
34	2-CF3	H	Me	Me	**122**	4-i-Bu	H	n-heptyl	Me
35	2-naphthyl	H	Me	Me	**123**	3,4-Me	H	C3CO2H	Me
36	4-N(Et)2	H	*i-Pr*	Me	**124**	3-pyridyl	H	Me	Me
37	4-OH	H	EtOH	Me	**125**	3-Br	H	n-Pr	Me
38	4-OH	H	CH2(CF2)7 CF3	Me	**126**	2,4-Cl	H	Me	Me
39	4-Et	H	n-Pr	Me	**127**	2-OH	H	Me	Me
40	2-Et	H	Me	Me	**128**	3-Br	H	Me	Me
41	2-Me	H	n-Pr	Me	**129**	4-PhC3H7	H	Me	Me
42	2-Me	H	CH2CF3	Me	**130**	3,5-t-Bu 4-OH	H	n-Pr	Me

Table B.1 continued

43	4-OH	H	PrOH	Me	**131**	3,5-t-Bu 4-OH	H	n-Pn	Me
44	2-Et	H	n-Pr	Me	**132**	3,5-t-Bu 4-OH	H	n-hexyl	Me
45	3-NO2	H	Me	Me	**133**	4-OMe	H	EtOH	Me
46	4-N(Et)2	H	n-Pr	Me	**134**	3,4-OMe	H	n-Pr	Me
47	2,6-Me	H	Me	Me	**135**	2-OH 3-OEt	H	2-phenol	Me
48	4-i-Pr	H	Me	Me	**136**	4-OH	H	C2N(Me)2	Me
49	4-t-Bu	H	Me	Me	**137**	3-OH	H	C2N(Me)2	Me
50	3-indole	H	Me	Me	**138**	2-OH	Me	Me	Me
51	2-F	H	n-Pr	Me	**139**	4-N(Et)2	H	C2-sym	Me
52	4-N(Me)2	H	*i-Pr*	Me	**140**	Benzyl	H	C2N(Me)2	Me
53	4-tetralin	H	Me	Me	**141**	3,5-t-Bu 4-OH	H	EtOH	Me
54	2-Me	H	Et	Me	**142**	2-OH 4-OMe	H	n-Pr	Me
55	4-N(Et)2	H	n-Pn	Me	**143**	2,4-Cl	H	n-Pr	Me
56	Benzyl	H	Me	Me	**144**	4-N(Et)2	H	C4-sym	Me
57	2-OH 3-OEt	H	Me	Me	**145**	2-OH 4-OMe	H	Me	Me
58	4-F	H	Me	Me	**146**	Piperonal	H	Me	Me
59	2-OH 4-N(Et)2	H	Me	Me	**147**	2-CF3	H	n-Pr	Me
60	2-imidazole	H	Me	Me	**148**	4-OH	H	Allyl	Me
61	2-Et	H	Et	Me	**149**	2,5-OMe	H	n-Pr	Me
62	3-Me	H	n-Pr	Me	**150**	4-N(Me)2	H	PrOH	Me
63	2-Me	H	n-Bu	Me	**151**	3-OH 4-Br	H	Me	Me
64	2-Me	H	n-Pn	Me	**152**	4-OH	H	2-heptyl	Me
65	2-Me	H	*i-Pr*	Me	**153**	4-Ph	H	Me	Me
66	3-OMe 4-OH	H	C3CO2H	Me	**154**	4-OMe	H	Allyl	Me

Table B.1 continued

67	4-Me	H	Et	Me	**155**	2-OH 4-OMe	H	PrOH	Me
68	2,3-OMe	H	C3CO2H	Me	**156**	4-N(Me)2	H	2-heptyl	Me
69	4-N(Et)2	H	C3CO2H	Me	**157**	4-OC4H9	H	Me	Me
70	4-Cl	H	Me	Me	**158**	4-N(Me)2	H	C3N(Me)2	Me
71	3-CF3	H	n-Pr	Me	**159**	4-N(Me)2	H	C2CN	Me
72	4-CF3	H	Me	Me	**160**	2-OH 4-N(Et)2	H	C2-sym	Me
73	4-OH	H	C3N(Me)2	Me	**161**	4-Me	H	C2H4CN	Me
74	3-CF3	H	Me	Me	**162**	2-Indole	H	n-Pn	Me
75	2,4-OH	H	C3CO2H	Me	**163**	3-OH	H	2-heptyl	Me
76	3,4-OH	H	C3CO2H	Me	**164**	3-OH	H	3-Pn	Me
77	2-Cl	H	Me	Me	**165**	2-Indole	H	C3N(Me)2	Me
78	2-Cl	H	n-Pr	Me	**166**	4-N(Me)2	H	EtOH	Me
79	4-CF3	H	n-Pr	Me	**167**	4-N(Et)2	H	C6-sym	Me
80	3,5-Me	H	Me	Me	**168**	2-Indole	H	n-Pr	Me
81	4-tetralin	H	C3CO2H	Me	**169**	3-OH	H	2-heptyl	Me
82	Benzyl	H	C3CO2H	Me	**170**	4-CN	H	PrOH	Me
83	2-OH 4-N(Et)2	H	C3CO2H	Me	**171**	4-OBu	H	n-Pn	Me
84	4-N(Me)2	H	C3CO2H	Me	**172**	4-OH	H	3-Pn	Me
85	4-OC6H13	H	Me	Me	**173**	4-OH	H	CH2CF3	Me
86	2,6-Me 4-OH	H	Me	Me	**174**	4-N(Me)2	H	Allyl	Me
87	3,5-t-Bu 4-OH	H	Benzyl	Me	**175**	4-OH	H	C2H4CN	Me
88		4-OH		H		Benzyl		Me	